



HAL
open science

Foamability of Oil Mixtures

Hoai-Phuong Tran

► **To cite this version:**

Hoai-Phuong Tran. Foamability of Oil Mixtures. Soft Condensed Matter [cond-mat.soft]. Sorbonne Université, 2022. English. NNT : 2022SORUS117 . tel-03850793

HAL Id: tel-03850793

<https://theses.hal.science/tel-03850793v1>

Submitted on 14 Nov 2022

HAL is a multi-disciplinary open access archive for the deposit and dissemination of scientific research documents, whether they are published or not. The documents may come from teaching and research institutions in France or abroad, or from public or private research centers.

L'archive ouverte pluridisciplinaire **HAL**, est destinée au dépôt et à la diffusion de documents scientifiques de niveau recherche, publiés ou non, émanant des établissements d'enseignement et de recherche français ou étrangers, des laboratoires publics ou privés.

Sorbonne Université

École doctorale Physique et Chimie des Matériaux (ED 397)

Moussabilité des Mélanges d'Huiles

Par **Hoai-Phuong TRAN**

Thèse de doctorat de Physique

Dirigée par Laurence TALINI et François LEQUEUX

Présentée et soutenue publiquement le 14 Janvier 2022

Devant un jury composé de :

M. Arnaud SAINT-JALMES	Directeur de Recherche <i>Université de Rennes 1</i>	Rapporteur
M. Thomas SALEZ	Chargé de Recherche <i>Université de Bordeaux</i>	Rapporteur
M. Thomas SÉON	Chargé de Recherche <i>Sorbonne Université</i>	Examinateur
Mme. Emmanuelle RIO	Professeure <i>Université Paris-Saclay</i>	Examinatrice
Mme. Laurence TALINI	Directrice de Recherche <i>CNRS</i>	Directrice de thèse
M. François LEQUEUX	Directeur de Recherche <i>ESPCI Paris</i>	Co-directeur de thèse
M. Nicolas PASSADE-BOUPAT	Chef de service <i>TotalÉnergies</i>	Invité

Sorbonne University

Doctoral School Physics and Chemistry of Materials (ED 397)

Foamability of Oil Mixtures

By **Hoai-Phuong TRAN**

Doctoral thesis in Physics

Directed by Laurence TALINI and François LEQUEUX

Presented and publicly defended on 14 January 2022

In front of a jury composed of:

M. Arnaud SAINT-JALMES	Research Director <i>University of Rennes 1</i>	Reviewer
M. Thomas SALEZ	Research Fellow <i>University of Bordeaux</i>	Reviewer
M. Thomas SÉON	Research Fellow <i>Sorbonne University</i>	Examiner
Mme. Emmanuelle RIO	Professor <i>Paris-Saclay University</i>	Examiner
Mme. Laurence TALINI	Research Director <i>CNRS</i>	Thesis supervisor
M. François LEQUEUX	Research Director <i>ESPCI Paris</i>	Thesis co-supervisor
M. Nicolas PASSADE-BOUPAT	Head of Department <i>TotalÉnergies</i>	Guest

ACKNOWLEDGEMENTS

TABLE OF CONTENTS

ACKNOWLEDGEMENTS	5 -
TABLE OF CONTENTS	6 -
LIST OF FIGURES	9 -
GLOSSARY OF ABBREVIATIONS	16 -
RÉSUMÉ	19 -
ABSTRACT	20 -
INTRODUCTION & BIBLIOGRAPHY	21 -
INDUSTRIAL PROBLEMS	21 -
LIQUID FOAM	22 -
<i>Plateau borders</i>	23 -
<i>Disjoining pressure</i>	23 -
ROLE OF MARANGONI EFFECT.....	26 -
<i>Film stabilization - Foam</i>	26 -
<i>Evaporation-induced foam stabilization</i>	28 -
<i>Questions about foam of binary and ternary mixtures</i>	29 -
<i>Our research with binary mixtures</i>	31 -
1. EXPERIMENTAL METHODS	33 -
1.1. DETERMINING THE FOAMABILITY OF BINARY MIXTURES WITH A BIKERMAN COLUMN ... -	34 -
<i>Experimental description</i>	34 -
1.1.1. <i>Measurement of the foam height</i>	35 -
1.1.2. <i>Determination of the foaming height by the measure of the total height.</i>	37 -
1.1.3. <i>Foam lifetime</i>	44 -
1.1.4. <i>Normalized foam lifetime</i>	45 -
1.1.5. <i>Effect of Evaporation</i>	46 -
1.1.6. <i>Interfacial tension of binary mixtures & Effect of composition and chemical natures on foamability</i> -	50 -
1.2. VARYING THE BUBBLE SIZE WITH AN ULTRA TURRAX SET-UP	59 -
<i>Geometry of Ultra Turrax</i>	59 -
<i>Experimental description</i>	59 -
1.2.1. <i>Measurement of bubble sizes by image analysis</i>	60 -
1.2.2. <i>Validation of bubble sizes by estimation from creaming phenomena</i>	62 -
1.2.3. <i>Influence of flowrate on bubble sizes</i>	63 -
1.2.4. <i>Normalized foam lifetime results</i>	64 -
1.3. MEASURING THE LIQUID FILM THICKNESS/LIFETIME BY A SINGLE BUBBLE EXPERIMENT -	65 -

<i>Experimental description</i>	- 65 -
1.3.1. <i>Methods</i>	- 66 -
1.3.2. <i>Thickness measurements</i>	- 73 -
1.4. CONCLUSION.....	- 74 -
2. SYMMETRIC BINARY MIXTURES	- 76 -
2.1. DEFINITIONS OF SYMMETRIC BINARY MIXTURES	- 77 -
2.1.1. <i>Used symmetric binary mixtures</i>	- 77 -
2.2. THEORETICAL INTERPRETATIONS & MODELLINGS.....	- 79 -
2.2.1. <i>Qualitative explanation of the stabilization mechanism</i>	- 79 -
2.2.2. <i>Picture of life and death of a foam</i>	- 80 -
2.2.3. <i>Shape of the film at mechanical equilibrium</i>	- 81 -
2.2.4. <i>Partition of molecules in the volume and at the interface</i>	- 84 -
2.2.5. <i>Characteristic length α – foamability</i>	- 87 -
2.3. COMPARISON TO EXPERIMENTAL DATA	- 88 -
2.4. CONCLUSION.....	- 91 -
2.5. PUBLICATION	- 92 -
3. ASYMMETRIC BINARY MIXTURES	- 100 -
3.1. DEFINITION OF ASYMMETRIC BINARY MIXTURES.....	- 101 -
3.1.1. <i>Used asymmetric binary mixtures</i>	- 102 -
3.1.2. <i>Summary of experimental results</i>	- 103 -
3.2. THEORETICAL INTERPRETATIONS & MODELLINGS.....	- 106 -
3.2.1. <i>Qualitative explanation about physical picture: Effect of molecular size on the non-linearity of the mixture’s surface tension</i>	- 106 -
3.2.2. <i>Partition of molecules in the volume and at the interface</i>	- 107 -
3.2.3. <i>Butler’s model and surface molar fraction Γ_1</i>	- 108 -
3.2.4. <i>Characteristic length α of asymmetric binary mixtures</i>	- 114 -
3.3. COMPARISON TO EXPERIMENTAL DATA	- 115 -
3.4. CONCLUSION.....	- 117 -
3.5. PUBLICATION	- 118 -
4. HYDRODYNAMICS AND PIERCING OF THIN LIQUID FILMS	- 128 -
4.1. SUMMARY OF SUBMITTED PUBLICATION “RUPTURE MECHANISMS OF FILM OF LIQUID MIXTURES”	- 129 -
4.2. SUBMITTED PUBLICATION	- 133 -
CONCLUSIONS & OUTLOOKS	- 156 -
APPENDICES	- 160 -

<i>Appendix A: Foaming systems – Measurement of liquid fraction in the foam Φ_L</i>	- 160 -
<i>Appendix B: Viscosity measurements</i>	- 164 -
<i>Appendix C: Estimation of bubble diameters based on creaming phenomena</i>	- 166 -
<i>Appendix D: Independence of bubble swelling time on injected flowrate</i>	- 168 -
<i>Appendix E: Determination of x_{1max} for symmetric mixtures</i>	- 171 -
<i>Appendix F: A linear link between surface tension γ and surface molar fraction Γ cannot reflect asymmetric mixtures.</i>	- 173 -
RÉSUMÉ EN FRANÇAIS	- 177 -
INTRODUCTION	- 177 -
CHAPITRE 1 : MÉTHODES EXPÉRIMENTALES	- 178 -
<i>Détermination de la moussabilité des mélanges binaires à l'aide d'une colonne Bikerman</i>	- 178 -
<i>Variation de la taille de la bulle avec un montage Ultra Turrax</i>	- 179 -
<i>Mesure de l'épaisseur et du temps de vie du film liquide par l'expérience d'une bulle unique</i>	- 181 -
CHAPITRE 2 : MÉLANGES BINAIRES SYMÉTRIQUES	- 183 -
CHAPITRE 3: MÉLANGES BINAIRES ASYMÉTRIQUES	- 187 -
CHAPITRE 4: HYDRODYNAMIQUE ET PERCEMENT DE FILMS LIQUIDES MINCES -	190 -
BIBLIOGRAPHIC REFERENCES	- 191 -
CONTACTS	- 195 -

LIST OF FIGURES

Figure Intro-1-1 : Electric motor rotates at high speeds. Air can infiltrate circuits and potentially trigger fluids to foam, causing device materials to be damaged.	21 -
Figure Intro-1-2 : Descriptive diagram of the structure of a foam [1].	22 -
Figure Intro-1-3 : Schematic of a horizontal film and a Plateau border.	23 -
Figure Intro-1-4 : Disjoining pressure ΠD between two interfaces as a function of liquid film thickness h . The different contributions to the disjoining pressure – van der Waals, electrostatic, steric – are represented by the dash lines and the continuous line represents their sum. [3]	24 -
Figure Intro-1-5 : (a) Stretching: plug-type flow velocity profile in the pure liquids.	26 -
Figure Intro-1-6 : Drainage: Poiseuille flow velocity profile with surface-active components.	27 -
Figure Intro-1-7 : Schematic showing the mechanism of bubble stabilization resulting from evaporation-induced Marangoni effect.	28 -
Figure Intro-1-8 : Phase diagram of ternary systems and lines of iso-foamability (dotted line) dotted lines): (a) ethanol/benzene/water system - (b) ethylene glycol/butanol/water system at 20 °C.	29 -
Figure Intro-1-9 : A molecule of the liquid having the lowest surface tension in the mixture inside a film. Its formation and spreading on the film surface, causing the film to thin and the liquid to flow. The film thins to the point where it breaks. [3]	30 -
Figure 1-10: No foam observed in pure liquid (left); a foam layer at the top of mixture of liquid (right)	31 -
Figure 1-1 : Schematic of the experimental set-up.	34 -
Figure 1-2 : (a) Binary mixtures in Birkman column; (b) Formation of foam in the top of the column after the air injection.	36 -
Figure 1-3 : ΦB is evaluated as a function of Q at a varied value of H_0 for Decane.	37 -
Figure 1-4 : ΦB is evaluated in terms of H_0 at a fixed value of $Q = 6 \text{ mL.s}^{-1}$ for 4 liquids of different viscosity: Water, Heptanol, Cyclopentanol and Decane.	38 -
Figure 1-5 : ΦB is evaluated as a function of Q at a varied value of H_0 from 10 cm to 15 cm for three liquids of different viscosity: Heptanol, Cyclopentanol and Decane.	39 -
Figure 1-6 : Calibration summary chart	40 -
Figure 1-7 : Forces acting on a rising bubble in the Birkman column	41 -
Figure 1-8 : Experimental fraction liquid ΦL of binary mixtures of linear alkanes and toluene as a function of μQ	43 -

Figure 1-9: Experimental foam height H of binary mixtures of linear alkanes and Toluene as a function of injected flowrate Q	44 -
Figure 1-10 : Experimental foam lifetimes of binary mixtures of linear alkanes and Toluene as a function of injected flow rate Q	45 -
Figure 1-11 : Issue of Evaporation for the studied mixtures. (left) Open system set-up; (right) Closed system set-up.	46 -
Figure 1-12 : Normalized foam lifetime of a Decane/Toluene mixture as a function of the Decane molar fraction x_1 in open system and closed system. The solid line is a guide for the eye.....	47 -
Figure 1-13 : Schematic showing the mechanism of bubble destabilization resulting from evaporation-induced Marangoni effect.....	48 -
Figure 1-14 : Experimental normalized foam lifetime $L\tau$ as a function of molar fraction of liquid 1 x_1 in the binary mixtures. (a) of linear alkanes and Toluene; (b) of linear alcohols and Cyclopentanol/ of 2 linear alcohols. The full lines are the guide for the eye.....	51 -
Figure 1-15 : Experimental normalized foam lifetime $L\tau$ as a function of molar fraction of liquid 1 x_1 in the alkane/alkane mixtures. Only 2 foaming mixtures are represented. C_7/C_8 and C_8/C_{10} are the non-foaming mixtures. The full lines are the guide for the eye.....	52 -
Figure 1-16 : Experimental normalized foam lifetime $L\tau$ as a function of molar fraction of PDMS ($M = 770 \text{ g.mol}^{-1}$; $\mu = 5 \text{ cst}$) in the mixture with Decane. Inset: same curve with x_1 in log scale.-	53 -
Figure 1-17 : Measurement of interfacial tension γ as a function of molar fraction of liquid 1 x_1 in the binary mixtures. (a) of linear alkanes and Toluene; (b) of linear alcohols and Cyclopentanol/ of 2 linear alcohols. For example, $x_1 = 0$ corresponds to surface tension of pure Toluene and $x_1 = 1$ corresponds to alkane's surface tension for the alkane/Toluene mixtures. The dashed line indicates linear variations.	54 -
Figure 1-18 : Measurement of interfacial tension γ as a function of molar fraction of liquid 1 x_1 in the binary mixtures of 2 linear alkanes. The dashed line indicates linear variations.	55 -
Figure 1-19 : Measurement of interfacial tension γ as a function of molar fraction of PDMS in the mixture with Decane. The dashed line indicates linear variations.	55 -
Figure 1-20 : Experimental normalized foam lifetime $L\tau$ of studied binary mixtures as a function of corresponding surface tension difference $\Delta\gamma$	56 -
Figure 1-21 : Experimental normalized foam lifetime $L\tau$ of studied binary mixtures as a function of corresponding $\sigma_{fit}\Delta\gamma RT$	58 -
Figure 1-22 : Schematic of the experimental set-up with Ultra Turrax device.	59 -
Figure 1-23 : Experimental images for different rotation speeds of Ultra Turrax device at fixed flowrate $Q = 100 \mu L.s^{-1}$	60 -

Figure 1-24 : Bubble diameter evaluated by image analysis based on rotation speed of the Ultra Turrax device at fixed flowrate $Q = 100 \mu\text{L} \cdot \text{s}^{-1}$. The diameter of the air bubbles is $D_b = 2.5 \text{ mm}$ when no Ultra turrax is used, i.e., $\omega = 0 \text{ rpm}$.	- 61 -
Figure 1-25 : Cumulative probability distribution of bubble sizes at the boundary foam – bubbly liquid for different rotation speeds of Ultra Turrax device at fixed flowrate $Q = 100 \mu\text{L} \cdot \text{s}^{-1}$.	- 62 -
Figure 1-26 : Bubble diameters as a function of injected flowrate Q (red squares) at a fixed Ultra Turrax rotation speed are in comparison to bubble diameter in Bikerman tests (blue circle) – Heptanol/Cyclopentanol mixture (at $x_{1\text{max}} = 0.12$).	- 63 -
Figure 1-27 : Normalized foam lifetime variations as a function of bubble diameters in the foam. Ultra Turrax experiments – red squares and Bikerman experiment – blue circle. Heptanol/Cyclopentanol mixture (at $x_{1\text{max}} = 0.12$).	- 64 -
Figure 1-28 : (a) Schematic of the set-up for single bubble experiments; (b) Schematic of the set-up from the side-view.	- 65 -
Figure 1-29 : (a) Formation of a single bubble in a Heptanol/Cyclopentanol mixture (at $x_{1\text{max}} = 0.12$); (b) and (c) Spatio-temporal diagram: bubble diameter versus time (horizontal axis). The first stage is represented in green area. The second stage – corresponding to the stable geometry prior bursting – is illustrated by cross pattern zone.	- 66 -
Figure 1-30 : Cumulative probability density function of bubble lifetimes measured at the surface of Decane/Toluene mixture at $x_{1\text{max}} = 0.12$.	- 67 -
Figure 1-31 : Cumulative probability distribution of bubble lifetimes in the single bubble experiments for different compositions of: (a) Octane/Toluene mixture; (b) Decane/Toluene mixture and (c) Heptanol/Cyclopentanol mixture. Continuous lines indicate the best fits of the data using a log-normal distribution function.	- 68 -
Figure 1-32 : Comparison between cumulative probability distribution of bubble lifetimes with three mixtures: Octane/Toluene, Decane/Toluene and Heptanol/Cyclopentanol at $x_{1\text{max}}$. Continuous lines indicate the best fits of the data using a log-normal distribution function.	- 68 -
Figure 1-33 : $L\tau$ obtained from single bubble experiments and foam experiments as a function of the molar fraction in the mixture of the species with the smallest surface tension. The full points represent the results of the single bubble experiments, while the foam experiments are shown as solid lines with the empty points: Octane/Toluene (green), Decane/Toluene (red) and Heptanol/Cyclopentanol (brown).	- 69 -
Figure 1-34 : (a) Image of a single bubble in the Heptanol/Cyclopentanol mixture at the air/liquid interface captured by a side-view camera; (b) Schematic of a bubble at the interface from the side. ϕ_0 is the angle between the upper part of the bubble and the interface.	- 69 -
Figure 1-35 : (a) The breaking point is the red dot. A spatio-temporal diagram in which the line taken from each image is represented horizontally, with time represented by the vertical axis; (b) Schematic	

of a bubble at the surface from the side. The curvilinear length travelled by the edge of the opening hole, $\mathbf{s}(t)$, is obtained from both its projection $\mathbf{r}(t)$ in the horizontal plane and the angle $\varphi(t)$ measured from top and side views of the bubble.	- 71 -
Figure 1-36 : Evolution of the curvilinear length travelled by the edge of the opening hole \mathbf{s} (brown circles, left axis) and of the angle φ (green circles, right axis) in the burst as a function of time (Heptanol/Cyclopentanol $x_1 = 0.12$). The hole opens at constant speed during a first stage (yellow zone). The slope of the full line is the Taylor-Culick speed from which the thickness at bursting is inferred.	- 71 -
Figure 1-37 : Experimental plot of normalized foam lifetime $L\tau$ as a function of liquid film thickness hb for studied binary mixtures. The full line is a guide to the eye.	- 73 -
Figure 2-1 : Schematical explanation of the thickness-dependent surface tension of a film of liquid mixture. As the film thins down at constant volume the concentrations at the interfaces cannot be kept constant, leading to a new equilibrium in which the interfacial concentration of the (red) species with the smallest surface tension is smaller, and thus the surface tension is larger. The thickness of the liquid film is designated by h	- 79 -
Figure 2-2 : Sketch illustrating the stretching phase. Two air bubbles encounter in the liquid mixture. These bubbles will deform and create a liquid film at the contact zone. It is a fast extension phase of the liquid film in the plug-shape ($\sim 10 - 4 s$).	- 80 -
Figure 2-3 : Diagram showing the forces acting on a fluid film of thickness hf connected to a Plateau border in the foam. The flat part's higher surface tension allows for mechanical balance even if the pressures are not equilibrated. A tension balance along the z-axis can be written on the film portion in red.	- 81 -
Figure 2-4 : Solution to Eq.2.10 giving the profile of the interface of a liquid film in mechanical equilibrium.	- 83 -
Figure 2-5 : Surface tensions of Decane/Toluene (red) and Octane/Decane (blue) mixtures as a function of the molar fraction of the species with the lowest surface tension (respectively, Decane and Octane). The full lines are guides for the eye.	- 84 -
Figure 2-6 : Experimental $L\tau$ (squares, left axis) as a function of Decane molar fraction for mixture of Toluene with Decane. Error bars correspond to uncertainties on measured foam heights. The length α (right axis) characterizing the relative surface tension variation with film thickness computed from Eq.2.25 is shown as a solid line.	- 88 -
Figure 2-7 : Molar fraction for which the foamability was measured to be maximum as a function of its value predicted.	- 89 -
Figure 2-8 : $L\tau$ as a function of α for 8 different liquid mixtures. Both $L\tau$ and α are normalized by their maximum values found in each mixture which are reached for the same composition. The full line is a guide to the eye.	- 90 -

Figure 3-1 : Foam formed in a Bikerman column using an asymmetric mixture of PDMS/Decane (L. Delance's experiment).....	- 101 -
Figure 3-2 : Normalized surface tensions of binary mixtures as a function of the molar fraction of liquid 1 – the species with the smallest surface tension. From left to right with full line and markers: PDMS/Decane (dark yellow), Octane/Toluene (green), Decane/Eicosane (light cyan) and Heptane/Hexadecane (violet). The dashed line indicates linear variations. All measurements were made at room temperature except the ones with the C ₁₀ /C ₂₀ mixture that were performed at 50°C.	- 103 -
Figure 3-3 : $L\tau$ computed following Eq.1.11 from the stationary foam heights measured with the same mixtures as in Figure 3-2 and as a function of the molar fraction of the species with the smallest surface tension. From left to right with full line and markers: PDMS/Decane (dark yellow), Octane/Toluene (green), Decane/Eicosane (light cyan) and Heptane/Hexadecane (violet). All experiments were performed at room temperature (20°C) but the one with Decane/Eicosane conducted at 50°C. Inset: same curves in log-log scale.....	- 104 -
Figure 3-4 : Liquid film of symmetric mixtures of molecules with similar sizes. The surface is enriched in the species with the lowest surface tension (red circles) compared to the bulk.	- 106 -
Figure 3-5 : Liquid film of asymmetric mixtures made of molecules of very different sizes. The surface is concentrated in species with low surface tension (red circles). The species with the higher surface energy (blue circles) has a significantly greater molecular size, resulting in a larger molecular surface area.	- 106 -
Figure 3-6 : Normalized surface tensions as a function of the bulk molar fraction of species 1: (a) Butler's model; (b) Experimental results. The dotted lines show the surface tensions computed from Butler's model with the liquid parameters and the adjusted surface ratios given in Table 8.	- 110 -
Figure 3-7 : Surface molar fraction Γ_1 as a function of the bulk molar fraction of species 1 for the studied mixtures.	- 111 -
Figure 3-8 : (a) Length α characterizing the increase of surface tension with decreasing thickness of a film of binary mixture, as a function of the mixture composition. The curves were computed using Eq.3.21 for different asymmetry ratios, derived in the case of ideal solutions. (b) Normalized foam height $L\tau$ as a function of the mixture composition. From left to right with full line and markers: PDMS/Decane (dark yellow), Octane/Toluene (green), Decane/Eicosane (light cyan) and Heptane/Hexadecane (violet).	- 115 -
Figure 4-1 : Experimental length $L\tau$ as a function of film thickness hb at bursting, both measured in single bubble experiments. The error bars on film thickness result from the uncertainty on the Taylor-Culick velocity.	- 129 -
Figure 4-2 : Illustration of the argument for considering constant composition of the liquid mixture during film pinching.	- 131 -
Figure 3 : Temps de vie expérimental normalisé de la mousse $L\tau$ en fonction de la fraction molaire du liquide 1 x_1 dans les mélanges binaires d'alcane linéaires et de Toluène.	- 179 -

Figure 4 : Diamètre des bulles évalué par analyse d'image en fonction de la vitesse de rotation du dispositif Ultra Turrax à débit fixe $Q = 100 \mu L \cdot s^{-1}$. Le diamètre des bulles d'air est $D_b = 2.5 mm$ lorsqu'aucun Ultra turrax n'est utilisé, soit $\omega = 0 rpm$.	- 179 -
Figure 5 : Images expérimentales pour différentes vitesses de rotation du dispositif Ultra Turrax à un débit fixe $Q = 100 \mu L \cdot s^{-1}$.	- 180 -
Figure 6 : Variations du temps de vie normalisée de la mousse $L\tau$ en fonction du diamètre des bulles dans la mousse. Expériences : Ultra Turrax - carrés rouges et expérience : Bikerman - cercle bleu. Mélange Heptanol/Cyclopentanol (à $x_1 = 0.12$).	- 180 -
Figure 7 : Le temps de vie normalisé de la mousse $L\tau$ en fonction de l'épaisseur du film liquide hb pour les mélanges binaires étudiés. La ligne en trait plein est un guide pour l'œil.	- 181 -
Figure 8 : Explication schématique de la tension superficielle en fonction de l'épaisseur d'un film de mélange liquide. Lorsque le film s'amincit à volume constant, les concentrations aux interfaces ne peuvent être maintenues constantes, ce qui conduit à un nouvel équilibre dans lequel la concentration interfaciale de l'espèce (rouge) ayant la plus petite tension superficielle est plus faible, et donc la tension superficielle est plus grande. L'épaisseur du film liquide est désignée par h .	- 183 -
Figure 9 : Diagramme montrant les forces agissant sur un film fluide d'épaisseur hf relié à une bordure de plateau dans la mousse. La tension superficielle plus élevée de la partie plate permet un équilibre mécanique même si les pressions ne sont pas équilibrées. Un équilibre de tension le long de l'axe z peut être écrit sur la partie du film en rouge.	- 184 -
Figure 10 : Tensions de surface des mélanges Décane/Toluène (rouge) et Octane/Décane (bleu) en fonction de la fraction molaire de l'espèce ayant la tension de surface la plus faible (respectivement, Décane et Octane). Les lignes en trait plein sont des guides pour l'œil.	- 185 -
Figure 11 : $L\tau$ en fonction de α pour 8 mélanges liquides différents. $L\tau$ et α sont normalisés par leurs valeurs maximales trouvées dans chaque mélange qui sont atteintes pour une même composition. La ligne en trait plein est un guide pour l'œil.	- 186 -
Figure 12 : (a) Film liquide de mélanges symétriques de molécules de tailles similaires. La surface est enrichie en espèces ayant la plus faible tension superficielle (cercles rouges) par rapport au volume. (b) Film liquide de mélanges asymétriques composés de molécules de tailles très différentes. La surface est concentrée en espèces à faible tension superficielle (cercles rouges). L'espèce ayant l'énergie de surface la plus élevée (cercles bleus) a une taille moléculaire nettement supérieure, ce qui se traduit par une plus grande surface moléculaire.	- 187 -
Figure 13 : (a) Tensions de surface normalisées de mélanges binaires en fonction de la fraction molaire du liquide 1 - l'espèce ayant la plus petite tension de surface. Les lignes pointillées montrent les tensions de surface calculées à partir du modèle de Butler. (b) $L\tau$ avec les mêmes mélanges en fonction de la fraction molaire de l'espèce ayant la plus petite tension de surface. Inset: mêmes courbes en échelle log-log.	- 188 -

Figure 14 : Longueur α caractérisant l'augmentation de la tension superficielle lorsque l'épaisseur d'un film de mélange binaire diminue, en fonction de la composition du mélange.- 189 -

GLOSSARY OF ABBREVIATIONS

A_h	Hamaker constant	R_f	Curvature radius of the border of Plateau
C_D	Drag coefficient	Re	Reynolds number
D	Diffusion coefficient	R	Gas constant
D_b	Bubble diameter	U	Bubble rising speed
D_0	Needle diameter	U_{TC}	Taylor-Culick speed
F_B	Buoyancy force	V	Volume
F_D	Drag force	V_b	Bubble volume
g	Gravitational acceleration	V_0	Needle volume
H_0	Initial liquid height	T	Temperature
H	Foam height	T_b	Boiling temperature
H_L	Bubbly liquid height	T_m	Melting temperature
H_F	Total liquid height	t	Time
h	Liquid film thickness	x_i	Molar fraction of species i
h_b	Liquid film thickness at bursting (bubble)	x_1^{max}	Molar fraction for maximum foamability
h_f	Liquid film thickness before drainage	α	Characteristic foam length (Eq.2.24)
h_{vdw}	Critical liquid film thickness (van der Waals)	δ_b	Geometric factor
l_c	Capillary length	γ	Surface tension
L_τ	Normalized foam lifetime (Eq.1.11)	γ_i	Surface tension of species i
M	Molar mass	$\Delta\gamma$	Difference of surface tension
N_A	Avogadro's number	E_γ	Excess surface tension (Eq.3.15)
P	Pressure	κ	Permeability
ΔP	Laplace pressure	μ	Viscosity of mixture
P_0	Pressure in liquid film	μ_i	Viscosity of species i
P_B	Pressure in Plateau border	Π_D	Disjoining pressure
Q	Injected air flowrate	Π_{el}	Electrostatic contribution
R	Column radius	Π_{vdw}	Van der Waals contribution
R_b	Bubble radius	Π_{st}	Steric contribution

ρ	Liquid density	τ	Lifetime of bubble/foam (Eq.1.10)
σ_i	Molar surface of species i (Eq.2.3)	Γ_i	Surface molar fraction of species i
S_i	Reduced molar surface of species i (Eq.3.14)	λ_D	Debye length
ω	Ultra Turrax rotating speed	Φ_L	Liquid volume fraction
v_i	Molar volume of species i	Φ_B	Volume fraction of gas in the bubbly liquid

RÉSUMÉ

La formation de mousse dans les mélanges d'huiles est un problème courant, par exemple dans les boîtes de vitesses de moteurs électriques. Des agents anti-mousses peuvent être utilisés, mais il est important de comprendre comment se forme la mousse. Les liquides purs ne forment pas de mousse en raison de la courte durée de vie des films liquides, où aucun effet ne s'oppose aux interactions attractives de van der Waals. Toutefois, l'effet permettant d'augmenter les temps de vie des films liquides dans les mélanges d'huiles, et en l'absence d'autres effets stabilisants connus, n'a pas été expliqué. Cette thèse propose un mécanisme à l'origine de cette augmentation. Nous avons mesuré le temps de vie de mousses dans des mélanges binaires dont la composition et la taille des bulles varient. Des expériences sur des bulles uniques formées à la surface d'un bain liquide ont permis de mesurer l'épaisseur du film liquide au moment de sa rupture. Nous démontrons que l'effet stabilisant est dû aux différences de concentration des espèces entre le volume et l'interface avec l'air : le liquide de tension de surface la plus faible a une concentration légèrement supérieure à l'interface et joue ainsi le rôle d'un tensioactif. Nous montrons ensuite comment ces différences de concentration sont reliées aux non-linéarités des variations de la tension de surface du mélange avec sa composition et quelles sont les conséquences sur le temps de vie des films liquides. Enfin, la rhéologie de surface de ces systèmes est plus simple que celle des films de savon et nous proposons une description quantitative de la formation, du drainage et de la rupture des films liquides.

ABSTRACT

Foaming in oil mixtures is a common problem, for example in electric motor gearboxes. Anti-foaming agents can be used, but it is important to understand how foam forms. Pure liquids do not form foams because of the short life of liquid films, where there is no effect against attractive van der Waals interactions. However, the effect at the origin of increased lifetimes of liquid films in oil mixtures, in the absence of other known stabilizing effects, has not been explained. This thesis proposes a mechanism for this increase. We have measured the lifetime of foams in binary mixtures of varying composition and bubble size. Experiments on single bubbles formed on the surface of a liquid bath allowed us to measure the thickness of the liquid film at the time of its rupture. We demonstrate the stabilizing effect is due to differences in species concentration between the volume and the interface with air: the liquid with the lowest surface tension has a slightly higher concentration at the interface and thus acts as a surfactant. We then show how these concentration differences are related to the non-linearities of the variations of the surface tension of the mixture with its composition and what are the consequences on the lifetimes of liquid films. Finally, we show that the surface rheology of these systems is simpler than that of soap films and propose a quantitative description of the formation, drainage and breakup of liquid films.

INTRODUCTION & BIBLIOGRAPHY

INDUSTRIAL PROBLEMS

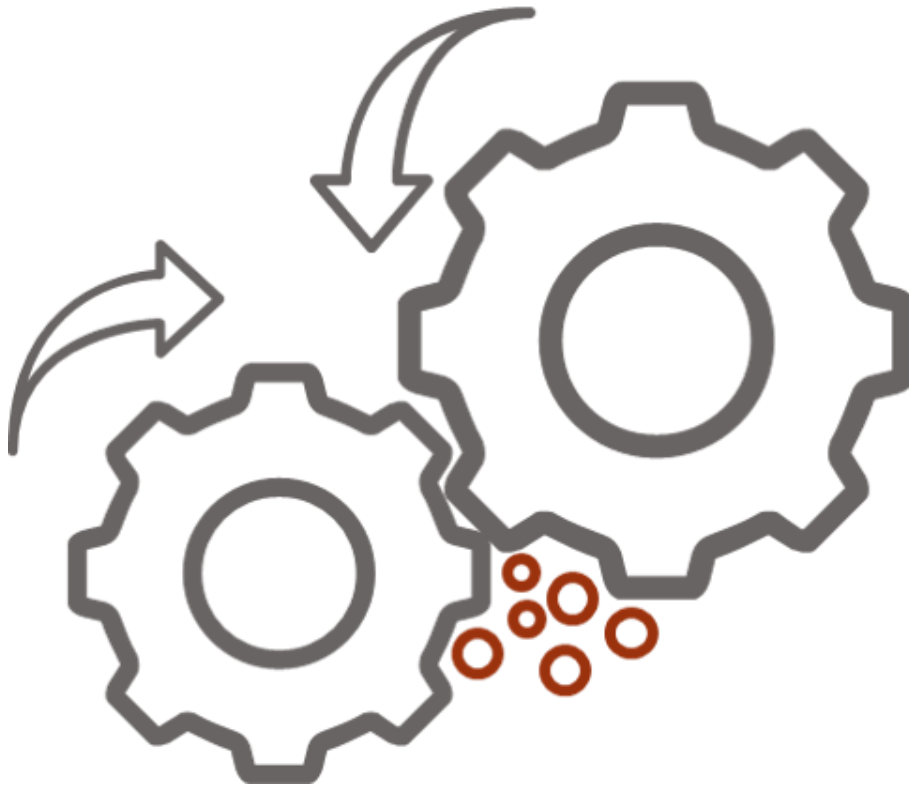


Figure Intro-1-1 : Electric motor rotates at high speeds. Air can infiltrate circuits and potentially trigger fluids to foam, causing device materials to be damaged.

The awareness of global climate change has finally encouraged people to rethink their means of transportation, and electric cars are becoming a replacement for classic petrol cars for a sustainable green energy future. At a glance, the main differences between these two types of cars lie in the points below.

Classic cars need gasoline or diesel to run, motor oil to lubricate their engine parts such as valves, pistons.

As the name suggests, electric cars run on electricity. However, they still need lubricants for their engines, lubricants and additives are indispensable to protect an electric vehicle's gearbox.

Foaming is a common problem with oil lubricated parts of car engines. But it is really drastic for electric car, as their motor and gearboxes operate at rotation speed five to ten times larger than the ones of classical cars. Gearboxes rotation generates small air bubbles can accumulate at liquid surface, and be convected by the flow near the gears, decreasing the lubricant effect of oil. The main objective of this work is to understand the origin of foaming of oil mixture, in order to control it.

LIQUID FOAM

First, we briefly recall what is a liquid foam. Liquid foam is a dispersion of gas bubbles in a liquid with a gas concentration large enough for the bubbles to be pressed one against the other. As a consequence, bubbles are faceted. The facets are liquid films that separate bubbles from their neighbor. Their structure is represented in the graph below.

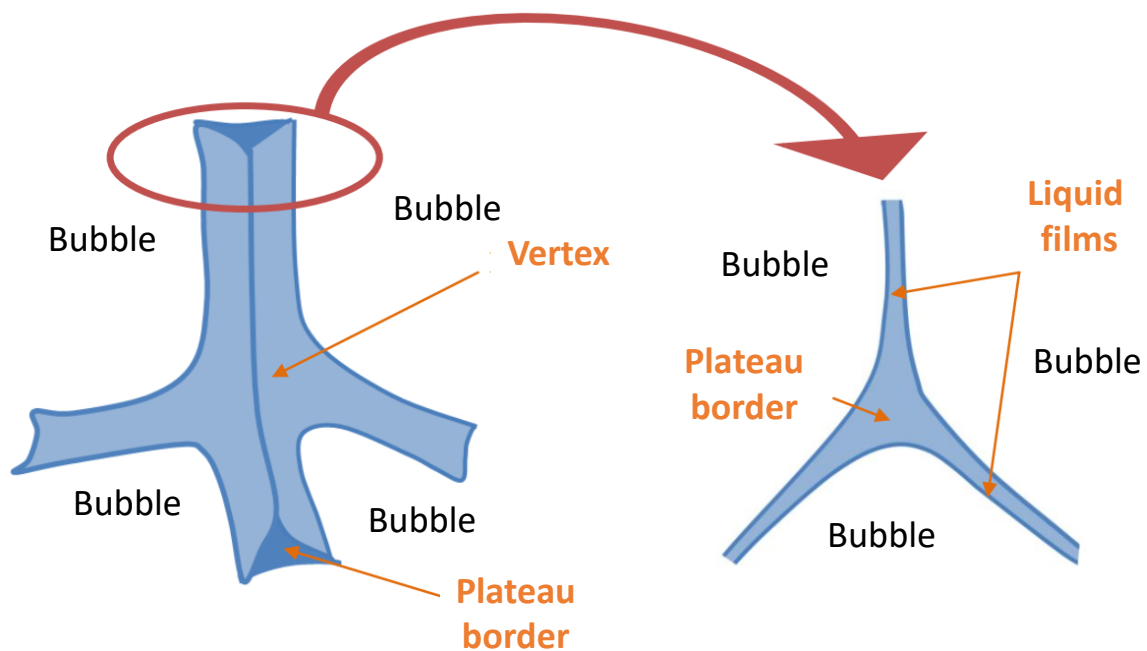


Figure Intro-1-2 : Descriptive diagram of the structure of a foam [1].

These liquid films are connected by 3 into channels, which are called Plateau borders. The liquid is mostly contained in these borders. They are themselves connected by 4 vertices as shown in **Figure Intro-1-2**.

Liquid foams offer a variety of unique and intriguing properties. They are employed in a variety of applications all around us, such as foods, cosmetics and oil recovery.

Plateau borders

One of the destabilizing mechanisms of the foams is the capillary suction of liquids from the films to the Plateau border. Indeed, the pressure in the Plateau border P_B is lower than the pressure inside the bubbles because of the curvature of the Plateau's borders. More precisely, the pressure in the Plateau border P_B is writes:

$$P_B = P_0 - \frac{\gamma}{R_f} \quad \text{Eq.Intro.1}$$

where P_0 is the gas pressure, γ is the surface tension of the liquid and R_f is the radius of curvature of the border of Plateau.

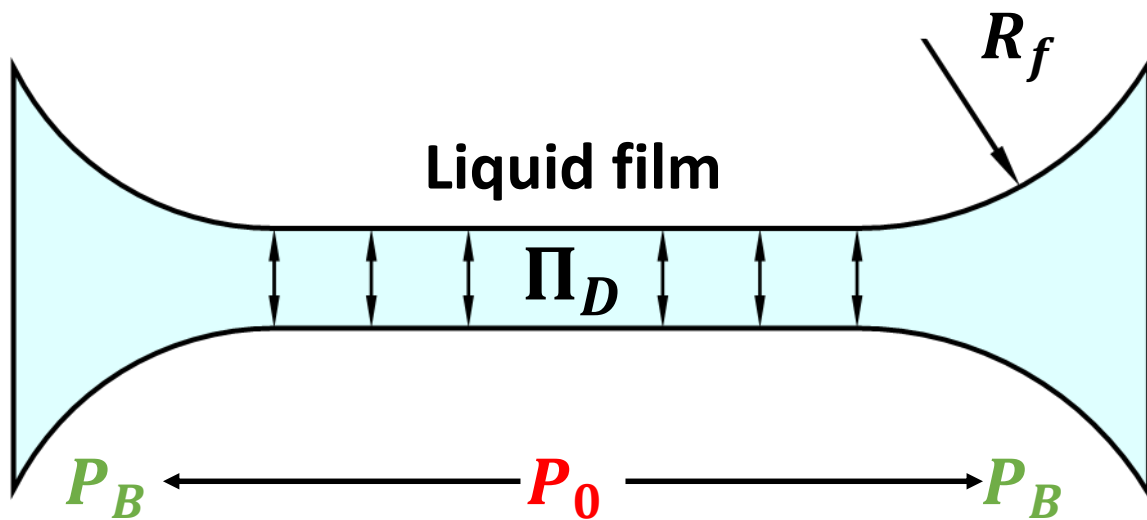


Figure Intro-1-3 : Schematic of a horizontal film and a Plateau border.

We will explain that the pressure in the film can be different from the gas one under the effect of molecular interactions disjoining, which can be described as a pressure term called disjoining pressure. This is the object of the following section.

Disjoining pressure

The concept of disjoining pressure, which has been defined by Derjaguin [2], describes the pressure difference between the pressure in a thin film and the pressure in the bulk fluid when the two are connected by a channel. The origins of the disjoining pressure are the molecular forces that may be attractive or repulsive and that become important when the film is very thin, that is of thickness smaller than about 100 nm.

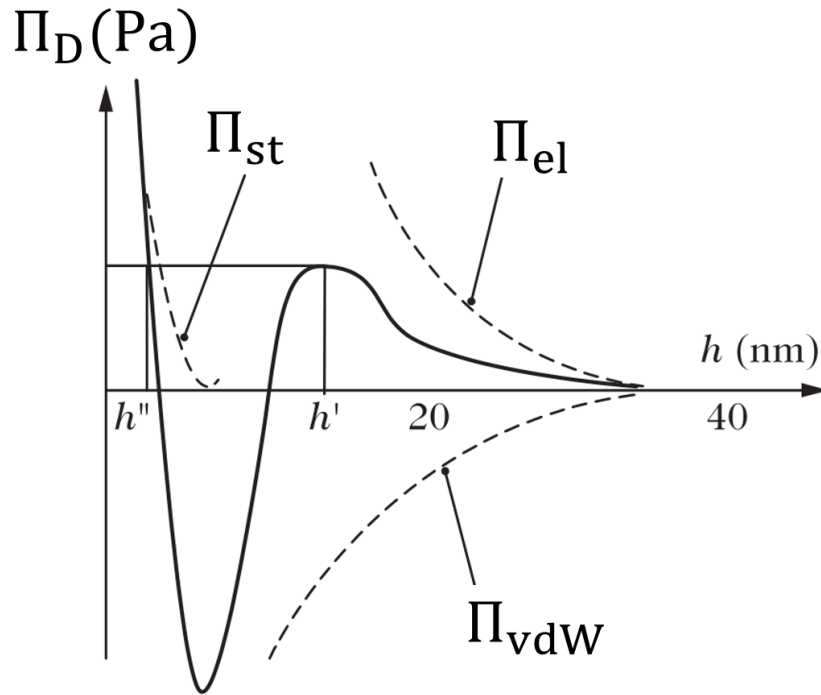


Figure Intro-1-4 : Disjoining pressure Π_D between two interfaces as a function of liquid film thickness h . The different contributions to the disjoining pressure – van der Waals, electrostatic, steric – are represented by the dash lines and the continuous line represents their sum. [3]

First, imagine a liquid film with two infinite interfaces separated by a liquid thickness h . This film is submitted to various short-range interactions, electrostatic, Van der Waals or steric, known as DLVO interaction [4,5]. They are responsible for the disjoining pressure that writes thus:

$$\Pi_D = \Pi_{el} + \Pi_{vdw} + \Pi_{st} \quad \text{Eq.Intro.2}$$

with the repulsive electrostatic contribution Π_{el} , the attractive Van der Waals contribution Π_{vdw} and the steric repulsive contribution Π_{st} . as illustrated in **Figure Intro-1-4**.

Electrostatic forces When ionic surfactants are adsorbed at interfaces, then those interfaces become electrically charged. The charged interfaces repel each other. The electrostatic contribution is:

$$\Pi_{el} \sim e^{-\frac{h}{\lambda_D}} \quad \text{Eq.Intro.3}$$

where λ_D is the Debye length. It is always repulsive and thus the electrostatic – disjoining pressure contribution is positive.

Van der Waals forces When the interfaces of a liquid film are close enough, van der Waals forces that are always attractive becomes to be predominant. The Van der Waal attraction contribution to the pressure is negative and writes:

$$\Pi_{vdW} = -\frac{A_h}{6\pi h^3} \quad \text{Eq.Intro.4}$$

where A_h is the Hamaker constant of the air/fluid system.

Steric forces Steric forces can appear if surfactants are adsorbed in monolayers on each interface. If the thickness of the film is smaller than twice the thickness of the monolayers, the energy of the system may increase. This may generate repulsive interactions, but that are short range and only with organized molecules layers.

The value of the disjoining pressure, and especially its sign, show how the two interfaces interact: a positive disjoining pressure corresponds to repelling interfaces, while a negative disjoining pressure indicates attracting interfaces. An equilibrium between the Laplace and disjoining pressures is may be attained if:

$$\frac{2\gamma}{R_f} + \Pi_D = 0 \quad \text{Eq.Intro.5}$$

As a result, equilibrium can be reached only if Π_D is repulsive, thus only if there are electrostatic or steric repulsions.

In the absence of any surface-active species, only the attractive contribution of Van der Waals intervenes. There is thus no solution for the equation above and thus films thin and hence coalesce. As a result, foams made from pure oil mixes are predicted to thin continuously and to break; thickness will decrease to zero, and then pinching will occur. Thus, the question of our PhD is the following: what determines the life-time of foams in the absence of repulsive interaction in the films? We show in the next section that mechanisms, including Marangoni flows, can slow down the thinning towards a few tens of seconds.

ROLE OF MARANGONI EFFECT

This section will go over the Marangoni effect and how it affects film stabilization.

Film stabilization - Foam

- Marangoni flow in a film containing surfactants

H. Lhuissier et al. [6] investigated the behaviour of bubbles at the surface of a tap water bulk. Bubbles are generated in the range of millimeters in size. Because the curvature of these bubbles is less than the capillary length, capillary pressure completely dominates hydrostatic pressure. Most of the liquid is drawn off the film in the beginning of drainage, known as capillary emptying time. This very first stage lasts just 10^{-2} s. However, they show that purity is an important component that controls the dynamics of thinning of the liquid film.

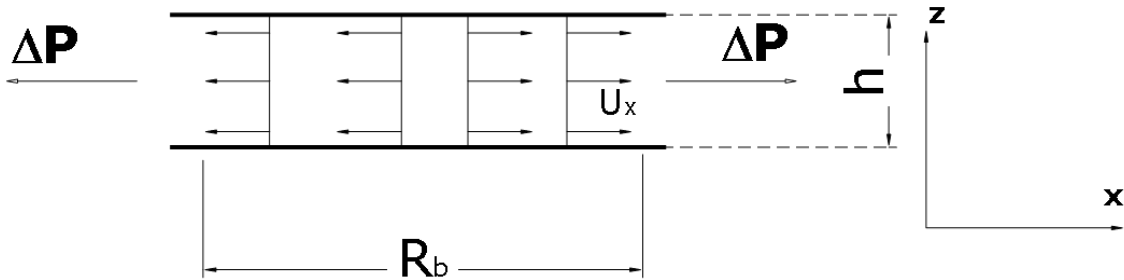


Figure Intro-1-5 : (a) Stretching: plug-type flow velocity profile in the pure liquids.

In the absence of Marangoni effect, i.e., in the case of pure liquid, surface tension is homogenous. The thinning of the film is done by a plug flow – or film stretching. The flow velocity profile will be of the plug type in this scenario, as indicated in **Figure Intro-1-5 (a)**, is:

$$U_{x-plug} \sim \frac{R_b^2}{\mu} \frac{\partial P}{\partial x} \sim \frac{R_b^2 \Delta P}{\mu R_b} \sim \frac{\gamma}{\mu} \quad \text{Eq.Intro.6}$$

The characteristic time can be estimated $\mu R_b / \gamma \sim 10^{-4}$ s, for $\mu = 10^{-3}$ Pa.s, surface tension $\gamma = 10^{-2}$ N.m⁻¹ and bubble size $R_b = 10^{-3}$ m.

However, in the presence of surface-active components, the interface cannot deform easily, and the drainage inside the film adopts a Poiseuille type velocity, see **Figure Intro-1-6**:

$$U_{x-Poiseuille} \sim \frac{h^2}{\mu} \frac{\partial P}{\partial x} \sim \frac{h^2 \Delta P}{\mu R_b} \sim \frac{\gamma h^2}{\mu R_b^2} \ll U_{x-plug} \quad \text{Eq.Intro.7}$$

The characteristic time can be estimated $\mu R_b^3 / \gamma h^2 \sim 10^2 \text{ s}$, for $\mu = 10^{-3} \text{ Pa.s}$, surface tension $\gamma = 10^{-2} \text{ N.m}^{-1}$, bubble size $R_b = 10^{-3} \text{ m}$ and film thickness $h = 10^{-6} \text{ m}$.

This long time has been observed for tap water in Lhuissier's article.

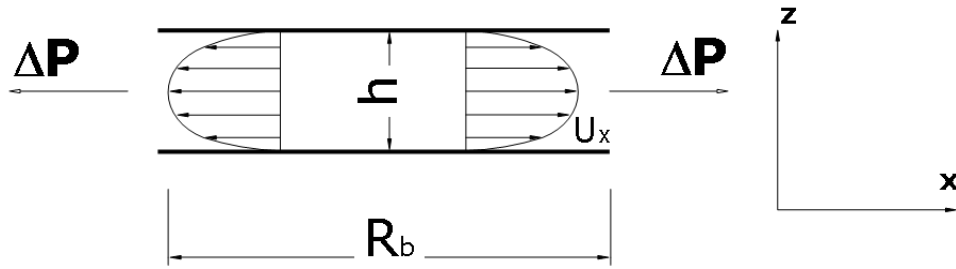


Figure Intro-1-6 : Drainage: Poiseuille flow velocity profile with surface-active components.

In order to quantify the Marangoni effect that is able to hinder the film stretching and thus to force Poiseuille flow, we have to estimate the gradient of surface tension in the case of Poiseuille flow. This writes:

$$\mu \frac{\partial U_x}{\partial z} \sim \frac{\partial \gamma}{\partial x} \quad \text{Eq.Intro.8}$$

Using the scaling law $\mu (\partial U_x) / \partial z \sim h \gamma / R_b^2$ and $\partial \gamma / \partial x \sim \Delta \gamma / R_b$, we obtain:

$$\Delta \gamma \sim \gamma \frac{h}{R_b} \ll \gamma \quad \text{Eq.Intro.9}$$

The order of magnitude of surface tension variations in the thin film sufficient to immobilize the surface is expected to be $\Delta \gamma \sim 10^{-3} \text{ N.m}^{-1} \ll \gamma$. Note that this effect is tiny. Such a variation of surface tension for instance is not measurable with a classical tensiometer.

To conclude, the tiny Marangoni effects can lead to Poiseuille flow and thus slow thinning of liquid films.

In addition, Marangoni effect can also be generated by evaporation. Following that, we will go through this impact in further depth.

Evaporation-induced foam stabilization

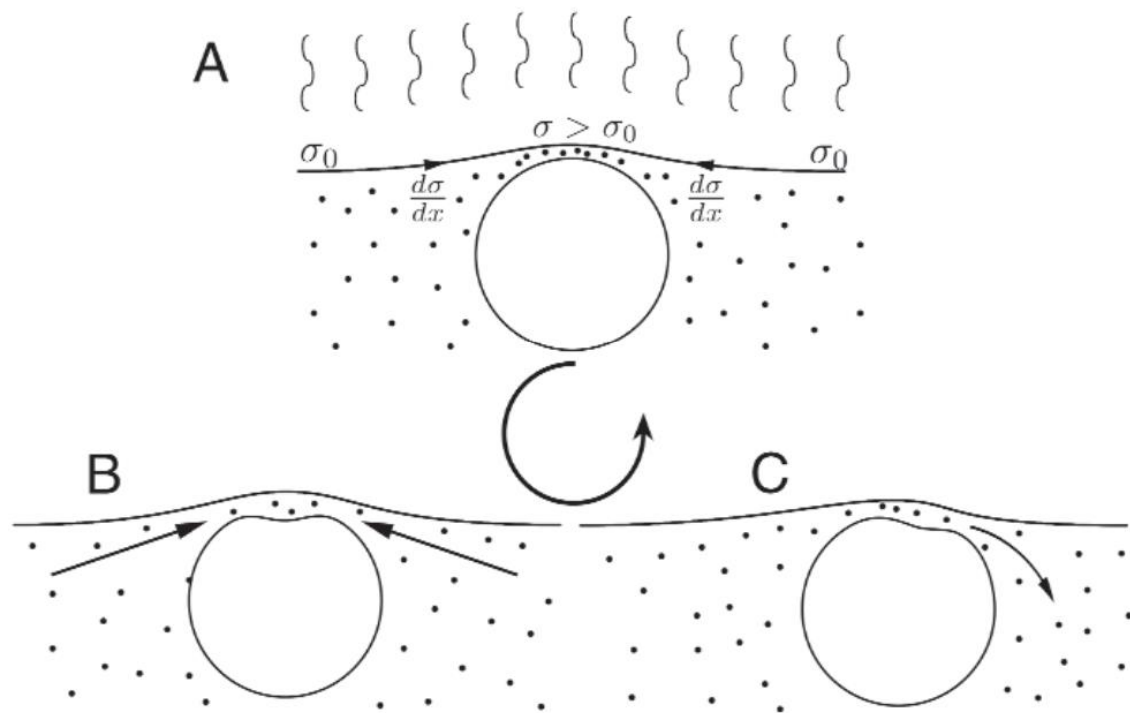


Figure Intro-1-7 : Schematic showing the mechanism of bubble stabilization resulting from evaporation-induced Marangoni effect.

Recently, Chandran Suja et al. [7] have performed an experiment with a single bubble to study the foam stabilization mechanism – for liquid mixtures with different evaporation rate of the constituents. This paper claims that the evaporation in liquid mixtures is implicated in the stability of foams in various oil combinations. When the component with the lower surface tension is the more volatile, its evaporation produces a surface tension gradient, resulting in a Marangoni flow. The mechanism underlying this phenomenon is illustrated in the above figure. We have a liquid mixture of two components: 1 and 2, with the former having a higher surface tension and being more volatile. Consider a bubble approaching the air/liquid interface and forming a liquid layer. Because the molecules in liquid 1 are more volatile, the proportion in this layer is decreased. Thus, a gradient of concentration between the film and the Plateau border is generated by evaporation. It results in a gradient of surface tension, with a surface tension larger in the film than in the Plateau border. Hence Marangoni flow occurs from the border to the film, forcing liquid to flow in the opposite direction of the drainage. As a result, in this case, the Marangoni effect stabilizes the liquid layer.

Questions about foam of binary and ternary mixtures

The pure liquid films without surface active species, as described in the preceding paragraphs, are extremely unstable. They will snap in a thousandth of a second. As a result, pure liquids cannot produce foam. However, mixtures of pure liquids do foam as shown by literature.

It has been observed that binary and ternary combinations of pure liquids put together can foam. And, more precisely, the ability to foam depends on the fractions of the components. S. Ross and G. Nishioka [8] noticed this, and their findings are displayed in the graph below.

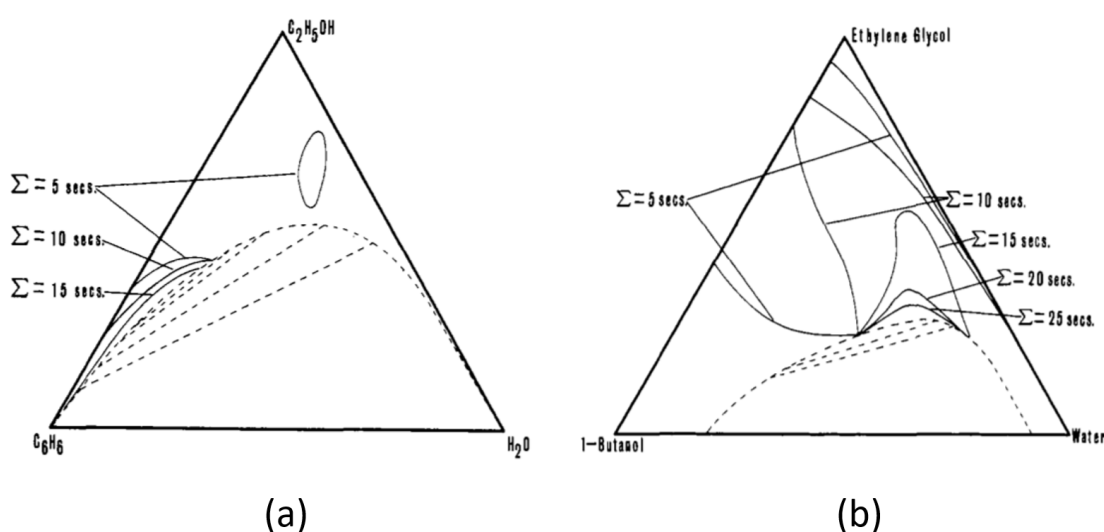


Figure Intro-1-8 : Phase diagram of ternary systems and lines of iso-foamability (dotted line) dotted lines): (a) ethanol/benzene/water system - (b) ethylene glycol/butanol/water system at 20 °C.

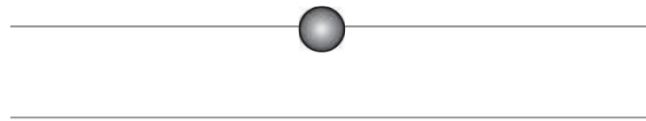
In the graphs of **Figure Intro-1-8**, they report the lines corresponding to foam lifetime of 5 to 25 seconds for various ternary mixtures. They observed that their foamability increases as one approaches the critical point, as long as one remains on the side where the mixture is a single homogeneous phase. This large foamability was attributed to the vicinity of a critical point but no understanding of the phenomena was proposed.

At opposite, in the region where the solvents separate into two immiscible mixtures, the lifetime of foams becomes extremely small. The authors hypothesize that one of the mixtures behaves as an antifoam of the other mixture. The system of lower surface tension will spontaneously spread on the surface of the other. The mechanism is the following. A droplet of the phase with

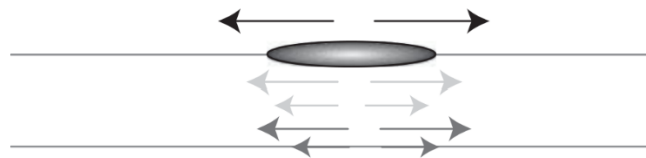
the lowest interfacial tension reaches the liquid gas interface, and spreads on it, leading to a thinning of the liquid film by Marangoni effect and then to its piercing. This effect is related to the effect of antifoams and will not be discussed in this work.



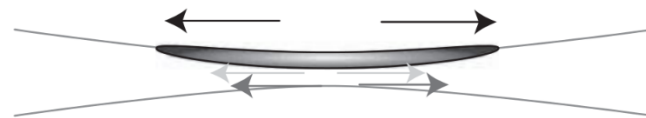
(a): Liquid molecule having the lowest surface tension inside the liquid film



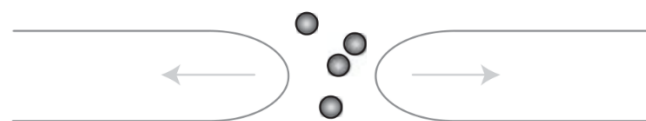
(b): It migrates to the gas/liquid interface



(c): Its spreading on the surface



(d): Marangoni spreading mechanism



(e): The liquid film thins and eventually breaks

Figure Intro-1-9 : A molecule of the liquid having the lowest surface tension in the mixture inside a film. Its formation and spreading on the film surface, causing the film to thin and the liquid to flow. The film thins to the point where it breaks. [3]

Our research with binary mixtures

Based on the observations and studies presented above, we focus our work on monophasic binary mixtures. A primary test consists in examining the levels of foaming in two bottles. The liquid in the first bottle 1 is pure (Decane), but the liquid in bottle 2 is a combination of two pure liquids (Decane and Toluene) that are miscible. When we shake the bottle 1, we are not able, with eyes to detect any bubbles formation. In contrast, by shaking bottle 2, we can clearly detect the creation of a foam layer, which remains for a few tens of seconds. Moreover, the liquids used have no surfactant nor impurity (because the polarity of the liquid used is lower than most of the pollutant contained in air). Furthermore, in contrast to the mixtures studied by Chandran Suja et al. [7], the effect of evaporation induced Marangoni effect is predicted to destabilize the films that are formed, because in the decane-toluene mixture the more volatile component (Toluene) has a higher surface tension.

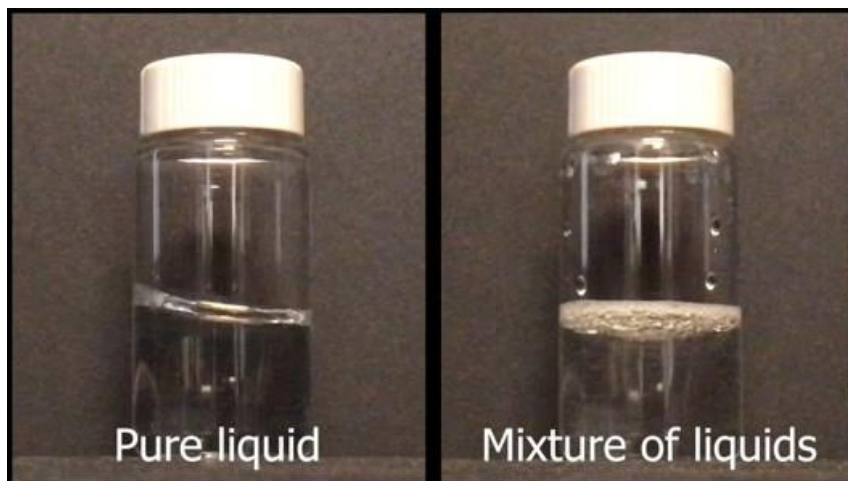


Figure 1-10: No foam observed in pure liquid (left); a foam layer at the top of mixture of liquid (right)

Thus, in the next chapters of this study, we will quantify the foaming capacity of various liquid mixtures, in order to understand these phenomena, and to model them. In **Chapter 1**, we will present the methods that we have used to characterize foaming, and film thickness before drainage. The **Chapter 2** will discuss and propose theoretical models to explain the origin of liquid mixture foaming of mixtures of liquids with very similar size. More complicated mixes, called asymmetric binary mixtures, will be addressed in greater depth in **Chapter 3**. Lastly in the last chapter, **Chapter 4**, we will explain how to model the lifetime of bubbles.

1. EXPERIMENTAL METHODS

This chapter will be divided into three sections that will discuss our approach for measuring foamability, the foamability dependence on bubble sizes, and the measurement of film thickness/bubble lifetime. First, foamability mixtures will be assessed using Bikerman columns. We will show that Bikerman test can provide an estimation of the bubble lifetime. We will then present our results on the foamability of various mixtures. Lastly, we will investigate the effect of bubble size on foamability. Finally, we present experiments performed on single bubbles, in order to measure the thickness of the liquid film at the onset of bursting.

1.1. DETERMINING THE FOAMABILITY OF BINARY MIXTURES WITH A BIKERMAN COLUMN

Experimental description

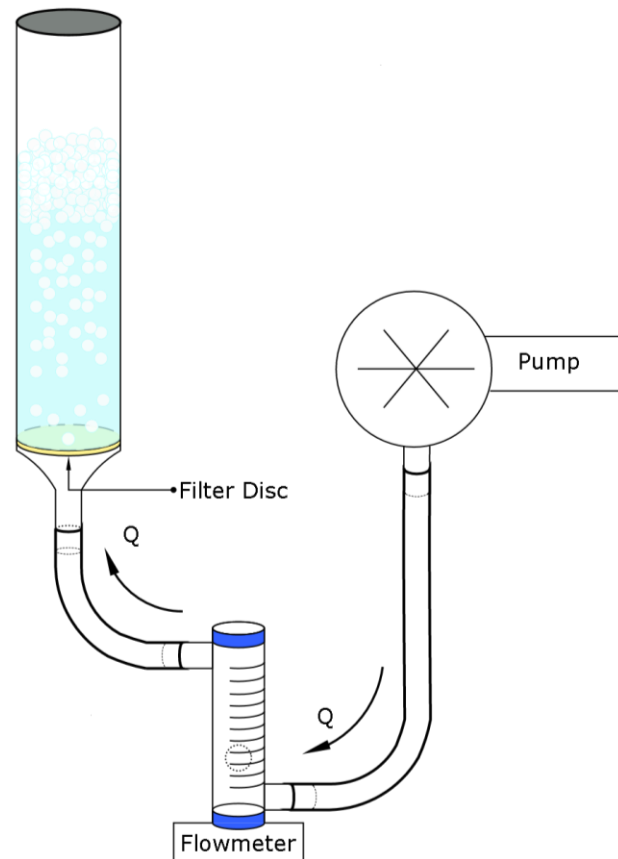


Figure 1-1 : Schematic of the experimental set-up

First, we describe our measurement of the foam lifetime measured with Bikerman columns.

According to literature, there are numerous methods [9–11] that have been mentioned and applied both in laboratory experiments and in the industry to study foam lifetimes. We have used the Bikerman method [12,13]. Gas is injected into liquids through a porous material to form foam. To measure formability, we determine the volume or the height of foam formed in the liquid.

This experiment is performed to measure the foam height of binary liquid mixtures. The experimental set-up is represented as shown in **Figure 1-1**. Our Bikerman test consists of a glass column (Robu Glass column - 85 mL, radius $R = 1\text{ cm}$) with a filter disc at its bottom (porosity: 10 – 16 μm). A studied liquid mixture is poured into the column with an initial

height of H_0 . Then, air is injected from the bottom of the column through the filter disc at constant flow rate Q . The flow rate is accurately controlled/measured by a flowmeter and can vary between $1 \text{ mL} \cdot \text{s}^{-1}$ and $8 \text{ mL} \cdot \text{s}^{-1}$. The experiment was carried out at room conditions: $T = 25^\circ\text{C}$ and $P = 1 \text{ atm}$. The whole experimental process is recorded by a side-view camera at 30 fps . The recorded images are processed by ImageJ software. During the air injection, a stationary state is established, and the final height H_F is reached a few seconds after the experiment begins.

In this work, we have investigated the foam behavior of binary mixtures of Toluene and linear alkanes; mixture of linear alkanes of different size and mixtures of Cyclopentanol with linear alcohols, respectively.

In addition, we will also discuss at the results on PDMS/Decane mixture that were performed by Léa Delance¹. The PDMS/Decane mixture strongly foams and a much smaller flowrate was used, $Q = 0.6 \text{ mL} \cdot \text{s}^{-1}$. In order to prevent retention of PDMS in the porous filter, it was chemically modified using a perfluorosilane.

For each tested binary mixture, mixture composition can also be varied in order to examine its relation to foam.

1.1.1. Measurement of the foam height

When gas is injected, the liquid and the foam phases reach a stationary state, see **Figure 1-2**. If we consider a column of radius R , the liquid volume fraction in the foam equal to Φ_L and the volume fraction of bubble in the liquid column below the foam Φ_B . The initial amount of liquid poured $H_0\pi R^2$ is divided between:

- A bubbly liquid forms in the lower part of height H_L . The liquid volume is equal to $H_L(1 - \Phi_B)\pi R^2$. In this part, air bubbles that are spherical in shape and have no interaction with one another. They are spread throughout the liquid phase and move towards the interface liquid/foam.
- The upper part consists of a foam of height H with liquid volume $H\Phi_L\pi R^2$.

¹ *The experimental results related to the PDMS/Decane mixture in this chapter were performed by Léa Delance in her PhD.*

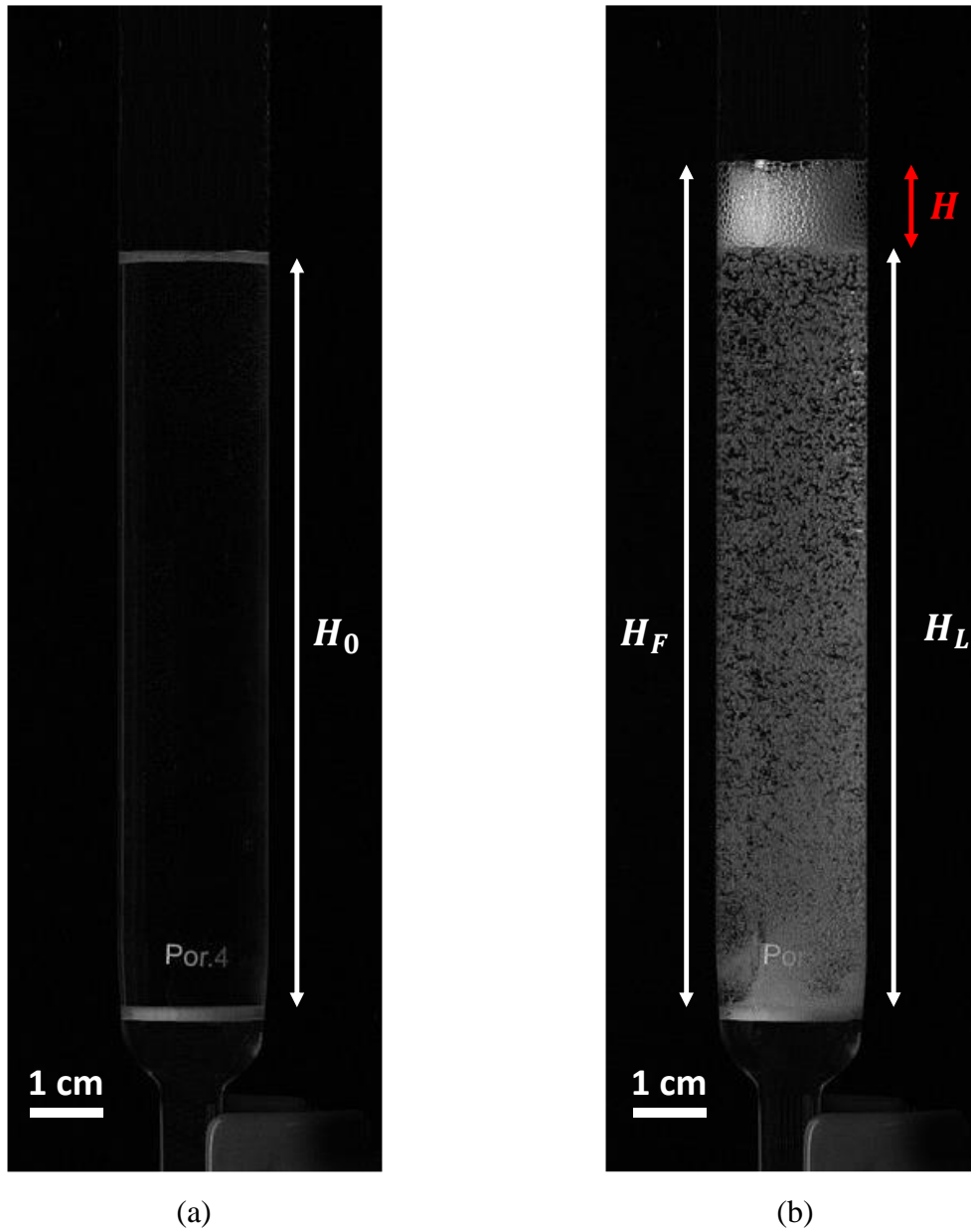


Figure 1-2 : (a) Binary mixtures in Bickerman column; (b) Formation of foam in the top of the column after the air injection

The volume conservation of liquid mixture gives us:

$$H_0\pi R^2 = H_L(1 - \Phi_B)\pi R^2 + H\Phi_L\pi R^2 \quad \text{Eq.1.1}$$

Besides, the total height H_F is written:

$$H_F = H_L + H \quad \text{Eq.1.2}$$

By combining **Eq.1.1** and **Eq.1.2**, we can deduce an expression for H-foam height:

$$H = \frac{H_F(1 - \Phi_B) - H_0}{1 - \Phi_B - \Phi_L} \quad \text{Eq.1.3}$$

1.1.2. Determination of the foaming height by the measure of the total height

In fact, we can directly measure the height of the foam H with most of the studied mixtures as shown in section 1.1.1. Nevertheless, the boundary between the bubbly liquid and the foam is sometimes difficult to discern for a variety of reasons, which we shall discuss later. In these circumstances, we had to measure the final height of liquid and foam H_F , and deduce H using Eq.1.3.

For that purpose, we need to estimate the other two parameters that affect the foam height. They are as follows: the volume fraction of gas in the bubbly liquid Φ_B and liquid volume fraction of foam Φ_L .

1.1.2.1. Case of non – foaming liquid

Since Φ_B is the volume fraction of gas in the bubbly liquid, we can perform the experiment with non-foaming systems to determine Φ_B . For that purpose, we use a pure liquid that does not form a foam. In this case, gas injection only increases the height of liquid in the Bikerman column.

Eq.1.1 becomes:

$$H_0 = H_L(1 - \Phi_B) \quad \text{Eq.1.4}$$

We can, therefore, deduce Φ_B as follows:

$$\Phi_B = \frac{H_F - H_0}{H_0} \quad \text{Eq.1.5}$$

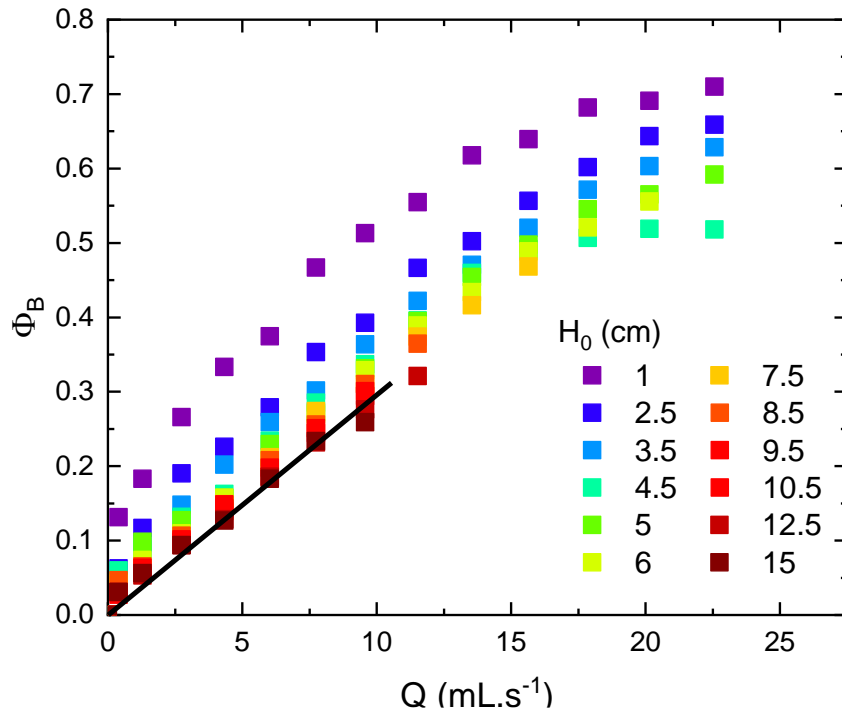


Figure 1-3 : Φ_B is evaluated as a function of Q at a varied value of H_0 for Decane.

We first worked at constant viscosity, exclusively conducting tests using Decane as shown in **Figure 1-3**. For each fixed value of H_0 between 1 – 15 cm, we vary the value of Q from 0.01 to 25 mL.s⁻¹. Experimentally, the final height clearly changes with flow rate Q and with the initial height H_0 . We remark in **Figure 1-3** that Φ_B is dependent on the initial liquid height, but only for small values of H_0 .

For small H_0 values ($H_0 \leq 7.5$ cm), we observe also non-linear dependence of Φ_B with Q .

For $H_0 > 8.5$ cm, we notice two distinct regimes depending on Q : Φ_B varies linearly with Q in the range 0 – 10 mL.s⁻¹. For Q larger than 10 mL.s⁻¹, the liquid height will not be stationary. It will produce massive air pockets and a large amplitude oscillation of the liquid/gas interface. Therefore, we cannot exactly determine Φ_B in this regime.

We now compare experiments on 4 liquids of different viscosity. For each liquid, we alternately modify 2 parameters which are the flow rate and the initial height H_0 of the liquid in each measurement in order to find optimal value of Φ_B .

It can be seen from **Figure 1-4** that Φ_B does not depend on the tested liquid. Thus, viscosity does not affect the value of gas volume fraction in the bubbly liquid. Φ_B decreases with H_0 and reach a plateau for $H_0 > 10$ cm. Thus, we choose in this work to use only values of H_0 larger than 10 cm, for which the plateau is reached.

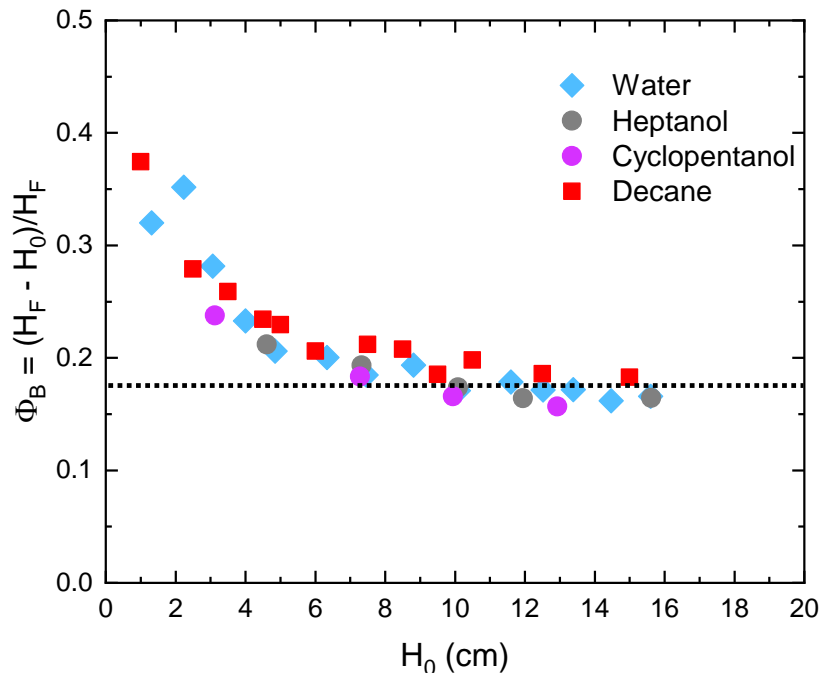


Figure 1-4 : Φ_B is evaluated in terms of H_0 at a fixed value of $Q = 6$ mL.s⁻¹ for 4 liquids of different viscosity: Water, Heptanol, Cyclopentanol and Decane.

The next parameter to consider which could affect the volume fraction of gas in the bubbling liquid is the injected flow rate. **Figure 1-3** and **Figure 1-5** describe the dependence of Φ_B on Q . We observe that throughout the examined range, Φ_B increases linearly as Q increases for all liquids (or in other words, for all viscosities tested), see **Figure 1-5**.

As mentioned above, Φ_B does not vary with viscosity μ . Hence, we can calibrate the volume fraction of gas in the bubble liquid and identify the right experimental range in which Φ_B is independent of the initial liquid height H_0 and flow rate Q . Experimentally, Φ_B is 0.18 as $H_0 \geq 10$ cm for $Q = 6$ mL.s⁻¹.

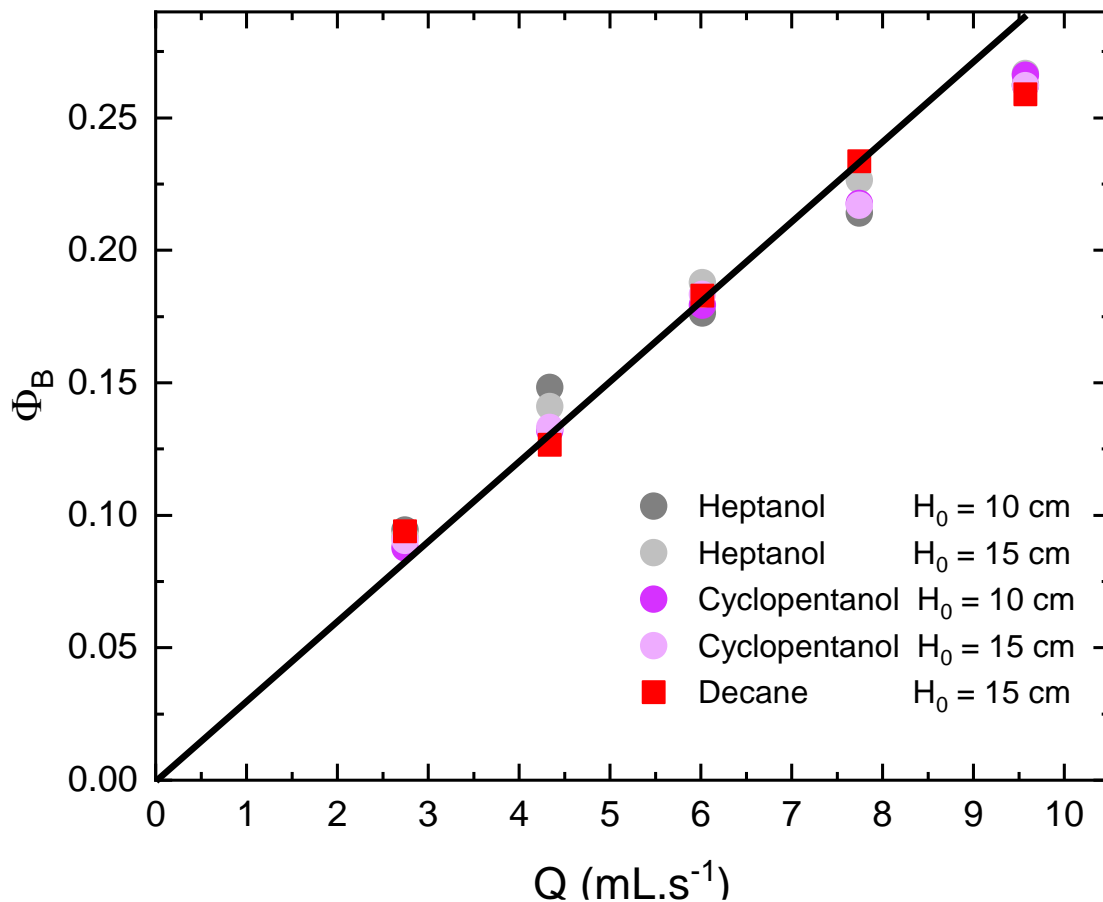


Figure 1-5 : Φ_B is evaluated as a function of Q at a varied value of H_0 from 10 cm to 15 cm for three liquids of different viscosity: Heptanol, Cyclopentanol and Decane.

In this manuscript we will use always a value of $Q = 6$ mL.s⁻¹ and a value of $H_0 = 10$ cm except when explicitly specified. The following is a summary graphic showing the calibration volume fraction of gas in the bubbly liquid based on the initial height of the liquid and the injected flowrate, see **Figure 1-6**.

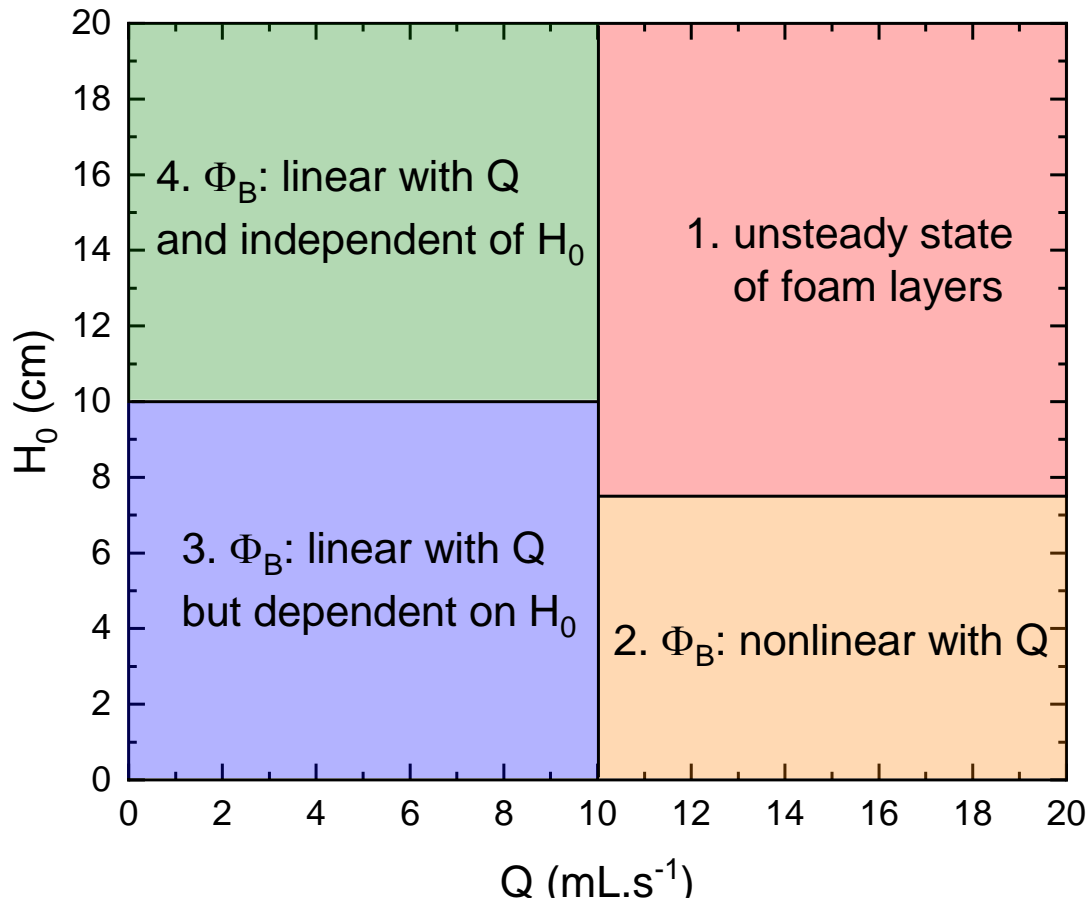


Figure 1-6 : Calibration summary chart

1. Red zone: for $Q > 10\text{mL}\cdot\text{s}^{-1}$ and for $H_0 > 7.5\text{ cm}$, the height of the foam layer is not steady in this scenario.
2. Orange zone: for $Q > 10\text{mL}\cdot\text{s}^{-1}$ and for $H_0 < 7.5\text{ cm}$, Φ_B has a nonlinear relationship with Q .
3. Violet zone: for $Q < 10\text{mL}\cdot\text{s}^{-1}$ and for $H_0 < 10\text{ cm}$, Φ_B varies linearly with Q , however, but its value depends on H_0 .
4. Green zone: for $Q < 10\text{mL}\cdot\text{s}^{-1}$ and for $H_0 > 10\text{ cm}$, Φ_B varies linearly with Q and Φ_B no longer depends on H_0 . This last domain is the only one used in the following.

We will now discuss the physics of the bubble rising in this liquid column.

1.1.2.2. Discussion of the non-foaming results

The fact that Φ_B does not depend on the viscosity suggests an inertial drag on rising bubbles. Moreover, the fact that Φ_B is proportional to the air flux, suggest that bubbles rise without interacting (and thus coalescing). We now estimate the rising velocity of the bubbles and compare it to the expected value from theory.

- Ascending bubble's speed in a column

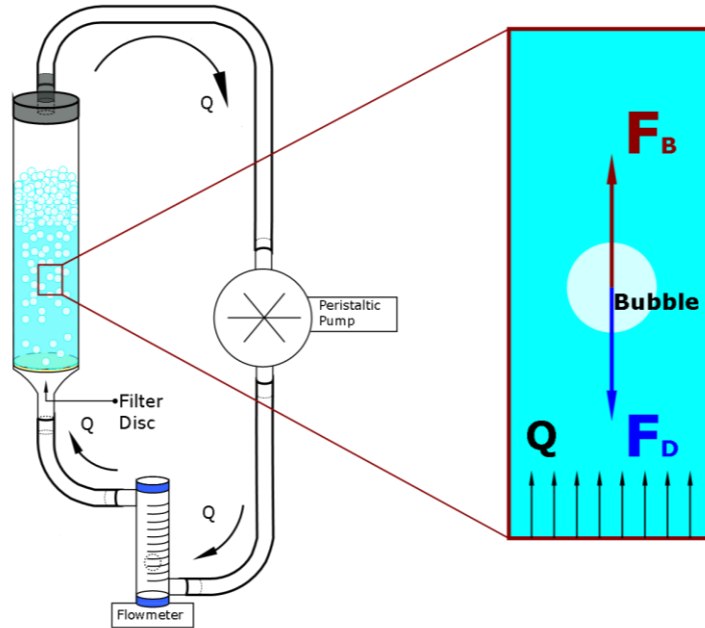


Figure 1-7 : Forces acting on a rising bubble in the Bickerman column

Consider a bubble of diameter D_b rising at speed U in the Bickerman column in a liquid of density ρ and viscosity μ , see **Figure 1-7**. The buoyancy force F_B and the drag force F_D are the only two forces impacting on the bubble. The drag force can be calculated using the Reynolds number Re and the drag coefficient C_D .

Table 1: Drag coefficient and drag force of a sphere at various Reynolds scales

$Re = \frac{\rho U D_b}{\mu}$	C_D	$F_D = \frac{1}{2} \frac{\rho \pi D_b^2}{4} C_D U^2$
$Re \leq 1$	$C_D = \frac{24}{Re}$	$F_D = 3\pi\mu D_b U$
$1 \leq Re \leq 10^3$	$C_D = \frac{18.5}{Re^{0.6}}$	$F_D = \frac{18.5}{8} \pi \rho^{0.4} \mu^{0.6} (D_b U)^{1.4}$
$10^3 \leq Re$	$C_D \approx 0.5$	$F_D = \frac{1}{16} \rho \pi D_b^2 U^2$

The bubble volume fraction in the liquid column is Φ_B . The flux of gas being imposed in the experiment, the average flux of gas is related to the rising speed of the air bubbles by:

$$U_{\text{exp}} \Phi_B = \frac{Q}{\pi R^2} \quad \text{Eq.1.6}$$

where U_{exp} is the experimental value of the bubble rising. Using the experimental values $\Phi_B = 0.18$ and $Q = 6 \text{ mL} \cdot \text{s}^{-1}$ gives us: $U_{\text{exp}} = 0.1 \text{ m/s}$.

The bubble diameter is approximately $D_b = 1.6 \pm 0.3 \text{ mm}$ for the Bikerman column. The number Re , thus, is:

$$Re = \frac{\rho U_{\text{exp}} D_b}{\mu} = 160 \quad \text{Eq.1.7}$$

with $\rho \approx 10^3 \text{ kg} \cdot \text{m}^{-3}$ and $\mu \approx 10^{-2} \text{ Pa} \cdot \text{s}$.

As a result, we are theoretically in the second regime of **Table 1**.

The drag force writes thus: $F_D = \frac{1}{2} \frac{\rho \pi D_b^2}{4} C_D U^2$, with $C_D = \frac{18.5}{Re^{0.6}}$.

The buoyancy force is: $F_B = \frac{1}{6} \pi D_b^3 \rho g$.

The force balance equation for a single bubble yields:

$$F_D = F_B \quad \text{Eq.1.8}$$

By replacing the expression of F_D and F_B in the previous equations, we obtain the expression of the bubble's rising speed:

$$U = \left(\frac{4}{3 \times 18.5} \left(\frac{\rho}{\mu} \right)^{0.6} g D_b^{1.6} \right)^{1/4} \quad \text{Eq.1.9}$$

The resulting theoretical value $U = 0.18 \text{ m/s}$ is quite close to the experimental one U_{exp} . This demonstrates that the drag is inertial and that the interaction between the bubbles and between bubbles and boundary of the glass column are negligible, in the non-foaming case. There is a small difference between the measured experimental findings and the theoretical value predicted from the model. The explanation for this mismatch might be that the modification of the flow in the case of many bubbles. This situation was reported by Richardson and Zaki [14] in their research, but only in the case of viscous drag, and will be discussed more below.

We have measured the liquid fraction in the foam using Eq.1.3. The results are the following section.

1.1.2.3. Foaming systems – Measurement of liquid fraction in the foam Φ_L

We turn now to foaming systems. First, we have measured the liquid fraction in the foam Φ_L . **Figure 1-8** depicts the experimental results demonstrating the relationship between liquid fraction and injected flowrate.

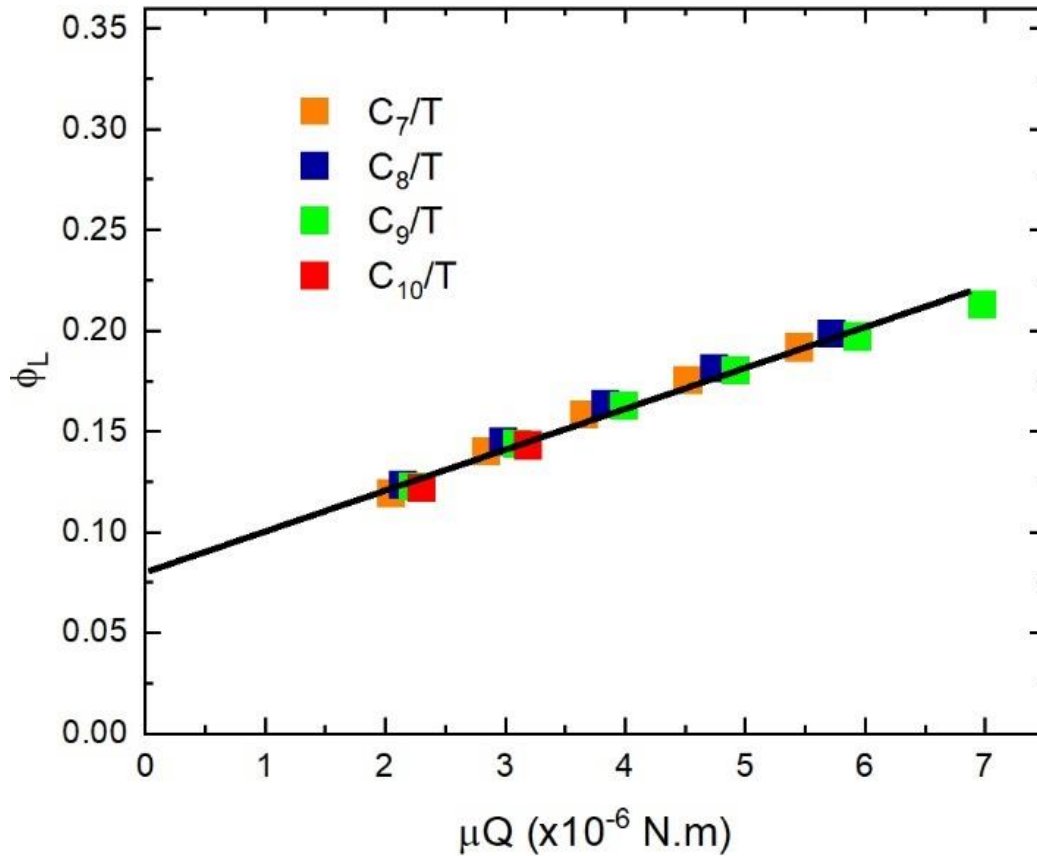


Figure 1-8 : Experimental fraction liquid Φ_L of binary mixtures of linear alkanes and toluene as a function of μQ .

As previously stated, when the border between the foam and bubbly liquid can be detected, it is simple to determine the liquid fraction Φ_L in the foam using **Eq.1.3**. However, in more complicated situations, the liquid fraction in the foam cannot be determined. In this circumstance, we require an estimating method for the liquid fraction's value in order to determine the foam's height. This estimation requires the use of the drainage equation and is described in the **Appendix A**.

1.1.3. Foam lifetime

It reasonable to wonder how the lifetime of bubbles is related to the foam height.

The height of the foam H , indeed, depends on injected flow rate Q . In the condition where H_0 is set at 10 cm, we conduct an experiment to measure H by varying Q . The results of the test are presented in the following graph.

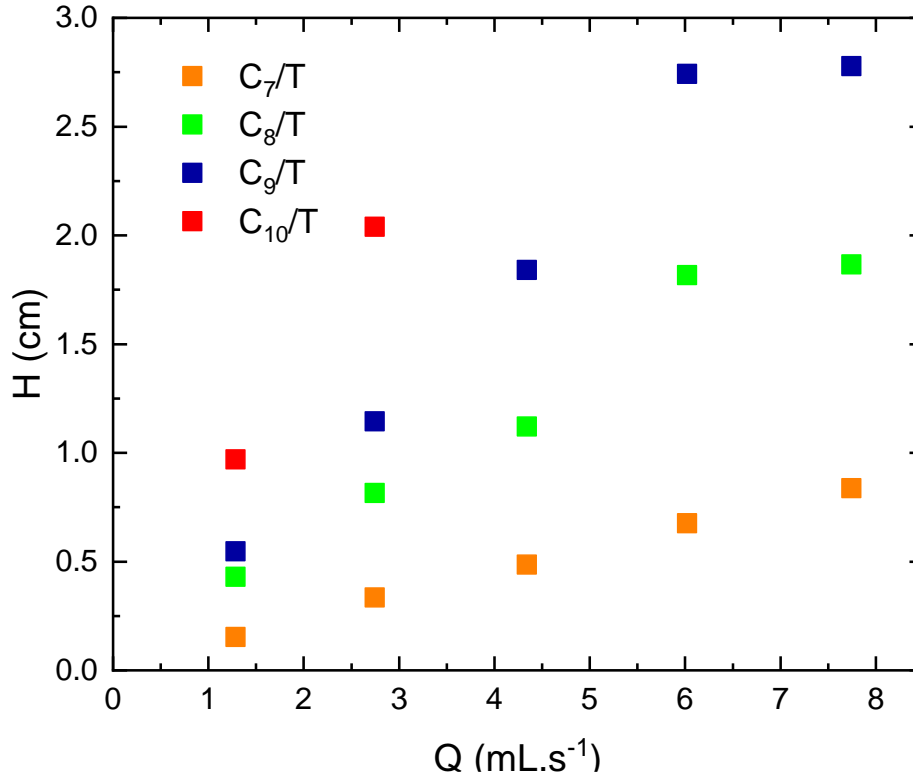


Figure 1-9: Experimental foam height H of binary mixtures of linear alkanes and Toluene as a function of injected flowrate Q .

From the values of experimental foam height H , we can calculate the foam lifetime, which is the average time that takes a bubble to go from the bottom to the top of the foam part.

Thus, the expression for the lifetime of foam is:

$$\tau = \frac{H\pi R^2}{Q} \quad \text{Eq.1.10}$$

We observe that these values are constant for any given liquid mixture and are unaffected by flow rate in our experiments as shown in **Figure 1-10** for different mixtures.

Thus, the Bikerman column allows, in our conditions, to measure lifetimes of foams that are independent of the injection conditions (flowrate and initial liquid height).

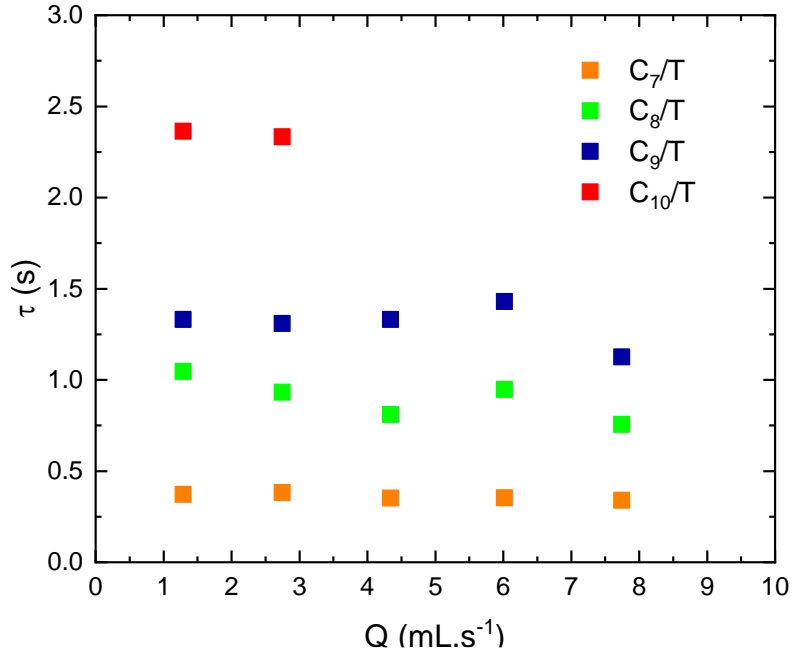


Figure 1-10 : Experimental foam lifetimes of binary mixtures of linear alkanes and Toluene as a function of injected flow rate Q .

1.1.4. Normalized foam lifetime

We will see later in the manuscript that it is convenient to write the lifetime as a normalized lifetime L_τ given by the product of the lifetime with the capillary velocity $\frac{\gamma}{\mu}$:

$$L_\tau = \frac{\tau\gamma}{\mu} \quad \text{Eq.1.11}$$

In order to evaluate L_τ , the viscosities of the investigated mixtures must be determined. Mixture viscosities were measured with a rheometer (Low Shear 400, Lamy Rheology) or calculated using the empirical Kendall-Monroe equation [15], which has been demonstrated to be appropriate for alkane-Toluene mixtures [16]. **Appendix B** has a detailed explanation and the experimental results. The typical value of this normalized height is typically 100 m and 10 m for the binary mixtures of Toluene and linear alkanes and of Cyclopentanol and linear alcohols, respectively. Definition of this height allows to include the effect of viscosity and of interfacial tension and compare lifetimes of foams formed in different mixtures.

The foamability of binary mixtures is of key interest in this research. To determine the relationship between foamability and composition as well as chemical nature, we will analyze the foaming capacity of each mixture using the normalized foam lifetime. Based on this quantity, we can furthermore develop a model to quantify the foamability. These concerns will be addressed in the following section.

1.1.5. Effect of Evaporation

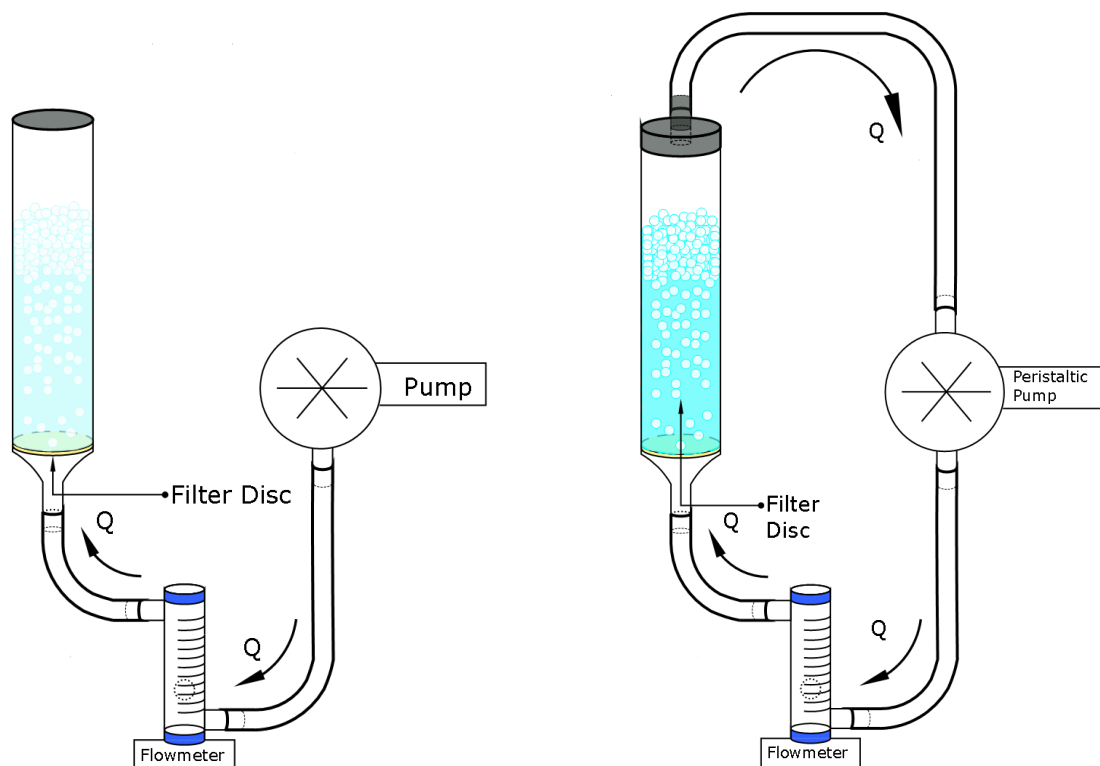


Figure 1-11 : Issue of Evaporation for the studied mixtures. (left) Open system set-up; (right) Closed system set-up.

As explained in the introduction, Chandran Suja et al. [7] have shown that the stability of foams in some oil mixtures has been linked to asymmetric evaporation in liquid mixtures. Thus, we can ask ourselves whether evaporation is of importance on foaming in our case. We thus check the effect of evaporation by performing experiments in closed and open systems, as described in **Figure 1-11**. In closed system, the gas equilibrates with the oil mixture and evaporation disappears. Thus, comparing closed and open experiments allows to detect whether evaporation in our situation has a role or not. All of the liquids in the studied mixtures are quite volatile. However, their evaporation rates are different. In addition to the fact that in open column, the ratio of the two species may drift with time, the lifetime of the foam may be affected by evaporation. **Figure 1-12** shows us the comparing results between two methods: empty squares and full squares represented the open and closed systems, respectively. For the small molar fraction of Decane $x_1 < 0.15$, the difference in normalized foam height L_τ is not truly clear. Nevertheless, starting from $x_1 > 0.2$, the distinction is fairly apparent.

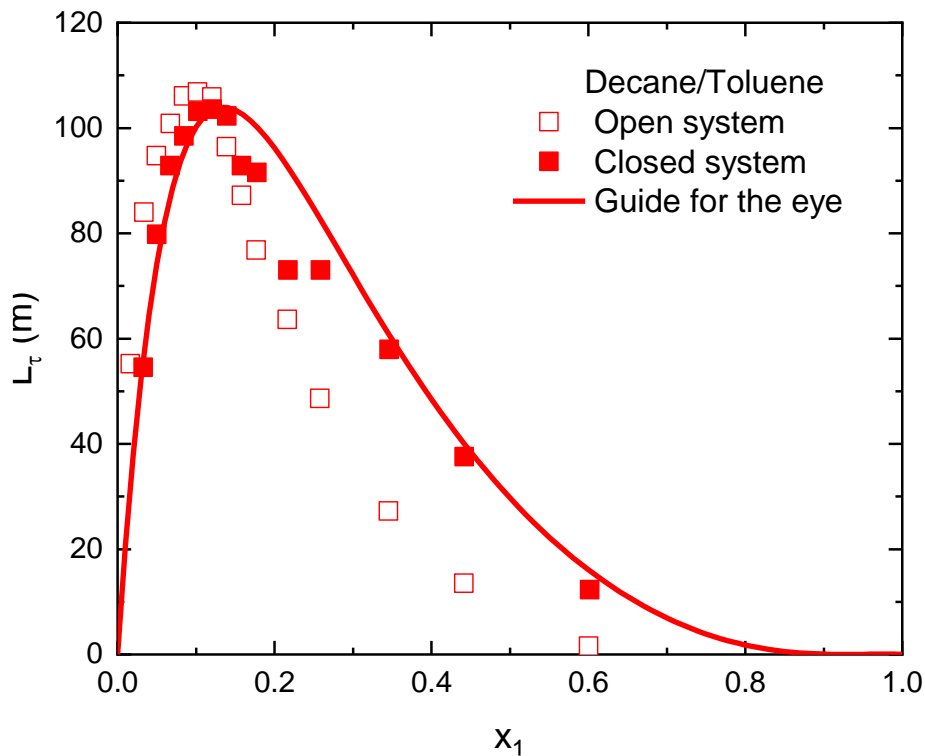


Figure 1-12 : Normalized foam lifetime of a Decane/Toluene mixture as a function of the Decane molar fraction x_1 in open system and closed system. The solid line is a guide for the eye.

This variation results from the volatile nature of the studied liquids. The boiling points T_b of Decane and Toluene are 174.1°C and 110.6°C , respectively. Toluene is therefore more volatile than Decane. The mechanism underlying this phenomenon is illustrated in **Figure 1-13**. We have a liquid mixture made up of two components: Toluene and Decane, with the former having a greater surface tension but being more volatile. Imagine that a bubble is now approaching the air/liquid interface and creating a liquid layer. Because Toluene molecules are more volatile, the Decane/Toluene proportion in this layer has been modified. A gradient of surface tension is caused by a gradient of concentration. In other words, the surface tension of the layer is lower than the surface tension of the surrounding liquid. Marangoni flow occurs, and liquid drains from the film in the same direction as the drainage. As a result, in this situation, the Marangoni effect totally destabilizes the liquid layer.

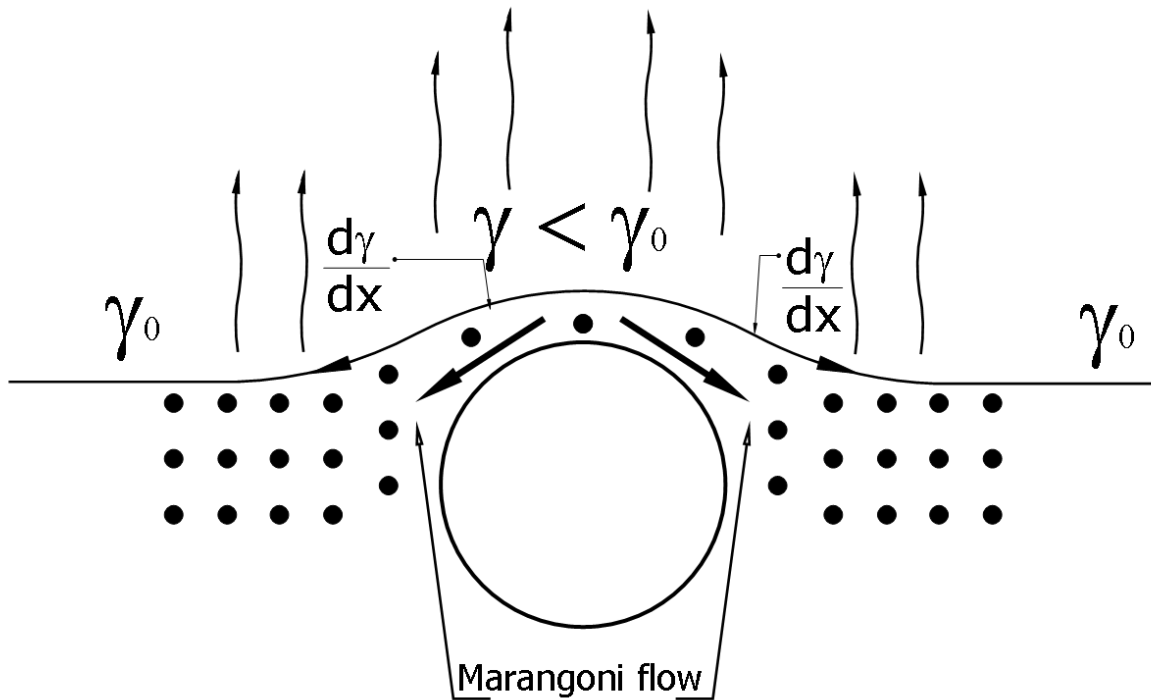


Figure 1-13 : Schematic showing the mechanism of bubble destabilization resulting from evaporation-induced Marangoni effect.

Clearly, the Marangoni effect resulting from evaporation destabilizes the liquid films in our case and makes L_τ smaller than real values.

This is contrary to the situation studied by Chandran Suja et al., where the Marangoni effect resulting from evaporation stabilizes the film. The explanation of the difference can be found in the liquids investigated. In their case, liquids having a lower surface tension are more volatile than liquids with a higher surface tension. Toluene, on the other hand, is a more volatile in our study yet has a higher surface tension than Decane in the binary mixture.

In the following we will only present results for which we assume that evaporation play no role, either using weak volatile liquids or using closed set-up. The properties of the used pure liquids are given in **Table 2** below.

Table 2 : Physico-chemical characteristics of the studied liquids

Name	Chemical formula	Abbreviation (used in this study)	Melting point (°C)	Boiling point (°C)	Density ($g.cm^{-3}$)	Molar mass ($g.mol^{-1}$)	Molar volume ($cm^3.mol^{-1}$)	Surface tension (25°C) ($mN.m^{-1}$)	Viscosity (25°C) ($mPa.s$)
Heptane	C ₇ H ₁₆	C ₇	-90.6	98.5	0.680	100.2	147.4	19.65	0.39
Octane	C ₈ H ₁₈	C ₈	-56.8	125.6	0.698	114.2	163.6	21.14	0.51
Nonane	C ₉ H ₂₀	C ₉	-53.5	150.8	0.714	128.3	179.6	22.37	0.65
Decane	C ₁₀ H ₂₂	C ₁₀	-29.7	174.1	0.727	142.3	195.8	23.37	0.85
Decane (50°C)	C ₁₀ H ₂₂	C ₁₀ (50°C)	-29.7	174.1	0.707	142.3	201.2	21.53	0.61
Hexadecane	C ₁₆ H ₃₄	C ₁₆	18.1	286.8	0.770	226.4	294.0	27.04	3.04
Eicosane (50°C)	C ₂₀ H ₄₂	C ₂₀ (50°C)	36.8	343.0	0.768	282.5	367.7	26.74	3.20
Toluene	C ₇ H ₈	T	-94.9	110.6	0.862	92.1	106.9	27.92	0.55
Pentanol	C ₅ H ₁₂ O	C ₅ OH	-78.9	137.9	0.811	88.2	108.7	25.51	3.51
Hexanol	C ₆ H ₁₄ O	C ₆ OH	-44.6	157.6	0.815	102.2	125.3	25.73	4.34
Heptanol	C ₇ H ₁₆ O	C ₇ OH	-34.0	176.4	0.819	116.2	141.9	26.21	5.90
Nonanol	C ₉ H ₂₀ O	C ₉ OH	-5.0	213.3	0.825	144.3	174.9	27.58	9.72
Cyclopentanol	C ₅ H ₁₀ O	Cyclo	-19.0	140.4	0.943	86.1	91.3	32.19	9.60
Polydimethylsiloxane	(C ₂ H ₆ OSi) _n	PDMS	-40.0	>205.0	0.918	770	838.8	18.76	5.00

1.1.6. Interfacial tension of binary mixtures & Effect of composition and chemical natures on foamability

1.1.6.1. Effect of composition and chemical natures on foamability

We now report foaming experiments performed with mixtures of fully miscible liquids that are either oils or alcohols. The studied binary mixtures are represented in the **Table 3**.

Table 3 : The studied binary mixtures

Binary mixtures	Liquid 1	Liquid 2	Observation
<i>Linear alkane</i> <i>/Toluene</i>	Heptane (C ₇)	Toluene (T)	Foam
	Octane (C ₈)	Toluene (T)	
	Nonane (C ₉)	Toluene (T)	
	Decane (C ₁₀)	Toluene (T)	
<i>Linear alcohol</i> <i>Cyclopentanol</i>	Pentanol (C ₅ OH)	Cyclopentanol (Cyclo)	
	Hexanol (C ₆ OH)	Cyclopentanol (Cyclo)	
	Heptanol (C ₇ OH)	Cyclopentanol (Cyclo)	
<i>Linear alcohol</i> <i>Linear alcohol</i>	Pentanol (C ₅ OH)	Nonanol (C ₉ OH)	
<i>PDMS</i> <i>Linear alkane</i>	PDMS	Decane (C ₁₀)	
<i>Linear alkane</i> <i>Linear alkane</i>	Heptane (C ₇)	Hexadecane (C ₁₆)	
	Decane (C ₁₀) (50°C)	Eicosane (C ₂₀) (50°C)	
	Heptane (C ₇)	Octane (C ₈)	No detectable
	Octane (C ₈)	Decane (C ₁₀)	foam

All the studied mixture are described in **Table 3**, and all the physicochemical useful parameters of each liquid are given in **Table 2**. In the manuscript, in all the mixtures, the species with the lowest surface tension, i.e., the linear alkane or linear alcohol, is referred to as liquid 1. On the other hand, liquid 2 refers to the component with the highest surface tension, such as Toluene or Cyclopentanol in the mixtures studied. In this study, we are also particularly interested in alkanes with long carbon chain, such as eicosane - C₂₀ (a paraffin). C₂₀, on the other hand, is solid in the laboratory conditions and has a melting point $T_m \approx 36.5^\circ\text{C}$. As a result, in order to perform the experiment and ensure that the resulting liquid mixture is homogeneous, the

experiment between Decane (C_{10}) and eicosane (C_{20}) was carried out at a temperature of $T_{exp} = 50^\circ C$, which is much higher than the melting point of C_{20} . All other experiments were conducted at room temperature ($T_{exp} = 25^\circ C$).

Mixture composition is varied for each tested binary mixture to check its capacity to foam. The foaming ability of the examined liquid mixtures is noted in the last column of this table. The majority of these mixtures can foam, as demonstrated by the Bikerman column experiment. However, in some of them, we only observe a thin layer of bubbles at the air/liquid surface, that means the foam height equals to diameter of these bubbles. So, this is also the error ΔH of the height of H in our experiments. To put it another way, it appears that these mixtures have no or very little foaming ability. We evaluate these mixtures as "No detectable foam" in **Table 3**.

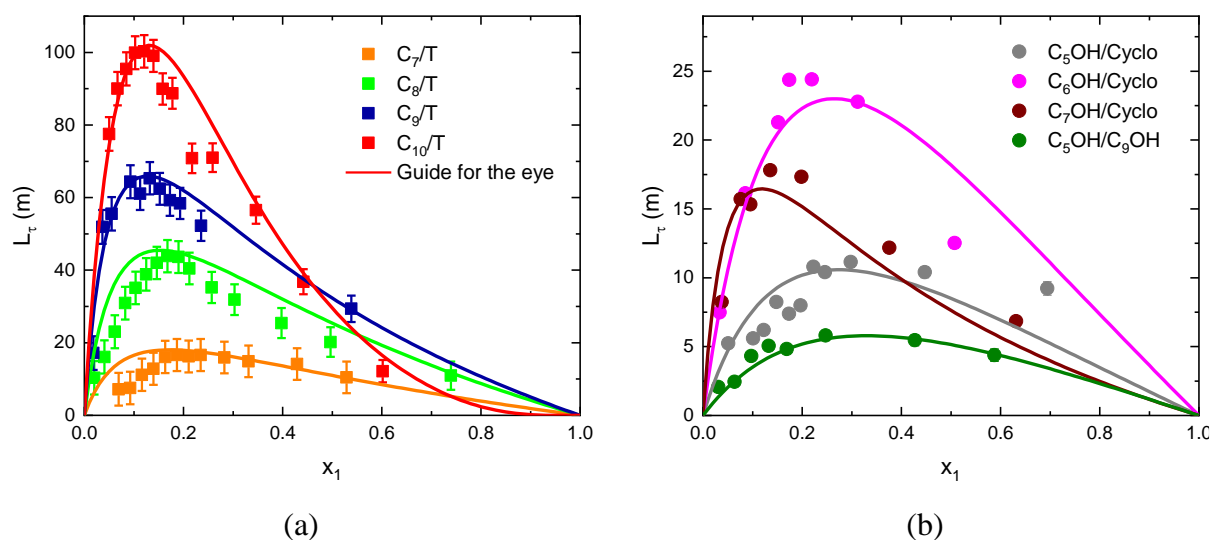


Figure 1-14 : Experimental normalized foam lifetime L_τ as a function of molar fraction of liquid 1 x_1 in the binary mixtures. (a) of linear alkanes and Toluene; (b) of linear alcohols and Cyclopentanol/ of 2 linear alcohols. The full lines are the guide for the eye.

Figure 1-14 (a) shows the normalized height of foam L_τ for various alkane-Toluene mixtures as a function of alkane molar fractions x_1 . Once again, we can observe that as x_1 is 0 (pure Toluene) or 1 (pure alkane), the normalized foam lifetime is 0. This confirms that pure liquids do not foams, and this also prove by the way that there are no contaminant species that could be responsible for some foaming. Between $0 < x_1 < 1$, the variations in lifetime τ and normalized foam lifetime L_τ are nonmonotonic, whereas the viscosity varies monotonically with composition [8]. A maximum for normalized foam lifetime is obtained at an alkane fraction that is depending on the length of

the alkane's carbon chain. The maximum value lifetime and L_τ is more strongly dependent on the alkane in the mixture with Toluene. For example, Decane/Toluene foams the most in liquid mixtures, whereas heptane/Toluene has a normalized foam lifetime which is five times smaller than that of Decane/Toluene.

Alcohol/Cyclopentanol mixtures have been shown in **Figure 1-14 (b)** to present similar properties. Experimentally, we have observed that the binary mixtures alkane/Toluene as well as alcohol/Cyclopentanol have varying normalized foam lifetimes depending on their compositions and chemical natures. In particular, in all situations, there is a ratio x_1 at which the degree of foaming is greatest. It's called as x_1^{max} .

Aside from the non-foaming mixes (C_7/C_8 or C_8/C_{10}), the other two liquid alkane/alkane mixtures exhibit roughly comparable foaming performance to alkane/Toluene or alcohol mixtures, see **Figure 1-15**. Like the previous two types of liquid mixtures, the alkane/alkane mixtures have also lifetime curves with a maximum.

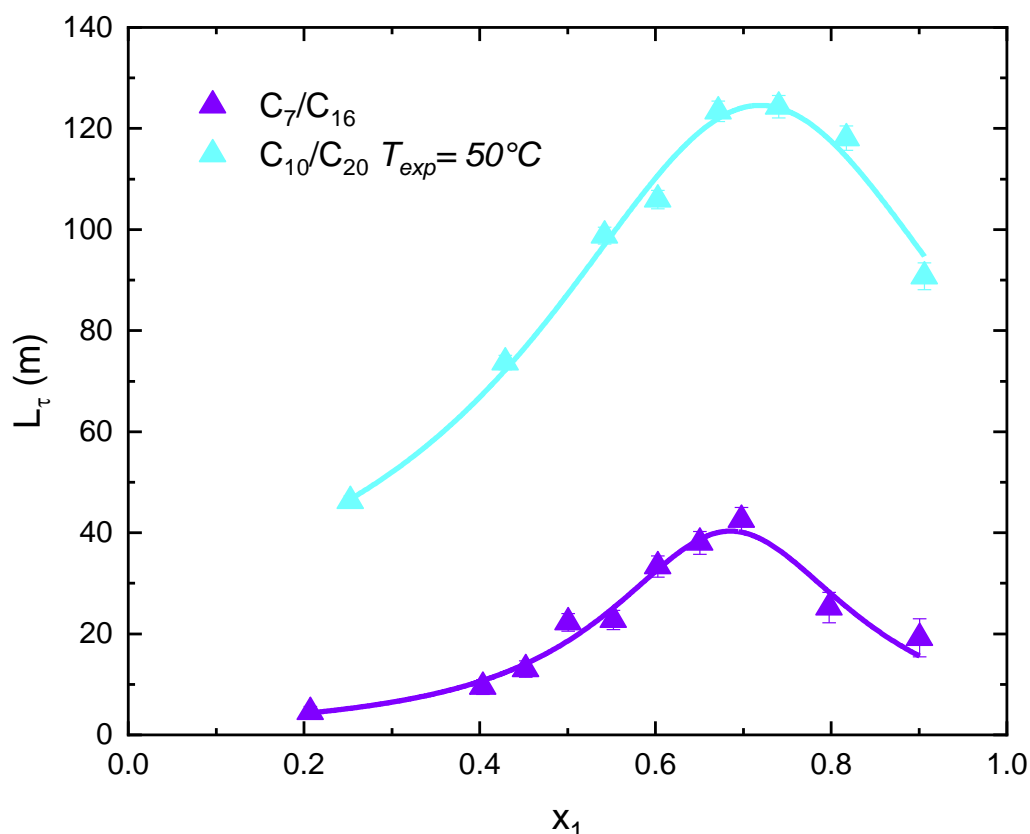


Figure 1-15 : Experimental normalized foam lifetime L_τ as a function of molar fraction of liquid 1 x_1 in the alkane/alkane mixtures. Only 2 foaming mixtures are represented. C_7/C_8 and C_8/C_{10} are the non-foaming mixtures. The full lines are the guide for the eye.

Finally, **Figure 1-16** illustrates the measured result L_τ of the PDMS/Decane mixture. As compared to the above mixtures, the PDMS/Decane is a strongly foaming mixture. The difference is that the maximum position is extremely near to 0. That is, even if only a tiny amount of PDMS is added to the Decane liquid, a considerable volume of foam will be produced. PDMS/Decane mixture exhibits also a maximum in foamability, for an amount of PDMS of about $x_1 \approx 10^{-3}$.

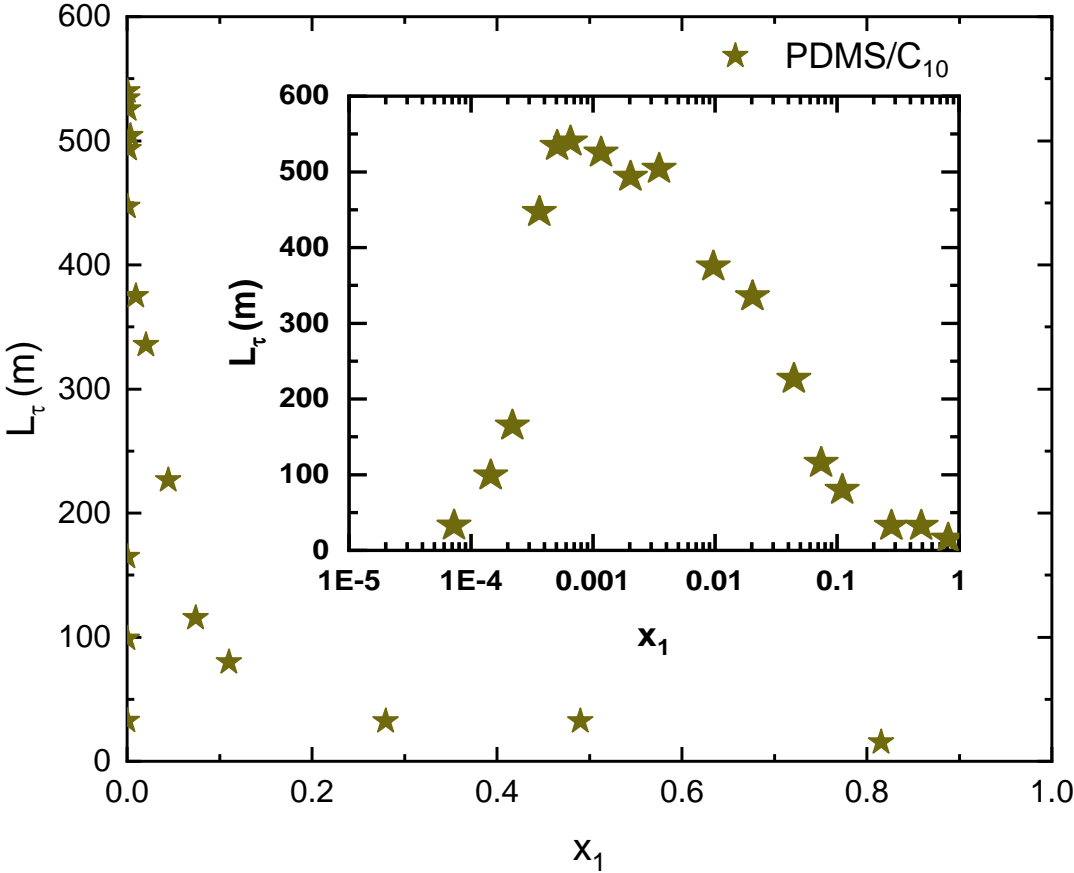


Figure 1-16 : Experimental normalized foam lifetime L_τ as a function of molar fraction of PDMS ($M = 770 \text{ g. mol}^{-1}$; $\mu = 5 \text{ cst}$) in the mixture with Decane. Inset: same curve with x_1 in log scale.

1.1.6.2. Interfacial tension of binary mixtures

We can ask ourselves whether foaming is related to the surface tension of the liquid mixture. For that, we have systematically measured the surface tension of mixtures as a function of their composition. The binary mixtures used are the compounds in **Table 3**. First, we use linear alkane/Toluene measurements and x_1 range from 0 to 1. As illustrated in **Figure 1-17**, the surface tension was discovered to vary in a nonlinear way. This deviation from linearity is clearly visible, and it has been noticed in a number of previous works [17–19]. Second, we do the same measurement on binary mixtures of various alcohols. Similar findings show that there is a sublinear relationship between surface tension and molar fraction. Nevertheless, the difference in these data is less pronounced than in the case of alkane/Toluene mixtures.

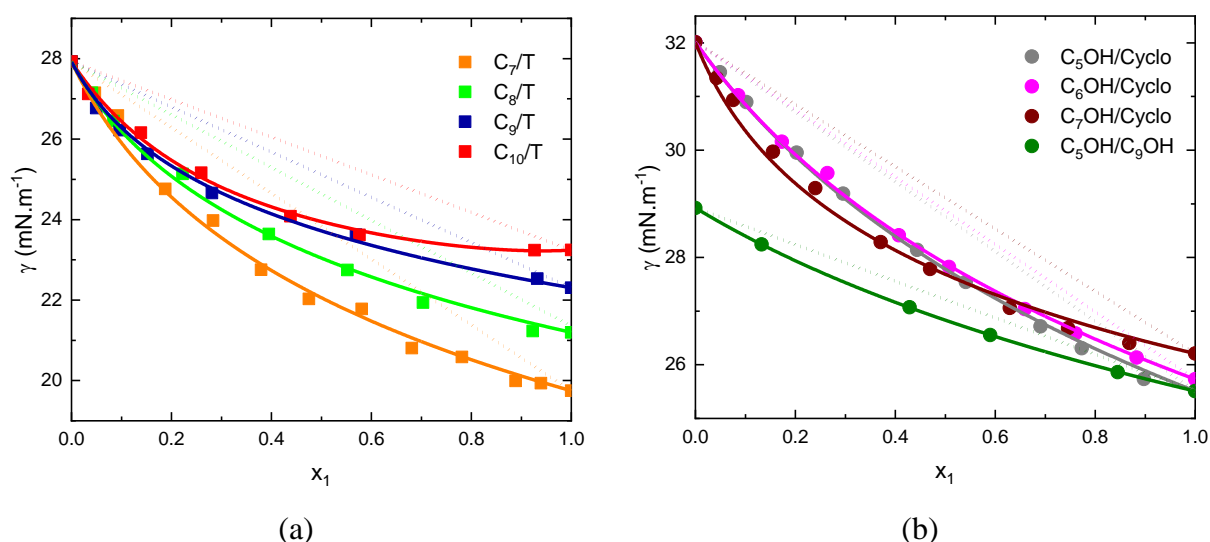


Figure 1-17 : Measurement of interfacial tension γ as a function of molar fraction of liquid 1 x_1 in the binary mixtures. (a) of linear alkanes and Toluene; (b) of linear alcohols and Cyclopentanol/ of 2 linear alcohols. For example, $x_1 = 0$ corresponds to surface tension of pure Toluene and $x_1 = 1$ corresponds to alkane's surface tension for the alkane/Toluene mixtures. The dashed line indicates linear variations.

Furthermore, we do the same experiment using a liquid mixture of two linear alkanes. We begin with two non-foaming liquid mixtures. Unlike the previous two types of mixtures, we do not see this sublinear connection in this situation; instead, the surface tension varies linearly with respect to the liquid composition in the mixture, see **Figure 1-18**. Nevertheless, the variation of surface tension with the liquid composition of two foaming alkane/alkane mixtures is entirely different from that of the other mixes. The surface tension in this situation was discovered to vary in a super-linear form. Several prior research with mixed alkanes have shown similar experimental results on this behavior [20].

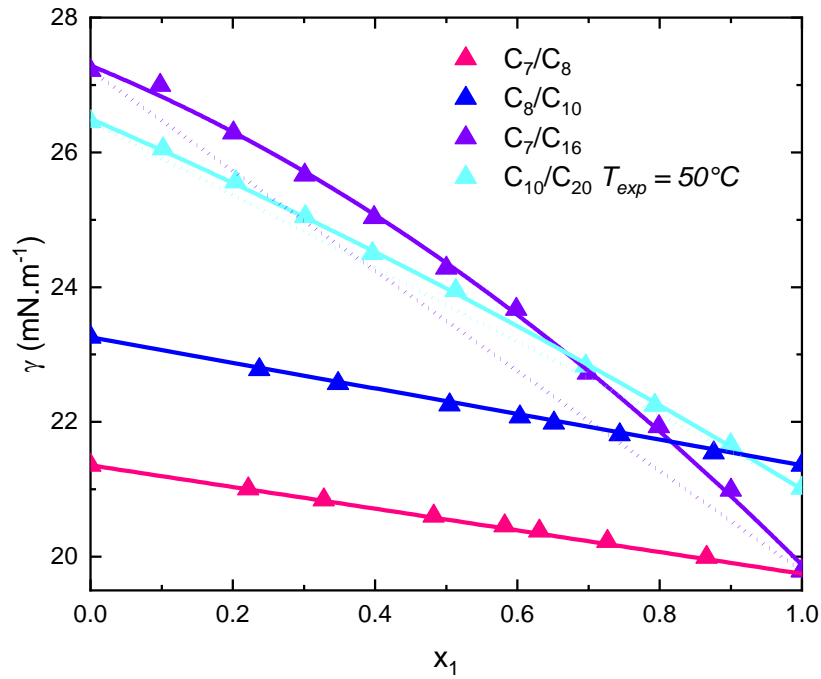


Figure 1-18 : Measurement of interfacial tension γ as a function of molar fraction of liquid 1 x_1 in the binary mixtures of 2 linear alkanes. The dashed line indicates linear variations.

Finally, we determine the surface tension of the PDMS/Decane mixture based on its composition. Surface tension varies non-linearly in this case, as it does in alkane/Toluene mixtures and mixtures of alcohols. The measurement exhibits a sublinear variation in more depth.

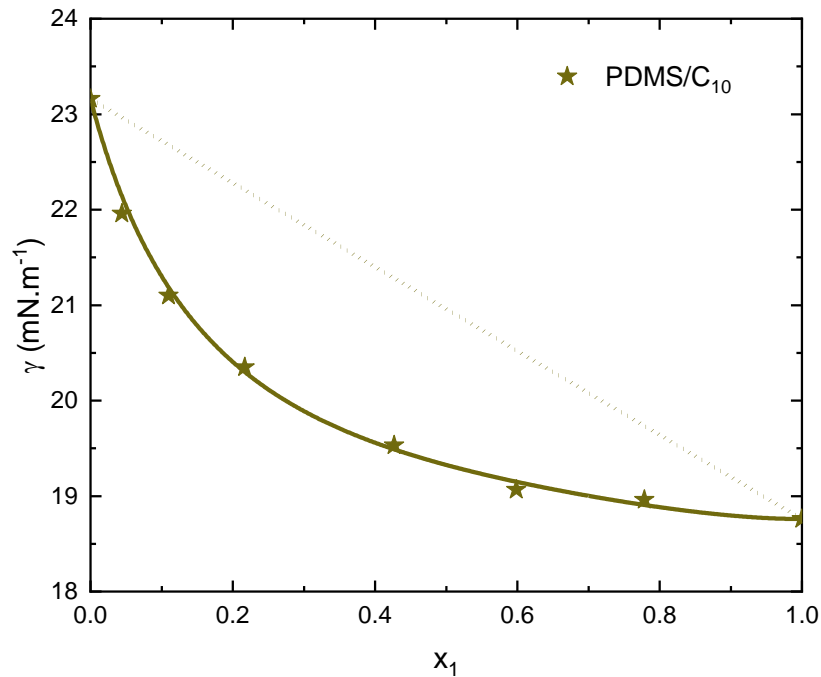


Figure 1-19 : Measurement of interfacial tension γ as a function of molar fraction of PDMS in the mixture with Decane. The dashed line indicates linear variations.

At this stage of our work, one can wonder how interfacial tension of the mixtures is related to foamability. Two tentative of correlations are described below.

(a) Relation between foamability and difference in interfacial tension

Figure 1-20 describes the correlation between normalized foam lifetime and the difference in surface tension between the components contained in the investigated liquid mixtures. We can observe that L_τ is small as $\Delta\gamma$ is small too. The Pentanol/Nonanol mixture is a typical example (shown by circle in olive color). However, this link between L_τ and $\Delta\gamma$ is not entirely obvious. This may be seen in Heptane/Toluene (orange square); while the difference in surface tension in this mixture is quite significant, L_τ is of modest value. Nevertheless, $\Delta\gamma$ is moderate in cases like Decane/Toluene (red square) and Decane/Eicosane (50°C) (cyan triangle), whereas these mixtures have very large value of L_τ .

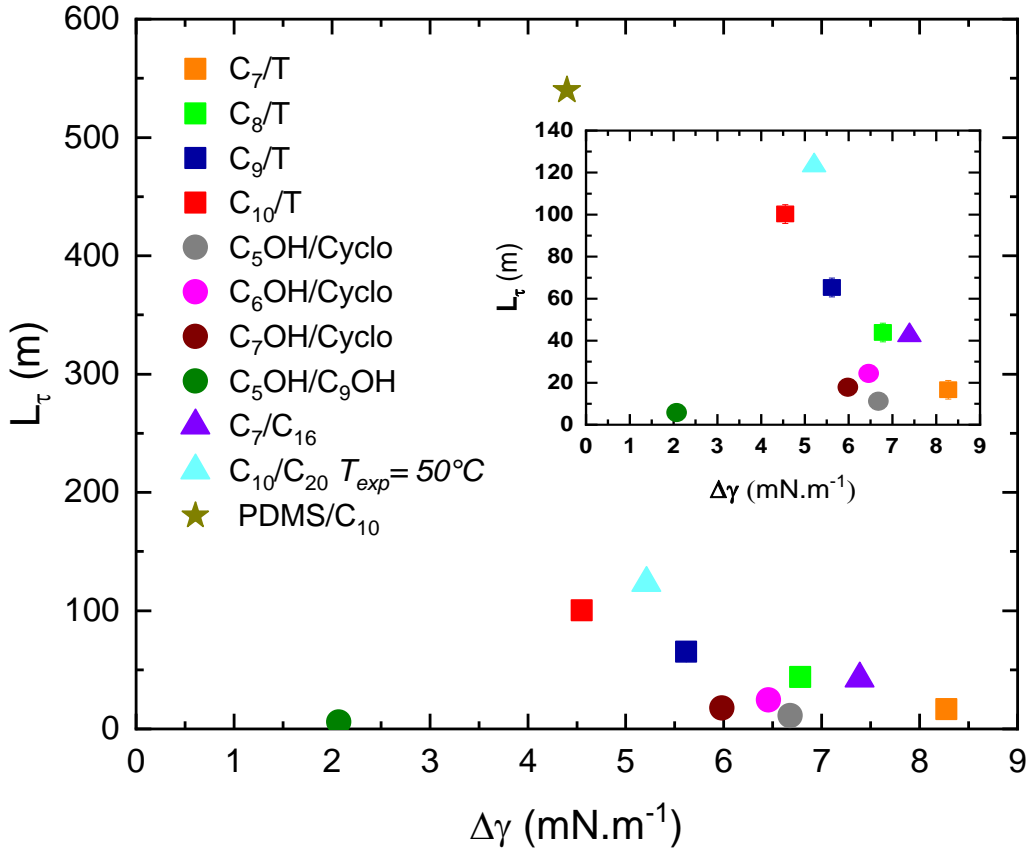


Figure 1-20 : Experimental normalized foam lifetime L_τ of studied binary mixtures as a function of corresponding surface tension difference $\Delta\gamma$.

We may conclude from data that the foamability cannot be explained merely by the difference in surface tension between the two liquids involved in the mixture.

(b) Relation between foamability and surface tension non-linearities

We can also wonder that the way the surface tension varies is also a contributing factor.

The surface tension of binary liquid mixtures can be fitted with their compositions using the equation below:

$$x_1 e^{\sigma_{fit} \frac{\gamma - \gamma_1}{RT}} + x_2 e^{\sigma_{fit} \frac{\gamma - \gamma_2}{RT}} = 1 \quad \text{Eq.1.12}$$

where γ_i is the surface tension of liquid i ($i = 1, 2$), x_i is molar fraction in the mixture with $x_1 + x_2 = 1$. And σ_{fit} is the area per mole, which, in a first approximation, is assumed to be the same for both liquids in the mixture. **Eq.1.12** is inspired from the well-known Butler equation [21], but as will be explained in the next chapter, the value of σ_{fit} may be in practice in some case very different from the real area per molecules.

We may deduce the relation between the surface tension and molar concentration from the above equation:

$$\gamma(x_1) = -\frac{RT}{\sigma_{fit}} \ln[x_1 e^{-\sigma_{fit} \frac{\gamma_1}{RT}} + (1 - x_1) e^{-\sigma_{fit} \frac{\gamma_2}{RT}}] \quad \text{Eq.1.13}$$

For all mixtures, this relation was fit to the experimental data using σ_{fit} as the only fitting parameter.

Table 4 : Values of σ_{fit} for used binary mixtures

Mixture	C ₇ / T	C ₈ / T	C ₉ / T	C ₁₀ / T	C ₅ OH/ Cyclo	C ₆ OH/ Cyclo	C ₇ OH/ Cyclo	C ₅ OH/ C ₉ OH	C ₇ / C ₁₆	C ₁₀ / C ₂₀ (50°)	PD MS /C ₁₀
σ_{fit} ($km^2 \cdot mol^{-1}$)	0.56	0.74	1.14	1.63	0.48	0.52	0.93	0.68	-0.32	-0.16	2.23

Note that σ_{fit} is positive when the interfacial tension/molar composition dependence is sublinear; and negative if it is super-linear. The graph above represents the normalized foam lifetime as a function of this value. The correlation is not very good between the two variables the normalized foam lifetime and $\sigma_{fit} \frac{\Delta\gamma}{RT}$, see **Figure 1-21**. For positive values of $\sigma_{fit} \frac{\Delta\gamma}{RT}$ foamability can be qualitatively related to the difference in surface tension between two liquids times the deviation from linearity. But the origin of foaming is more complicated and will be explored in detail in the following chapter.

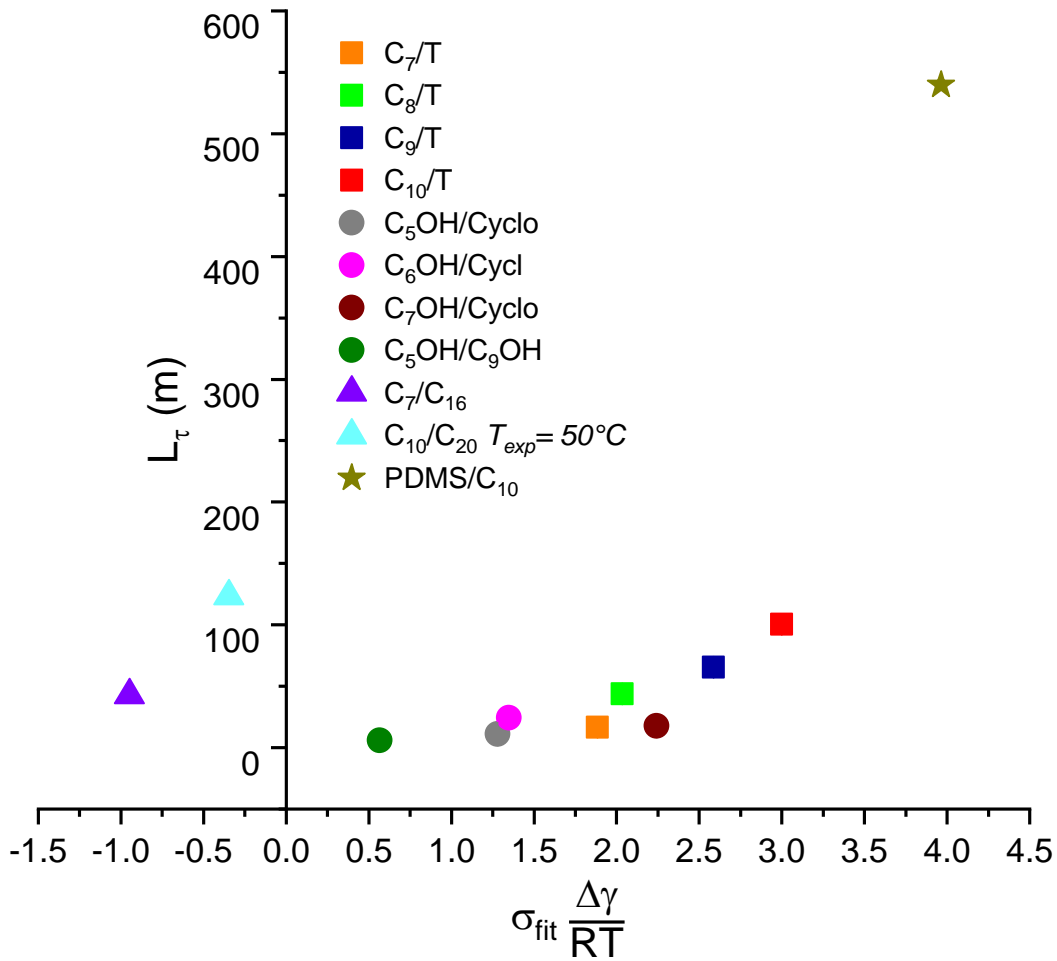


Figure 1-21 : Experimental normalized foam lifetime L_τ of studied binary mixtures as a function of corresponding $\sigma_{fit} \frac{\Delta\gamma}{RT}$.

Table 3 shows which mixture foams and which does not foam. In general, we can see that the majority of liquid mixtures foam. Understanding the origin of foaming and quantifying foamability, on the other hand, is more challenging. Detailed theoretical calculations will be discussed in the following chapters. Before we get into these discussions, let's look at some further behaviors: the effect of bubble size on foamability and experiments with single bubble.

The bubble diameter is nearly unchanged in Bikerman columns studies, $D_b = 1.6 \text{ mm}$, whatever the porosity of the filter disc. To investigate the effect of foams resulting from bubble sizes, we have developed a set up using an Ultra Turrax device that allows to control the bubble sizes.

1.2. VARYING THE BUBBLE SIZE WITH AN ULTRA TURRAX SET-UP

Geometry of Ultra Turrax

Ultra Turrax is a dispersion device that is used for homogenization, emulsification, and suspension. It allows to strongly shear a liquid. In this investigation, we use the T18 digital Ultra Turrax from IKA Dispersers. It has a rotation speed range of 3000 – 25000 *rpm*, allowing us to work at high circumferential speeds. This device is utilized for amounts ranging from 1 to 1500 *mL* and comes equipped with a dispersing tool. The dispersing tool (S18 N - 10 G) having a diameter of 10 *mm* and an immersion length of 70 *mm* is also provided by IKA.

Experimental description

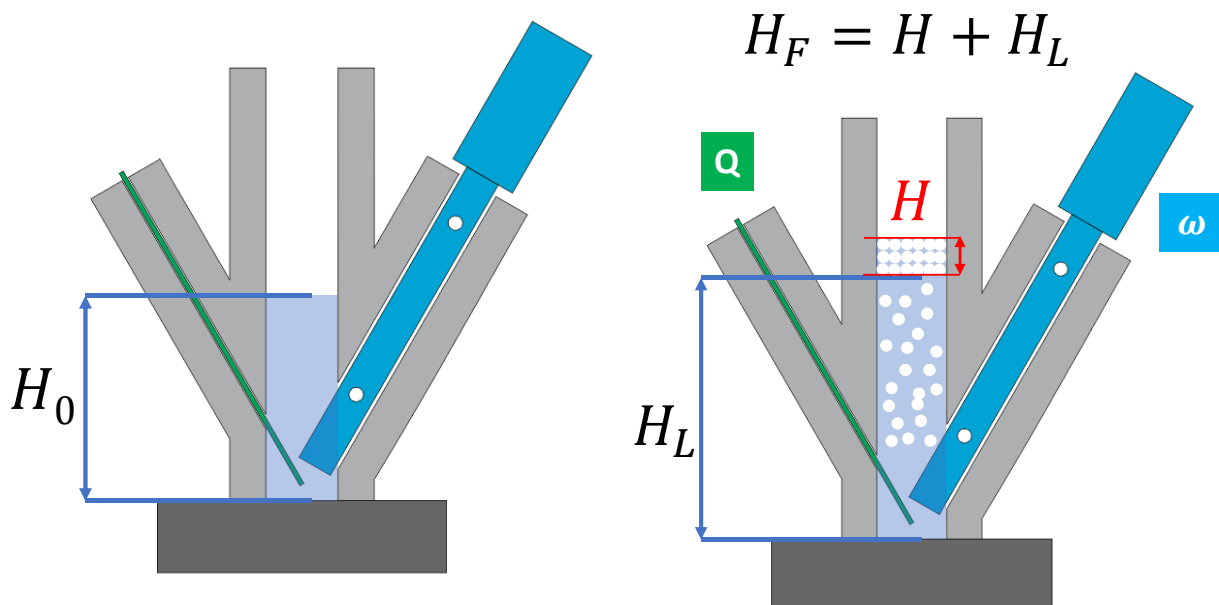


Figure 1-22 : Schematic of the experimental set-up with Ultra Turrax device.

Based on the function and design of the Birkman column, we have built a customized glass instrument that is compatible with the Ultra Turrax device, see **Figure 1-22**. It is made up of a primary column with a radius of $R = 1 \text{ cm}$, which is utilized to contain the liquid mixture. The two sides of the main column consist of two auxiliary pipes of different purposes. The left pipe has a diameter of 1.3 *mm* that works as a needle holder to inject air into the liquid mixture at a constant flowrate Q . The flowrate can be varied between 10 $\mu\text{L} \cdot \text{s}^{-1}$ and 5000 $\mu\text{L} \cdot \text{s}^{-1}$. In the meantime, the right pipe is bigger of diameter 12 *mm* to fit the dispersing tool of Ultra Turrax.

The rotation speed ω of this dispersion tool may be readily modified between 3000 *rpm* and 18000 *rpm* using Ultra Turrax. To prevent producing vortexes during Ultra Turrax operation, we installed a fiberglass grill ($D_{grille} = 2\text{ cm}$; mesh size is $1\text{ mm} \times 1\text{ mm}$) in the main column just above the position of the dispersion tool. In addition, we have to avoid the temperature changes of the device as the dispersing tool rotates. The temperature is measured using an electronic thermometer with a precision of at least 0.1°C . Each experimental measurement lasted between $30\text{ s} - 1\text{ min}$. During this period of the experiment, the reported temperature did not change. The delay between each operation, however, is typically 10 minutes to guarantee that the liquid temperature is constantly at room temperature.

The fluid mixtures utilized was identical to that used in the Bikerman column experiment. They are also poured to the initial height H_0 . The task to determine foam layer height H and final height H_F during the air injection process is likewise entirely comparable to the prior experiment. However, it is harder to identify the boundary between the foam layer and the bubbly liquid layer as the dispersive device rotates at high speed in this operation. Therefore, characteristics like volume fraction of gas Φ_B or liquid fraction Φ_L are necessary to estimate H from H_F .

To prevent evaporation, the experiment was carried out with a closed system, like set-up with Bikerman column.

1.2.1. Measurement of bubble sizes by image analysis

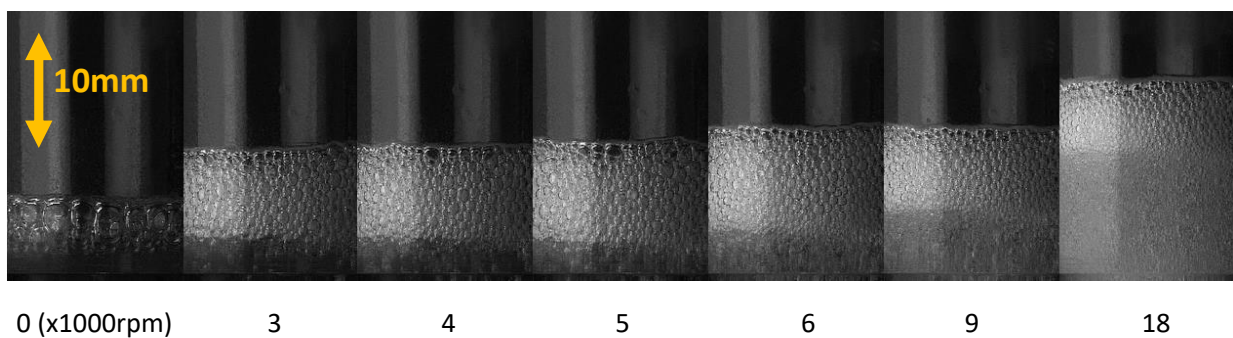


Figure 1-23 : Experimental images for different rotation speeds of Ultra Turrax device at fixed flowrate $Q = 100\ \mu\text{L}\cdot\text{s}^{-1}$.

First of all, we have to examine the experiment's effectiveness. The aim of this experimental system is to use the Ultra Turrax to create bubbles that are smaller in size than the previous

experiment – the Bikerman column. To begin, we will examine the diameters of bubbles generated in two cases: without and with Ultra Turrax (at the minimum rotational speed ω , i.e., 3000 rpm). We'll then gradually increase ω to see how Ultra Turrax affects the size of the bubbles in the foam, see **Figure 1-23**. All studies in this section were carried out at a constant flowrate $Q = 100 \mu\text{L} \cdot \text{s}^{-1}$, with a liquid mixture of Heptanol/Cyclopentanol at $x_1^{max} = 0.12$. x_1^{max} is the molar fraction of liquid 1 in the mixture at which normalized foam lifetime L_τ , or the degree of foaming, is maximum.

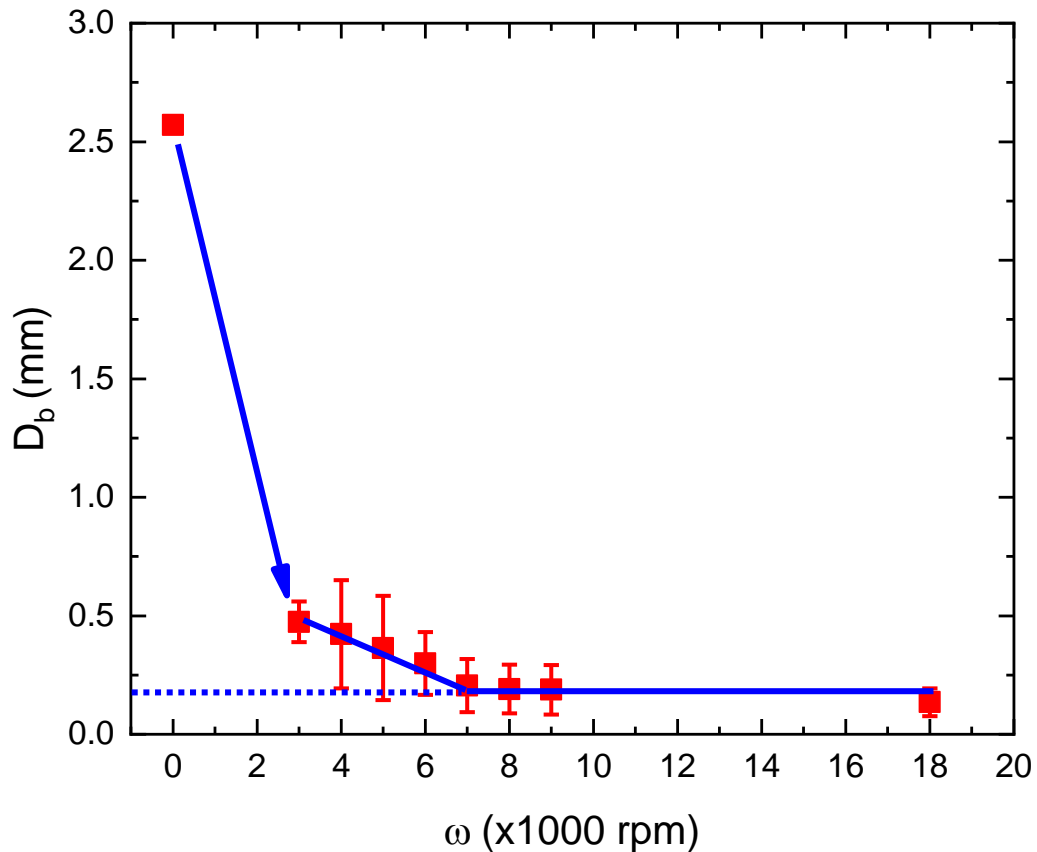


Figure 1-24 : Bubble diameter evaluated by image analysis based on rotation speed of the Ultra Turrax device at fixed flowrate $Q = 100 \mu\text{L} \cdot \text{s}^{-1}$. The diameter of the air bubbles is $D_b = 2.5 \text{ mm}$ when no Ultra turrax is used, i.e., $\omega = 0 \text{ rpm}$.

The results are depicted in **Figure 1-24**. As illustrated in this figure, we can subdivide the air bubbles injected into the column of studied liquid mixtures by using Ultra Turrax. Average bubble diameter is approximately $D_b = 0.5 \text{ mm}$ ($\omega = 3000 \text{ rpm}$), 5 times smaller than the initial size without Ultra Turrax. As the speed of the rotation increases, the size of these bubbles falls linearly until it reaches a critical size $D_b = 0.25 \text{ mm}$ at $\omega = 9000 \text{ rpm}$. From this rotating velocity on, the diameter of the bubbles remains nearly constant, and 6 times smaller than the Bikerman experiment bubbles.

To be more specific, the mean bubble diameters are statistically determined for each rotating speed over a total of 50 consecutive measurements. Similarly, as **Figure 1-25** shows, the size of bubbles in the foam system is reduced when the rotational speed of the device is increased. However, the bubble's size distribution remained practically unchanged afterwards.

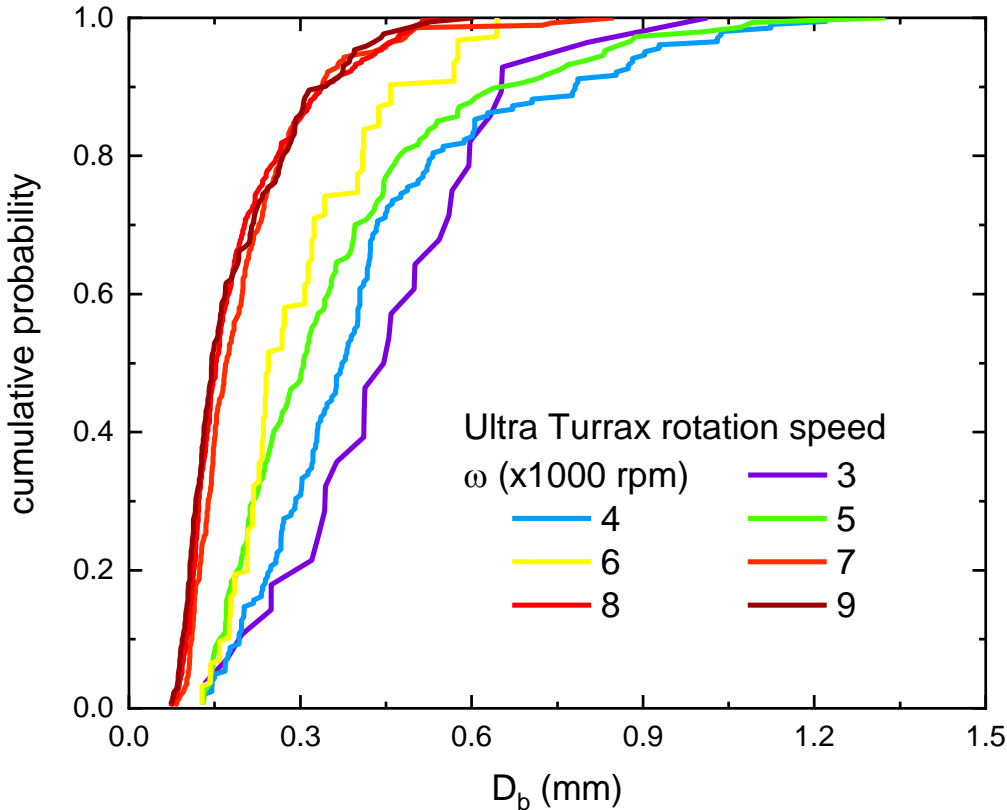


Figure 1-25 : Cumulative probability distribution of bubble sizes at the boundary foam – bubbly liquid for different rotation speeds of Ultra Turrax device at fixed flowrate $Q = 100 \mu L. s^{-1}$.

1.2.2. Validation of bubble sizes by estimation from creaming phenomena

The previous section showed the findings of the experiment to measure the size of the bubbles. We employed the Richardson and Zaki model [14] in size bubble estimation from creaming phenomena to better understand this phenomenon and observed outcomes.

From this model, we can estimate the diameter of bubbles:

$$\langle D_b \rangle = 0.34 \text{ mm}$$

The values above show that the two methods, measurement from image analysis or estimation with creaming phenomena, produce the same results.

A detailed description of calculations using this model is given in the **Appendix C**.

1.2.3. Influence of flowrate on bubble sizes

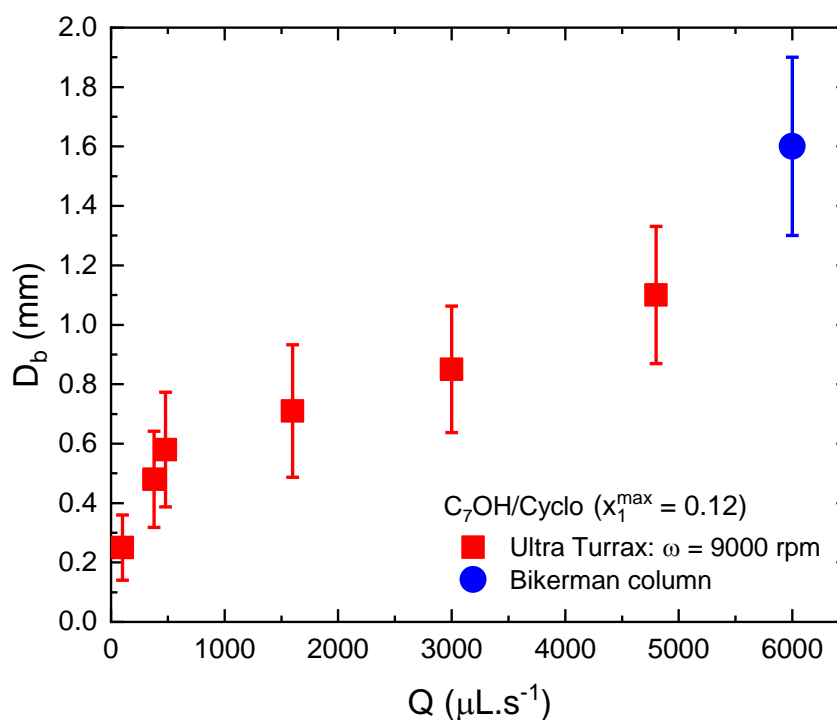


Figure 1-26 : Bubble diameters as a function of injected flowrate Q (red squares) at a fixed Ultra Turrax rotation speed are in comparison to bubble diameter in Bikerman tests (blue circle) – Heptanol/Cyclopentanol mixture (at $x_1^{\text{max}} = 0.12$).

In fact, it appears that if the velocity of the rotor has a little impact on the bubble diameter, the air flux has a great importance. The rotational speed chosen is the optimum rotational speed stated in the previous section $\omega = 9000$ rpm. The flowrate of air injection Q is adjusted between $100 \mu\text{L}\cdot\text{s}^{-1}$ and $4800 \mu\text{L}\cdot\text{s}^{-1}$ – which is similar to the flowrate used in the Bikerman case ($\sim 6000 \mu\text{L}\cdot\text{s}^{-1}$).

The data acquired in measuring the bubble size of the Ultra Turrax at a fixed rotational velocity revealed that raising the flowrate did actually increase the average diameter of the bubbles created in the foam, see **Figure 1-26**. When their flowrates are essentially comparable, their average diameter appears to be approaching the value observed in the Bikerman column experiment.

In summary, using a specially designed set-up, we are able to form bubbles of size varying between 0.2 mm and 1.2 mm.

1.2.4. Normalized foam lifetime results

To summarize, as seen in the preceding sections, we were able to inject smaller air bubbles into the liquid mixture using Ultra Turrax than in the case of Bikerman column. the diameter of these bubbles depends weakly on the variation in rotation speed, but can be easily tuned varying the injected flowrate. We measure the height of the layer of foam created by these air bubbles, similarly to prior research.

Finally, we attempt to compare the normalized height of foam according to bubble size.

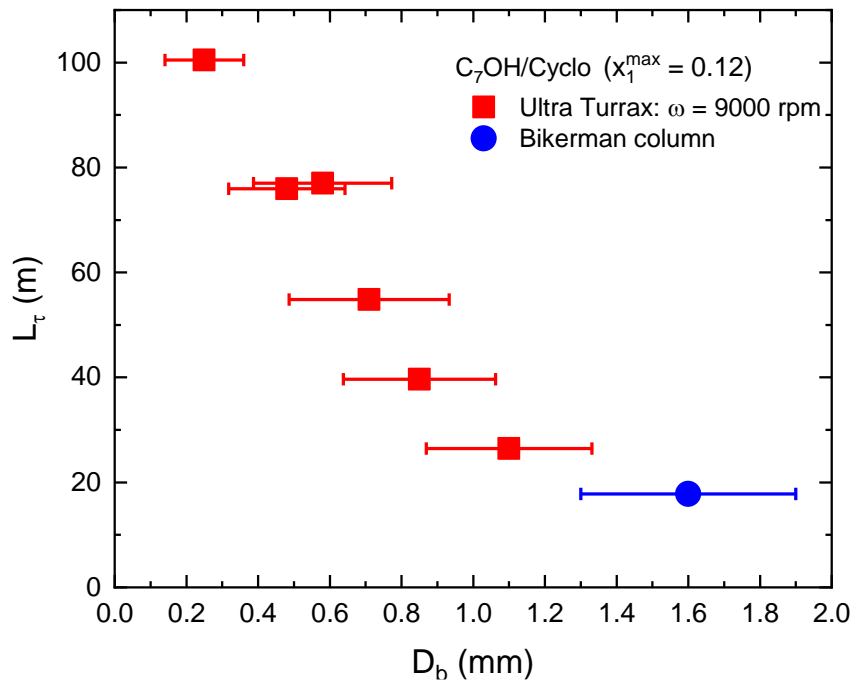


Figure 1-27 : Normalized foam lifetime variations as a function of bubble diameters in the foam. Ultra Turrax experiments – red squares and Bikerman experiment – blue circle. Heptanol/Cyclopentanol mixture (at $x_1^{max} = 0.12$).

Figure 1-27 above depicts the relationship between L_τ and the size of the air bubble introduced into the liquid, obtained from different air flow rates. L_τ decreases with increasing bubble size., the measured test results reveal that when the average size of the bubbles in the foam is reduced by about 10 times, the normalized foam lifetime increases more than 5 times.

To conclude this section, we conducted an experiment using a device called the Ultra Turrax. We can indeed generate bubbles five times smaller than in Bikerman column with this equipment. We may then test the foaming level with the studied liquid mixtures when the bubble sizes are changed. Experiment results demonstrate that the bubble lifetime decreases for increasing bubbles diameter.

1.3. MEASURING THE LIQUID FILM THICKNESS/LIFETIME BY A SINGLE BUBBLE EXPERIMENT

As we've seen in earlier sections, the experiment with the Bikerman column yielded quantitative data on the foamability. Experiments at the macro level, on the other hand, make it impossible to exactly estimate the thickness of liquid films between bubbles as they burst. As a result, we developed a novel measurement method to determine this thickness with single bubble.

Experimental description

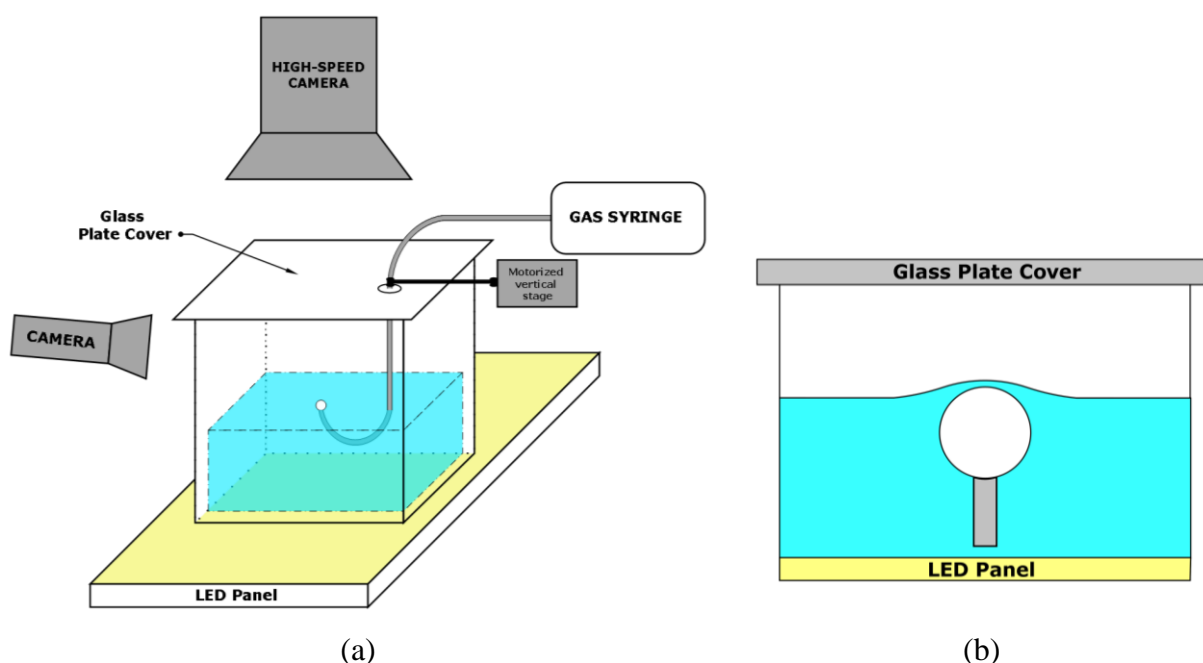


Figure 1-28 : (a) Schematic of the set-up for single bubble experiments; (b) Schematic of the set-up from the side-view.

In order to study thin films of binary liquid mixtures, we have an experimental setup allowing us to measure the bursting speed as well as the life time of single bubble, see **Figure 1-28**. In our experiments, the studied mixture is placed in a reservoir. The size of the box ($5 \times 5 \times 5 \text{ cm}^3$) is much larger than the diameter of the bubbles to avoid any boundary effect. Using a syringe pump, air is injected at a constant flow rate into the mixture through a tube and a metal needle of 1mm diameter, and stopped when a bubble is formed. The needle is placed vertically at a distance of 1 mm from the surface of liquid bath. A motorized vertical translation stage is used to control this distance. A glass cover plate is used to avoid the evaporation effect. A bubble is then formed and

touches the surface in being held with the needle. The volume of the bubble is fixed at $5 \mu\text{L}$. The experiments are performed at the laboratory temperature (25°C). The life time of the bubble is measured with a high-speed camera above of the bath. The bursting speed of the bubble is also estimated from the videos filmed with this high-speed camera.

The whole process is observed by 2 cameras as illustrated in **Figure 1-28**. An LED panel is placed under the liquid bath to illuminate the whole experimental system.

The top view is recorded by a high-speed camera (PHOTRON) and the side view is recorded by a normal camera with a respective framerate of 37500 fps and 30 fps , respectively. The side view camera is tilted at an angle of 5° to avoid meniscus effect on the bath wall. In addition, the camera on the side of the bath also plays a role in capturing the bubble shape which is important, as explained in the next section.

1.3.1. Methods

1.3.1.1. Top-view camera

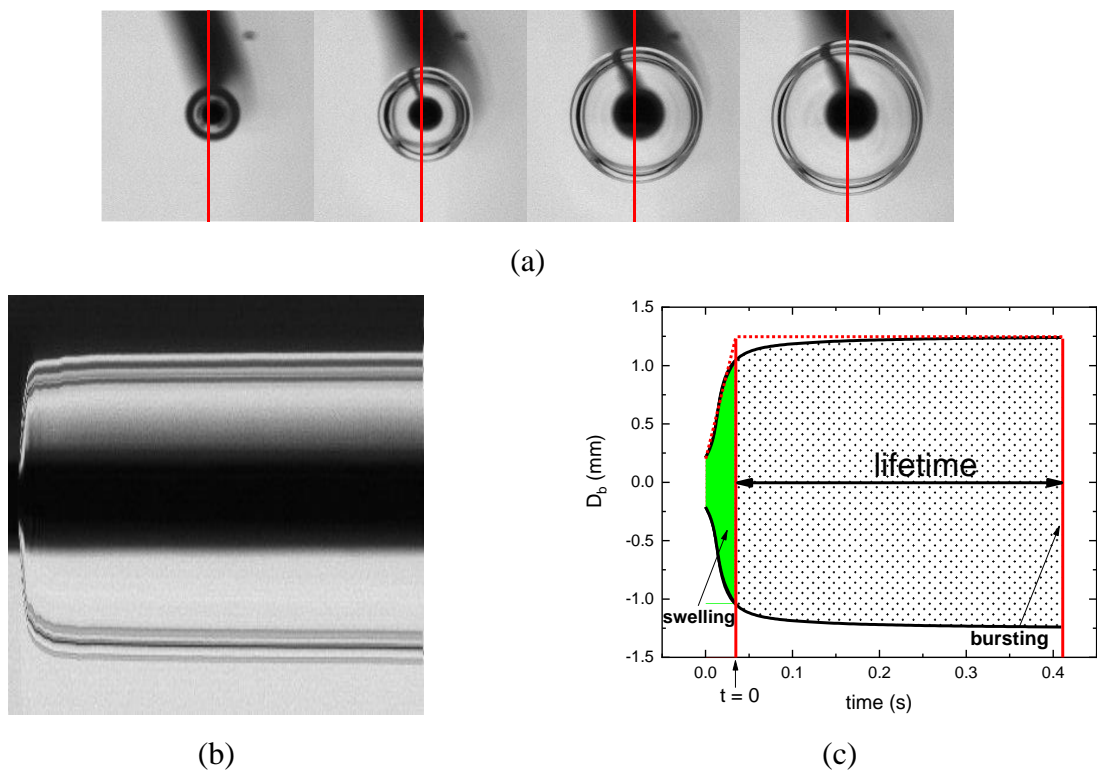


Figure 1-29 : (a) Formation of a single bubble in a Heptanol/Cyclopentanol mixture (at $x_1^{max} = 0.12$); (b) and (c) Spatio-temporal diagram: bubble diameter versus time (horizontal axis). The first stage is represented in green area. The second stage – corresponding to the stable geometry prior bursting – is illustrated by cross pattern zone.

The top-view camera is used to observe the formation, evolution and bursting of bubbles. With this high-speed camera, we can directly determine the size of the bubble and its lifetime when it is visible on the surface. D_b is diameter of the bubble.

The diameter of the bubble is determined from top view images recorded during its swelling. It also deforms the air/liquid interface before bursting. It is clear that the diameter of the bubble always increases due to air injection. **Figure 1-29** shows the bubble diameter as a function of time. Two stages taking place at very different time scales can be considered. In the first stage, the bubble expands linearly with time. This swelling process occurs very quickly, in a few tens of milliseconds. Remarkably, this duration does not appear to be affected by the injected flowrate. This due to the gas compressibility and detailed explanation is given in the **Appendix D**. Then, its size remains practically unchanged during the second stage, until its rupture. The diameter of the bubble is about 2.5 mm.

As a result, we can also define that the bubble lifetime τ is the period of second phase. The initial time $t = 0$ is the intersection of 2 peripheral red dot lines, see **Figure 1-29 (c)**.

Figure 1-30 reports results of the cumulative distribution of bubble lifetimes measured over 50 different experiments of 12% in molar fraction of Decane in the mixture with Toluene. From the collected data, we can observe that the distributions are rather narrow.

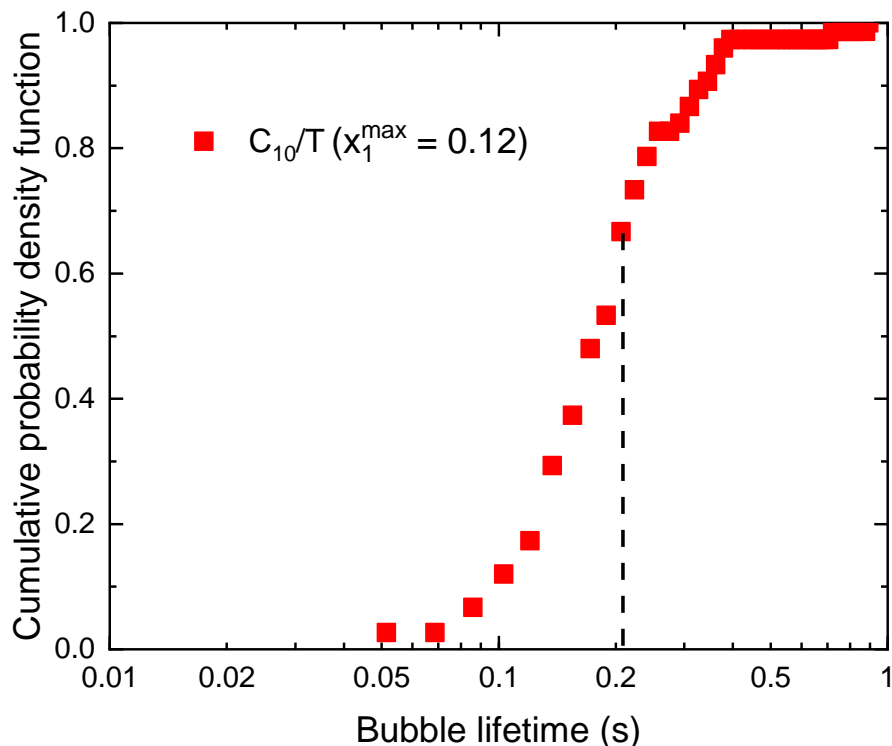


Figure 1-30 : Cumulative probability density function of bubble lifetimes measured at the surface of Decane/Toluene mixture at $x_1^{max} = 0.12$.

In other mixtures, for each composition, the mean bubble lifetimes are statistically determined over a total sampling of 25 experiments under the same experimental conditions, see **Figure 1-31**.

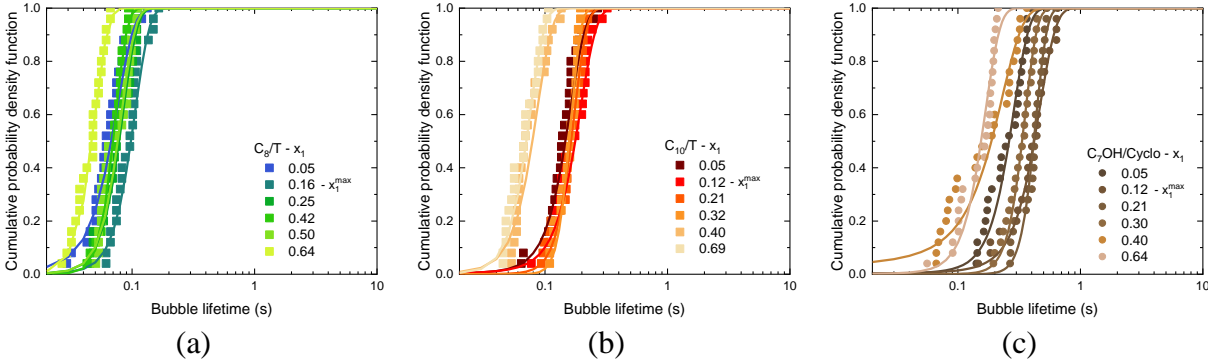


Figure 1-31 : Cumulative probability distribution of bubble lifetimes in the single bubble experiments for different compositions of: (a) Octane/Toluene mixture; (b) Decane/Toluene mixture and (c) Heptanol/Cyclopentanol mixture. Continuous lines indicate the best fits of the data using a log-normal distribution function.

As can be seen in graph above, there is a proportion for each mixture where the lifetime of the bubbles is the maximum. It's defined as x_1^{max} . The difference in bubble lifetimes between the compositions of these mixtures is truly quite small, barely approximately 0.5 s.

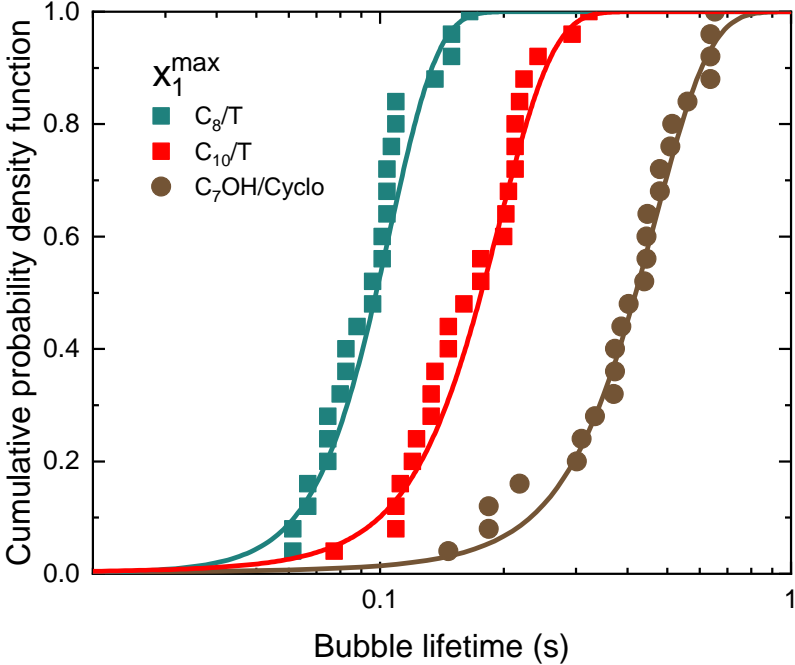


Figure 1-32 : Comparison between cumulative probability distribution of bubble lifetimes with three mixtures: Octane/Toluene, Decane/Toluene and Heptanol/Cyclopentanol at x_1^{max} . Continuous lines indicate the best fits of the data using a log-normal distribution function.

In **Figure 1-33**, we compare the bubble lifetime at x_1^{max} between three different mixtures: Octane/Toluene, Decane/Toluene and Heptanol/Cyclopentanol. As shown by the graph, the life time of the bubbles (scale on the left) has similar variations with composition as the one of the foams measured by Bikerman tests (scale on the right). But there is a factor ten between the respective lifetimes.

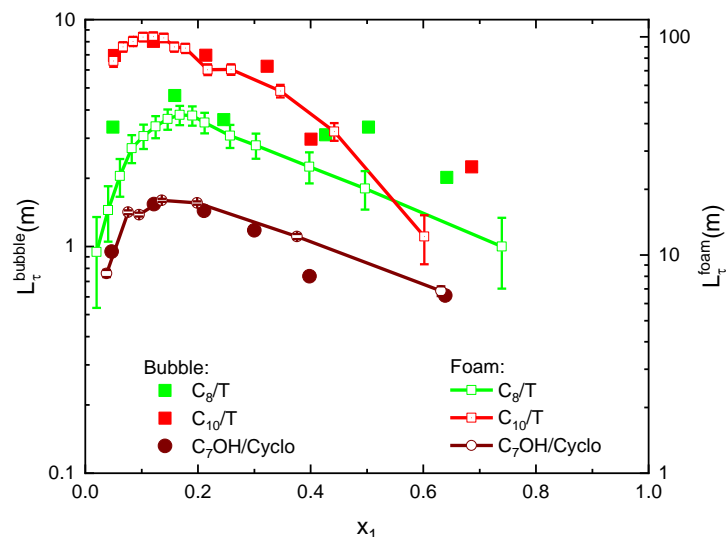


Figure 1-33 : L_t obtained from single bubble experiments and foam experiments as a function of the molar fraction in the mixture of the species with the smallest surface tension. The full points represent the results of the single bubble experiments, while the foam experiments are shown as solid lines with the empty points: Octane/Toluene (green), Decane/Toluene (red) and Heptanol /Cyclopentanol (brown).

In addition, we have measured the film thickness.

1.3.1.2. Side-view camera

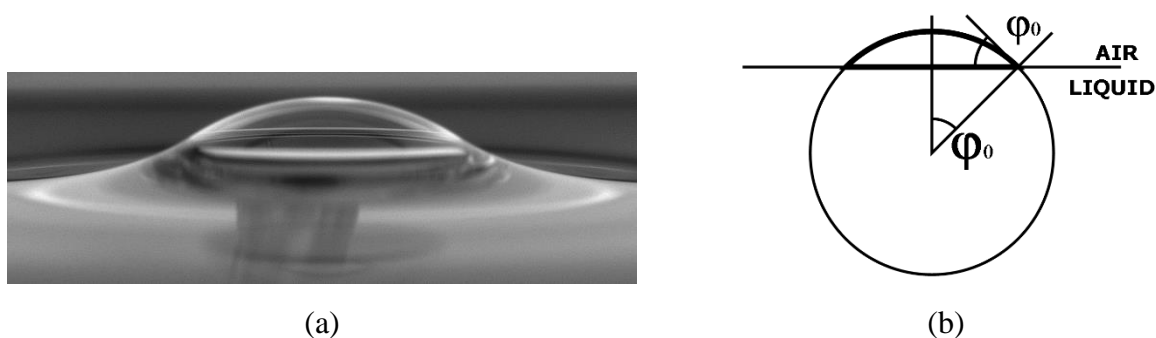


Figure 1-34 : (a) Image of a single bubble in the Heptanol/Cyclopentanol mixture at the air/liquid interface captured by a side-view camera; (b) Schematic of a bubble at the interface from the side. φ_0 is the angle between the upper part of the bubble and the interface.

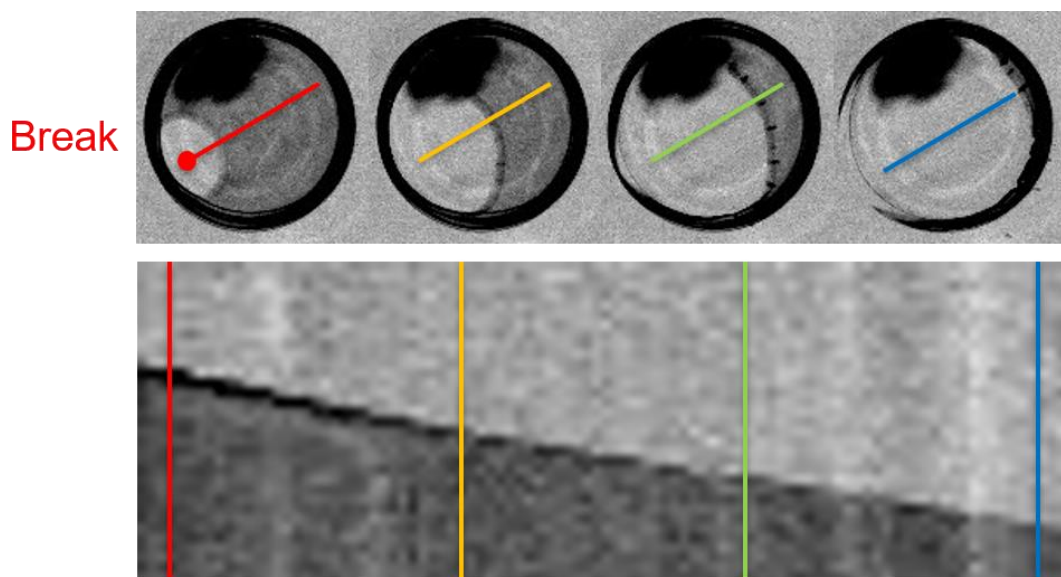
To measure the film thickness, we will measure the growth velocity of the holes in a film after spontaneous piercing. The bubble burst is recorded at 37500fps using the top-view camera. The bubble bursting speed allows us to estimate the film thickness at the time of rupture using Taylor-Culick relation in following section.

The side-view camera also plays an important role in capturing the bubble shape and projection angle of the top view. Bubbles are formed at the air/liquid interface, see **Figure 1-34 (a)**. The upper part of the bubble (above the bath interface) can be fitted by a spherical cap, see **Figure 1-34 (b)**. This cap creates an angle of about $\varphi_0 = 38.5 \pm 1.5$ degrees with the interface. We have found that the value of this angle is found to be nearly independent of the mixture utilized, leading to the conclusion that in our system the piercing is deterministic contrary to what is observed in surfactant foams [22].

1.3.1.3. Taylor-Culick relation

The entire bursting process is recorded to measure Taylor-Culick speed.

From the top view, we can examine break-up kinetics, as shown as in **Figure 1-35 (a)**. A red dot represents the point at which the bubble begins to burst in this graph. We draw a line connecting this breaking point and the center of the bubble. Using Image J, we can obtain a spatio-temporal diagram in which the line taken from each image is represented horizontally, with time represented by the vertical axis. The value received from this opening of the hole with the top view camera, on the other hand, is merely the projections on the horizontal plane.



(a)

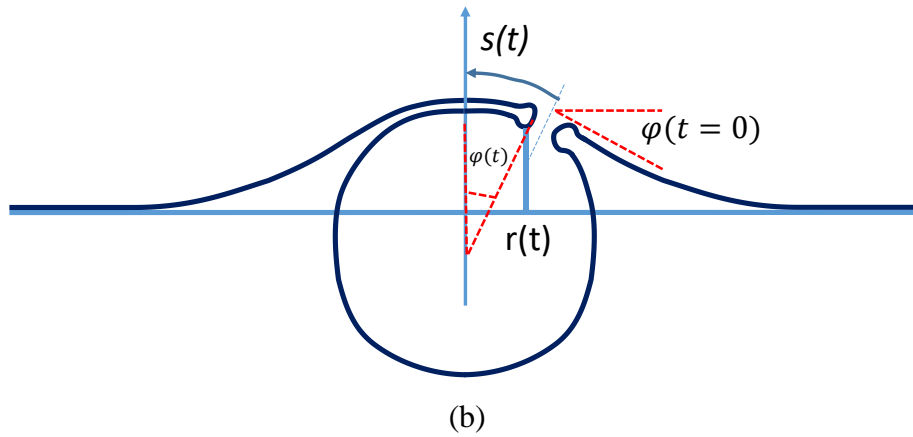


Figure 1-35 : (a) The breaking point is the red dot. A spatio-temporal diagram in which the line taken from each image is represented horizontally, with time represented by the vertical axis; (b) Schematic of a bubble at the surface from the side. The curvilinear length travelled by the edge of the opening hole, $s(t)$, is obtained from both its projection $r(t)$ in the horizontal plane and the angle $\varphi(t)$ measured from top and side views of the bubble.

In order to obtain the projection angle of the top view, we need analyze the supplementary information from the side view, see **Figure 1-35 (b)**. the curvilinear distance travelled by the edge of the opening hole, $s(t)$, is obtained by correcting $r(t)$ with the angle $\varphi(t)$.

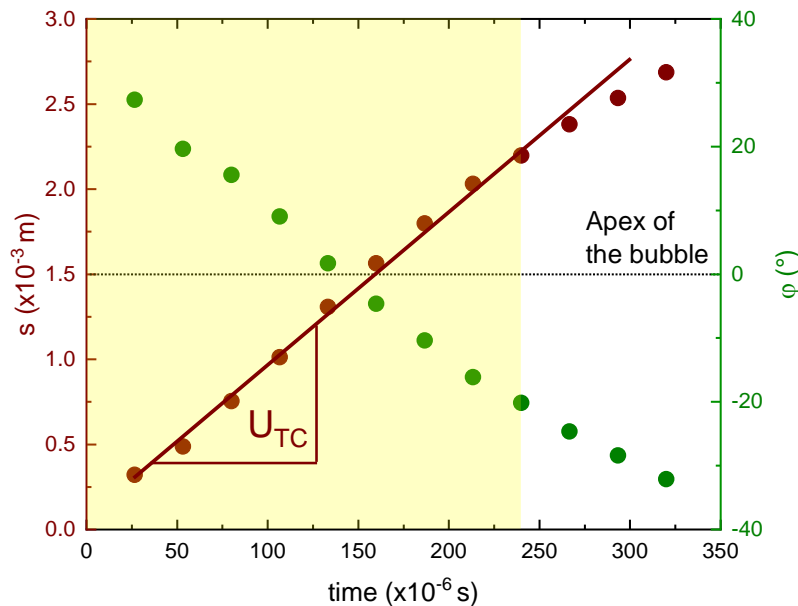


Figure 1-36 : Evolution of the curvilinear length travelled by the edge of the opening hole s (brown circles, left axis) and of the angle φ (green circles, right axis) in the burst as a function of time (Heptanol/Cyclopentanol $x_1 = 0.12$). The hole opens at constant speed during a first stage (yellow zone). The slope of the full line is the Taylor-Culick speed from which the thickness at bursting is inferred.

Figure 1-36 represents the results about the evolution of the opening hole and the angle measurement at the opening hole's edge. As obvious from the figure, $\varphi(t)$ progressively drops to 0 - this position corresponds to the apex of the bubble. After that, it subsequently changes its sign to negative values, indicating that the hole expands on the other half of the air bubble.

This graph also shows us that opening length s increases linearly with the time. The hole opens at constant speed during a first stage. This process is indicated by the yellow zone on the graph, suggesting that the film has a nearly constant thickness. Therefore, we can deduce the opening speed of the hole U_{TC} – the Taylor-Culick speed. We have performed several experiments to determine this speed. From these values, we can also estimate the error bar of the measurements.

The film thickness is determined by using the Taylor-Culick relation between the hole opening speed U_{TC} and film thickness h_b at bursting **[23,24]**:

$$h_b = \frac{2\gamma}{\rho \cdot U_{TC}^2} \quad \text{Eq.1.14}$$

As demonstrated in this "Methods" section, we may quantify the liquid film thickness of a single bubble from the investigated foaming liquid mixtures using the Taylor-Culick relation.

1.3.2. Thickness measurements

We measured the thickness of a thin liquid layer using three different liquid mixtures: Heptanol/Cyclopentanol, Octane/Toluene and Decane/Toluene. We selected three compositions to conduct the experiment for each mixture. The composition corresponds to the maximum foaming level, and the other 2 compositions correspond to the average foam level obtained from the Bikerman column experiment. The measured L_τ are shown in **Figure 1-37**. The normalized foam lifetimes are represented by the thickness of the liquid thin layer, which is computed using the Taylor-Culick speed.

According to **Figure 1-37**, the film has a thickness in the micro-size range, and the normalized foam lifetime changes proportionately to the squared thickness of this film. The h_b error is computed from the Taylor-Culick speed error and is around 30%. We will explain the found variation in the following chapters.

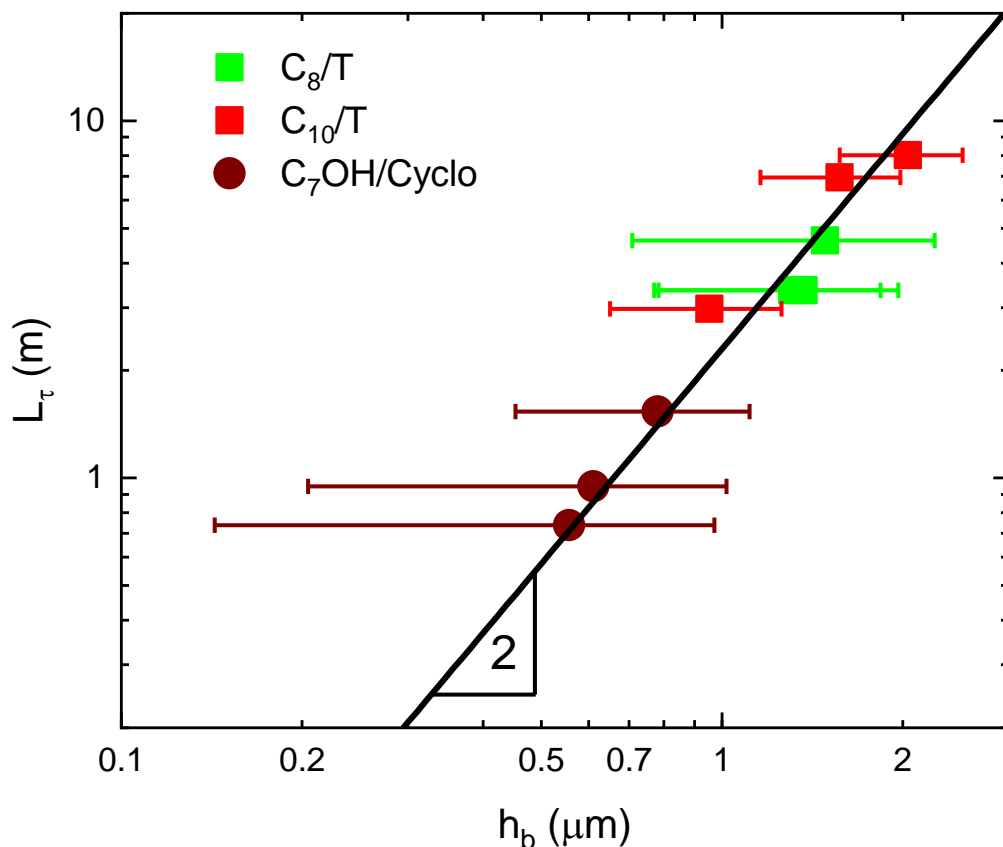


Figure 1-37 : Experimental plot of normalized foam lifetime L_τ as a function of liquid film thickness h_b for studied binary mixtures. The full line is a guide to the eye.

1.4. CONCLUSION

To summarize, we measured normalized foam lifetime L_τ and thickness h_b using different liquid mixes in this chapter.

We observed the following tendencies:

The film lifetime decreases for increasing diameter of bubbles.

The film thickness increases with the film lifetime as a power law with an exponent 2.

In these mixtures, surface tensions vary sublinearly or superlinearly with composition. There is no simple relation between the interfacial tension of mixtures and foamability.

In the following chapters, we will go through these experimental results in further insight. The **Chapter 2** will demonstrate the relationship between normalized foam lifetime L_τ and the physicochemical characteristics of symmetric liquid mixes. **Chapter 3** will discuss asymmetry in liquid mixes and explain why this feature shifts the surface tension curve $\gamma(x)$ from sublinear to super-linear. Furthermore, we will show how the asymmetry and change in shape of the gamma curve have an effect on the normalized foam lifetime L_τ .

Finally, in **Chapter 4**, we will explain why normalized foam lifetime varies as a quadratic function of liquid film thickness h_b .

2. SYMMETRIC BINARY MIXTURES

In the previous chapter, we have shown that stability measurable lifetime – of the order of a few seconds - can be observed in foams and single bubbles of most of the liquid mixtures. In the present chapter, we investigate the mechanisms leading to this effect. In order to keep things simple, this chapter will exclusively cover symmetric mixtures, i.e., mixtures of liquids of similar molecular volumes and surfaces. We will show that differences in concentration in bulk and at interfaces are at the origin of a thickness-dependent surface tension for liquid films, and that this effect is responsible for the existence of a life-time of a few seconds.

The results presented here have been published in a paper that we reproduce at the end of the chapter. Note that in this paper, equations have been derived in the more general case of liquids with different molar surfaces. However, the results were not valid for very asymmetric mixtures, which will be considered in **Chapter 3**. So, in this text we will limit ourselves to the case of symmetric (same molar volume and surface) molecules.

In the present chapter, in a first part, we will introduce the experimental liquid mixtures tested. Then, in the next part, we propose a mechanism for the stabilization of thin films of liquid mixtures based on the non-linear variation of the mixture's surface tension with its composition. We show that this phenomenon is at the origin of a thickness-dependence of the surface tension. Lastly, we present experimental data on the lifetimes of foams in binary mixtures and compare them to the predictions made by this proposed mechanism.

2.1. DEFINITIONS OF SYMMETRIC BINARY MIXTURES

2.1.1. Used symmetric binary mixtures

Table 5 : The characteristics of used liquids. The molar surfaces were calculated using the cuboid molecule approximation from the molar volumes.

Mixture	Liquid 1	Liquid 2	σ_1 ($km^2.mol^{-1}$)	σ_2 ($km^2.mol^{-1}$)
<i>Linear alkane</i> <i>/Toluene</i>	Heptane (C ₇)	Toluene (T)	0.24	0.19
	Octane (C ₈)	Toluene (T)	0.25	0.19
	Nonane (C ₉)	Toluene (T)	0.27	0.19
	Decane (C ₁₀)	Toluene (T)	0.28	0.19
<i>Linear alcohol</i> / <i>Cyclopentanol</i>	Pentanol (C ₅ OH)	Cyclopentanol (Cyclo)	0.19	0.17
	Hexanol (C ₆ OH)	Cyclopentanol (Cyclo)	0.21	0.17
	Heptanol (C ₇ OH)	Cyclopentanol (Cyclo)	0.23	0.17
<i>Linear alcohol</i> / <i>Linear alcohol</i>	Pentanol (C ₅ OH)	Nonanol (C ₉ OH)	0.19	0.26
<i>Linear alkane</i> / <i>Linear alkane</i>	Heptane (C ₇)	Octane (C ₈)	0.24	0.25
	Octane (C ₈)	Decane (C ₁₀)	0.25	0.28

In the present chapter, we focus on binary mixtures that are symmetric in size, i.e., those in which the surface area of the molecules has close values:

$$\sigma_1 \approx \sigma_2 \quad \text{Eq.2.1}$$

where σ_i is the molar surface of species i in the liquid mixture.

Assuming that the molecules are cubic in shape, we can compute the surface of a molecule $\sigma_{molecule}$ from its volume:

$$\sigma_{molecule} = v_{molecule}^{\frac{2}{3}} \quad \text{Eq.2.2}$$

For one mole of N_A molecules, the molar surface σ , thus, is:

$$\sigma = v^{\frac{2}{3}} N_A^{\frac{1}{3}} \quad \text{Eq.2.3}$$

In **Table 5**, we report the molar surface values of the investigated alcohol/alcohol as well as alkane/Toluene mixtures. Since for each mixture the molar surfaces differ by less than 40%, we will consider them as symmetric mixtures in the following.

2.2. THEORETICAL INTERPRETATIONS & MODELLINGS

2.2.1. Qualitative explanation of the stabilization mechanism

We suggest that the stabilization mechanism of liquid films in mixtures is based on the fact that the concentrations of species are different in the bulk and at the interfaces with air. The species with the smallest surface tension are always more concentrated at the interfaces than in the bulk. In the case of symmetric mixtures, this difference results in sublinear variations of surface tension with composition, as observed in most of the mixtures listed in **Table 5**.

Because of these concentration differences, the surface tension is expected to be thickness-dependent in thin films: if a film thins down while its volume remains constant, its interfaces area increase modifying the partition between interfaces and bulk as schematized in **Figure 2-1**. As a result, the interfaces of thin films are less concentrated in species with the smallest surface tension as compared to the one of large thicknesses. This leads to an increase of the surface tension of the film for decreasing thicknesses.

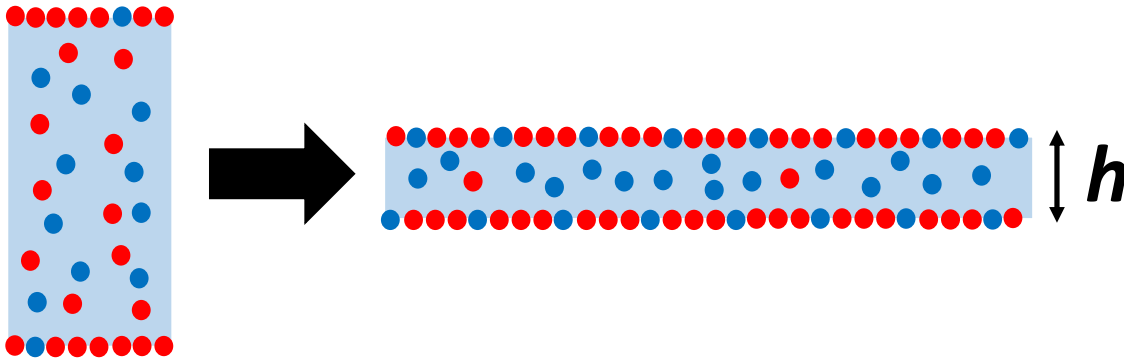


Figure 2-1 : Schematical explanation of the thickness-dependent surface tension of a film of liquid mixture. As the film thins down at constant volume the concentrations at the interfaces cannot be kept constant, leading to a new equilibrium in which the interfacial concentration of the (red) species with the smallest surface tension is smaller, and thus the surface tension is larger. The thickness of the liquid film is designated by h .

In the following, we show the increase of surface tension can be written as:

$$\gamma(h) = \gamma \left(1 + \frac{\alpha}{h} \right) + O(h^{-2}) \quad \text{Eq.2.4}$$

where γ is the surface tension of the liquid in an infinitely large liquid reservoir, h the local thickness of the film. In addition, α is a length characteristic of the mixture and depending on its composition, which will be explained in more detail later.

In the following, we show that the increase of surface tension in films that thins down make a partial mechanical equilibrium possible at the end of the formation process of films. We make the assumption that the film's thermodynamic equilibrium is instantaneous between the bulk and the film's surfaces. Indeed, for a 1 micron-thick film, the characteristic time of diffusion over the film thickness h^2/D , with D the diffusion coefficient of molecules (typically $10^{-9} \text{ m}^2 \cdot \text{s}^{-1}$), is of the order of 1 ms. It is actually rather short in comparison to the other characteristic times involved in the life and death of a liquid film. So, in all this work, we will assume an instantaneous equilibrium between bulk and interfaces concentrations.

2.2.2. Picture of life and death of a foam

Within the foam, films are connected to menisci called Plateau borders in which the capillary pressure drop induces a suction. As liquid is drawn off the film, foam destabilization may be separated into two distinct stages, each happening at different timescales. Stretching of liquid films occurs as a first stage as depicted in **Figure 2-2**. The surface tension is homogeneous and an extensional flow is created, like in liquid films with mobile surfaces in which no pinching occurs [25]. During this stage, liquid drainage is negligible and the film can be considered to stretch at constant volume. As a result, its surface to volume ratio grows. Because the species with the lowest surface tension are more prevalent on the surface than in the bulk, thinning is associated with an increase in surface tension in the flat parts of the liquid films.

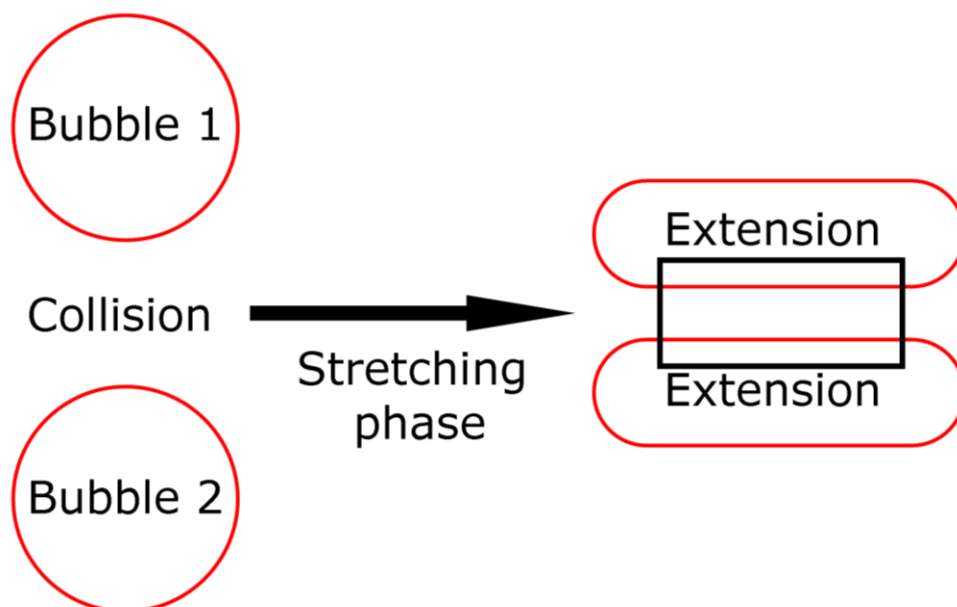


Figure 2-2 : Sketch illustrating the stretching phase. Two air bubbles encounter in the liquid mixture. These bubbles will deform and create a liquid film at the contact zone. It is a fast extension phase of the liquid film in the plug-shape ($\sim 10^{-4} \text{ s}$).

The increase of surface tension allows equilibrium of the liquid film tension (that is sum of the pressure times thickness and surface tension contribution) to be reached between the flat part of the film and the Plateau border it is connected with. This equilibrium is reached at the end of the first “stretching” stage.

However, film tension balance equilibrium does not mean that there is a pressure balance and in a second stage, the film drains because of pressure difference between the flat and curved parts of the films. We can expect the interfaces experience zero-velocity (solidlike) conditions [26] and the drainage flow is Poiseuille flow. Due to the short duration of the first stretching stage, it is the slowest draining stage that determines the film lifetime. The key parameter for this lifetime is the thickness of the film at the beginning of the drainage stage. In the following we denote h_f this thickness. Since it corresponds to the thickness reached when a tension equilibrium is attained, we show in the following it is possible to derive h_f , and that the only parameters it depends on are the length α and the radius of curvature of the Plateau border R_f .

2.2.3. Shape of the film at mechanical equilibrium

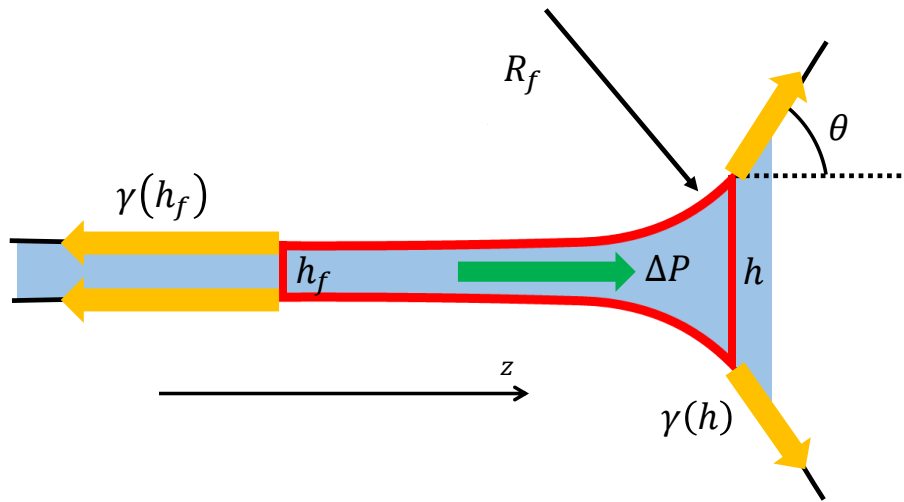


Figure 2-3 : Diagram showing the forces acting on a fluid film of thickness h_f connected to a Plateau border in the foam. The flat part's higher surface tension allows for mechanical balance even if the pressures are not equilibrated. A tension balance along the z-axis can be written on the film portion in red.

In this section we show that, when mechanical equilibrium of film tension is reached, the shape of the film can be determined analytically. We consider the film of thickness h_f is connected to a Plateau border schematized in **Figure 2-3**.

Film tensions write: $2\gamma(h) \cos[\theta(z)] + \Delta P(h)h(z)$. The film equilibrium imposes this tension to be constant. Because the film is in its middle part flat, the constant is simply two times the interfacial tension for which $\theta = 0$ and $\Delta P(h) = 0$. This yielding at any z :

$$2\gamma(h_f) = 2\gamma(h) \cos[\theta(z)] + \Delta P(h)h(z) \quad \text{Eq.2.5}$$

where $\theta(z)$ is the local angle of the film with the z -axis direction. $\Delta P(h) = \gamma(h)d^2(h/2)/dz^2$ is the Laplace pressure difference between the gas and the liquid in the meniscus written in the thin-film approximation with first-order terms only.

It is also important to note that at small angles, the angle between the film and the z -direction may be approximated by $\cos(\theta(z)) \cong 1 - \frac{1}{2} \left(\frac{\partial h/2}{\partial z} \right)^2$.

Substituting the expression of γ for two parts from **Eq.2.4** in **Eq.2.5**, the mechanical equilibrium for the film becomes:

$$2\gamma \left(1 + \frac{\alpha}{h_f} \right) = \gamma \left(1 + \frac{\alpha}{h} \right) \left(2 - \frac{1}{4} \left(\frac{\partial h}{\partial z} \right)^2 + h \frac{\partial^2 h}{2\partial z^2} \right) \quad \text{Eq.2.6}$$

Here, we present the dimensionless variables $H(\zeta)$, which are defined as $h(z)/h_f$ and $\xi = z/w$, respectively, where w denotes an unknown characteristic length in the direction of z . Additionally, we add the dimensionless number, $Y = \alpha/h_f$. In practice, $Y \ll 10^{-3}$, as will be demonstrated in the next section. Expanding **Eq.2.6** in Y leads at first order to:

$$\frac{4Yw^2}{h_f^2} \left(\frac{1}{H} - 1 \right) + \left(-\frac{1}{2} H'^2 + HH'' \right) + O(Y^2) = 0 \quad \text{Eq.2.7}$$

We emphasize the equation simplifies to the basic equation of pressure equilibrium in the film when $Y = 0$, i.e., the surface tension is constant. This means that for $Y=0$, $H = a(\xi - b)^2$ is the unique solution, and a and b are constants. Thus, a flat film cannot be connected to a Plateau boundary with this parabolic solution and is thus not physically sound. As a result, only if the surface tension is thickness dependent can a meaningful solution to **Eq.2.6** be obtained. A natural value of lateral length is $w = h_f Y^{-1/2} = h_f^{3/2} / \alpha^{1/2}$. **Eq.2.7** can then be solved by using H as a variable. We denote $\Theta(H) = \frac{1}{2} \frac{dH}{d\xi}$ the dimensionless slope of the interface.

Therefore, $H'' = 2\Theta' \frac{dH}{d\xi} = 4\Theta\Theta'$, and **Eq.2.7** becomes, if expressed as a function of the variable H :

$$\left(\frac{1}{H} - 1 \right) - \frac{\Theta(H)^2}{2} + H\Theta(H)\Theta'(H) = 0 \quad \text{Eq.2.8}$$

The general solution is $\Theta = \frac{\sqrt{1-2H+H^2k}}{\sqrt{H}}$ where k is a constant to be determined. The value of k must be such that Θ tends toward zero when H approaches unity, where the flat film is reached. This

leads to $k = 1$. To sum-up, if the thickness of the film is dependent on the surface tension, a solution exists linking a flat film and a Plateau boundary. This solution writes:

$$\theta = \frac{H - 1}{\sqrt{H}} \quad \text{Eq.2.9}$$

Integrating with respect to ξ yields the explicit inverse function of the solution to the implicit equation in Eq.2.9:

$$\sqrt{H} - 2 + \frac{1}{2} \text{Log} \left(3 - \frac{6}{\sqrt{H} + 1} \right) = \xi - c \quad \text{Eq.2.10}$$

where c is an integration constant.

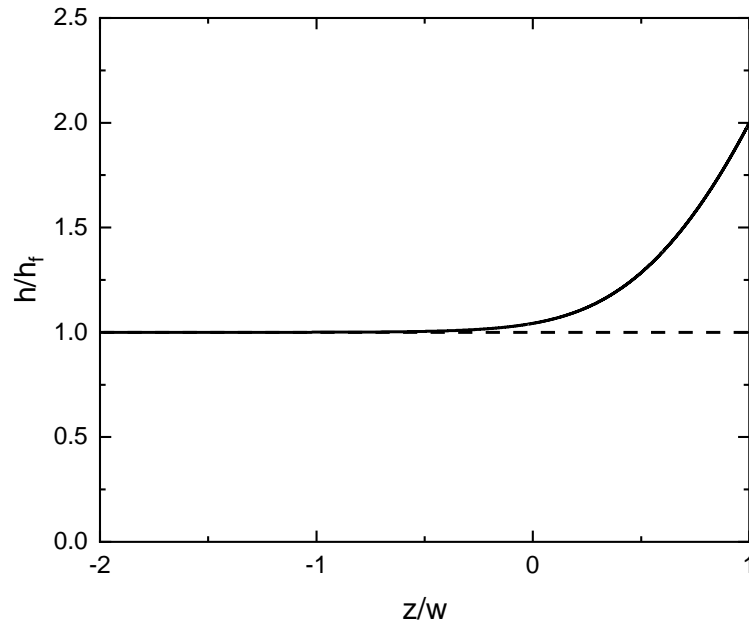


Figure 2-4 : Solution to Eq.2.10 giving the profile of the interface of a liquid film in mechanical equilibrium.

$H = 2$ at $\xi = 1$ is an arbitrarily chosen value. The solution is plotted in **Figure 2-4**

In a foam, the curvature of the Plateau border and the meniscus curvature are both equal to the meniscus curvature for a single bubble, as one might predict from the meniscus curvature $h''/2$.

The curvature is $1/R_f$, which we lead to:

$$\lim_{z \rightarrow \infty} h''/2 = \frac{h_f}{w^2} = \frac{1}{R_f} \quad \text{Eq.2.11}$$

Combining **Eq.2.11** and **Eq.2.8** gives the relations:

$$h_f = \sqrt{\alpha R_f} \quad \text{Eq.2.12}$$

And:

$$w = \alpha^{1/4} R_f^{3/4} \quad \text{Eq.2.13}$$

After the stretching stage and before considerable drainage, the film thickness and the characteristic lateral length are simply functions of the Plateau border radius and the microscopic length α , which originates from the concentration partition of molecules between the bulk and surface.

In the next sections we consider the differences in concentration in the bulk and at the interfaces with and we further derive the microscopic length α .

2.2.4. Partition of molecules in the volume and at the interface

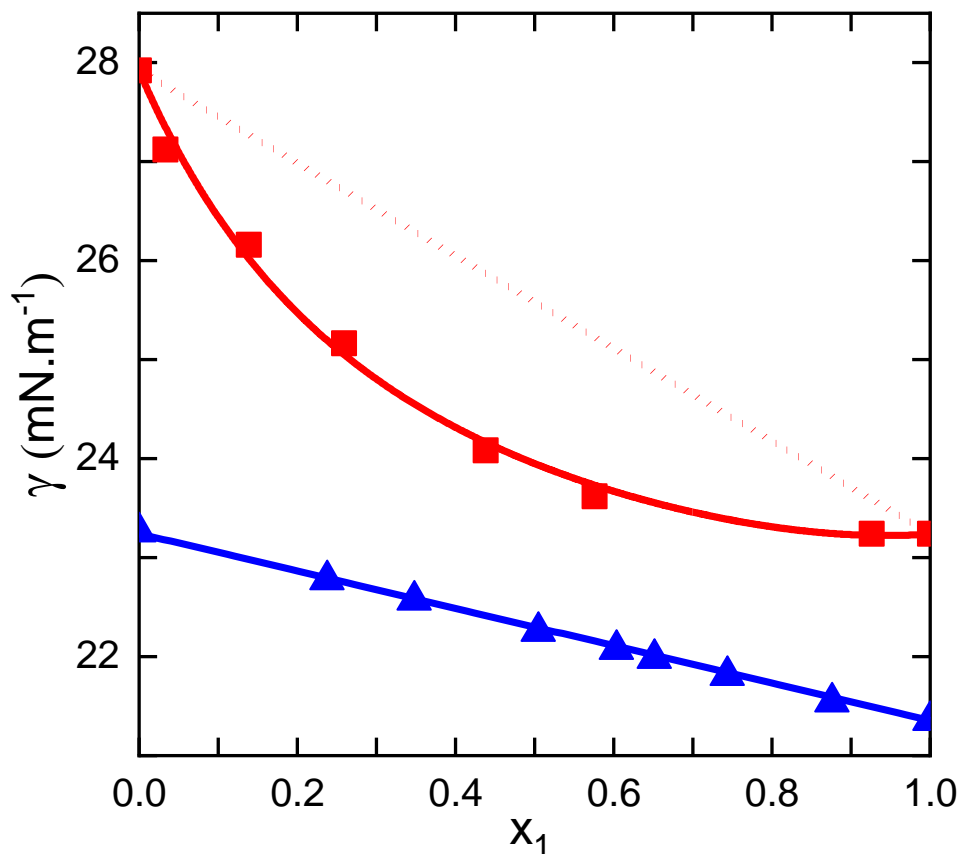


Figure 2-5 : Surface tensions of Decane/Toluene (red) and Octane/Decane (blue) mixtures as a function of the molar fraction of the species with the lowest surface tension (respectively, Decane and Octane). The full lines are guides for the eye.

As pointed out above, in symmetric binary mixtures, the sublinear variation of surface tension with composition result from concentration differences in the bulk and at the interfaces with air: the species with the smallest surface tension is more concentrated at the interfaces than in the bulk. Different models are available to relate surface tension and surface concentrations.

Here, we use a very simple phenomenological relation in which a linear relationship between surface tension γ and the molar fractions of each species on the surface Γ_i ($i = 1, 2$) is thus assumed [27]:

$$\gamma = \Gamma_1\gamma_1 + \Gamma_2\gamma_2 \quad \text{Eq.2.14}$$

where γ and γ_i ($i = 1, 2$) are the surface tensions of the mixture and of the pure components, respectively. Note that in this relation, there is no assumed partitions between the interface and bulk. In **Chapter 3**, we will use an exact model assuming ideal solutions and interfaces to describe the surface tension of binary mixtures, including very asymmetric ones, and we will detail the link between bulk and interface concentrations. But for the purpose of the discussion in the present chapter, the phenomenological relation of **Eq.2.15** is enough to describe the main features of symmetric mixtures.

Substituting $\Gamma_2 = 1 - \Gamma_1$ in **Eq.2.14**, a relation is established between γ and Γ_1 :

$$\Gamma_1 = \frac{\gamma - \gamma_2}{\gamma_1 - \gamma_2} \quad \text{Eq.2.15}$$

By measuring the surface tension of the binary mixture, it is possible to deduce the surface concentrations from this relation. We can remark that the surface population is the same as the bulk population when the interfacial tension varies linearly with the bulk composition, i.e. $\Gamma_1 = x_1$, see **Figure 2-5**. Further, we show that this scenario relates to non-foaming mixtures in the next section.

We consider a mixture of two liquids with two molecules 1 and 2 of initial molar fraction x_1^0 (respectively x_2^0) measured in mol/mol.

A film of thickness h and surface area S is created from a volume V^0 of this mixture, of initial molar fraction x_1^0 (respectively x_2^0) measured in mol/mol.

The surface-to-volume ratio S/V increases with decreasing film thickness, affecting bulk molar fractions x_i . Therefore, we note x_1 (respectively x_2) the molar fraction of molecules 1 (respectively 2) in the bulk in the case of a film.

By definition of the molar fraction, we have:

$$x_1^0 + x_2^0 = x_1 + x_2 = 1 \quad \text{Eq.2.16}$$

For both liquids, the volume per mole, as well as the area per mole, is considered to be the same, and that-is-to-say: $v_1 = v_2 = v$ and $\sigma_1 = \sigma_2 = \sigma$. On the surface, we have obviously:

$$\Gamma_1 + \Gamma_2 = 1 \quad \text{Eq.2.17}$$

The total amount of species 1 writes:

$$\frac{\Gamma_1}{\sigma} S + \frac{x_1}{v} V = \frac{x_1^0}{v} V^0 \quad \text{Eq.2.18}$$

with V the volume of the bulk of film, and V^0 the initial volume.

Similarly, we get the conservation equation for molecules of liquid 2:

$$\frac{\Gamma_2}{\sigma} S + \frac{x_2}{v} V = \frac{x_2^0}{v} V^0 \quad \text{Eq.2.19}$$

Combining molecular conservation with constant volume and surface densities and replacing $S = 2V^0/h$, a geometrical relation between x_1 and x_1^0 may be obtained:

$$x_1 - x_1^0 = \frac{2v}{h\sigma} (x_1^0 - \Gamma_1) \quad \text{Eq.2.20}$$

Linearizing the dependence of the surface tension with composition yields:

$$\gamma(h) - \gamma = \left(\frac{\partial \gamma}{\partial x_1} \right)_{x_1=x_1^0} (x_1 - x_1^0) \quad \text{Eq.2.21}$$

with γ is the surface tension of the binary mixture at $x_1 = x_1^0$.

Substituting **Eq.2.15** in the above expression, the final relation giving the thickness-dependent surface tension of a film of a binary mixture is:

$$\gamma(h) - \gamma = \frac{2}{h} \left(\frac{\partial \gamma}{\partial x_1} \right)_{x_1=x_1^0} \frac{v}{\sigma} (x_1^0 - \Gamma_1) \quad \text{Eq.2.22}$$

Eq.2.22 is true in the limit $h \gg v_i/\sigma_i$ (with species i having the largest molecules), corresponding to thicknesses ten times larger than the molecular size, i.e., to about 10 nm.

The derivative of $\gamma(x_1)$ is calculated using experimental data surface tension dependence on the molar fractions.

Note that in the case of linear variation of the surface tension with the initial composition, that writes $\gamma = \gamma_1 x_1^0 + \gamma_2 (1 - x_1^0)$ as explained in the beginning of this section, leads to $\Gamma_1 = x_1$. From eq.2.22 we deduce: $\gamma(h) - \gamma = 0$. It follows as a result that for liquid mixtures with a linear variation of the surface tension, there is no possible foaming. This is indeed what we observed experimentally for alkane/alkane mixtures. The thickness-dependent surface tension is consequently related to nonlinear variations in surface tension. Note that this result only valid if $\sigma_1 = \sigma_2$ ($v_1 = v_2$), or, to put it another way, for symmetric mixtures.

2.2.5. Characteristic length α – foamability

Following, we write **Eq.2.22** in the form of:

$$\gamma(h) = \gamma \left(1 + \frac{\alpha}{h} \right) \quad \text{Eq.2.23}$$

Or, α – the characteristic length can be expressed as the following, which is equivalent to the previous equation:

$$\alpha = \frac{\gamma(h) - \gamma}{\gamma} h \quad \text{Eq.2.24}$$

Therefore, the increase in surface tension in a thin film may be estimated if α is known. To put that into perspective, we can evaluate the foaming capacity of symmetric liquid mixtures by finding α .

It is possible to calculate α using the molar volumes and surfaces of the two liquids and the derivative of $\gamma(x_1)$:

$$\alpha = \frac{2}{\gamma} \left(\frac{\partial \gamma}{\partial x_1} \right)_{x_1=x_1^0} \frac{v}{\sigma} (x_1^0 - \Gamma_1) \quad \text{Eq.2.25}$$

Using the data acquired from foaming tests with Bikerman column experiments, we will compare our predictions to the experimental data in the next section to see if our theoretical model is correct. To obtain α , we use the fit of **Eq.1.13** to get the derivative of the interfacial tension versus x and $(x_1^0 - \Gamma_1)$ from **Eq.2.14** with **Eq.2.25**.

2.3. COMPARISON TO EXPERIMENTAL DATA

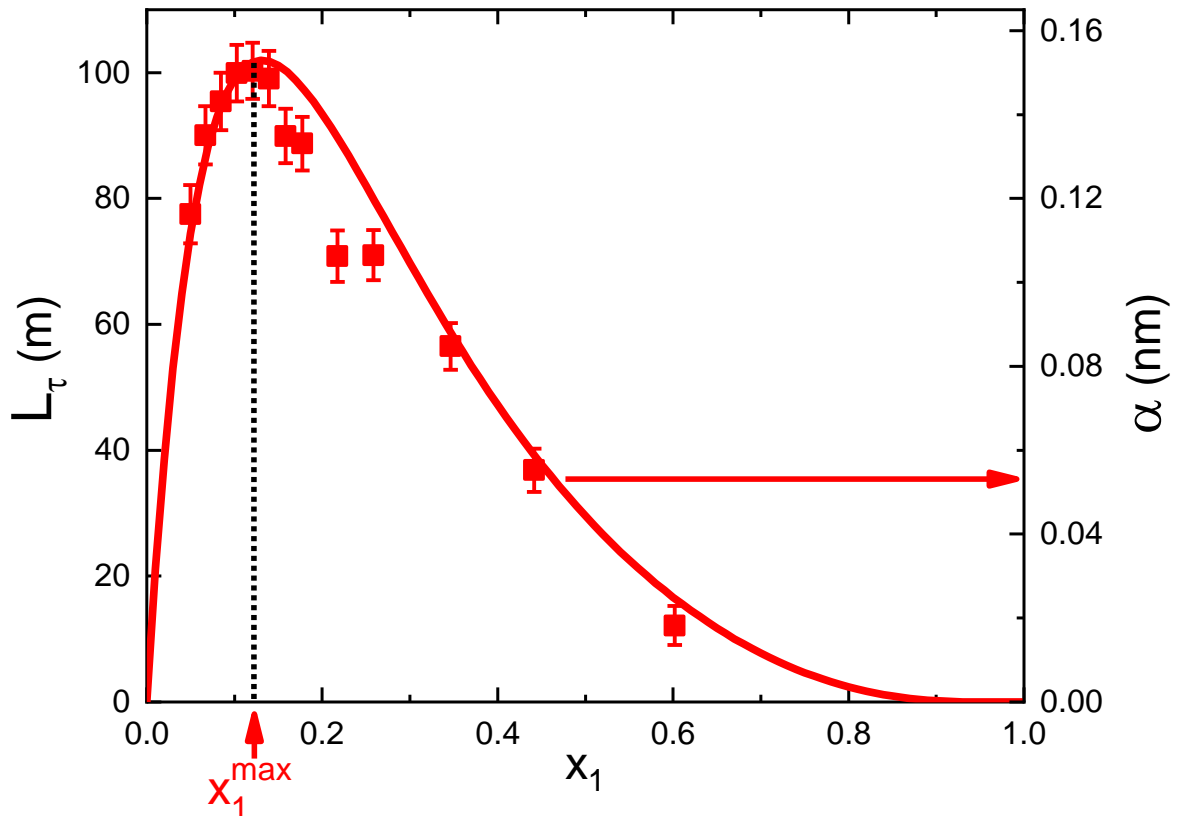


Figure 2-6 : Experimental L_τ (squares, left axis) as a function of Decane molar fraction for mixture of Toluene with Decane. Error bars correspond to uncertainties on measured foam heights. The length α (right axis) characterizing the relative surface tension variation with film thickness computed from Eq.2.25 is shown as a solid line.

We show here that the experimental variations in L_τ with mixture composition are correlated with the variations of α . According to **Eq.2.25**, all of the parameters are either constants of liquids or deduced from the fit of surface tension data. For Decane/Toluene mixtures, the comparative results are shown in **Figure 2-6**. Reminding that the ability to foam, as computed by the length α , occurs at the nanoscopic scale. Meanwhile, the measured lifetimes specify the length L_τ ranging from meters to 100 m . A linear correlation between two quantities is seen. It is important to note that the length α is of the order of a tenth of nanometer, i.e., very small, yet the difference in surface tension is substantial, $\Delta\gamma \sim 10^{-3} \text{ mN} \cdot \text{m}^{-1}$ for a film thickness $h = 1 \mu\text{m}$.

We can in addition compare the maximum foamability composition next denoted by x_1^{\max} , using equation **Eq.1.13** and **Eq.2.25** (see also how to compute the maximum foam position in the **Appendix E**). We see in **Figure 2-7** that the position of maximum foamability is quantitatively predicted.

Furthermore, there was no foam in alkane mixtures. Since the surface tensions of these mixtures vary in a quasi-linear way (see **Figure 2-5**), so the thickness dependence of the surface tension is not expected, according to **Eq.2.25**, in agreement with the data.

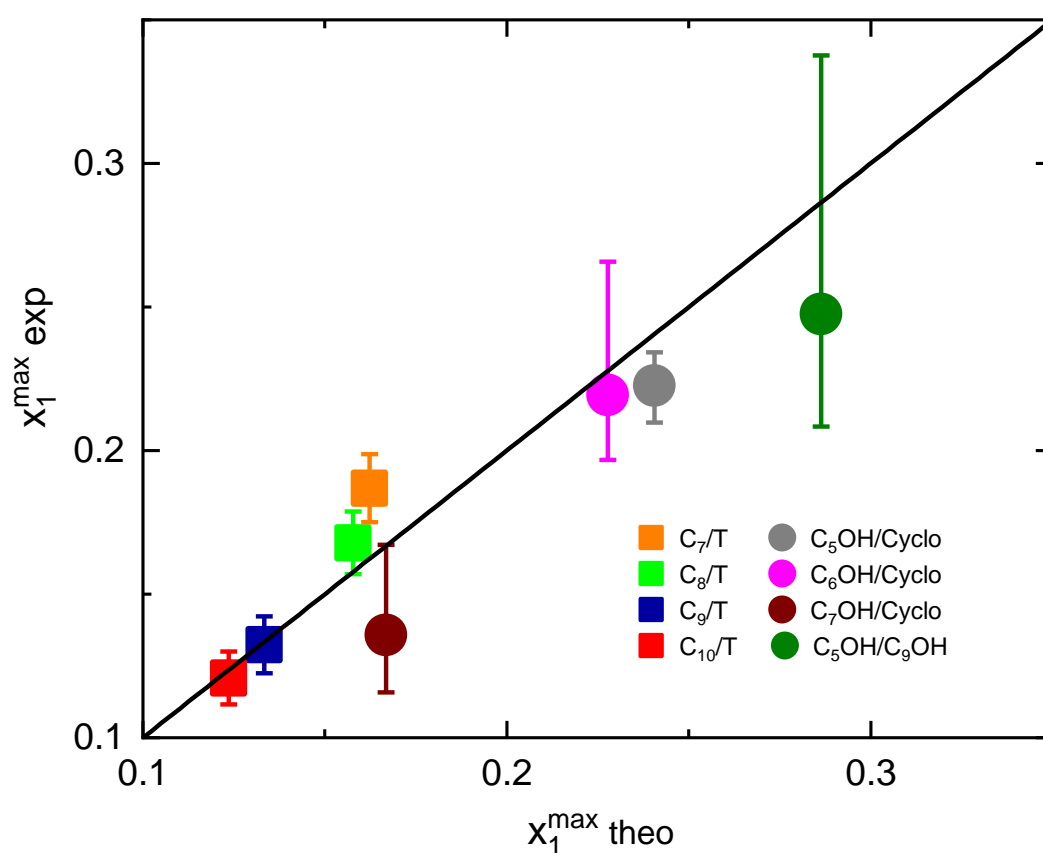


Figure 2-7 : Molar fraction for which the foamability was measured to be maximum as a function of its value predicted.

In **Figure 2-8**, the experimental data L_τ obtained in a Bikerman column are compared to the length α estimated for all mixtures. L_τ and α are both normalized by the maximum values found in each mixture. A master curve for symmetric mixtures can be seen in **Figure 2-8**, which shows that both polar and non-polar liquids have their data plotted onto it. It suggests that L_τ is proportional to α . Since we have shown that $h_f = \sqrt{\alpha R_f}$, it implies that L_τ should vary with h_f^2 . This is indeed what we have observed (see section 1.3.2). We will explain this dependency in **Chapter 4**, in which we consider the last instants of liquid films.

We attribute the dispersion of the data to the poor determination of the molar surfaces. We recall we have made the rough approximation of cuboid molecules in order to compute the molar surfaces from the molar volumes. Molar surfaces cannot be directly measured; therefore, a model must always be used to determine them. In **Chapter 4**, we further investigate the link between foam and bubble lifetimes (or length L_τ) and we will show that it is possible to compare them with only measured quantities instead of using the non-measured length α , that is estimated from an estimated value for molar surface.

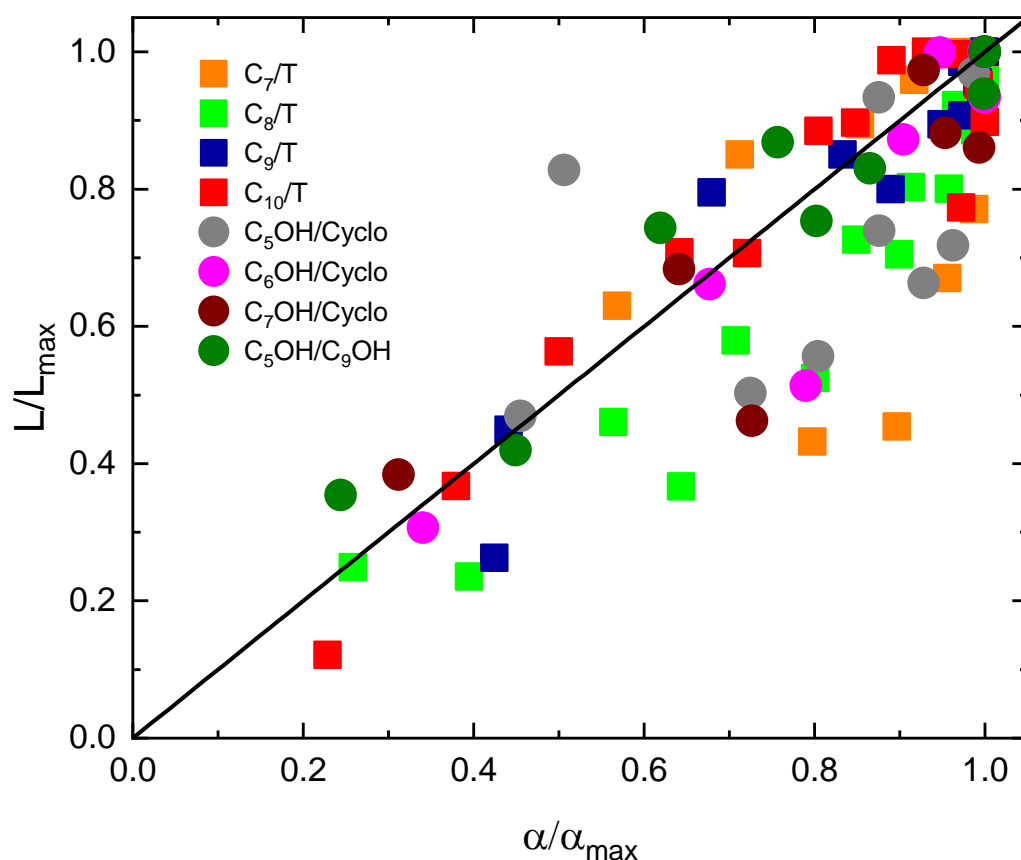


Figure 2-8 : L_τ as a function of α for 8 different liquid mixtures. Both L_τ and α are normalized by their maximum values found in each mixture which are reached for the same composition. The full line is a guide to the eye.

2.4. CONCLUSION

We have shown that partition of species between bulk and interfaces controls mixture foamability. This is in fact a surfactant-like behavior, where the species with the smallest interfacial tension plays the role of surfactant for the other species. This mechanism is at the origin of the enhanced stability of foams in liquid mixtures, as demonstrated in this chapter. The molecules of the liquid in the mixture with the lowest surface tension are concentrated at the interface. This results in a non-linear variation in surface tension in symmetric mixtures as a function of composition. Due to this non-linear variation, the mixture has a thickness-dependent surface tension. Moreover, the thickness-dependent surface tension of liquid films is related to foamability. Finally, the experimental variations of surface tension with composition may be used to estimate the thickness of the liquid films before drainage. All these results are presented in our published paper that shows that the thickness of the liquid film and foamability are correlated for liquids of different polarity. The precise relation between the foam life-time and the physico-chemistry will be explained more detail in **Chapter 4**.

Remark on the notations: in the following article, we have used the notation γ_{∞} , while we use γ in all the manuscript, because the subscript ∞ is not necessary for the understanding of the manuscript.

2.5. PUBLICATION

GLOSSARY OF ABBREVIATIONS

γ	<i>Surface tension</i>	γ_{∞}	<i>Surface tension</i>
σ	<i>Molar area</i>	ν	<i>Molar volume</i>
L	<i>Column height</i>	R	<i>Column radius</i>
Q	<i>Injected air flowrate</i>	D	<i>Diffusion coefficient</i>
ΔP	<i>Laplace pressure</i>	Γ	<i>Surface molar concentration</i>
H	<i>Foam height</i>	H_0	<i>Initial liquid height</i>
τ	<i>Foam lifetime</i>	μ	<i>Viscosity of mixture</i>
V	<i>Liquid film volume</i>	S	<i>Liquid film surface</i>
h	<i>Liquid film thickness</i>	h_f	<i>Liquid film thickness before drainage</i>
x	<i>Molar fraction</i>	α	<i>Length characterizing the foamability</i>
R_b	<i>Bubble radius</i>	φ_l	<i>Liquid volume fraction of foam</i>

Understanding Frothing of Liquid Mixtures: A Surfactantlike Effect at the Origin of Enhanced Liquid Film Lifetimes

H.-P. Tran,^{1,2} M. Arangalage,^{1,2} L. Jørgensen^{1,2}, N. Passade-Boupat^{3,4}, F. Lequeux,^{1,2} and L. Talini^{1,2,*}

¹*CNRS, Sciences et Ingénierie de la Matière Molle, ESPCI Paris, PSL Research University, Sorbonne Université, 75005 Paris, France*

²*Laboratoire Physico-Chimie des Interfaces Complexes, ESPCI, 10 rue Vauquelin, 75005 Paris*

³*Laboratoire Physico-Chimie des Interfaces Complexes, Bâtiment CHEMSTARTUP, Route Départementale 817, 64170 Lacq, France*

⁴*Total S.A., 64170 Lacq, France*



(Received 22 May 2020; accepted 8 September 2020; published 21 October 2020)

The formation of froth in mixtures of liquids is well documented, particularly in oil mixtures. However, in nonvolatile liquids and in the absence of surface-active molecules, the origin of increased liquid film lifetimes had not been identified. We suggest a stabilizing mechanism resulting from the nonlinear variations of the surface tension of a liquid mixture with its composition. We report on experimental lifetimes of froths in binary mixtures and show that their variations are well predicted by the suggested mechanism. We demonstrate that it prescribes the thickness reached by films before their slow drainage, a thickness which correlates well with froth lifetimes for both polar and nonpolar liquids.

DOI: 10.1103/PhysRevLett.125.178002

Foams are metastable dispersions of gas in liquids. In recent decades, the processes at the origin of their finite lifetimes have been extensively studied in surfactant solutions [1]. Among the destabilizing mechanisms, one results from the capillary drainage of liquid films in the Plateau borders where three liquid films meet. The pressure drop associated with the curved gas-liquid interfaces at the Plateau borders induces a capillary suction of the liquid, leading to film thinning. In the presence of surfactants adsorbed at the interfaces, thinning can be opposed by a repulsion between both film interfaces, of either a steric or a charge-induced nature. In addition, film rupture can be delayed by the surface tension gradient originating from a local extension of the film surface. A local decrease in surfactant concentration generates an increase in surface tension, driving a Marangoni flow opposing drainage [2]. A measurement of that effect is the Gibbs elasticity, whose associated modulus relates the excess surface tension to the relative increase of surface area [3,4]. However, the influence of Gibbs elasticity on foam stability is still an open question [5].

Marangoni flows are also invoked to explain the large influence of contaminants on the stability of liquid films, even in the absence of purposely added surfactants [6]. However, in pure liquids of low surface tensions such as oils, contaminant-induced effects are small and the lifetime of films is so short that no foaming is generally observed in pure nonpolar liquids. In contrast, mixtures of liquids have been shown to form froths, i.e., poorly stable foams, even with nonpolar liquids, as first evidenced decades ago [7]. Using binary and ternary mixtures, froth lifetimes up to a

few tens of seconds were reported that increased in the vicinity of critical points. As in pure liquids, the net interaction between interfaces of a liquid film are attractive owing to van der Waals forces. Since they are also free of surfactants, a new stabilizing mechanism has to be invoked in these liquids. In order to clearly distinguish the mechanism of thin films stabilization from the effect of disjoining pressure, we will call the phenomenon frothing instead of foaming. The frothing behavior was attributed to the variations of surface activity occurring before phase separation but was not quantitatively described. Similar findings were reported in the literature for mixtures of partially miscible liquids [8,9]. One of the salient features is the existence of a sharp maximum of a foam lifetime at a given mixture composition.

More recently, asymmetric evaporation in liquid mixtures has been pointed out to be responsible for the stabilization of foams in some oil mixtures [10]. When the component with the smaller surface tension is the more volatile, its evaporation results in a surface tension gradient generating a Marangoni flow that stabilizes a liquid film. In contrast, when the more volatile component has the larger surface tension, the Marangoni effect is expected to destabilize films.

In this Letter, we report on frothing experiments with mixtures of fully miscible liquids that are either polar or nonpolar. In agreement with past results, the lifetimes of the formed foams are small (a few tens of seconds) and exhibit a maximum with compositions of mixtures. Stabilization does not result from evaporation-induced Marangoni effects since evaporation has a destabilizing effect in most

mixtures. In addition, in the peculiar systems in which surface and bulk are of close compositions with extremely fast exchanges between them, there is no effect of interfacial viscosity. In contrast, we show that the experimental data can be quantitatively described by introducing a thickness-dependent surface tension of the liquid mixture, resulting from concentrations of the species at the interface with air slightly different from the bulk ones. Within this context, we will show that the only condition for frothing consists of nonlinear variations of surface tensions of mixtures with their compositions.

We have investigated the frothing behavior of binary mixtures of toluene and linear alkanes and of cyclopentanol and linear alcohols, respectively. An additional mixture of linear alcohols was tested. All liquids were high purity (>99%) ones supplied by Sigma-Aldrich. The linear species were of different carbon chain lengths: from heptane to decane for the alkanes and from pentanol to heptanol for the alcohols. The surface tension of alkanes (alcohols) increases with the length of the carbon chain but is smaller than the surface tension of toluene (cyclopentanol) in the investigated range [11]. The surface tensions of all liquids were systematically measured with a Teclis rising bubble tensiometer. In the following, the surface tension of a mixture is denoted as γ ; γ_i ($i = 1, 2$) is the surface tension of pure liquid i , and x_i is its molar fraction in the mixture. Liquid 1 refers to the species with the lowest surface tension, i.e., either the linear alkane or linear alcohol. The surface tension difference is $\Delta\gamma = \gamma_2 - \gamma_1$ and $\Delta\gamma > 0$.

For all alkane-toluene and alcohol-cyclopentanol mixtures, the surface tension was found to exhibit a sublinear variation [12] similar to the one for decane and toluene shown in Fig. 1. It suggests the existence of a surface adsorption layer for the species with the lower surface tension, such as the one evidenced both numerically [12] and experimentally [13] in water-alcohol mixtures. We show in the following that it is at the origin of the enhanced lifetimes of films of liquid mixtures. In contrast, the surface tension of alkane mixtures (such as the one in Fig. 1) varies linearly, with the composition indicating identical bulk and surface compositions.

Surface tension variations can be described using available models for binary mixtures. A simple approximation considers linear variation of surface tension with surface molar concentrations of each species Γ_i ($i = 1, 2$) [14]:

$$\gamma \approx \Gamma_1 \sigma_1 \gamma_1 + \Gamma_2 \sigma_2 \gamma_2, \quad (1)$$

where σ_i is the molar area of species i .

Writing $\Gamma_2 \sigma_2 = 1 - \Gamma_1 \sigma_1$ and replacing it in Eq. (1) provides a relation between γ and Γ_1 . Surface concentrations can thus be inferred from the surface tension values of the binary mixture. In the case of a linear variation of the interfacial tension with bulk composition, the surface

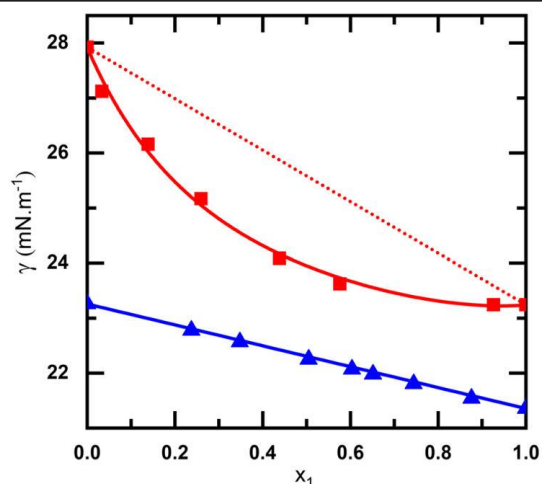


FIG. 1. Surface tensions of decane-toluene (red) and octane-decane (blue) mixtures as a function of the molar fraction of the species with the lowest surface tension (respectively, decane and octane). The full lines are guides for the eye.

population is the same as the bulk one, i.e., $\Gamma_i \sigma_i = x_i$. In the following we show that case corresponds to non-foaming mixtures.

More elaborate models for surface tensions of mixtures are available; we have tested one in which molecular interactions are accounted for by a Flory parameter [15] and found that it equivalently described our frothing data. Therefore, our analysis is not model dependent, and in the following we use the simple approximation of Eq. (1).

Foaming experiments were performed with Bikerman columns [16,17], i.e., glass columns of radius $R = 1$ cm and height $L = 30$ cm with a porous filter at their bottom (Robu; porosity, 10–16 μm). The columns were filled with liquids up to a height $H_0 = 10$ cm and were part of a closed air circuit, in which air was continuously pumped and injected through the porous at flow rate $Q = 6$ ml s⁻¹ [11]. The stationary froth height H reached was measured from video images. The froth lifetime, corresponding to the time during which bubbles were convected before bursting, is defined as $\tau = H\pi R^2/Q$. We have checked to see that it does not depend on initial height H_0 and flow rate Q in the probed ranges. Since capillary drainage is the destabilizing mechanism of the studied froths, time τ is expected to linearly vary with liquid viscosity μ [18,19]. Mixture viscosities were either measured with a rheometer (Low Shear 400, Lamy Rheology) or computed using the empirical Kendall-Monroe equation [20], shown to be adequate for alkane-toluene mixtures [21]. In the following, we report on values of the ratio τ/μ , which provides a measurement of foamability that is independent of both the injection conditions and liquid viscosity.

Figure 2 shows the ratio τ/μ as a function of the alkane molar fraction x_1 for the different alkane-toluene mixtures.

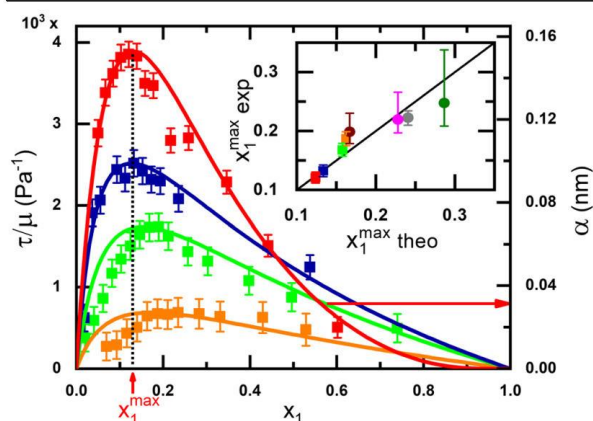


FIG. 2. Experimental foamability (squares) defined as the ratio of foam lifetimes and liquid viscosities (left axis) as a function of alkane molar fraction for mixtures of toluene with decane (red), nonane (blue), octane (green), and heptane (orange). Error bars correspond to uncertainties on measured foam heights. The length α characterizing the relative surface tension variation with film thickness [Eq. (5)] is shown as a solid line. The scale of right axis is for the decane-toluene mixture only; other α curves are in arbitrary units. Inset: molar fraction for which the foamability was measured to be maximum as a function of its value predicted by Eq. (4). Data for alkane-toluene (squares) and alcohol-cyclopentanol mixtures (circles, as in Fig. 4). Horizontal error bars are too small to be visible.

In agreement with past results [7], the variations of both time τ and foamability τ/μ are nonmonotonic, whereas the viscosity varies monotonically with composition. A maximum for τ/μ is reached at an alkane fraction slightly dependent upon the length of the carbon chain of the alkane. The maximum value of the foamability more strongly depends on the alkane: it is, for instance, about 4 times larger for decane than for heptane. Similar features were found with alcohol-cyclopentanol mixtures [11].

We attribute the frothing behavior of mixtures to the role of the different species at the interface: the nonlinear variations of surface tension of mixtures with linear alkane or alcohol fraction indicates that the surface concentration of alkane or alcohol, respectively, is larger than its bulk one. It suggests the existence of a surface adsorption layer of molecular thickness such as the one in water-alcohol mixtures [12,13]. The ability to quickly pump molecules from the bulk to the layer results in a thickness-dependent surface tension, which is at the origin of the enhanced stability of thin films in liquid mixtures.

More precisely, we consider a liquid film of thickness h and surface S . As the thickness h is much smaller than the other dimensions, all processes occurring along the h direction can be considered instantaneous compared to the ones in lateral directions. In particular, the characteristic molecular diffusion time through the film thickness $h^2/D \approx 1$ ms (with D the diffusion coefficient and $h = 1 \mu\text{m}$), is

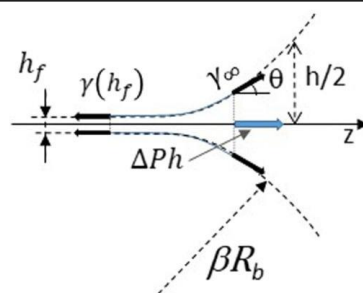


FIG. 3. Schematic of a liquid film of thickness h_f connected to a Plateau border in the foam and the forces (per unit length) it is submitted to.

small compared to the timescales of the processes we consider. Consequently, we assume that thermodynamical equilibrium between bulk and surfaces of the film is reached instantaneously.

Within the foam, films are connected to menisci called Plateau borders in which the capillary pressure drop induces a suction (see Fig. 3). As liquid is drawn off the film, two stages occurring at very different timescales can be considered. At a first stage, surface tension is uniform and an extensional flow is established, as in liquid films with mobile interfaces in which no pinching occurs [22]. The film is stretched and gets thinner at almost constant volume, and, at one point, its surface concentration in the species with the lowest surface tension must decrease because its surface-to-volume ratio has increased. Surface tension thus increases in the film, allowing equilibrium of tensions to be reached. From that instant, thinning is further associated with surface tension gradient, resulting in a zero-velocity (solidlike) condition at the interfaces [23]. The flow is therefore a much slower Poiseuille flow, and the film is further subjected to marginal pinching [24]. No full theoretical description is available for the latter process, and it is out of the scope of this Letter. However, since the first stretching stage is short, it is the slow drainage stage that sets the film lifetime, which therefore depends on the initial thickness. The latter, which we denote as h_f , is the one reached at the end of the first stage, when the increase of surface tension in the film exactly compensates for the capillary suction and tension in the meniscus. Considering that the equilibrium reached at that point allows for the determination of h_f , our analysis is based on the assumption that the film lifetime correlates with the value of h_f .

As schematized in Fig. 3, the film of thickness h_f is connected to a Plateau border. Pressure equilibrium is not reached, but equilibrium of the tensions in the film is nevertheless satisfied, yielding at any z

$$2\gamma(h) \cos[\theta(z)] + \Delta P(h)h(z) = 2\gamma(h_f), \quad (2)$$

where $\theta(z)$ is the local angle of the film with the z -axis direction and $h(z)$ is the local film thickness.

$\Delta P(h) = \gamma(h)d^2(h/2)/dz^2$ is the Laplace pressure difference between the gas and the liquid in the meniscus written in the thin-film approximation with first-order terms only. The right-hand term of Eq. (2) is the left-hand term written in the flat part of the film for which $\theta = 0$ and $\Delta P(h) = 0$. Equation (2) is similar to the one for film equilibrium with significant disjoining pressure [25]. Here, disjoining pressure is negligible since h_f is assumed to be large, and equilibrium is reached because surface tension in the flat film is larger than at the Plateau border.

We now show that the thickness-dependent surface tension $\gamma(h)$ can be derived from the variations of surface tension with composition. We assume that the film, of total surface S , is formed from a volume V_0 of the mixture, of the initial molar fractions x_i^0 in the species of the respective molar volumes v_i ($i = 1, 2$), and of the equilibrium surface tension $\gamma_\infty = \gamma(x_i^0)$. As the film thins down and

its surface-to-volume ratio S/V increases, its bulk molar fractions x_i vary. A geometrical relation between x_i and x_i^0 can be derived by combining the conservation of molecules $\Gamma_i S + x_i V/v_i = x_i^0 V_0/v_i$ and the constant volume and surface densities $\sum_i x_i^0 = \sum_i x_i = \sum_i \Gamma_i \sigma_i = 1$:

$$x_1 - x_1^0 = \frac{S[v_1 \Gamma_2 \sigma_2 (-1 + x_1^0) + v_2 (1 - \Gamma_1 \sigma_1) x_1^0]}{S v_2 (-1 + \Gamma_1 \sigma_1) + (V_0 - S v_1 \Gamma_1) \sigma_2}. \quad (3)$$

Further expanding that relation in powers of S and using the linearized relation $\gamma(h) - \gamma_\infty = (x_i - x_i^0)(\partial\gamma/\partial x_i)_{x_i=x_i^0}$, we obtain the asymptotical limit of surface tension variation. Replacing surface concentrations with their expressions, inferred from Eq. (1), and replacing S with V_0/h finally yields

$$\gamma(h) - \gamma_\infty = \frac{2}{h} \left(\frac{\partial\gamma}{\partial x_1} \right)_{x_1=x_1^0} \left(\frac{\frac{v_1}{\sigma_1} (\gamma_\infty - \gamma_2) (1 - x_1^0) + \frac{v_2}{\sigma_2} (\gamma_\infty - \gamma_1) x_1^0}{\gamma_2 - \gamma_1} \right) + O\left(\frac{1}{h^2}\right). \quad (4)$$

Equation (4) is valid in the limit $h \gg v_i/\sigma_i$ (with species i being the one with the largest molecules), corresponding to thicknesses much larger than the molecular size. In this range, the second-order term of the expansion is smaller than the first-order one and $\gamma(h)$ remains larger than γ_∞ .

According to Eq. (4), the effect of stabilizing liquid films vanishes for finite thicknesses provided that the surface tension varies linearly with composition, i.e., $\gamma_\infty = \gamma_1 x_1^0 + \gamma_2 (1 - x_1^0)$. Nonlinear variations of surface tensions are therefore at the origin of the thickness-dependent surface tension.

In the following, we write Eq. (4) under the form

$$\gamma(h) = \gamma_\infty (1 + \alpha/h), \quad (5)$$

where α is a characteristic length that can be computed from molar volumes and surfaces of the two liquids and from the derivative of $\gamma(x_1)$. Calculation of the latter is performed with empirical functions fitting the experimental data (full line in Fig. 1). We have found α ranges from 10^{-2} to 10^{-1} nm, which corresponds to surface tension variations of a few $\mu\text{N m}^{-1}$ for a $1\text{-}\mu\text{m}$ -thick film. The increase of surface tension is therefore very small but large enough to induce Marangoni effects.

In light of the previous analysis, the experimental variations of foamability with mixture composition can be compared to the ones of α , and they are in excellent agreement, as shown in Fig. 2. The values of α correspond to the decane-toluene mixture only, with other α curves being shown in arbitrary units to superimpose with foamability, with which the relation is not linear (see the following). A similar agreement was found for polar mixtures [7], in

particular, the composition for maximum foamability was quantitatively predicted (inset of Fig. 2). In addition, no froth could be observed in alkane mixtures. As detailed above, these mixtures exhibit quasilinear variations of their surface tensions and, according to Eq. (4), vanishing film lifetimes are expected, which is consistent with observations.

Furthermore, the thickness h_f reached by the film before it significantly drains can be determined using Eq. (2). Injecting the expression for $\gamma(h)$ yields a differential equation satisfied by $h(z)$ at equilibrium. The equation can be solved numerically and we have found that, in the meniscus, the asymptotical solution to that equation is of parabolic form, $h(z) \cong 2h_f + z^2 \alpha/h_f^2$, provided that $\alpha/h_f \ll 1$ [11]. In foams, the meniscus corresponds to a Plateau border whose curvature radius can be written as βR_b , where R_b is the bubble radius and β is a numerical prefactor that depends on the liquid volume fraction of the foam, φ_l , following $\beta = \sqrt{\varphi_l/0.33}$ [26]. Within this framework, a simple relation is obtained for the thickness h_f reached by the liquid films before their slow drainage:

$$h_f \cong \sqrt{\alpha \beta R_b}. \quad (6)$$

In addition, an estimate of the liquid volume fraction of the foam can be obtained by writing the drainage equation of foams in a stationary state [26]. Assuming that the foam is a packing of bubbles whose permeability is given by the Kozeny-Carman equation, we find $\varphi_l \approx 0.1$ for all mixtures, yielding $\beta = 0.55$.

Thickness h_f can thus be computed for all mixtures from Eq. (6), and in Fig. 4 it is compared to the experimental

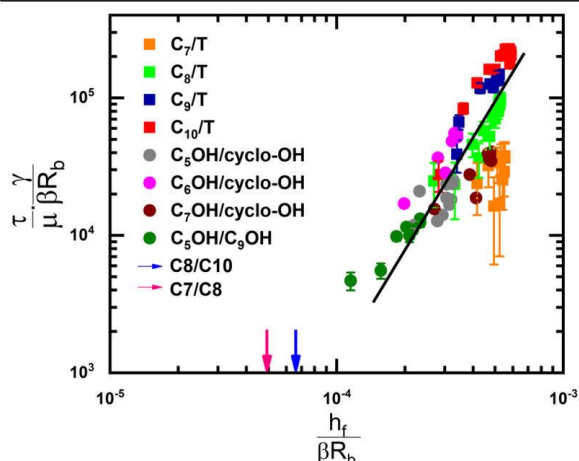


FIG. 4. Dimensionless foamabilities of alkane-toluene and alcohol-cyclopentanol mixtures as a function of the ratio of the predicted film thickness computed from Eq. (6) and the radius of curvature of the Plateau border, βR_b . The full line is a guide for the eye. Bubble radius $2R_b = (1.6 \pm 0.3)$ mm was measured to be independent of the nature and composition of the mixture, as well as $\beta = 0.55$. Arrows indicate the thickness values predicted in mixtures in which no foam could be observed.

foamability, made dimensionless by multiplying it by the Laplace pressure difference. Despite the strong approximation of Eq. (1), foamability and thickness h_f correlate and Fig. 4 clearly evidences the existence of a master curve, onto which the data fall for both polar and nonpolar liquids in which frothing is observed. In the case of alkane mixtures, thicknesses h_f computed from the quasilinear variations of surface tension with composition are shown by arrows. In these mixtures, no froth height could be measured, and the found values of h_f were consistently the smallest of all mixtures.

Finally, we emphasize that $h_f \approx 100$ nm, which correspond to negligible van der Waals attraction. It demonstrates that, consistently, the stabilizing effect we depict is of larger range than the van der Waals forces.

In conclusion, we have shown that the frothing of liquid mixtures is explained by a surfactantlike behavior of the liquid of smaller surface tension. A thickness-dependent surface tension of the mixture results from the nonlinear variations of surface tension with composition and it is the resulting thickness-dependent surface tension of liquid films that quantifies the foamability of the mixture. Within this framework, the thickness reached by the liquid films before drainage can be computed from the experimental variations of surface tension with composition. As expected, this thickness and the foamability correlate for liquids of different polarities. This demonstrates the universal nature of the effect, which can have large consequences on processes in which mixtures of liquids are in contact with gases, such as transport of oil in pipes or food processing.

*Corresponding author.

laurence.talini@espci.fr

Present address: CNRS, Surface du Verre et Interfaces, Saint-Gobain, 93300 Aubervilliers, France.

- [1] B. Petkova, S. Tcholakova, M. Chenkova, K. Golemanov, N. Denkov, D. Thorley, and S. Stoyanov, Foamability of aqueous solutions: Role of surfactant type and concentration, *Adv. Colloid Interface Sci.* **276**, 102084 (2020).
- [2] Y. Couder, J.M. Chomaz, and M. Rabaud, On the hydrodynamics of soap films, *Physica (Amsterdam)* **37D**, 384 (1989).
- [3] A. Prins, C. Arcuri, and M. Vandente, Elasticity of thin liquid films, *J. Colloid Interface Sci.* **24**, 84 (1967).
- [4] M. Vandente, J. Lucassen, and E. Lucassen, Application of surface thermodynamics to Gibbs elasticity, *J. Phys. Chem.* **69**, 1798 (1965).
- [5] S. D. Stoyanov and N. D. Denkov, Role of surface diffusion for the drainage and hydrodynamic stability of thin liquid films, *Langmuir* **17**, 1150 (2001).
- [6] H. Lhuissier and E. Villermaux, Bursting bubble aerosols, *J. Fluid Mech.* **696**, 5 (2012).
- [7] S. Ross and G. Nishioka, Foaminess of binary and ternary solutions, *J. Phys. Chem.* **79**, 1561 (1975).
- [8] J. Gracia, C. Guerrero, J.G. Llanes, and A. Robledo, Transient foaminess, aggregate formation, and wetting behavior in water-phenol mixtures, *J. Phys. Chem.* **90**, 1350 (1986).
- [9] R. Tuinier, C. G. J. Bisperink, C. van den Berg, and A. Prins, Transient foaming behavior of aqueous alcohol solutions as related to their dilational surface properties, *J. Colloid Interface Sci.* **179**, 327 (1996).
- [10] V. C. Suja, A. Kar, W. Cates, S. M. Remmert, P. D. Savage, and G. G. Fuller, Evaporation-induced foam stabilization in lubricating oils, *Proc. Natl. Acad. Sci. U.S.A.* **115**, 7919 (2018).
- [11] See Supplemental Material at <http://link.aps.org/supplemental/10.1103/PhysRevLett.125.178002> for properties of pure liquids, additional experimental data and video of an experiment.
- [12] M. Matsumoto, Y. Takaoka, and Y. Kataoka, Liquid-vapor interface of water-methanol mixture. I. Computer simulation, *J. Chem. Phys.* **98**, 1464 (1993).
- [13] H. Chen, W. Gan, R. Lu, Y. Guo, and H.-f. Wang, Determination of structure and energetics for Gibbs surface adsorption layers of binary liquid mixture 2. Methanol plus water, *J. Phys. Chem. B* **109**, 8064 (2005).
- [14] J. G. Eberhart, The surface tension of binary liquid mixtures, *J. Phys. Chem.* **70**, 1183 (1966).
- [15] J. C. Eriksson, On the thermodynamics of surface systems, *Adv. Chem. Phys.* **6**, 145 (1964).
- [16] J. J. Bikerman, *Methods of Measuring Foaminess in Foams: Theory and Industrial Applications* (Reinhold, New York, 1953).
- [17] J. J. Bikerman, *Measurement of Foaminess in Foams* (Springer-Verlag, New York, 1973).
- [18] A. P. Brady and S. Ross, The measurement of foam stability, *J. Am. Chem. Soc.* **66**, 1348 (1944).
- [19] G. Verbist, D. Weaire, and A. M. Kraynik, The foam drainage equation, *J. Phys. Condens. Matter* **8**, 3715 (1996).

- [20] J. Kendall and K. P. Monroe, The viscosity of liquids. II. The viscosity-composition curve for ideal liquid mixtures, *J. Am. Chem. Soc.* **39**, 1787 (1917).
- [21] H. Iloukhani, M. Rezaei-Sameti, and J. Basiri-Parsa, Excess molar volumes and dynamic viscosities for binary mixtures of toluene plus *n*-alkanes (C_5 - C_{10}) at $T = 298.15$ K—Comparison with Prigogine-Flory-Patterson theory, *J. Chem. Thermodyn.* **38**, 975 (2006).
- [22] P. D. Howell and H. A. Stone, On the absence of marginal pinching in thin free films, *Eur. J. Appl. Math.* **16**, 569 (2005).
- [23] S. A. Koehler, S. Hilgenfeldt, E. R. Weeks, and H. A. Stone, Drainage of single Plateau borders: Direct observation of rigid and mobile interfaces, *Phys. Rev. E* **66**, 040601(R) (2002).
- [24] A. Aradian, E. Raphael, and P. G. de Gennes, “Marginal pinching” in soap films, *Europhys. Lett.* **55**, 834 (2001).
- [25] B. V. Toshev and I. B. Ivanov, Thermodynamics of thin liquid films. I. Basic relations and conditions of equilibrium, *Colloid Polym. Sci.* **253**, 558 (1975).
- [26] I. Cantat, S. Cohen-Addad, F. Elias, F. Graner, R. Höhler, O. Pitois, F. Rouyer, and A. Saint-Jalmes, *Foams: Structure and Dynamics* (Oxford University Press, New York, 2013).

3. ASYMMETRIC BINARY MIXTURES

In the previous chapter, we demonstrated that the nonlinearity of the mixtures interfacial tension in relation to their compositions results in foaming. Surface tension was observed to vary sublinearly in general for symmetric mixtures. By symmetric mixtures, we mean mixtures of molecules with similar molar surfaces and molar volumes. A simple theoretical model was developed to describe the foamability, based on the respective liquid component bulk/surface partition. In the present chapter, we investigate stability of foams for asymmetric mixtures or mixtures of molecules with significantly different sizes. We have observed significant nonlinearity – either sublinearity or superlinearity – in surface tension for asymmetric binary mixtures. We have also observed that mixtures can foam whatever the sign of the surface tension non-linearity. We will explore these variations using a thermodynamic model for ideal mixtures. We will show how asymmetry is related to the sign of the surface tension non-linearity and discuss in this frame the foamability of asymmetric mixtures.

3.1. DEFINITION OF ASYMMETRIC BINARY MIXTURES

According to the conclusions of the previous chapter, the enhanced stability of foams in binary mixtures is caused by partitions of the molecules between interface and bulk, which are related with nonlinear surface tensions. This effect allows an equilibrium of film tension (but not pressure) and thus causes a slow drainage of liquid films. Our earlier experiments were carried out with mixtures of molecules of fairly similar sizes. In this chapter, we extend our approach to molecules of different sizes. Surface tension of mixtures will indeed not only be related to partitions of the molecules between bulk and surfaces, but also to their molar surface. We will study here the relationship between foaming and variations in surface tension of mixtures of molecules with a large size ratio, which can exhibit some counter-intuitive behavior at points. In this chapter, we will limit ourselves to the case of the ideal solution theory.

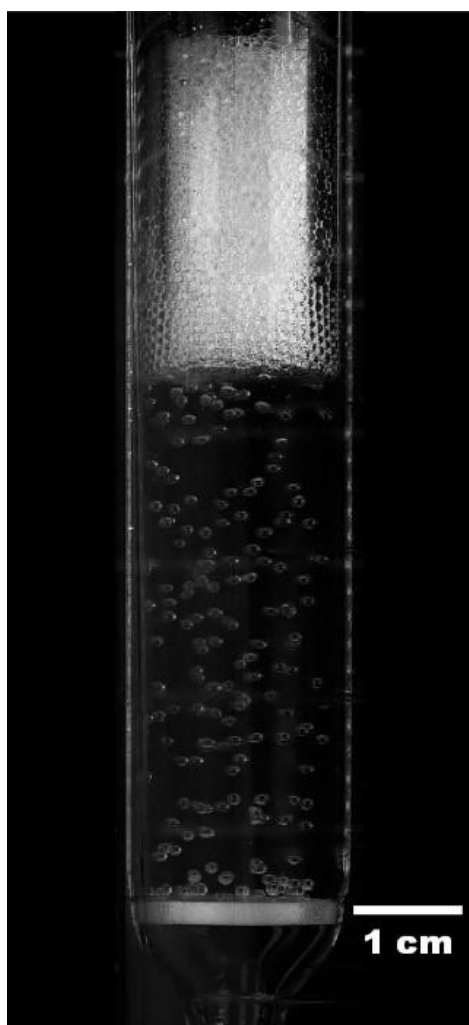


Figure 3-1 : Foam formed in a Bikerman column using an asymmetric mixture of PDMS/Decane (L. Delance's experiment).

3.1.1. Used asymmetric binary mixtures

In contrast to symmetric binary mixtures, asymmetric binary mixtures contain molecules with significantly different specific surface areas.

$$\sigma_1 \neq \sigma_2 \quad \text{Eq. 3.1}$$

where σ_i is the molar surface of species i in the liquid mixture.

The asymmetry ratio is defined as the ratio of the molar surface of liquid 2 to that of liquid 1, σ_2/σ_1 . The asymmetric binary mixtures researched are shown in **Table 6**.

Table 6 : The characteristics of used liquids for asymmetric mixtures. The molar surfaces were calculated using the cuboid molecule approximation from the molar volumes. We recall that we choose the following convention: liquid 1 has the smallest interfacial tension.

Mixture	Liquid 1	Liquid 2	σ_1 ($km^2 \cdot mol^{-1}$)	σ_2 ($km^2 \cdot mol^{-1}$)	$\frac{\sigma_2}{\sigma_1}$ Asymmetry Ratio
<i>PDMS/ Linear alkane</i>	PDMS	Decane (C ₁₀)	0.75	0.29	0.38
<i>Linear alkane/ Linear alkane</i>	Heptane (C ₇)	Hexadecane (C ₁₆)	0.24	0.37	1.49
	Decane (C ₁₀) (50°C)	Eicosane (C ₂₀) (50°C)	0.29	0.43	1.58
<i>Nearly Symmetric Mixture (used in Chap 2)</i>	Octane (C ₈)	Toluene (T)	0.25	0.19	0.75

The molar surface values shown above are computed from the molar volume, assuming that the molecules are cubic in form, as already assumed in symmetric mixtures, see **Eq.2.3**. The values of the molar surface are quite dissimilar, with an asymmetry ratio of at least 1.5 times (ratio of the larger molecule divided by the smaller one). Additionally, we will compare the results from the

above asymmetric mixtures to those from a nearly symmetric mixture (Octane/Toluene) obtained in **Chapter 2**.

3.1.2. Summary of experimental results

We recall experimental data from surface tension measurements of mixtures with varying compositions. In **Figure 3-2**, the reduced surface tension of four mixtures is plotted as a function of the molar fraction of liquid 1 with the lowest surface tension.

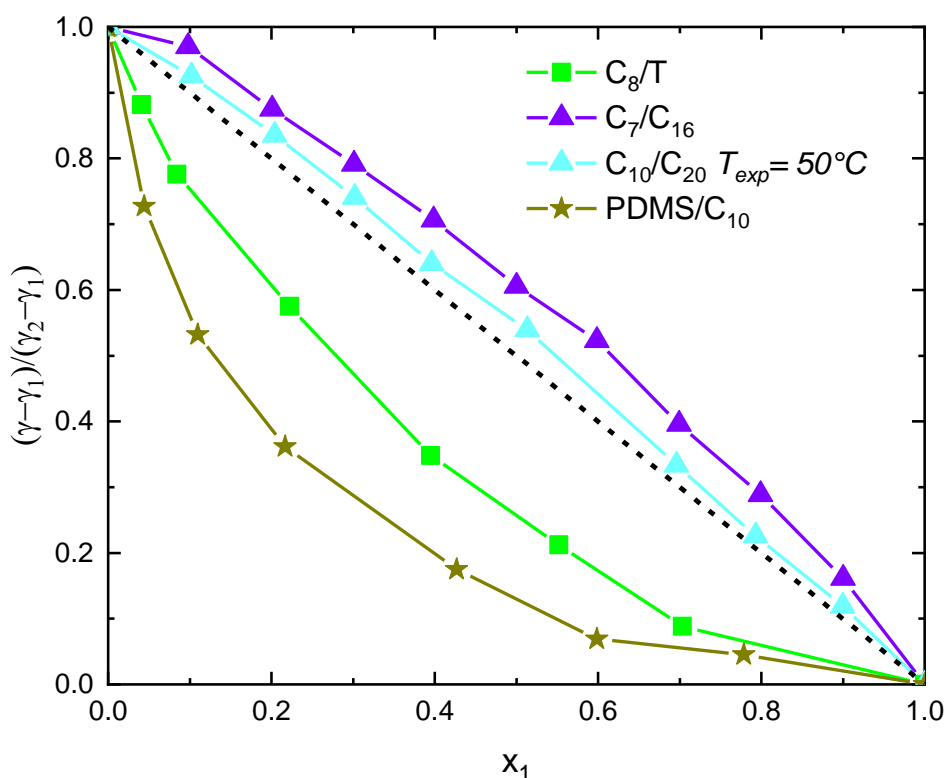


Figure 3-2 : Normalized surface tensions of binary mixtures as a function of the molar fraction of liquid 1 – the species with the smallest surface tension. From left to right with full line and markers: PDMS/Decane (dark yellow), Octane/Toluene (green), Decane/Eicosane (light cyan) and Heptane/Hexadecane (violet). The dashed line indicates linear variations. All measurements were made at room temperature except the ones with the C_{10}/C_{20} mixture that were performed at $50^\circ C$.

There are two distinct behaviors noticed. On the one hand, the surface tension of both the PDMS/Decane and Octane/Toluene mixtures varies sublinearly with composition. This leads to a surface composition that is concentrated in the species with the lowest surface tension and the largest molar volume, namely PDMS or Octane. Similar observations have been documented often

with mixtures of various kinds [28–34]. PDMS/Decane has a higher asymmetry ratio than Octane/Toluene and that the former's sublinearity is more notable than the latter's one.

The surface tensions of Heptane/Hexadecane and Decane/Eicosane (50°C), on the other hand, vary superlinearly with their compositions. This effect, which has been observed infrequently to date, occurs when the species with the lowest surface tension also has the smallest molar volume, resulting in surface ratios greater than 1, which is consistent with prior findings [20,35,36]. We will demonstrate in the following that whatever the sign of the surface tension non-linearity, the molar concentrations at the interfaces differ from the one in the bulk, and the species with the lowest surface tension is always more concentrated (in moles) at the surface than in the bulk. The sign of the nonlinearity is determined by the molecules' surface ratio.

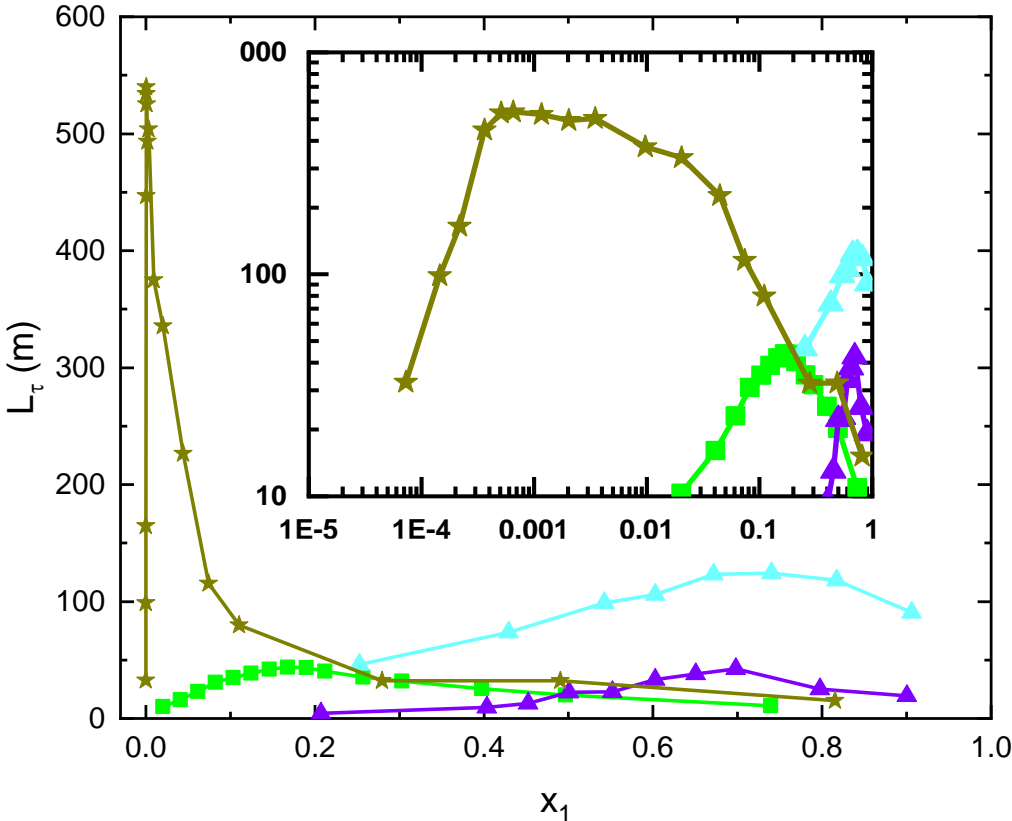


Figure 3-3 : L_τ computed following Eq.1.11 from the stationary foam heights measured with the same mixtures as in Figure 3-2 and as a function of the molar fraction of the species with the smallest surface tension. From left to right with full line and markers: PDMS/Decane (dark yellow), Octane/Toluene (green), Decane/Eicosane (light cyan) and Heptane/Hexadecane (violet). All experiments were performed at room temperature (20°C) but the one with Decane/Eicosane conducted at 50°C. Inset: same curves in log-log scale.

Additionally, we examine the capacity of foaming between different asymmetric mixtures and Octane/Toluene symmetric mixture. **Figure 3-3** illustrates the values of L_τ obtained using **Eq.1.11** as a function of the molar fraction x_1 of the mixtures utilized from the Bikerman column experiment. The normalized foaming heights range from a few tens to a few hundreds of meters.

For smaller values of the asymmetry ratios, corresponding to sublinear variations of surface tension, the position of the maximum is reached for $x_1 < 0.5$. In contrast, it corresponds to $x_1 > 0.5$ for surface ratios larger than unity, for which superlinear variations of surface tension are observed. As a result, we can observe that the mixture's asymmetrical ratio has an effect on the composition value for maximum foamability.

Correlation between the asymmetry ratio values and the amplitude of the maximum foaming height L_τ are not easy to find. For instance, PDMS/Decane mixture generated foams with surprising large lifetimes, as shown in **Figure 3-3**, even with a very tiny quantity of PDMS ($\sim 10^{-3}$) in the mixture with decane. The amount of foam created is relatively considerable when compared to other liquid mixtures examined in this investigation.

3.2. THEORETICAL INTERPRETATIONS & MODELLINGS

3.2.1. Qualitative explanation about physical picture: Effect of molecular size on the non-linearity of the mixture's surface tension

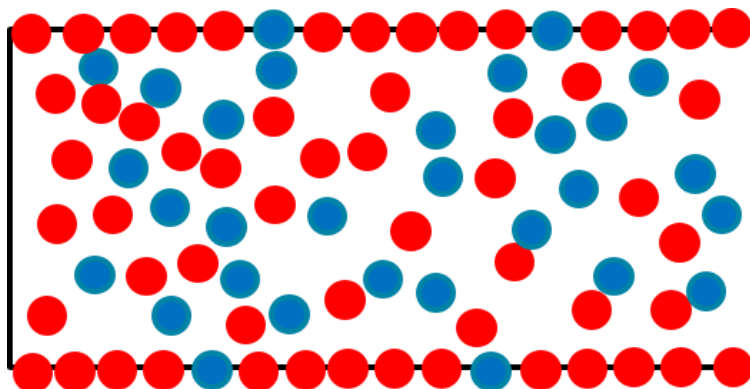


Figure 3-4 : Liquid film of symmetric mixtures of molecules with similar sizes. The surface is enriched in the species with the lowest surface tension (red circles) compared to the bulk.

As discussed previously in Chapter 2, the stabilizing mechanism for liquid films in mixtures is based on the fact that species concentrations are different in the bulk and at air interfaces. At the interface, the species with the lowest surface tension is always more concentrated than in the bulk, see **Figure 3-4**. If the films are composed of molecules of comparable size $\sigma_1 \approx \sigma_2$, the species with the highest surface energy will be depleted from the surface. As a consequence, the surface tension was found to exhibit a sublinear variation for symmetric mixtures.

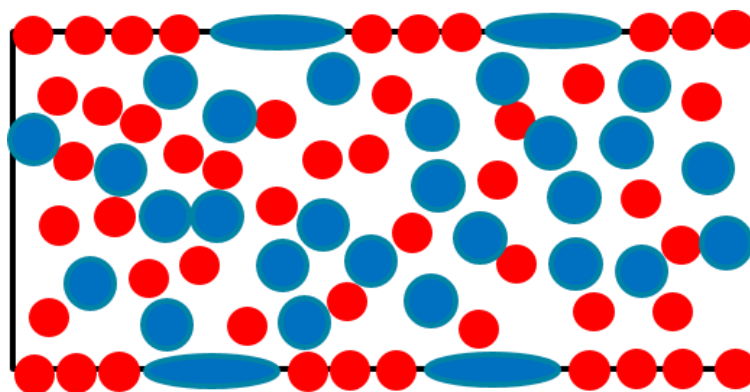


Figure 3-5 : Liquid film of asymmetric mixtures made of molecules of very different sizes. The surface is concentrated in species with low surface tension (red circles). The species with the higher surface energy (blue circles) has a significantly greater molecular size, resulting in a larger molecular surface area.

When compared to symmetric mixtures, species with a larger molecular size cover a larger surface area and thus may impact the surface tension in a more complex way, see **Figure 3-5**.

For instance, if $\sigma_1 < \sigma_2$ and $\gamma_1 < \gamma_2$, despite being depleted on the surface, species 2 with higher surface energy will be able to contribute more to interfacial tension. This may lead to a superlinear interfacial tension variation. As a result, the surface tension of asymmetric mixtures may exhibit a sublinear or superlinear variation. This explains the experimentally determined surface tension values given in **Figure 3-2**. Beyond this hand-waving argument, we will now estimate the surface tension variation of asymmetric mixtures using ideal solution thermodynamics.

3.2.2. Partition of molecules in the volume and at the interface

Consider a liquid film with a thickness of h made of an asymmetric binary mixture of liquids 1 and 2, with species 1 having the lowest surface tension. As with symmetric mixtures, we designate N_0 as the total mole number; x_1^0 and x_2^0 as the initial molar fractions. Using volume additivity, the total volume of the liquid creating the film V^0 is as follows:

$$V^0 = (x_1^0 v_1 + x_2^0 v_2) N_0 \quad \text{Eq. 3.2}$$

When the liquid film forms, N moles of respective molar fractions in species 1 – x_1 and in species 2 – x_2 occupy its bulk. Meanwhile, $N_S = N_0 - N$ moles with surface molar fractions Γ_1 and Γ_2 , respectively, are at the interfaces with air.

The bulk volume V (excluding the surface layer) and total surface area S of the film are calculated as follows:

$$V = (x_1 v_1 + x_2 v_2) N \quad \text{Eq. 3.3}$$

$$S = (\Gamma_1 \sigma_1 + \Gamma_2 \sigma_2) N_S \quad \text{Eq. 3.4}$$

For species 1, the conservation equations yield the following result:

$$\Gamma_1 N_S + x_1 N = x_1^0 N_0 \quad \text{Eq. 3.5}$$

Eq. 3.2, **Eq. 3.4** and **Eq. 3.5** finally yield the following relations:

$$N_S = \frac{S}{\Gamma_1 (\sigma_1 - \sigma_2) + \sigma_2} \quad \text{Eq. 3.6}$$

$$N_0 = \frac{V^0}{x_1^0 (v_1 - v_2) + v_2} \quad \text{Eq. 3.7}$$

$$x_1 = x_1^0 \frac{N_0}{N} - \Gamma_1 \frac{N_S}{N} \quad \text{Eq. 3.8}$$

Assuming $N_S - N_0 \approx N_S$ and introducing $S = 2V/h$, it is possible to construct a geometric relationship between x_1 and x_1^0 from **Eq. 3.8**:

$$x_1 - x_1^0 = \frac{2 v_2(1 - x_1^0) + v_1 x_1^0}{h \Gamma_1(\sigma_1 - \sigma_2) + \sigma_2} (x_1^0 - \Gamma_1) \quad \text{Eq. 3.9}$$

Using the linearized relation $\gamma(h) - \gamma = \left(\frac{\partial \gamma}{\partial x_1} \right)_{x_1=x_1^0} (x_1 - x_1^0)$, the final relation giving the thickness-dependent surface tension of a film of an asymmetric binary mixture is:

$$\gamma(h) - \gamma = \frac{2}{h} \left(\frac{\partial \gamma}{\partial x_1} \right)_{x_1=x_1^0} \frac{v_2(1 - x_1^0) + v_1 x_1^0}{\Gamma_1(\sigma_1 - \sigma_2) + \sigma_2} (x_1^0 - \Gamma_1) \quad \text{Eq.3.10}$$

where γ is the surface tension of the binary mixture at $x_1 = x_1^0$.

Making the approximation $x_1 \approx x_1^0$, yields:

$$\gamma(h) - \gamma = \frac{2}{h} \frac{\partial \gamma}{\partial x_1} \frac{v_2(1 - x_1) + v_1 x_1}{\Gamma_1(\sigma_1 - \sigma_2) + \sigma_2} (x_1 - \Gamma_1) \quad \text{Eq.3.11}$$

As with symmetric mixtures, **Eq.3.11** holds true in the limit $h \gg v_i/\sigma_i$ (species i containing the largest molecules), which corresponds to thicknesses many orders of magnitude bigger than the molecular size.

Once again, as shown in the above equation, the thickness-dependent surface tension of a film of an asymmetric binary mixture is proportional to the surface-bulk partition of species 1 ($x_1 - \Gamma_1$). Let us note that, **Eq.3.11** becomes identical to **Eq.2.22**, obtained in **Chapter 2**, for symmetric mixtures composed of molecules with the same molar surface and volume.

To provide an estimate of $\frac{\partial \gamma}{\partial x_1}$, we will now use the ideal solution thermodynamics introduced by Butler.

3.2.3. Butler's model and surface molar fraction Γ_1

In **Chapter 2**, we used a fairly simple phenomenological model, assuming that surface tension γ is a linear function of the surface molar fraction Γ . Comparison of experimental and theoretical data demonstrates that this model is appropriate for symmetric mixtures **[37,38]**. However, for asymmetric ones, this approach does not adequately account for observed phenomena such as surface tension superlinearity. This is demonstrated in further detail in the **Appendix F**. Consequently, a more accurate theoretical model for the physicochemical features of asymmetric

liquid mixtures is required. For the sake of simplicity, we will choose the ideal solution approximation.

The ideal solution approximation has been introduced by Butler [21] to describe the surface/volume partition of ideal mixtures. The relation between bulk fraction and interfacial tension writes:

$$x_1 e^{\frac{\sigma_1}{RT}(\gamma - \gamma_1)} + x_2 e^{\frac{\sigma_2}{RT}(\gamma - \gamma_2)} = 1 \quad \text{Eq.3.12}$$

where R the ideal gas constant and T the absolute temperature.

Indeed, this equation expresses the relation $\Gamma_1 + \Gamma_2 = 1$, where the surface molar fractions Γ_i , follows the Boltzman's law:

$$\Gamma_i = x_i e^{E_i/RT} \quad \text{Eq.3.13}$$

where $E_i = \sigma_i(\gamma - \gamma_1)$ the surface energy variation when one mole of species i ($i = 1,2$) is displaced from the bulk to the interface.

This model gives thus the relations between bulk and interface concentrations, as well as the liquid's surface tension.

We introduce several dimensionless parameters: the reduced molar surfaces of species i :

$$S_i = \sigma_i \frac{(\gamma_2 - \gamma_1)}{RT} \quad \text{Eq.3.14}$$

The values these parameters are of the order of unity (see **Table 7**).

Table 7 : Reduced molar surfaces of two liquids in used mixtures

Liquid 1	Liquid 2	σ_2/σ_1	S_1	S_2
PDMS	Decane (C ₁₀)	0.38	1.36	0.53
Heptane (C ₇)	Hexadecane (C ₁₆)	1.49	0.66	0.50
Decane (C ₁₀) (50°C)	Eicosane (C ₂₀) (50°C)	1.58	0.64	0.96
Octane (C ₈)	Toluene (T)	0.75	0.72	1.11

We introduce also the excess surface tension, characterizing the non-linearity of the interfacial tension:

$$E_\gamma = \frac{\gamma - (\gamma_1 x_1 + \gamma_2 x_2)}{\gamma_2 - \gamma_1} \quad \text{Eq.3.15}$$

This excess value characterizes the deviation from linearity. For superlinear surface tension variations, $E_\gamma > 0$ whereas for sublinear surface tension variations, $E_\gamma < 0$.

Introducing **Eq.3.14**, **Eq.3.15** and using $x_2 = 1 - x_1$, the Butler's equation **Eq.3.12** may be written as:

$$x_1 e^{S_1(E_\gamma + 1 - x_1)} + (1 - x_1) e^{S_2(E_\gamma - x_1)} = 1 \quad \text{Eq.3.16}$$

According to **Eq.3.16**, E_γ is a function of the composition of the mixture and is solely dependent on two parameters S_1 and S_2 .

Following that, we will exploit this model to determine the specific form of the characteristic length of asymmetric binary mixtures.

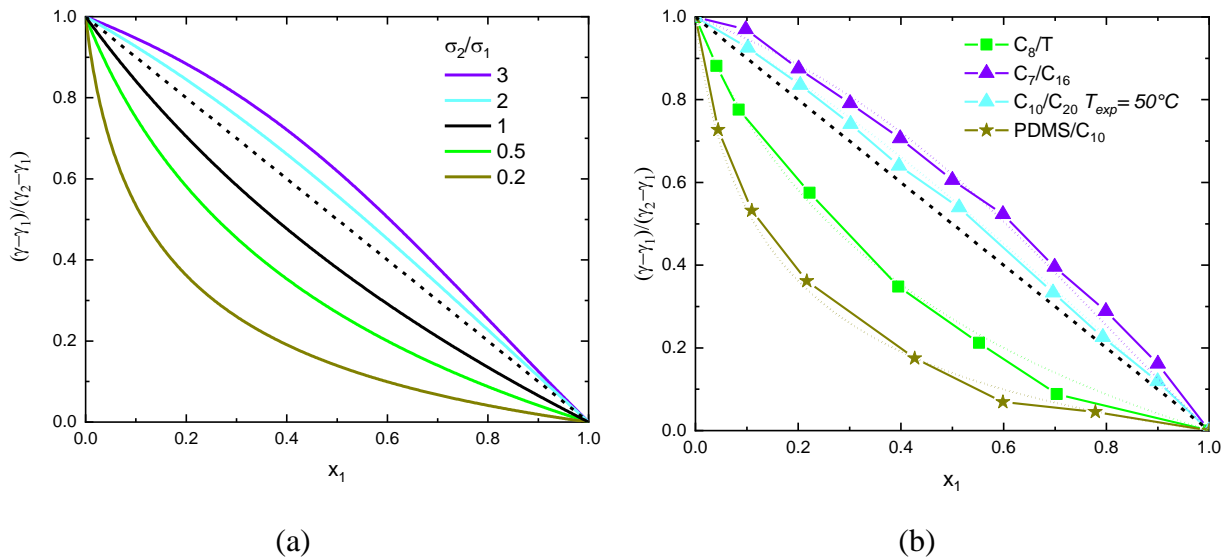


Figure 3-6 : Normalized surface tensions as a function of the bulk molar fraction of species 1: (a) Butler's model; (b) Experimental results. The dotted lines show the surface tensions computed from Butler's model with the liquid parameters and the adjusted surface ratios given in Table 8.

Figure 3-6 (a) depicts the variations in normalized surface tension of studied mixtures as a function of the bulk molar fraction of the species with the lowest surface tension, which are

predicted by **Eq.3.16** with arbitrarily chosen values: $S_1 = 1$ and different surface ratios $S_2/S_1 = \sigma_2/\sigma_1$.

The variations are sublinear for surface ratios ranging from 0.2 to 1, and the nonlinearity increases as the ratio decreases. For surface ratios $S_2/S_1 = 2$ and 3, on the other hand, the variations are superlinear and the nonlinearity grows with the ratio. This is in accordance with the experiment's findings, see **Figure 3-6 (b)**.

Although the surface tension varies superlinearly with their composition, the molecules in the mixture with the highest surface tension (species 2) are always less concentrated at the interface than in the bulk. This relation is seen in the graph below.

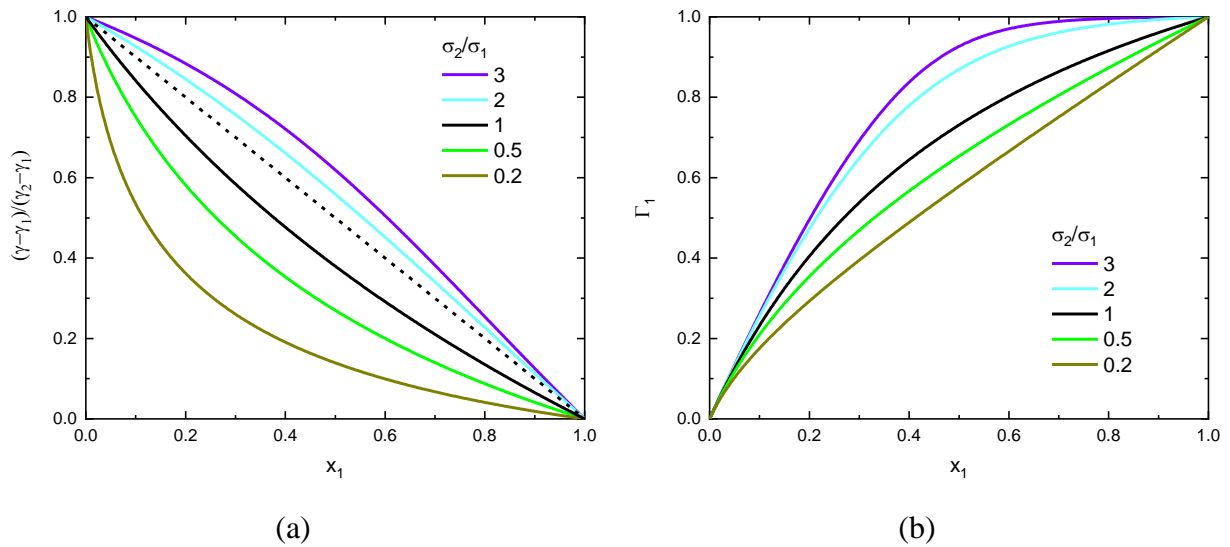


Figure 3-7 : Surface molar fraction Γ_1 as a function of the bulk molar fraction of species 1 for the studied mixtures.

We can compute the surface molar fraction $\Gamma(x)$ from **Eq.3.13** by determining the values of surface tension $\gamma(x)$ and bulk molar fraction x . The surface molar fraction Γ_1 as a function of the bulk molar fraction x_1 of species 1 (the lowest surface tension ones) is illustrated in **Figure 3-7** for examined mixtures with a typical value of S_1 and various surface ratios S_2/S_1 as mentioned in the previous paragraph.

From this figure, it highlights that Γ_1 is always a superlinear function with respect to x_1 in all circumstances and for all asymmetric ratio values investigated. Indeed, this outcome is observable

mathematically. The surface tension of the mixture is always larger than the surface tension of liquid 1, hence $\gamma - \gamma_1$ is always positive. Following **Eq.3.13**, the molar fraction in species 1 at the surface is larger than the one in the bulk $\Gamma_1 = x_1 e^{\sigma_1(\gamma - \gamma_1)/RT} > x_1$.

In addition, the related nonlinearity grows monotonically with the molecule surface ratio. The surface tension of a mixture is given by the product of the surface concentrations and the molecular surfaces. Surface tension can be superlinearly if the species with the highest surface tension has simultaneously a highly large surface area, even while its concentration at the surface is lower than the bulk. The associated nonlinearity increases monotonically with the molecule's surface ratio.

Expanding **Eq.3.16** for S_1 and $S_2 \ll 1$, which corresponds to the limit of an entropy-dominated partition between surface and bulk explains our conclusion. The excess surface tension in this situation is denoted by:

$$E_\gamma = \frac{x_1(1-x_1)}{x_1 + \frac{S_2}{S_1}(1-x_1)} \left(\frac{S_2}{S_1} - 1 \right) \quad \text{Eq.3.17}$$

Due to the fact that $0 < x_1 < 1$, the ratio in the right-hand term of **Eq.3.19** is always positive. As a result, the sign of nonlinearity is determined by the sign of $\left(\frac{S_2}{S_1} - 1\right)$. When surface ratios are different from unity, this finding is qualitatively consistent with the results shown in **Figure 3-7**, for which a sublinear behavior is described for ratios of 0.2 to 0.5 with $S_2/S_1 < 1$ and a superlinear behavior is recorded for ratios of 3 to 5 in the case of $S_2/S_1 > 1$. In comparison, although the approximated **Eq.3.19** predicts that the surface tension would vary linearly for $S_1 = S_2$ (i.e., $E_\gamma = 0$) the full resolution of Butler's equation shown in Fig. 5 results in sublinear variations. According to the full Butler's equation, a linear behavior is expected for a surface ratio S_2/S_1 close to 2. To make sense of this results, the contribution of surface energy, which are assumed to be extremely tiny in the derivation of eq. (16), must be examined. Indeed, the mixture's surface tension is defined by the product of the molecular surfaces and the difference in their surface energies. If two molecules have identical surface energies, their partitions between surface and bulk are likewise similar. As a result, if the species with the highest surface tension also has the highest molar surface, its contribution to surface tension is proportional to its bulk concentration multiplied by its molar surface, resulting in superlinear variations of surface tension. This limit is predicted by **Eq.3.19**. However, if the difference in surface energies is significant, this impact is counterbalanced by the fact that a lower surface concentration of the species with a higher surface

energy is preferred over bulk. Because the value of the reduced molar surface is on the order of unity, these two effects (ratio between occupied surfaces and partition) are of the same order of magnitude. This explains why the surface tension of a mixture varies superlinearly only when the species with the highest surface tension also has the highest molar surface and when the ratio of the two species' molar surfaces surpasses a critical value. Resolution of Butler's equation for $E_\gamma = 0$ and $x_1 = 0.5$ allows one to determine the crossover of sub and superlinear variations of the interfacial tension. We obtain:

$$S_2 = -2 \ln(2 - e^{\frac{S_1}{2}}) \quad \text{Eq. 3.18}$$

which yields $S_2/S_1 = 2.09$ for $S_1 = 1$.

Thus, the crossover between super and sub linear superficial tensions is highly dependent on the values of the molar surfaces and the difference in surface energies. Sublinear behavior is encouraged by large differences in surface energies, whereas differences in molar surfaces cause either superlinear or sublinear behavior, depending on the surface ratio. We now compare Butler's equation's predictions to the experimental results in **Figure 3-2**. In **Figure 3-2**, we show the calculated surface tensions for each mixture. The molar surfaces are unknown; a common estimate used in the literature is cuboid molecules, which allows for the determination of the molar surfaces using the molar volumes.

Table 8 : The molar surfaces were computed from the molar volumes in the cuboid molecule approximation. The best surface ratio are the values for which the best agreement was found between the experimental and predicted variations of surface tension with the ones predicted by Butler's equation Eq.3.16.

Liquid 1	Liquid 2	σ_2/σ_1 (Cuboid surface ratio)	σ_2/σ_1 (Best surface ratio)
PDMS	Decane (C ₁₀)	0.38	0.2
Heptane (C ₇)	Hexadecane (C ₁₆)	1.49	2
Decane (C ₁₀) (50°C)	Eicosane (C ₂₀) (50°C)	1.58	3
Octane (C ₈)	Toluene (T)	0.75	0.5

However, we discovered that the experimental surface tensions cannot be described using the values for molar surfaces obtained in this approximation; a more accurate description requires more asymmetric molar surfaces, as shown in **Table 8**, where we report the surface ratios that are most consistent with the experimental data. The molar surface of species 1 was randomly chosen to be the one predicted by the cuboid approximation in each example, and the surface ratio was changed to match the surface tension curves predicted by **Eq.3.16**.

There have been several attempts [27,30,34,35,39–41] to establish a quantitative description of the surface tension of mixtures as a function of their composition. However, due to the lack of information about the molecular surface, no acceptable model exists, regardless of the nature of the mixture. As previously stated, the molar surfaces of a particular molecule may differ from one mixture to another depending on the nature of the molecule with which it is mixed. The molar surfaces of a mixture may also differ in composition [42]. Additionally, nonideal behavior, both in bulk and on surfaces, can result in variations from Butler's equation. We did not attempt to offer a more quantitative description of the surface tensions of the mixtures studied since we are interested in the relationship between surface tension nonlinearity and foamability.

3.2.4. Characteristic length α of asymmetric binary mixtures

Within the context of ideal mixtures, we can now give an expression for α . For that, we derive **Eq.3.16** with respect to x_1 . We thus get:

$$\frac{\partial \gamma}{\partial x_1} = RT \frac{x_1 - \Gamma_1}{(1 - x_1)x_1(\Gamma_1 S_1 + (1 - \Gamma_1)S_2)} \quad \text{Eq.3.19}$$

Substituting **Eq.3.19** into the thickness-dependent surface tension **Eq.3.11**, we obtain:

$$\gamma(h) - \gamma = \frac{RT (\Gamma_1 - x_1)^2}{2h (1 - x_1)x_1} \frac{v_1 x_1 + v_2 (1 - x_1)}{(\Gamma_1 \sigma_1 + (1 - \Gamma_1)\sigma_2)^2} \quad \text{Eq.3.20}$$

Finally, the expression for the microscopic length α that characterizes the capacity to produce foams is determined in the case of ideal solution:

$$\alpha = \frac{RT (\Gamma_1 - x_1)^2}{2\gamma_\infty (1 - x_1)x_1} \frac{v_1 x_1 + v_2 (1 - x_1)}{(\Gamma_1 \sigma_1 + (1 - \Gamma_1)\sigma_2)^2} \quad \text{Eq.3.21}$$

Note that α is always positive. The next part will compare the theoretical model's outcomes to those obtained experimentally.

3.3. COMPARISON TO EXPERIMENTAL DATA

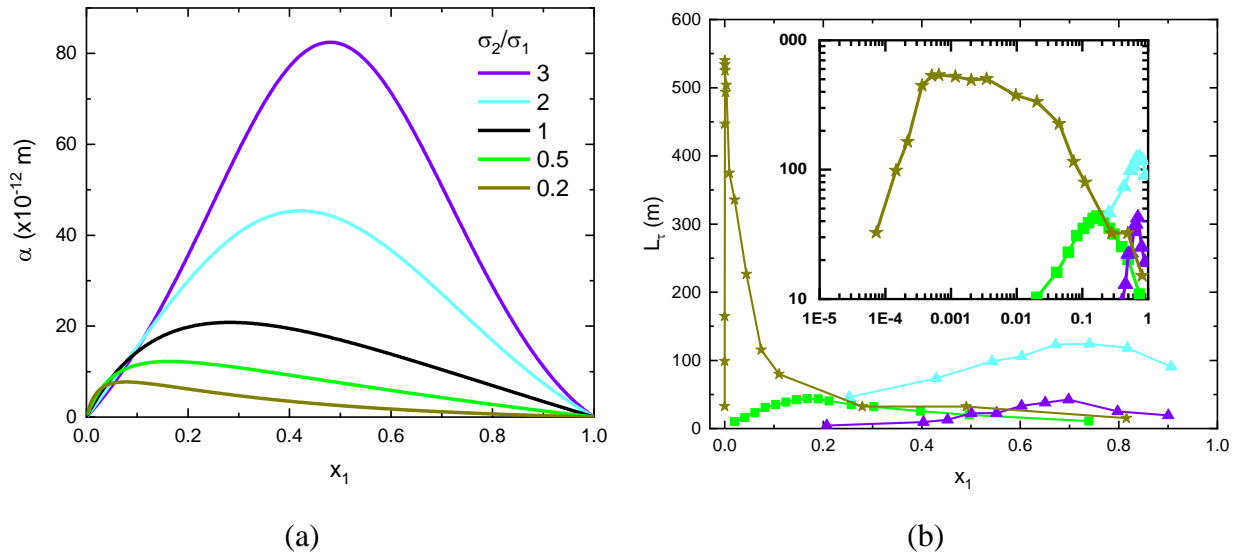


Figure 3-8 : (a) Length α characterizing the increase of surface tension with decreasing thickness of a film of binary mixture, as a function of the mixture composition. The curves were computed using Eq.3.21 for different asymmetry ratios, derived in the case of ideal solutions. (b) Normalized foam height L_τ as a function of the mixture composition. From left to right with full line and markers: PDMS/Decane (dark yellow), Octane/Toluene (green), Decane/Eicosane (light cyan) and Heptane/Hexadecane (violet).

We have determined α using Eq.3.21 with $S_1 = 1$ and the asymmetry ratios S_2/S_1 determined from the experimental surface tensions. Figure 3-8 (a) shows the variation of alpha as a function of mixture composition. Generally, the length α is of a fraction of nanometer. We also observe that all curves accept a maximum composition dependent on the asymmetry of the mixture. As the asymmetry ratio grows, the maximum for foamability shifts toward the greater molar fractions in species 1. Moreover, the maximum's amplitude grows monotonically as the asymmetry ratio increases.

The estimated values of α – assuming ideal solution thermodynamics - may be compared to the experimental values L_τ for the liquid mixes under investigation, which are presented in Figure 3-8 (b) with mixture's composition. As observed for symmetric case and discussed in the next chapter, α is around 10^{13} times less than the value of L_τ . Foaming height L_τ , like α , exhibit a maximum when composition is varied. The positions of the maxima, in particular, follows qualitatively the

model, i.e., higher molar fractions in species 1 for larger asymmetric ratios. However, the amplitude variations of α and L_τ as a function of the asymmetry ratio are obviously quantitatively different. For example, PDMS/C₁₀ mixture generated foams with extremely long lifetimes, resulting in large value of L_τ which is not predicted by our model. Moreover, the position with the greatest amount of foaming is only qualitative. As predicted by the **Eq.3.21**, PDMS/C₁₀ creates the most foam when roughly 5% PDMS is added to Decane. We see, however, that a minimal quantity of PDMS ($\sim 10^{-3}$ in molar fraction) is sufficient for this mixture to create maximal foam.

Clearly, α represented by **Eq.3.21** does not encompass all of the effects seen throughout the experiment. The way we determine the asymmetry ratio results in significant inaccuracies. The non-ideal behavior of the foaming properties, such as the fugacity of the different species in bulk and at the interfaces, would necessitate a more quantitative description. However, determining the fugacity of molecules at an interface experimentally is challenging, and molecular dynamics simulations are more likely to shed fresh information on the relationship between species partition and foamability **[18,43]**.

3.4. CONCLUSION

In this chapter, we have examined foams created in asymmetric liquid mixtures containing molecules of different sizes. Using a model for surface tension in the case of ideal solutions, we show surface tension of a mixture may change superlinearly with composition provided that the species with the highest surface energy has a sufficiently large molar surface, corresponding with our experimental observations on mixtures with different surface ratios. However, regardless of the sign of the nonlinearity, the surface concentration of the species with the lowest surface energy is always greater than the bulk concentration and this partition is responsible for foaming of mixtures.

3.5. PUBLICATION

Foaming of Binary Mixtures: Link with the Nonlinear Behavior of Surface Tension in Asymmetric Mixtures

H. P. Tran, L. Delance, N. Passade-Boupat, E. Verneuil, F. Lequeux, and L. Talini*



Cite This: <https://doi.org/10.1021/acs.langmuir.1c02198>



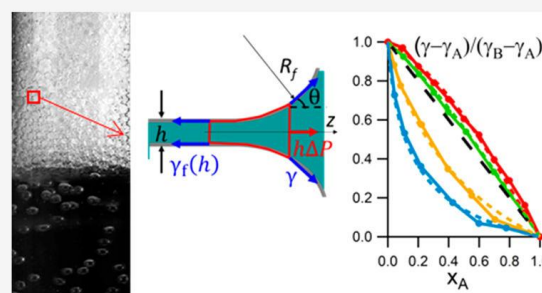
Read Online

ACCESS |

Metrics & More

Article Recommendations

ABSTRACT: The lifetimes of single bubbles or foams that are formed in mixtures of liquids can be several orders of magnitude larger than the ones formed in pure liquids. We recently demonstrated that this enhanced stability results from differences between bulk and interfacial concentrations in the mixture, which induce a thickness dependence of the surface tension in liquid films, and thus a stabilizing Marangoni effect. Concentration differences may be associated with nonlinear variations of surface tension with composition and we further investigate their link with foamability of binary mixtures. We show that, for asymmetric binary mixtures, that is, made of molecules of very different sizes, strong nonlinearities in surface tension can be measured, that are associated with large foam lifetimes. When the molecules that occupy the largest surface areas have the smallest surface tension, the surface tension of the mixture varies sublinearly with composition, reflecting an enrichment in this species at the interface with air, as classically reported in the literature. In contrast, when they exhibit the largest surface tension, superlinear variations of surface tension are observed, despite a similar enrichment. We discuss these variations in light of a simple thermodynamic model for ideal mixtures and we demonstrate why foam stability is enhanced for both sublinear and superlinear surface tension variations, thus, shedding new light on foamability without added surfactants.



INTRODUCTION

More than a century ago, it was observed that the surface tensions of some binary mixtures do not vary linearly with their composition.¹ For instance, it is well-known that the surface tension of water/alcohol mixtures is smaller than the one predicted by a linear variation with composition. This effect was further ascribed to the presence of a surface layer of composition different from the one of the bulk; in the case of water/alcohol mixtures, the surface layer is enriched in alcohol, which has a smaller surface tension than water, resulting in sublinear variations with a composition of the surface tension of the mixture. Thermodynamical models were developed in that framework,² and the detailed description of this effect remains a current research subject,³ as well as the properties of the surface layer.⁴

In parallel, it has been shown that some binary mixtures have foaming properties: whereas the lifetimes of bubbles formed in pure low-viscosity liquids are expected to be smaller than 1 ms in the absence of contaminants,⁵ the lifetimes of bubbles in binary mixtures of similar viscosities can reach several tens of seconds⁶ and transient foams are observed. Consequences of the foaming behavior of liquid mixtures impact multiple applications in which control of foaming is needed; when foaming is desired, it provides a way to produce foams without adding surfactants by simply mixing different liquids. In

contrast, when unwanted, foaming of mixtures can be detrimental to applications; for instance, it impedes lubrication by oils in car gear boxes.

We have recently demonstrated that the enhanced stability of foams in binary mixtures results from the differences in concentrations at the interface and in the bulk,⁷ that are associated with nonlinear surface tensions. Because of these differences, the increase of surface to volume ratio of liquid films that occurs during the stage of foam formation requires changes in both surface and bulk concentration. As a result, the surface tension of a liquid film increases with decreasing thicknesses. This effect induces a slowing down of the drainage of the liquid films between bubbles in foams and, thus, increases the lifetimes of these films.

Our previous experiments were conducted with mixtures of molecules with similar sizes.⁷ In that case, because the surfaces of molecules have close values, the variations of surface tension

Received: August 18, 2021

Revised: October 7, 2021

Table 1. Used Liquids and Their Properties^a

mixture A/B	surface tensions (mN m ⁻¹)		molar volumes (10 ⁻⁴ m ³ mol ⁻¹)		vol ratio V_B/V_A	cuboid molar surfaces (10 ⁹ m ² mol ⁻¹)		cuboid surface ratio σ_B/σ_A	best surfaces ratio σ_B/σ_A	$\sigma_A(\gamma_B - \gamma_A)/RT$ S_A	$\sigma_B(\gamma_B - \gamma_A)/RT$ S_B
	γ_A	γ_B	V_A	V_B		σ_A	σ_B				
PDMS/decane	18.8	23.3	8.39	1.96	0.23	0.75	0.29	0.38	0.2	1.36	0.53
octane/toluene	21.4	27.9	1.64	1.07	0.65	0.25	0.19	0.75	0.4	0.66	0.50
decane/eicosane (50 °C)	21.0	26.5	2.01	3.67	1.86	0.29	0.43	1.49	2	0.64	0.96
heptane/hexadecane	19.8	27.2	1.47	2.94	1.99	0.24	0.37	1.58	3	0.72	1.11

^aThe surface tension values were measured and the molar volumes found in the literature. The molar surfaces were computed from the molar volumes in the cuboid molecule approximation. The best surface ratio are the values for which the best agreement was found between the experimental and predicted variations of surface tension with the ones predicted by Butler's equation (eq 13).

with composition simply reflect the population at the interface with air. In contrast, for mixtures of molecules with very different surfaces, hereafter called asymmetric, the situation is more complex. Here, we investigate the link between foaming and surface tension variations of mixtures of molecules with a large size ratio, which can present some counterintuitive behavior. We discuss them in light of the ideal solution approximation for surface tension of binary mixtures.

EXPERIMENTAL SECTION

Materials. The binary mixtures were made with *n*-heptane, *n*-decane, *n*-hexadecane, and toluene (all with a purity >99%, Sigma-Aldrich), as well as polydimethylsiloxane (PDMS, ABCR, viscosity ScSt). Experiments were also conducted with *n*-eicosane (>99%, Sigma-Aldrich), which has a melting point at 36.65 °C. The measurements made with eicosane were performed at 50 °C, whereas all other measurements were made at room temperature. Liquids were mixed and stirred to obtain homogeneous mixtures with different compositions. We list in Table 1 the properties of the used binary mixtures A/B, A being the species with the smallest surface tension. In particular, we report the volume ratio of the mixture which we define as the ratio of the molar volume of species B, v_B , and the molar volume of A, v_A . The surface areas σ_A and σ_B occupied in the gas/liquid interface by, respectively, molecules A and B are expressed as molar surfaces; in a first approximation, they are computed from molar volumes as the areas of cuboid molecules.

Tensiometry. The surface tensions of all binary mixtures were measured as a function of their composition with a tensiometer (Teclis) that measured the shapes of rising bubbles formed in mixtures. We have found that, in all mixtures, a constant value of surface tension is reached instantaneously, indicating relaxation times smaller than the time resolution of the tensiometer (0.1 s). Measurement conducted over long times (up to 1 h) did not show any variation of surface tension showing evaporation is negligible. The densities of the mixtures were computed in the approximation of volume additivity that has been validated in previous studies for some mixtures.⁸ This assumption was checked for the other mixtures by weighing a given volume of liquid.

Viscosimetry. The viscosities of PDMS/decane and octane/toluene mixtures were measured (Rheometer Low Shear 400, Lamy rheology). The viscosities of alkane mixtures were computed using the empirical Kendall-Monroe equation.⁹

Foaming Experiments. Bikerman columns constituted by a glass column of diameter 2 cm with a porous glass filter at the bottom (Robu, porosity: 10–16 μm), were used to form foams and measure their lifetimes.¹⁰ The column was filled with the binary mixture up to a height of 10 cm. Air pumped in a closed loop was injected at the bottom of the column at a flow rate corresponding to the average velocity $V_{\text{gas}} = 1.9 \times 10^{-2} \text{ m}\cdot\text{s}^{-1}$. The PDMS/decane mixture strongly foams and a much smaller gas velocity was used, $V_{\text{gas}} = 2 \times 10^{-3} \text{ m}\cdot\text{s}^{-1}$. Evaporation effects are expected to destabilize foams in all mixtures except hexane-hexadecane,⁷ and larger foam heights were

accordingly measured with negligible evaporation, that is, in the closed loop in which air saturates in volatile species. In order to prevent retention of PDMS in the porous filter, it was chemically modified using a perfluorosilane. Briefly, the inner column was set to low pressure, and an air plasma was generated for 60 s. A droplet of perfluorotrichlorosilane was then evaporated at low vapor pressure inside the column, leading to chemical modification of the glass filter and no imbibition of the filter by the PDMS/decane mixture. The bubble radius in the formed foams was found to slightly depend on the liquid mixture but nevertheless remained within the range 500–800 μm. During gas injection, a foam forms at the top of liquid, as shown in Figure 1. Its height reaches a stationary value H within a few

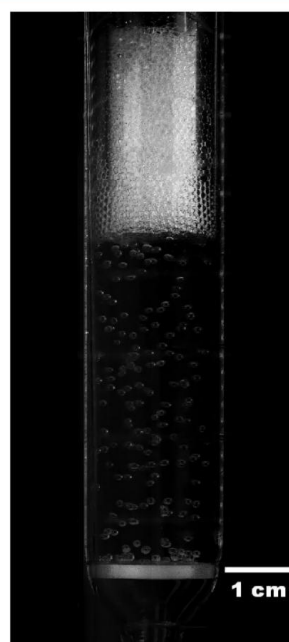


Figure 1. Foam formed in a Bikerman column. The white part at the bottom of the column is the porous filter through which vapor-saturated air is injected.

seconds. The lifetime of the foam we define is the ratio of the foam height and the average gas injection velocity, H/V_{gas} . We have checked that the height varied linearly with injection velocity in the investigated flow rate range and did not depend on the initial liquid height in the column.

In order to compare the foaming properties of mixtures of different viscosity μ and surface tension γ on which lifetimes depend, it is

convenient to consider the product of average bubble lifetime and capillary velocity γ/μ

$$L_\tau = \frac{\gamma H}{\mu V_{\text{gas}}} \quad (1)$$

For all mixtures, L_τ is independent of injection conditions within the investigated range.

RESULTS

Surface Tension of Mixtures. The reduced surface tensions of four A/B mixtures are shown in Figure 2 as a

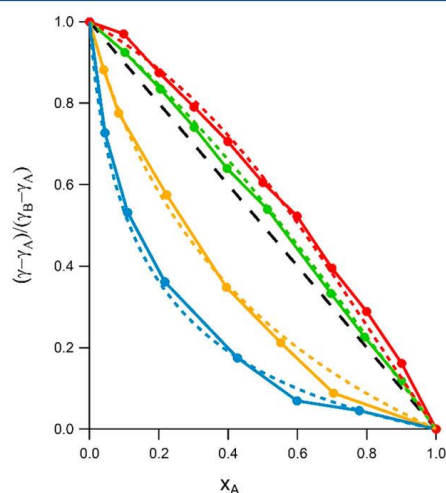


Figure 2. Normalized surface tensions of binary mixtures A/B as a function of the molar fraction of A, the species with the smallest surface tension. From left to right with full line and markers: PDMS/decane (blue), octane/toluene (orange), decane/eicosane (green), and heptane/hexadecane (red). The dashed line indicates linear variations. The dotted lines show the surface tensions computed from eq 13 with the liquid parameters and the adjusted surface ratios given in Table 1. All measurements were made at room temperature, except the ones with the decane/eicosane mixture that were performed at 50 °C.

function of the molar fraction of the species A that has the smallest surface tension. Two different behaviors are observed. On the one hand, in both the PDMS/decane and octane/toluene mixtures, the surface tension exhibits sublinear variations with composition. It corresponds to a surface composition enriched in the species with the smallest surface tension, which has also the largest molar volume, that is, either PDMS or octane. Similar variations have been widely reported with mixtures of different natures.^{3b,8,11} Clearly, the sublinearity is more marked for the PDMS/decane, which has the largest surface ratio. On the other hand, the surface tensions of heptane/hexadecane and decane/eicosane vary superlinearly with their compositions. This effect has been scarcely evidenced up to date, it is observed when the species with the smallest surface tension has the smallest molar volume, yielding surface ratios larger than unity, consistent with previous findings.¹² We will show in the following that the superlinearity of surface tension in these mixtures results from the same effect as in mixtures with sublinear variations of surface tension; in both cases, the concentrations at the interfaces differ from the ones in the bulk, the species with the smallest surface tension is always more concentrated at the

surface than in the bulk. The sign of the nonlinearity depends on the surface ratio of the molecules.

Lifetimes of Foams in Mixtures. We have found that foam forms during Bikermann tests with all investigated mixtures. The measured lifetimes are multiplied by the capillary velocity in the same mixture, in order to account for viscosity and surface tension effects following eq 1. The resulting values L_τ are shown in Figure 3 as a function of

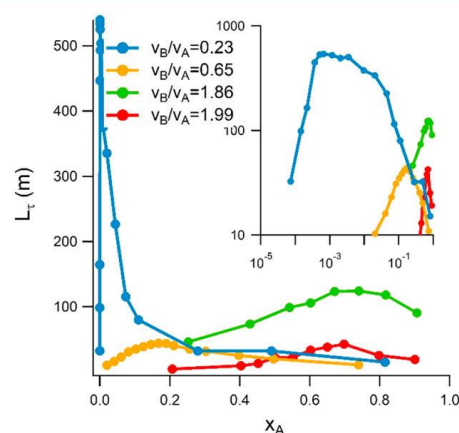


Figure 3. Product L_τ of measured lifetimes and capillary velocities computed following eq 1, obtained in the same mixtures as in Figure 2 and as a function of the molar fraction of the species with the smallest surface tension. All experiments were performed at room temperature (20 °C), but the one with decane/eicosane was conducted at 50 °C. Inset: same curves in log–log scale.

volume fraction of the species with the smallest surface tension. The values of L_τ range from a few tens to a few hundreds of meters. They are therefore larger by more than 10^4 than the bubble size in the formed foams. Very large typical lengths were similarly found to be involved in the bursting of bubbles at the surface of tap water,⁵ and are currently not understood. However, L_τ provides a convenient way to compare lifetimes obtained in mixtures with different viscosities and surface tensions, and we will consider it as a normalized lifetime rather than a physical length.

All curves of Figure 3 exhibit a maximum at a composition that depends on the asymmetry of the mixture. For smaller values of the volume ratios, corresponding to sublinear variations of surface tension, the position of the maximum is reached for $x_A < 0.5$. In contrast, it corresponds to $x_A > 0.5$ for surface ratios larger than unity, for which superlinear variations of surface tension are observed. However, there is no correlation between the values of the volume ratio and the amplitude of the maximum L_τ . In particular, we have found the PDMS/decane mixture formed foams with very large lifetimes yielding very large values of L_τ . The position of the maximum in the latter curve is also reached for a strikingly small ($\sim 10^{-3}$) molar fraction in PDMS. Remarkably, PDMS is widely used as an antifoaming agent in aqueous solutions¹³ whereas it clearly promotes foaming when added to decane, with which it is miscible. We will show later that the profoaming property of PDMS added to decane results from both the rather large difference between their surface tensions and the large volume ratio of the two molecules.

C

<https://doi.org/10.1021/acs.langmuir.1c02198>
Langmuir XXXX, XXX, XXX–XXX

Thickness-Dependent Surface Tension. We have shown that the differences in bulk and surface concentrations in binary mixtures result in a thickness dependence of the interfacial tension.⁷ Actually, since thinning implies an increase of surface to volume ratio, a thin liquid film cannot further thin down without modifying its bulk and surface concentrations. Consequently, thinning implies a decrease of the surface concentration of species A, and therefore an increase of surface tension, which itself opposes thinning. As a liquid film forms in the foam between two bubbles coming closer, in a first and fast stage it is stretched without significant drainage, that is, at constant volume. Its surface to volume ratio increases and, as a consequence of the partition of species between bulk and interfaces, the surface tension γ_f in its flat part increases with decreasing thicknesses h following

$$\gamma_f(h) - \gamma = \gamma \frac{\alpha}{h} \quad (2)$$

where γ is the surface tension of the liquid mixture as measured in a tensiometry experiment and α is a microscopic length that is derived in the following.

The resulting thickness-dependent interfacial tension allows a transient mechanical equilibrium of the film connected to a meniscus, called a Plateau border in foams. As detailed in a previous publication⁷ and schematized in Figure 4, equilibrium

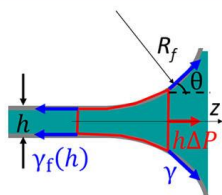


Figure 4. Schematics of a liquid film between two bubbles of radius R in the foam. The flat part of the film is connected to the Plateau border (meniscus). The larger surface tension in the flat part allows establishment of a mechanical equilibrium, although the pressures are not equilibrated. A balance of tensions along the z -axis can be written, for instance, on the film portion in red.

of the tensions in the film is reached because the tension is larger in the flat part than in the curved part of the film. Although the increase in surface tension in the flat part is very small (less than 1%), it allows the film tension, that is, the sum of surface tension and pressure times thickness, to be balanced between the flat and curved parts of the film. We emphasize no equilibrium could be reached without the increase of surface tension. Once the equilibrium is reached for a given shape of the film, the pressure is nevertheless smaller in the Plateau border than in the film and the liquid is further sucked from the film to the Plateau border. The lifetimes of the liquid films are determined by the duration of film drainage, which is a relatively slow process (typically seconds).¹⁴ This duration depends on the initial film geometry (i.e., on the curvature radius of the Plateau border) and is observed to vary proportionally with the length α .⁷ This is why the relation between partition of molecules at the interface and in the bulk and its role on the interfacial tension is crucial to understand the lifetime of foams formed in mixtures.

We now derive the expression of the microscopic length α . We consider a liquid film of thickness h of a binary mixture A/B, species A having the smallest surface tension, and we derive

its thickness-dependent surface tension. We denote N_0 its total mole number and x_A^0 and x_B^0 its initial molar fractions. We make the approximation of volume additivity, the total volume of the liquid forming the film V_0 is thus $V_0 = (x_A^0 v_A + x_B^0 v_B) N_0$. When the liquid film forms, N moles occupy its bulk, of respective molar fractions in species A and B x_A and x_B , whereas $N_S = N_0 - N$ moles are at the interfaces with air, of respective molar fractions Γ_A and Γ_B . The bulk volume (without the surface layer) and total surface of the film are respectively

$$V = (x_A v_A + x_B v_B) N \quad (3)$$

$$S = (\Gamma_A \sigma_A + \Gamma_B \sigma_B) N_S \quad (4)$$

Using the conservation equations of species A yields

$$\Gamma_A N_S + x_A N = x_A^0 N_0 \quad (5)$$

From eqs 3, 4, and 5 and using $\Gamma_A + \Gamma_B = 1$, we obtain the following relations

$$N_S = \frac{S}{\Gamma_A(\sigma_A - \sigma_B) + \sigma_B} \quad (6)$$

$$N_0 = \frac{V_0}{x_A^0(v_A - v_B) + v_B} \quad (7)$$

$$x_A = x_A^0 \frac{N_0}{N} - \Gamma_A \frac{N_S}{N} \quad (8)$$

From the last equations, we derive the variation in bulk molar fraction resulting from the creation of an interface

$$x_A - x_A^0 = \frac{N_S}{N_0 - N_S} (x_A^0 - \Gamma_A) \quad (9)$$

Making the approximation $N_0 - N_S \approx N_0$ and using the geometrical relation between the total surface of the liquid film and its volume and thickness, $S = 2V/h$, yields

$$x_A - x_A^0 = -\frac{2}{h} \frac{(\Gamma_A - x_A^0)(v_B(1 - x_A^0) + v_A x_A^0)}{(\Gamma_A(\sigma_A - \sigma_B) + \sigma_B)} \quad (10)$$

Finally, the increase of surface tension of the film of thickness h is obtained from the expansion $\gamma_f(h) - \gamma = (d\gamma/dx_A)(x_A - x_A^0)$ and eq 10, yielding

$$\gamma_f(h) - \gamma = \frac{2}{h} \left(\frac{d\gamma}{dx_A} \right) (x_A - \Gamma_A) \frac{(v_B(1 - x_A) + v_A x_A)}{(\Gamma_A(\sigma_A - \sigma_B) + \sigma_B)} + o\left(\frac{1}{h^2}\right) \quad (11)$$

where the approximation $x_A^0 \approx x_A$ has been made and where values of γ and its derivative are taken for $x_A = x_A^0$, that is, $\gamma = \gamma(x_A^0)$ and $(d\gamma/dx_A) = (d\gamma/dx_A)_{x_A^0}$.

Equation 11 is valid only for thicknesses that are large compared to the molecular sizes, $h \gg v_i/\sigma_i$. Note that eq 11 is not based on any thermodynamical hypothesis since it is derived only from molar conservation considerations. For symmetric mixtures, that is, made of molecules of same molar surface and volume, one obtains from eq 2 and 11

$$\alpha = \frac{2}{\gamma} \left(\frac{d\gamma}{dx_A} \right) (x_A - \Gamma_A) \frac{v_A}{\sigma_A} \quad (12)$$

Therefore, the ability to foam, as measured by the length α , is related to the surface-bulk partition of species A ($x_A - \Gamma_A$). As a result, with symmetric molecules, foamability is associated with the nonlinearity of surface tension with composition, as

previously demonstrated for binary mixtures of different natures.⁷

In asymmetric mixtures, the surface-bulk partition is also at the origin of a thickness-dependent surface tension, as explicit in eq 11. As in symmetric mixtures, length α and $(x_A - \Gamma_A)$ are proportional, but with a positive geometric coefficient that depends on x_A . However, the term $(x_A - \Gamma_A)$ is not necessarily associated with a nonlinearity of surface tension. Further discussion on this point requires to examine the variations of surface tension and surface fractions as a function of bulk fractions. We have chosen to use the relation between these quantities known as Butler's equation.

Predictions of Butler's Equation. We consider the equation first introduced by Butler^{2a} that describe the surface/volume partition for ideal mixtures. It has been widely used in the literature, and assumes an ideal behavior of molecules both in bulk and at interfaces.^{2b} In the picture suggested by Butler, the surface molar fractions follow a Boltzman's law $\Gamma_i = x_i e^{\sigma_i(\gamma - \gamma_i)/RT}$, with $\sigma_i(\gamma - \gamma_i)$, the surface energy variation when one mole of species i is displaced from the bulk to the interface, R is the ideal gas constant, T is the absolute temperature, and γ is the surface tension of the mixture. Since $\Gamma_A + \Gamma_B = 1$, the surface tension γ verifies the relation

$$x_A e^{\sigma_A/RT(\gamma - \gamma_A)} + (1 - x_A) e^{\sigma_B/RT(\gamma - \gamma_B)} = 1 \quad (13)$$

We introduce several dimensionless parameters: the effective reduced molar surface areas occupied by A and B, respectively, $S_A = \sigma_A(\gamma_B - \gamma_A)/RT$, $S_B = \sigma_B(\gamma_B - \gamma_A)/RT$, and the dimensionless excess surface tension

$$E_\gamma = \frac{\gamma - (\gamma_A x_A + \gamma_B x_B)}{\gamma_B - \gamma_A} \quad (14)$$

This excess value characterizes the deviation from linearity and is positive for superlinear variations of surface tension and negative for sublinear variations. Using these quantities, Butler's equation (eq 13) can be written as

$$x_A e^{S_A(E_\gamma + 1 - x_A)} + (1 - x_A) e^{S_B(E_\gamma - x_A)} = 1 \quad (15)$$

Following eq 15, the dimensionless excess surface tension $E_\gamma(x_A)$ is a function of mixture composition and only depends on two parameters, S_A and S_B . In practice, these parameters are of the order of unity (see Table 1).

We have solved eq 15 numerically with a typical value of $S_A = 1$ and different surface ratios $\sigma_B/\sigma_A = S_B/S_A$. The corresponding normalized surface tension variations are shown in Figure 5a as a function of the bulk molar fraction of the species having the smallest surface tension. For surface ratios ranging from 0.2 to 1, the variations are sublinear and the nonlinearity increases as the ratio decreases. Conversely, for surface ratios of 3 and 5, the variations are superlinear and the nonlinearity increases as the ratio increases. However, it does not mean that the species B with the largest surface tension concentrates at the surface. From the computed values of $\gamma(x_A)$, we also determine $\Gamma_A(x_A)$ in Figure 5b: Clearly, whatever the surface ratio of the molecules, the molar fraction in species A at the surface is larger than the one in the bulk. The associated nonlinearity increases monotonically with the surface ratio of the molecules.

This result can be understood by expanding eq 15 for S_A and $S_B \ll 1$, in the limit of an entropy-dominated partition between

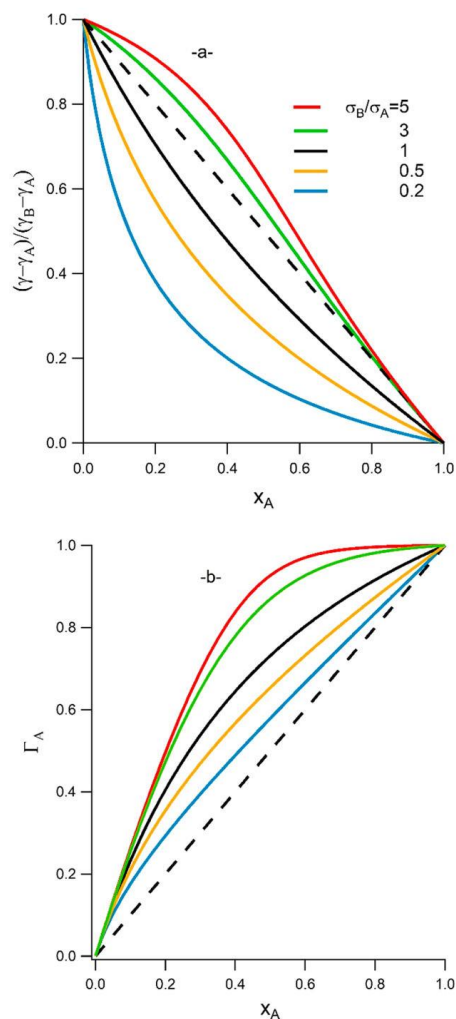


Figure 5. (a) Normalized surface tensions as a function of the bulk molar fraction of species A, predicted by Butler's equation (eq 14) with arbitrarily chosen values: $S_A = 1$ and different S_B/S_A ratios. (b) Corresponding surface molar fraction of species A.

surface and bulk. In that case, the dimensionless excess surface tension is given by

$$E_\gamma = \frac{x_A(1 - x_A)}{x_A + \frac{S_B}{S_A}(1 - x_A)} \left(\frac{S_B}{S_A} - 1 \right) \quad (16)$$

The ratio in the right-hand term of eq 16 is positive. Therefore, the sign of the nonlinearity is given by the sign of $\left(\frac{S_B}{S_A} - 1\right)$.

This result is in qualitative agreement with the data of Figure 5 for surface ratios different from unity, for which a sublinear behavior is reported for ratios of 0.2 and 0.5 (i.e., $S_B/S_A < 1$) and a superlinear behavior for ratios of 3 and 5 ($S_B/S_A > 1$). In contrast, while the approximated eq 16 predicts the surface tension to vary linearly for a ratio of 1 (i.e., $E_\gamma = 0$), full resolution of Butler's equation with the parameters of Figure 5 yields sublinear variations for the latter ratio. Instead a linear behavior is predicted for a surface ratio close to 2 according to the complete Butler's equation. The contribution of surface

energies, which are assumed to be very small in the derivation of eq 16, must be considered to understand the latter results.

Actually, the surface tension of the mixture is determined by the product of molecular surfaces and the difference between the surface energies. If the surface energies of the two molecules are close, their partitions between surface and bulk are also similar. As a result, if the species with the largest surface tension has also the largest molar surface, its contribution to surface tension will be proportional to its concentration in bulk times its molar surface, leading to superlinear variations of surface tension. This limit is predicted by eq 16. However, if the difference between surface energies is large, this effect is counterbalanced by the fact that a smaller surface concentration of the species with the larger surface energy is favored, as compared to bulk. These two effects (ratio between occupied surfaces and partition) are of the same order of magnitude because the value of the effective reduced molar surface is of the order of unity. This explains why the surface tension of a mixture varies superlinearly only if the species with the largest surface tension also has the largest molar surface and if the ratio of the molar surfaces of the two species exceeds some critical value. The crossover between sub and superlinear variations of the interfacial tension can be found by solving Butler's equation for $E_\gamma = 0$ and $x_A = 1/2$. The following relation is obtained

$$S_B = -2 \ln(2 - e^{S_A/2}) \quad (17)$$

which yields $S_B/S_A = 2.09$ for $S_A = 1$. Therefore, the crossover between super and sub linear superficial tension depends in a subtle way on the respective values of the molar surfaces and on the difference between surface energies. Sublinearity is favored by large differences in surface energies whereas difference of molar surfaces are at the origin of either superlinear or sublinear behaviors, depending on the surface ratio. Similar conclusions were drawn by Prigogine and his co-workers for nonideal solutions.¹² They, in particular, showed that, in addition to surface ratio, the heat of mixing contributes to a lower surface tension of mixtures.

We now compare the predictions of Butler's equation with the experimental data of Figure 2. For each mixture, we have reported the computed surface tensions in Figure 2. The molar surfaces are unknown; a usual approximation made in the literature considers cuboid molecules, allowing computation of the molar surfaces from the molar volumes. However, we have found the experimental surface tensions are not described using values for molar surfaces obtained in this approximation; a correct description requires more asymmetric molar surfaces, as can be seen in Table 1, in which we report the value of surface ratios in best agreement with the experimental data. In each case, the molar surface of species A was arbitrarily chosen to be the one given by the cuboid approximation, and the surface ratio was adjusted in order to match the surface tension curves following eq 13.

Numerous attempts have been made to provide a quantitative description of the surface tension of mixtures as a function of their composition.^{2c,e,3a,11a,d,12,15} However, because of the missing information on the molecular surface, there is no available model valid, whatever the nature of the mixture. As reported, molar surfaces of a given molecule may vary from one mixture to another, depending on the nature of the molecule it is mixed with. For a given mixture, the molar surfaces may as well vary with composition. In addition, nonideal behavior in bulk, but also at the surfaces, can induce

deviations from Butler's equation. We have not tried to provide a more quantitative description of the surface tensions of the mixtures investigated since we focus here on the link between surface tension nonlinearity and foamability.

Microscopic Length α of the Studied Mixtures. We establish the expression for α in the framework of ideal mixtures. The derivative of surface tension ($\frac{\partial\gamma}{\partial x_A}$) is readily obtained by computing the derivative of Butler's equation (eq 13) with respect to x_A

$$\frac{\partial\gamma}{\partial x_A} = \frac{RT(x_A - \Gamma_A)}{(1 - x_A)x_A(\Gamma_A S_A + (1 - \Gamma_A)S_B)} \quad (18)$$

Equation 11, giving the thickness-dependent surface tension, then becomes

$$\gamma_j(h) - \gamma = \frac{1}{h} \frac{RT(\Gamma_A - x_A)^2}{2(1 - x_A)x_A} \frac{(v_B(1 - x_A) + v_A x_A)}{(\Gamma_A \sigma_A + (1 - \Gamma_A)\sigma_B)^2} + o\left(\frac{1}{h^2}\right) \quad (19)$$

Finally, the expression for the microscopic length α , in the case of ideal solutions, characterizing the ability to form foams is deduced from eqs 19 and 2

$$\alpha = \frac{RT(\Gamma_A - x_A)^2}{\gamma} \frac{(v_B(1 - x_A) + v_A x_A)}{(1 - x_A)x_A 2(\Gamma_A \sigma_A + (1 - \Gamma_A)\sigma_B)^2} \quad (20)$$

Mixtures with identical bulk and surface compositions, for which $\Gamma_A = x_A$ are characterized by $\alpha = 0$, meaning that foams are as unstable as in pure liquids for which bubble lifetimes are of the order of 1 ms. However, as emphasized above, the species with the smallest surface tension is always more concentrated at the surface than in the bulk, that is, $\Gamma_A - x_A > 0$, whatever the surface ratio of molecules. As a result, provided the surface tensions are different, the microscopic length is nonzero and foam lifetimes are enhanced.

We have computed the variations of length α following eq 20 and they are reported as a function of mixture composition in Figure 6. Cuboid molecules have been considered in order to determine the molar surfaces, with surface ratios close to the ones determined for the used liquid mixtures (see Table 1). The length α is at most of a molecular size. Similar to the variation of L_r shown in Figure 3, all curves for length α exhibit a maximum at a composition that depends on the asymmetry of the mixture; in addition, the position of the maximum is shifted toward the larger molar fractions in species A as the surface ratio increases, as found for L_r . A qualitative correlation between the two lengths is therefore observed.

However, the amplitudes of length α and L_r vary differently with the volume ratio. In particular, we have found the PDMS/decane mixture formed foams with very large lifetimes, yielding very large values of L_r . The position of the maximum in the experimental curve is also reached for a strikingly small ($\sim 10^{-3}$) molar fraction in PDMS. As reported in Figure 6 (dashed line), such a value corresponds to a surface ratio close to 10^{-2} , much smaller than the one determined from surface tension variations. Clearly, eq 20, derived in the framework of ideal mixtures, does not capture the effects at stake in this mixture. A more quantitative description of the foaming properties would require one to consider nonideal behaviors, that is, fugacities of the different species in bulk and at the interfaces. Nevertheless, experimental determination of the fugacity of molecules at an interface is difficult and molecular dynamics simulations are more likely to help bring new light on the link between species partition and foamability.¹⁶

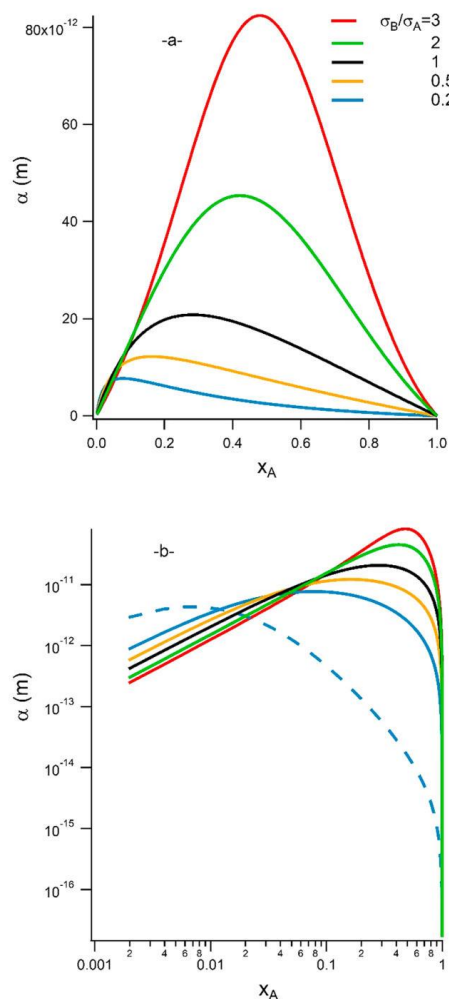


Figure 6. Length α characterizing the increase of surface tension with decreasing thickness of a film of binary mixture, as a function of the mixture composition in linear (a) and log (b) plots. The curves were computed using eq 20, derived in the case of ideal solutions. The additional dashed line in (b) was obtained with a volume ratio of 10^{-2} .

CONCLUSION

We have shown previously that the foams formed in liquid mixtures of molecules with similar surfaces have lifetimes 3–4 orders of magnitude larger than the ones formed in pure liquids and that it was a consequence of the sublinear variations of their surface tension with composition. Here we demonstrate that the case of mixtures of molecules with different sizes is more complex. We show that, in the case of ideal solutions, the surface tension may vary superlinearly with composition, provided the species with the largest surface energy has a large enough molar surface, consistently with our experimental findings on mixtures with different surface ratios. However, whatever the sign of the nonlinearity, the surface concentration of the species with the smallest surface energy is always larger than the bulk one; we show the ability to foam originates from this concentration difference and confirm that finding experimentally. As a result, mixtures of species of

asymmetric molecular sizes may exhibit either sub or superlinear variations of their surface tension with composition and nonetheless have a stronger ability to foam than pure liquids.

AUTHOR INFORMATION

Corresponding Author

L. Talini – CNRS, Surface du Verre et Interfaces, Saint-Gobain, 93300 Aubervilliers, France; orcid.org/0000-0001-7309-7673; Email: laurence.talini@espci.fr

Authors

H. P. Tran – CNRS, Sciences et Ingénierie de la Matière Molle, ESPCI Paris, PSL Research University, Sorbonne Université, 75005 Paris, France; Laboratoire Physico-Chimie des Interfaces Complexes, ESPCI, 75005 Paris, France; Bâtiment CHEMSTARTUP, 64170 Lacq, France

L. Delance – CNRS, Sciences et Ingénierie de la Matière Molle, ESPCI Paris, PSL Research University, Sorbonne Université, 75005 Paris, France; Laboratoire Physico-Chimie des Interfaces Complexes, ESPCI, 75005 Paris, France; Bâtiment CHEMSTARTUP, 64170 Lacq, France

N. Passade-Boupat – Laboratoire Physico-Chimie des Interfaces Complexes, ESPCI, 75005 Paris, France; Bâtiment CHEMSTARTUP, 64170 Lacq, France; Total S.A., 64170 Lacq, France; orcid.org/0000-0003-2913-0864

E. Verneuil – CNRS, Sciences et Ingénierie de la Matière Molle, ESPCI Paris, PSL Research University, Sorbonne Université, 75005 Paris, France; Laboratoire Physico-Chimie des Interfaces Complexes, ESPCI, 75005 Paris, France; Bâtiment CHEMSTARTUP, 64170 Lacq, France; orcid.org/0000-0002-7829-0795

F. Lequeux – CNRS, Sciences et Ingénierie de la Matière Molle, ESPCI Paris, PSL Research University, Sorbonne Université, 75005 Paris, France; Laboratoire Physico-Chimie des Interfaces Complexes, ESPCI, 75005 Paris, France; Bâtiment CHEMSTARTUP, 64170 Lacq, France; orcid.org/0000-0003-4076-3988

Complete contact information is available at: <https://pubs.acs.org/10.1021/acs.langmuir.1c02198>

Notes

The authors declare no competing financial interest.

REFERENCES

- (1) von Szyszkowski, B. Experimental studies of the capillary properties of aqueous solutions of fatty acids. *Z. Phys. Chem.* **1908**, *64*, 385–414.
- (2) (a) Butler, J. A. V. The thermodynamics of the surfaces of solution. *Proceedings of the Royal Society of London Series A* **1932**, *135* (827), 348–375. (b) Eriksson, J. C. On the thermodynamics of surface systems. *Advances in Chemical Physics* **2007**, *6*, 145–174.
- (c) Eberhart, J. G. The Surface Tension of Binary Liquid Mixtures. *J. Phys. Chem.* **1966**, *70* (4), 1183–1186. (d) Guggenheim, E. A.; Adam, N. K. The thermodynamics of adsorption at the surface of solutions. *Proceedings of the Royal Society of London Series a-Containing Papers of a Mathematical and Physical Character* **1933**, *139* (837), 218–236.
- (e) Belton, J. W.; Evans, M. G. Studies in the Molecular Forces Involved in Surface Formation. 2. The Surface Free Energies of Simple Liquid Mixtures. *Trans. Faraday Soc.* **1945**, *41* (1), 1–12.
- (3) (a) Santos, M. S. C. S.; Reis, J. C. R. Partial molar surface areas in liquid mixtures. Theory and evaluation in aqueous ethanol. *J. Mol. Liq.* **2019**, *273*, 525–535. (b) Shardt, N.; Wang, Y.; Jin, Z.; Elliott, J.

A. W. Surface tension as a function of temperature and composition for a broad range of mixtures. *Chem. Eng. Sci.* **2021**, *230*, 116095.

(4) (a) Chen, H.; Gan, W.; Lu, R.; Guo, Y.; Wang, H. F. Determination of structure and energetics for Gibbs surface adsorption layers of binary liquid mixture 2. Methanol plus water. *J. Phys. Chem. B* **2005**, *109* (16), 8064–8075. (b) Kirschner, J.; Gomes, A. H. A.; Marinho, R. R. T.; Bjorneholm, O.; Agren, H.; Carravetta, V.; Ottosson, N.; de Brito, A. N.; Bakker, H. J. The molecular structure of the surface of water-ethanol mixtures. *Phys. Chem. Chem. Phys.* **2021**, *23* (19), 11568–11578.

(5) Lhuissier, H.; Villermaux, E. Bursting bubble aerosols. *J. Fluid Mech.* **2012**, *696*, 5–44.

(6) (a) Ross, S.; Nishioka, G. Foaminess of binary and ternary solutions. *J. Phys. Chem.* **1975**, *79* (15), 1561–1565. (b) Tuinier, R.; Bisperink, C. G. J.; vandenBerg, C.; Prins, A. Transient foaming behavior of aqueous alcohol solutions as related to their dilational surface properties. *J. Colloid Interface Sci.* **1996**, *179* (2), 327–334.

(7) Tran, H. P.; Arangalage, M.; Jorgensen, L.; Passade-Boupat, N.; Lequeux, F.; Talini, L. Understanding Frothing of Liquid Mixtures: A Surfactantlike Effect at the Origin of Enhanced Liquid Film Lifetimes. *Phys. Rev. Lett.* **2020**, *125* (17), 178002.

(8) Gaines, G. L. Surface Tension of Polymer Solutions. I. Solutions of Poly(dimethylsiloxanes). *J. Phys. Chem.* **1969**, *73* (9), 3143.

(9) Kendall, J.; Monroe, K. P. The viscosity of liquids. II. The viscosity-composition curve for ideal liquid mixtures. *J. Am. Chem. Soc.* **1917**, *39*, 1787–1802.

(10) Bikerman, J. J. *Measurement of Foaminess in Foams*; Springer-Verlag: New York, 1973.

(11) (a) Suarez, J. T.; Torresmarchal, C.; Rasmussen, P. Prediction of Surface Tensions of Nonelectrolyte Solutions. *Chem. Eng. Sci.* **1989**, *44* (3), 782–786. (b) Nath, S. Surface tension of nonideal binary liquid mixtures as a function of composition. *J. Colloid Interface Sci.* **1999**, *209* (1), 116–122. (c) Kahl, H.; Wadewitz, T.; Winkelmann, J. Surface tension of pure liquids and binary liquid mixtures. *J. Chem. Eng. Data* **2003**, *48* (3), 580–586. (d) Kaptay, G. Partial Surface Tension of Components of a Solution. *Langmuir* **2015**, *31* (21), 5796–5804. (e) Santos, M. S. C. S.; Reis, J. C. R. Thermodynamic evaluation of molar surface area and thickness of water plus ethanol mixtures. *J. Mol. Liq.* **2018**, *255*, 419–428.

(12) Prigogine, I.; Marechal, J. The Influence of Differences in Molecular Size on the Surface Tension of Solutions. 4. *J. Colloid Sci.* **1952**, *7* (2), 122–127.

(13) Pugh, R. J. Foaming, foam films, antifoaming and defoaming. *Adv. Colloid Interface Sci.* **1996**, *64*, 67–142.

(14) Koehler, S. A.; Hilgenfeldt, S.; Weeks, E. R.; Stone, H. A. Drainage of single Plateau borders: Direct observation of rigid and mobile interfaces. *Phys. Rev. E: Stat. Phys., Plasmas, Fluids, Relat. Interdiscip. Top.* **2002**, *66* (4), 04601.

(15) Santos, M. S. C. S.; Reis, J. C. R. New Thermodynamics for Evaluating the Surface-phase Enrichment in the Lower Surface Tension Component. *ChemPhysChem* **2014**, *15* (13), 2834–2843.

(16) (a) Matsumoto, M.; Takaoka, Y.; Kataoka, Y. Liquid vapor interface of water-methanol mixture. I. Computer-simulation. *J. Chem. Phys.* **1993**, *98* (2), 1464–1472. (b) Chang, T. M.; Dang, L. X. Liquid-vapor interface of methanol-water mixtures: A molecular dynamics study. *J. Phys. Chem. B* **2005**, *109* (12), 5759–5765.

4. HYDRODYNAMICS AND PIERCING OF THIN LIQUID FILMS

In previous chapters, we show that foaming of liquid mixtures – based on experimental data and theoretical models – is due to the partitioning of molecules between bulk and surface. Indeed, the liquid film layers generated between the two bubbles exhibit thickness-dependent surface tension. The difference in surface tension creates the Marangoni effect, which delays the drainage in thin films. However, this drainage always occurs as a consequence of a pressure imbalance between the liquid film and the Plateau border. This results in a pinching effect on the liquid thin film.

In this chapter, we will continue our investigation of the relations between foam and bubble lifetimes and demonstrate that they may be compared to measurable values. Finally, we can develop our approach only because the surface rheology of these systems is rather simple in comparison to that of soap films formed from aqueous surfactant solutions, for which no complete prediction of the lifetimes has been made. For that purpose, we give an analytical description of liquid film formation, drainage, and breakup.

4.1. SUMMARY OF SUBMITTED PUBLICATION “RUPTURE MECHANISMS OF FILM OF LIQUID MIXTURES”

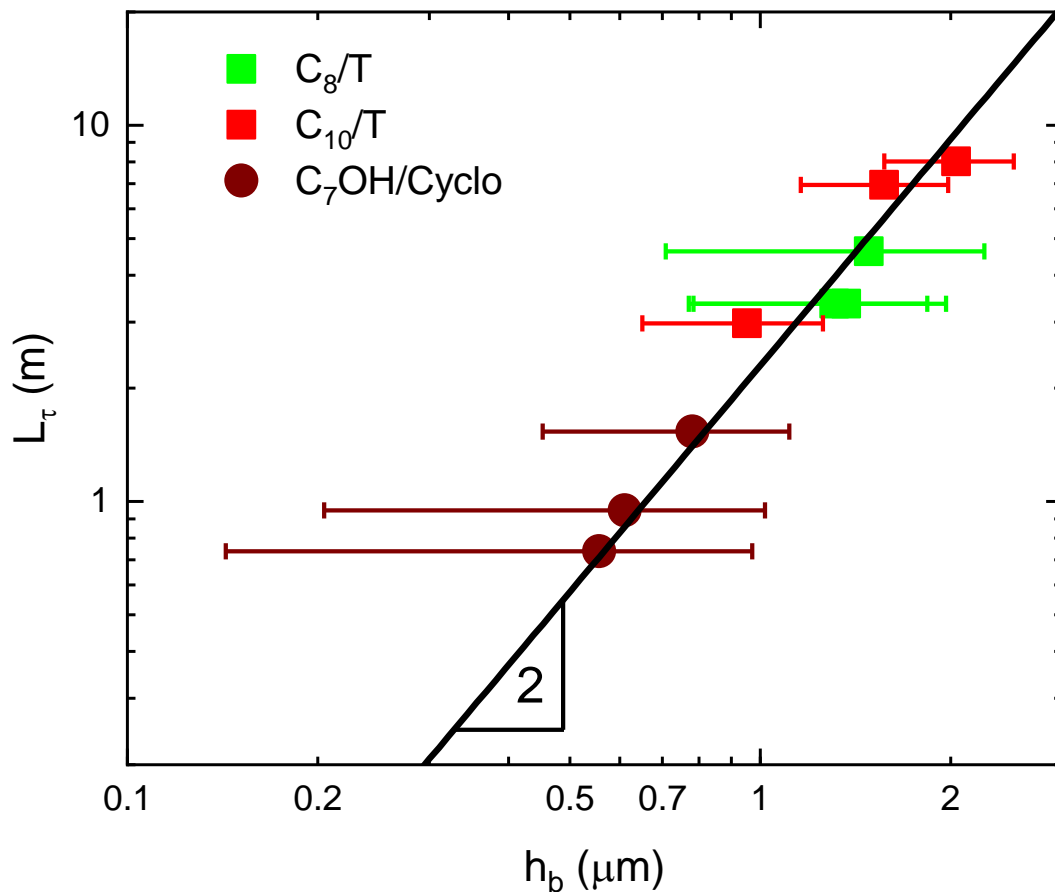


Figure 4-1 : Experimental length L_τ as a function of film thickness h_b at bursting, both measured in single bubble experiments. The error bars on film thickness result from the uncertainty on the Taylor-Culick velocity.

In **Chapter 1**, we conducted an experiment with a single bubble at the liquid's surface in order to determine the thickness of the liquid film when the bubble bursts. The thickness of the liquid thin layer is nearly uniform at this stage. This result demonstrates that the thickness h_b is close 1 micrometer and spatially homogeneous, which indicates that drainage has not significantly affected the film but at the piercing location. Hence the piercing is very localized, and we can assume that $h_b = h_f$ since no significant drainage, except at the position of piercing was observed. Moreover, the radial position of piercing is extremely reproducible. Its suggest that the origin of bursting is controlled by hydrodynamics. We also measured the lifetime of the

bubble at the surface in these tests. We derived the foaming length L_τ from this value and illustrated the correlation between this length L_τ and the film thickness h_b (which is also h_f) in the **Figure 4-1**. This graph indicates that the lifetime of the bubble changes proportionately to the squared thickness of its film $\tau \sim L_\tau \sim h_b^2$.

In **Chapter 2**, we also addressed the formation of film layers and suggested an analytical description of the shape of the film at mechanical equilibrium in tension. The liquid film consists of two parts: a flat thin film and a curved part due to the meniscus effect. The surface tension in the former is higher than in the latter. A length α is provided to account for the variation in surface tensions in this thin film: $\gamma(h) = \gamma(1 + \alpha/h)$.

Moreover, α is related to the thickness of thin layer at the moment before the liquid in this film begins to drain in the following way: $h_b = h_f = \sqrt{\alpha R_f}$. R_f is the curvature radius of the film. In **Chapter 2**, we have measured a correlation between the foamability of mixes and the characteristic length α that leads to the phenomenological law $L_\tau \sim \alpha$. As a result, it also suggests that L_τ or foam lifetime τ should vary with h_f^2 . We will in the following discuss the pinching mechanism and show that a scaling analysis of the pinching dynamics gives a lifetime dependence on thickness in h_f^2 .

The mechanical equilibrium between Plateau boarder and film is not pressure-balanced and in the absence of repulsive disjunction pressure, drainage leads to film thinning and piercing. In this frame, Aradian et al. [43] predict that the film is expected to thin down at a precise location, and forms a pinch. The proposed mechanism leading to the film bursting is as follows: when the pinched part thins – due to hydrodynamics - down to a critical thickness, van der Waals attraction becomes effective [44,45]; the film then pierces extremely quickly. The film lifetime is thus determined by the time required for the pinched part to reach the critical thickness, which is significantly longer than the durations of the first stretching stage and the last piercing stage under van der Waals forces action. It thus determines the lifetime of the bubbles.

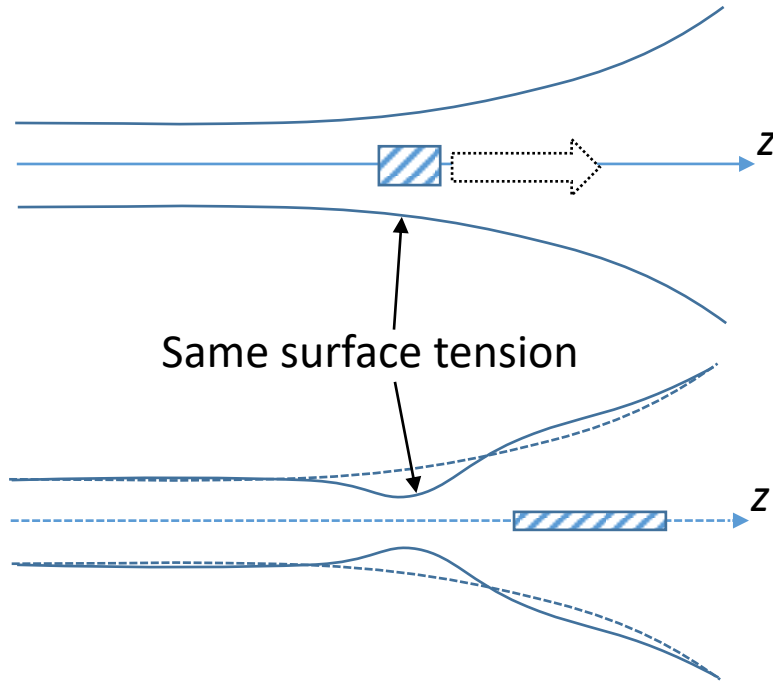


Figure 4-2 : Illustration of the argument for considering constant composition of the liquid mixture during film pinching.

Due to the high rate of fluid drainage at the pinching spot, a relative displacement of the film's bulk and interfaces is predicted at this point. Because pinching results in a localized thinning of the film, it is equal to removing some liquid volume from a specific location within the film's bulk, as seen in **Figure 4-2**.

It obviously reduces the thickness at the surrounding area, but it has no effect on the thermodynamic equilibrium between the interfaces and the bulk. As a result, we can assume that removing a fluid element from a part of the film results in its thinning without affecting the surface tension at that point.

We will examine the scaling of the lubrication equation at the pinching level in our paper, which is attached below. Scaling gives a relation between the foam/bubble lifetime τ and the characteristic length α :

$$\tau \approx \frac{\mu 3\alpha R_f^3}{\gamma h_{vdW}^3} \quad \text{Eq. 4.1}$$

where h_{vdW} is the critical thickness reached at which van der Waals forces are effective.

With $\alpha = 0.1 \text{ nm}$, $h_{vdW} = 100 \text{ nm}$, and $R_f = 1 \text{ mm}$, we find $L_\tau = \frac{\tau\gamma}{\mu} = 300 \text{ m}$, which is less than one order of magnitude larger than the experimental lengths in foam experiments. Note this value strongly depends on the chosen value of h_{vdW} .

Comparison to soap films

Finally, we will compare the outcomes of our investigation on liquid thin films in mixtures to those obtained with soap films.

Investigations on soap films are well documented in the literature [46,47]. With aqueous surfactant solutions, the exchange of surfactant molecules between bulk and interfaces is slow. At opposite, in our situation, the interchange of molecules between bulk and surfaces is fast because they are the constituent of the liquids. As a result, h^2/D represents the typical period of equilibration between bulk and film interfaces. This period is of the order of a millisecond, which is extremely brief in comparison to the time required for film formation. Therefore, our situation appears as a very specific situation of the surface rheology of complex fluids, different from the one of surfactant solutions, and this allows an efficient relation between lifetime and physico-chemistry.

4.2. SUBMITTED PUBLICATION

Rupture mechanisms of films of liquid mixtures

H.-P. Tran^{1,2}, N. Passade-Boupat^{2,3}, L. Talini^{4†} and F. Lequeux^{1,2}

¹ CNRS, Sciences et Ingénierie de la Matière Molle, ESPCI Paris, PSL Research University, Sorbonne Université, 75005 Paris, France.

² Laboratoire Physico-Chimie des Interfaces Complexes, ESPCI, 10 rue Vauquelin, 75005 Paris, Bâtiment CHEMSTARTUP, Route Départementale 817, 64170 Lacq, France.

³ Total S.A. 64170 Lacq, France.

⁴ CNRS, Surface du Verre et Interfaces, Saint-Gobain, 93300 Aubervilliers, France

(Received xx; revised xx; accepted xx)

Foams that are formed in liquid mixtures have longer lifetimes than the ones formed in pure liquids of similar viscosities. We have shown recently that this effect results from a mechanical equilibrium of the liquid films between bubbles reached before drainage, and that the equilibrium is made possible by the partition of molecules between bulk and surfaces. In this equilibrium situation, the pressure is nevertheless not constant and the film pinches and further ruptures. This last process controls the lifetimes of foam or single bubbles. We show how the problem is simplified compared to the one in soap films and we suggest its analytical description. This description is in agreement with experimental data on both foam and single bubble lifetimes measured in mixtures of different liquids.

Key words: Foams, Bubble Breakup/coalescence, Thin films

1. Introduction

Foams of surfactant solutions have been widely described in literature (Denkov et al 2020). Their lifetimes, and thus the ones of the liquid films between bubbles, can exceed days. These very long times are explained by the large repulsion induced by surfactants between the interfaces of the liquid films; the resulting disjoining pressure is able to balance the capillary pressure that induces a suction of the liquid from the flat parts of the films to their curved parts (Ivanov 1988), the so-called Plateau borders, schematized in figure 1.

In contrast, foams formed in liquids with attractive interactions between their interfaces are less stable; in practice, they are promised to a rapid death typically after a few milliseconds for viscosities close to the one of water. Among them, the foams formed in liquid mixtures have been scarcely discussed in the literature despite the simplicity of their physico-chemistry (Ross and Nishioka 1975; Tran et al 2020). In practice, foaming of solvent mixtures can be detrimental in many processes of e.g. oil industry, from crude

[†]Email address for correspondence: laurence.talini@cnrs.fr

oil extraction to car tank filling or of food industry where it is for instance observed in frying oils. As a matter of fact, addition of anti-foaming additives is often required in these processes (Pugh 1996).

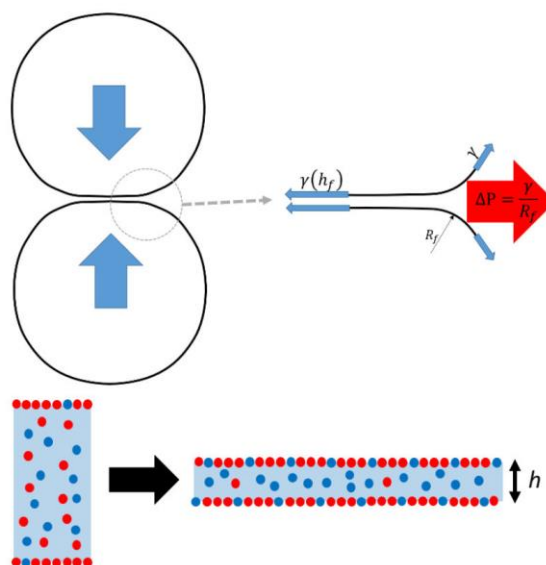


Figure 1: (Top) Scheme of a liquid film formed between two bubbles in a foam. The film is connected to a meniscus of radius of curvature R_f and can reach a mechanical equilibrium after stretching because of the increase of surface tension in its flat part. (Bottom) Illustration of the mechanism leading to increased surface tension when a flat film of liquid mixture is stretched at constant volume. Initially the surface is enriched in the species with the lowest surface tension (red circles) compared to the bulk. Because the surface to volume ratio of the film increases during stretching, the surface and bulk concentrations of the different species (blue and red circles) cannot be kept constant. A new equilibrium is reached, in which the surface concentration of the red species is smaller than initially, resulting in a larger surface tension, which value depends on film thickness, h .

We have recently shown that, whereas pure liquids do not foam because the bubbles that form in these liquids have very small lifetimes, most solvent mixtures do foam. The phenomenon at the origin of the longer bubble lifetimes in mixtures is the difference of concentration in molecules at the film surface and in the bulk of the liquid films when the two liquids have different surface tensions (Tran et al 2020; Tran et al 2021). It is well known that, in mixtures, the molecules with the smallest surface energy are more concentrated at the interface than in bulk (Butler 1932; Eriksson 1964; Prigogine and Marechal 1952) and we have demonstrated that they can play a surfactant-like role for the other molecules. To understand the consequences on film lifetimes, two stages must be distinguished between film formation and rupture. As described for small concentrations of surfactants (Lhuissier and Villermaux 2012), when a foam forms (or equivalently when a bubble approaches the surface of a liquid bath), a liquid film is first stretched and then drains in a second stage. Since stretching is associated with an increase

of surface to volume ratio, in the case of liquid mixtures, it always results in the pumping of the low surface energy species from the interfaces to the bulk, as schematized in figure 1. As a consequence, the interfacial tension of the stretched film increases. This effect can be described with a thickness-dependent surface tension of liquid films. In particular, it allows flat films that are connected to Plateau borders to reach a mechanical equilibrium when they form, and this *before they significantly drain*. The whole film tension – i.e. the sum of pressure multiplied by film thickness and surface tension – is constant in this situation, and liquid films of thicknesses determined by the curvature of the Plateau borders are in equilibrium. However, even if the whole film tension is constant, a pressure gradient persists between the flat and curved parts of the films. In summary, when a film of a liquid mixture connected to a Plateau border forms between bubbles, an equilibrium is reached - within milliseconds for low-viscosity liquids - for film *tension*, but not for *pressure*. In a second stage, drainage driven by the pressure gradient occurs. Drainage corresponds to a motion the bulk of the film relatively to its surfaces. It is slow and its duration sets the lifetimes of bubbles that are of the order of seconds. The liquid film will finally pinch, pierce and disappear. The pinching and piercing process leading to the film death has been studied in literature in different unstable systems (Champougny et al 2016; Lhuissier and Villermaux 2012). The pressure gradient between the Plateau border and the flat part of the film drives a localised thinning of the film in the crossover region between the Plateau border and the film. When the crossover region is thin enough, the film pierces at some point, generating a single hole. Owing to film tension, the hole further extends and destroys the liquid film. In this paper, we will focus on the pinching process of films of liquid mixtures. We will explain that, in this particular case, the lifetimes of the films depend on the partition coefficient of molecules between bulk and surfaces. We will compare our experimental observations to our model. We will finally discuss why the situation is very different from the one encountered in surfactant solutions.

The complex problem of the pinching of liquid films has been the object of different approaches. Theoretical considerations have been limited to the simple situation of rigid interfaces, i.e. interfaces at which the liquid velocity vanishes in the laboratory frame. In this case, the equation of evolution - the so-called thin film equation - is difficult to solve, because it is a fourth order partial equation, and scaling approaches are not straightforward (Aradian et al 2001). Nevertheless, the approximation of rigid surfaces makes the problem similar to the drainage of films squeezed between a solid surface and a liquid/liquid interface, which has been solved by different authors (Bluteau et al 2017; Connor and Horn 2003; Jain and Ivanov 1980). However, this approximation sweeps the initial configuration of the liquid film under the rug. Moreover, the precise description of pinching remains an open problem, due to the complexity of the mechanisms involved, namely surface rheology and surfactant transfers. Indeed various simulations including some surface rheology are currently developed to describe pinching (Chatzigiannakis et al 2021).

In the case of liquid mixtures that is considered herein, the surface rheology and the film mechanics are extremely simple, because exchanges between bulk and surfaces are fast compared to the other mechanisms at stake; we show in the following that, in liquid mixtures, film lifetimes can simply be expressed as a function of geometrical parameters. The paper is organized as follows: We first present experimental results on the lifetime of foams and bubbles in polar and nonpolar liquid mixtures. We further give the analytical solution for the shape of a liquid film connected to a Plateau border before it drains. We then write the dimensionless hydrodynamical equation for drainage, and explain how the film lifetime can be inferred. Lastly, we discuss our results in light of the ones established for thin films of surfactant solutions.

2. Experimental procedures and results

In the following, we describe and give the results of experiments performed either with single bubbles or foams.

1.1 Bursting bubbles

Air bubbles are formed at the tip of a tube immersed in a tank filled with liquid mixture. The dimensions of the tank are large compared to the size of the bubble (diameter 2.5mm). The bubbles are held at a distance 1 mm from the free surface of the bath. They are imaged from the top using at a framerate of 37500 fps and from the side at 30 fps. The top view allows measurements of both bubble lifetimes and break-up kinetics. The side view is used to measure the bubble size and projection angle of the top view.

The bubbles are swollen by injecting air at constant flow rate. We have found that the swelling dynamics does not depend on air flow rate. Actually, the pressure in a bubble varies inversely with its radius of curvature; as a result, pressure first increases until the bubble radius is the one of the tube, and further decreases. Because of gas compressibility, the pressure drop is associated with air expansion in the whole circuit (syringe and tubing), which drives the kinetics of bubble expansion and make it independent of flowrate, in the conditions investigated herein.

Bubble lifetimes were measured from top views and defined as the time elapsed between the end of the swelling stage and bubble bursting. As illustrated in figure 2 that shows the cumulative distribution of bubble lifetimes measured over 50 different experiments in decane-toluene mixtures, the distributions are rather narrow. In other mixtures, the lifetimes were averaged over 25 experiments for each set of experimental conditions.

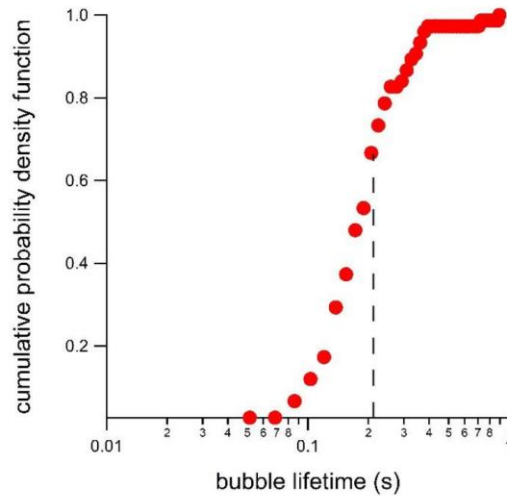


Figure 2: Cumulative probability density function of bubble lifetimes measured at the surface of a liquid mixture (decane-toluene, $x_1=0.12$). The result of 50 different experiment is shown and the dotted line indicates the average value of bubble lifetime.

Bubbles were found to puncture at a reproducible location on their side, of radius making an angle of $26 \pm 3^\circ$ with respect to the vertical axis. No significant differences in angles were observed between the different mixtures nor between different compositions of the same mixture. Interestingly, in viscous oils, bubbles were observed to puncture at the apex (Debregeas et al 1998), similarly to bubbles formed in concentrated (above the critical micellar concentration) aqueous surfactant solutions (Champougny et al 2016). In contrast, holes open close to the foot when the liquid is either a low concentration surfactant solution (Champougny et al 2016) or tap water (Lhuissier and Villermaux 2012). Remarkably, the bursting location in fluid mixtures are similar to the ones reported in moderately concentrated surfactant solutions.

We have investigated the kinetics of hole opening when bubbles burst. The curvilinear distance travelled by the edge of the opening hole, $s(t)$, is obtained from analysis of top view images. As shown in figure 3, the hole opens at constant velocity during a first stage, after which the velocity slightly decreases. The first stage ends when the hole extends beyond the bubble apex (corresponding to $\varphi = 0$ in figure 3).

The film thickness is determined by using the Taylor-Culick's relation between hole opening velocity v and film thickness h_b at bursting (Culick 1960)

$$h_b = \frac{2\gamma}{\rho v^2}, \quad (1)$$

where ρ is the liquid density and γ its surface tension.

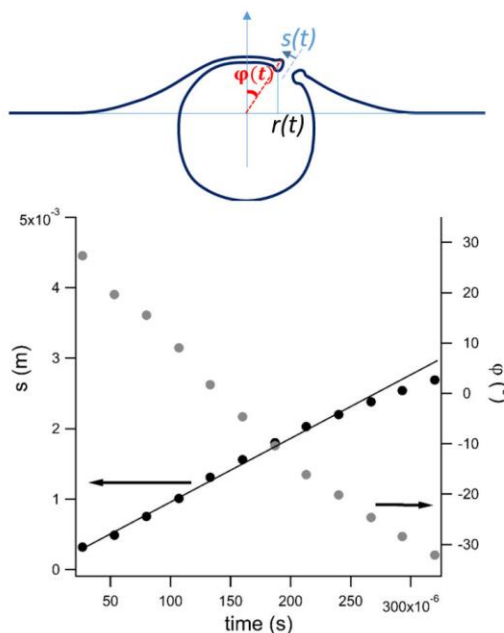


Figure 3: (Top) Scheme of a bursting bubble. The curvilinear length travelled by the edge of the opening hole, $s(t)$, is obtained from both its projection $r(t)$ in the horizontal plane and the angle $\varphi(t)$ measured from top and side views of the bubble. (Bottom) Variations with time of distance s (left axis, black circles) and angle φ (right axis, grey circles). Both s and φ were measured during bursting of a bubble in a heptanol/cyclopentanol mixture of heptanol molar fraction $x_1=0.12$. The slope of the full line is the Taylor-Culick velocity from which the thickness at bursting is inferred.

The resulting thicknesses are in the micron range, and depend on the nature of the mixture and its composition. The thickness values that are reported in the following are the one found at the first and constant-velocity stage of hole opening, and thus corresponds to the homogeneous thickness of the film when it punctures. The observed kinetics of bursting reveals that, at the onset of bursting, the liquid film has a homogeneous thickness, which is indicative of negligible drainage occurring before bursting.

2.2 Foaming experiments

The experiments with single bubbles have been compared with ones made with foams, which results have already been reported elsewhere (Tran et al 2020). Briefly, they consist in forming foams by injecting gas in a Bikerman column (Bikerman 1973), i.e. a cylindrical glass column at the bottom of which lies a porous filter. The column is first filled with a liquid mixture, and the conditions are such that, when gas is injected, a foam forms with a stationary height. The sizes of the bubbles were measured and found to weakly vary with height in the foam and from one liquid mixture to another. The

average diameter is 1.6 ± 0.3 mm. The foam lifetime is defined as the ratio of foam height and gas velocity. It is independent of the gas velocity in the investigated range.

2.3 Measured characteristic lengths

Both bubble rupture and foaming experiments have been performed in three different liquid mixtures: octane-toluene, decane-toluene and heptanol-cyclopentanol. The properties of each liquid are reported in Table 1. Their viscosities and surface tensions differ and, so do the properties of their mixtures.

Liquid	Octane	Decane	Toluene	Heptanol	Cyclo pentanol
γ (N.m ⁻¹) $\times 10^{-3}$	21.6	23.8	28.5	26.2	32.7
μ (Pa.s) $\times 10^{-3}$	0.51	0.85	0.55	5.76	9.60

Table 1: Investigated liquids and their surface tension and viscosity values.

In order to compare lifetimes measured in liquid mixtures of different compositions, and to account for the differences in viscosities and surface tensions, we introduce a length L that is the product of the lifetime (either of bubbles or foams) measured in a mixture and the capillary velocity in the same mixture, $V^* = \gamma/\mu$. The lifetimes range from seconds to tens of seconds and the capillary velocities from meters per second to tens of meters per second; as a result, the length L ranges from a few meters to 100m. This characteristic length is therefore much larger than the other lengths of the problem. Similar “giant” characteristic lengths were found to be involved in the bursting of bubbles in water (Lhuissier and Villermaux 2012). Actually, the bubble size was expressed as the geometric mean of the film thickness at bursting and a giant length, making the length scales of the problem ranging from hundreds of nanometers to tens of meters. The meaning of these lengths remains to be determined. Interestingly, we will show in the following that the characteristic length scales of the problem we consider span an even broader range; the effect stabilizing liquid films in mixtures actually requires the introduction of a molecular length, extending the spanned range to more than ten decades. In the following, we do not consider L as a physical length of the problem but rather as a convenient quantity for comparing lifetimes of bubbles or foams in liquids with different viscosities and surface tensions.

We report in figure 4 the variations of L obtained from the measured lifetimes of bubbles and foams in the different mixtures as a function of their compositions. As for

lifetimes (Tran et al 2020), a maximum is found for L in each nature of mixture. The maximum occurs at a molar fraction which values depends on the mixture, and can be predicted from the surface tension variations of the mixture with composition (Tran et al 2020). Interestingly, the values of the lengths L determined in single bubble experiments are smaller by one order of magnitude than the lengths obtained in foaming experiments. In both experiments, liquid films are connected to a curved meniscus and drain. But the curvature of the meniscus differs: whereas it is given by the capillary length for single bubbles at the surface of a liquid bath, it depends on the size of the bubbles and on the liquid fraction in foams (Cantat 2013). In the foams we consider, we roughly estimate the average liquid fraction to be close to 10% and thus the radius of curvature of the Plateau border to be approximately half the bubble radius, i.e. close to 500 μm (Cantat 2013), which is smaller than the capillary length. We emphasize this value is approximate and, in particular, is not expected to be constant over the foam height, because of gravity-induced drainage. As a result, it is difficult to precisely account for the role of the curvature of the Plateau border in foams. Even if the absolute values of L that are measured are different in single bubble and foam experiments, figure 4 shows their relative variations are nevertheless in good agreement in both experiments. In particular, a maximum lifetime with mixture composition is found in all cases. In the following, we suggest a generic model for both bubbles and foams that successfully predicts the relation between the lengths L , characterising the film lifetimes, and the thickness at the onset of bursting, independently of the details of the drainage mechanism.

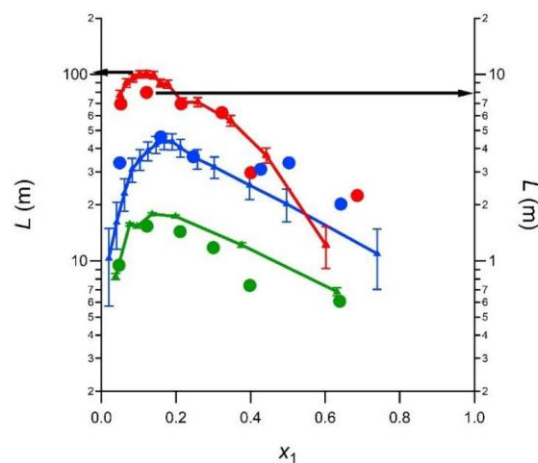


Figure 4: Characteristic lengths defined as the products of lifetimes and capillary velocities as a function of the molar fraction in the mixture of the species with the smallest surface tension. Results of both foaming experiments (left axis and triangles) and single bubble experiments (right axis and circles) are shown. Solid lines are guides to the eye. The error bars result from the uncertainty on foam height in foams. The lifetimes of single bubbles were averaged over 25 experiments performed in the same conditions.

In summary, a length L ranging from meters to 100m is defined from the measured lifetimes of foams and single bubbles formed in liquid mixtures. Its variations with mixture composition are the same in both experiments. In addition, we measure the thickness of liquid films at the onset of bubble bursting; remarkably, this thickness is spatially homogeneous. We now detail the theoretical analysis we conduct on the mechanism driving film bursting, in order to find a relation between film lifetime and its thickness at bursting.

3. Theoretical analysis and discussion

3.1 Tension equilibrium before drainage

As explained above, two stages can be considered before film rupture: in a first stage, a film forms between two bubbles by stretching until a mechanical equilibrium is reached; in a second stage, the film drains because of the pressure difference between its flat and curved parts. This picture is relevant provided the duration of the drainage stage is much larger than the time needed for film formation. We will come back to this point later. We first write the mechanical equilibrium for the film considered as a whole (bulk and interfaces). We emphasize an equilibrium is reached for film tension but not for pressure. The pressure gradient driving drainage will be discussed in the next section.

In our analysis, we neglect the effect of intermolecular forces, i.e. the disjoining pressure term, since its influence is limited to the very final stage, as explained below. In the case of liquid mixtures, the partition of species between bulk and interface, leads - in the absence of relative motion between the film surfaces and its bulk, or more precisely in the absence of drainage - to the following relation for the local superficial tension γ_f (Tran et al 2020)

$$\gamma_f(h) = \gamma \left(1 + \frac{\alpha}{h} \right) + O(h^{-2}), \quad (2)$$

where γ is the surface tension of the liquid in an infinitely large liquid reservoir, α a length characteristic of the mixture and depending on its composition (Tran et al 2020; Tran et al 2021), h the local thickness of the film.

Equation (2) is derived by considering the partition of molecules in mixtures and it describes the increase of surface tension in a thin film resulting from the concentration differences between bulk and surfaces. It is valid provided h remains larger than molecular sizes. As discussed in previous works (Tran et al 2020; Tran et al 2021), the length α varies with mixture composition and reaches a maximum at a composition depending on the species at stake; its value is of a few tenths of nanometers at most for the mixtures investigated herein. The length α also depends on the surfaces of the molecules at the interface, which are poorly known quantities since they are not measured

but extrapolated from other properties (Eriksson 1964; Santos and Reis 2014). The value of α is particularly difficult to determine in mixtures of molecules of very different sizes (Tran et al 2021). As a result, in the present work we limit our analysis to mixtures of molecules that have similar sizes, for which the uncertainty on α is smaller. In summary, equation (2) provides the expression of the increase of surface tension expected in a liquid film of mixtures. The resulting increase of surface tension is very small (0.01% for a 1 μ m-thick film), but nevertheless allows the stretching film to reach a mechanical equilibrium.

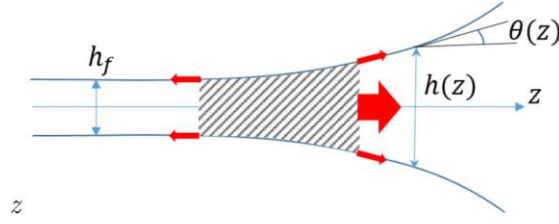


Figure 5: Scheme of a liquid film and equilibrium of its whole tension.

As schematized in figure 5 and already discussed in a previous work (Tran et al 2020), the forces exerted on a film in the z -direction (per unit length in the direction perpendicular to the plane) consists of interfacial tension and of the product of pressure in the liquid and local thickness. We refer to the sum of these forces by unit length as the film tension, which differs from the interfacial tension. At equilibrium, the film tension is constant and therefore

$$2\gamma(h) \cos(\theta(h)) + h(z)\Delta P(h) = cste, \quad (3)$$

with $\theta(h)$ the local angle of the film surface with the z -direction at x and ΔP the difference of pressure between the curved part of the film and the gas. We will here limit our analysis to small curvatures (for the sake of simplicity) and therefore the pressure difference is simply given by $\Delta P(h) \cong \gamma(h) \partial^2(h/2)/\partial z^2$. In addition, for small angles $\cos(\theta(h)) = 1 - (\partial(h/2)/\partial z)^2/2$. The constant in equation (3) is determined by considering the tension of the film in its flat part. As the reference for pressure is the one in the gas phase, and because we do not consider the effect of disjoining pressure, the film tension in the flat part of thickness h_f (see figure 5) is simply $2\gamma(1 + \alpha/h_f)$. Equation (3) finally becomes

$$\gamma \left(1 + \frac{\alpha}{h}\right) \left(2 - \frac{1}{4} \left(\frac{\partial h}{\partial z}\right)^2 + h \frac{\partial^2 h}{2 \partial z^2}\right) = 2\gamma \left(1 + \frac{\alpha}{h_f}\right). \quad (4)$$

We introduce the dimensionless variable $H(\xi) = h(z)/h_f$ and $\xi = z/w$, where w is an unknown characteristic length in the z -direction. We also introduce the dimensionless number $Y = \alpha/h_f$. In practice, $Y \ll 10^{-3}$, as will be shown in the following. Expanding equation (3) in Y leads at first order to:

$$\frac{4Yw^2}{h_f^2} \left(\frac{1}{H} - 1 \right) + \left(-\frac{1}{2}H'^2 + HH'' \right) + O(Y^2) = 0. \quad (5)$$

We emphasize that for $Y = 0$, i.e. a constant surface tension, the equation reduces to the simple equation of pressure equilibrium in the film. The only solution is then $H = a(\xi - b)^2$ where a and b are constants. However, this parabolic solution cannot connect a flat film with a Plateau border and is therefore not physically sound. As a result, a relevant solution to equation (5) can be found only if surface tension is thickness-dependent.

A natural value of lateral length is $w = h_f Y^{-1/2} = h_f^{3/2} / \alpha^{1/2}$. Equation (5) can then be solved by using H as a variable. We denote $\Theta(H) = (dH/d\xi)/2$ the dimensionless slope of the interface. Therefore, $H'' = 2\Theta' dH/d\xi = 4\Theta\Theta'$, and equation (5) becomes, if expressed as a function of the variable H

$$\left(\frac{1}{H} - 1 \right) - \frac{\Theta(H)^2}{2} + H\Theta(H)\Theta'(H) = 0. \quad (6)$$

The general solution is $\Theta = \sqrt{1 - 2H + H^2 k} / \sqrt{H}$ where the constant k remains to be determined. The value of k is such that Θ tends toward zero when H tends toward unity, which yields $k = 1$. A solution connecting a flat film and a Plateau border can therefore be found provided the surface tension is thickness-dependent. This solution is given by

$$\Theta = \frac{H-1}{\sqrt{H}}. \quad (7)$$

Equation (7) is an implicit equation, and the explicit inverse function of the solution can be obtained by integration with respect to ξ

$$\sqrt{H} - \sqrt{2} + \text{Log} \left(3 - \frac{6}{\sqrt{H}+1} \right) = \xi - c, \quad (8)$$

where c is an integration constant.

We arbitrarily choose $H = 2$ for $\xi = 1$. The corresponding variations of $h(z)/h_f$ as a function of the dimensionless position are shown in figure 6.

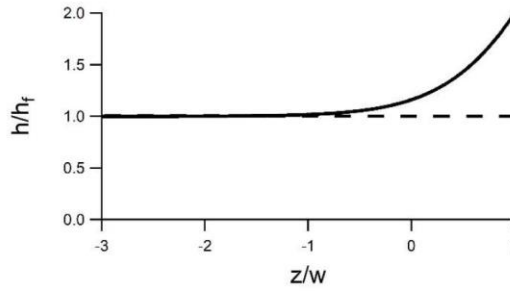


Figure 6: Solution to equation (8) giving the profile of the interface of a liquid film in mechanical equilibrium.

As expected, the curvature of the meniscus, $h''/2$ tends toward a constant value for large thicknesses, and this value corresponds to either the curvature of the Plateau border

in a foam, or the one of the meniscus for a single bubble. We denote the curvature as $1/R_f$, which yields

$$\text{Lim}_{z \rightarrow \infty} \frac{h''}{2} = \frac{h_f}{w^2} = \frac{1}{R_f}. \quad (9)$$

Combining (8) and (5) gives the relations

$$h_f = \sqrt{\alpha R_f}, \quad (10)$$

and

$$w = \alpha^{1/4} R_f^{3/4}. \quad (11)$$

At equilibrium, i.e. after the stretching stage and before significant drainage, the film thickness and the characteristic lateral length are therefore functions only of the radius of the Plateau border and of the microscopic length α ; the latter characterizes the concentration differences between bulk and surface in the liquid mixture. Since α is subnanometric and R_f is millimetric, the thickness of the film at equilibrium is within the micron range, and the lateral length is roughly ten times larger. Importantly, w is two orders of magnitude smaller than the radius of the Plateau border. In other works focusing on film pinching (Aradian et al 2001; Chan et al 2011), the initial shape of the film was not determined and the lateral scale was assumed to be of the same order of magnitude as the radius of the Plateau border; herein, the mechanism we suggest for the formation of liquid films allows the full determination of the shape of the film before drainage, as well as of the characteristic horizontal lengthscale. In the following, we discuss the pinching dynamics in light of these results.

3.2 Dynamics of pinching

The previous picture describes the film that is formed after simultaneous stretching of the interface of the film and its bulk and therefore only gives the initial thickness profile before drainage. As emphasised above, the pressure inside the film is not balanced, resulting in a further stage of drainage. Because of the non-zero pressure gradient, the film is expected to thin down at some location, forming a pinch, during this stage (Aradian et al 2001). The suggested scenario conducting to the film bursting is that, as the pinched part further thins down, a critical thickness is reached for which van der Waals attraction becomes effective (Chatzigiannakis and Vermant 2020; Shah et al 2021); the film then pierces and this process is very fast. The film lifetime is therefore given by the time needed for the pinched part to reach the critical thickness, which is much larger than both the durations of the first stretching stage and of the last piercing stage under the action of van der Waals forces. In the following, we examine the pinching dynamic in order to determine the lifetimes of the liquid films.

Consistently with the uniform thickness of the liquid film measured in single bubble experiments, we will assume that drainage is actually localised at the point of pinching but does not significantly affect the thickness of the film. Since fluid drains significantly

at the pinching location, a relative displacement of the bulk and the interfaces of the film is expected at this point. A displacement results in a variation with time of the concentration fields of species and consequently the relation $\gamma_f(h) = \gamma(1 + \alpha/h)$ valid in thermodynamical equilibrium, should not be satisfied any more. Description of this complex behaviour is out of the scope of the present work, and the analysis of pinching dynamics made in the following is limited to a simple approximation: since pinching consists in a local thinning of the film, it is equivalent to the removal of some liquid volume at a given position in the bulk of the film, as schematised in figure 7. Obviously, it results in a decrease of the thickness at the corresponding position, but does not modify the thermodynamical equilibrium between the interfaces and the bulk. As a result, removing a fluid element from some part of the film leads to a thinning of the film without any modification of the surface tension at this location.

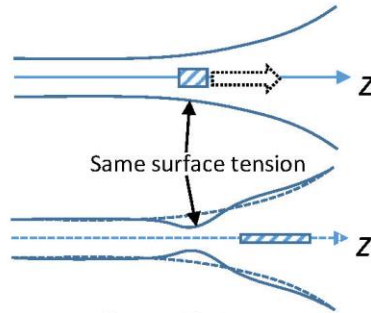


Figure 7: Illustration of the argument for considering constant composition of the liquid mixture during film pinching.

Consequently, we expect the pinching process not to be significantly influenced by the concentration field: a flow in a region where the horizontal gradient of concentration is small modifies the thickness but not the interfacial tension. In addition, we assume that film stretching is negligible in the vicinity of the pinched part, because of the very small evolution of surface tension in this region. The latter approximation is equivalent to considering rigid interfaces, which constitutes a very general assumption provided Marangoni flows are expected. The thin film equation describing pinching dynamics is

$$\frac{\partial h}{\partial t} + \frac{\gamma}{3\mu} \frac{\partial}{\partial z} h^3 h''' = 0, \quad (12)$$

where μ is the viscosity of the liquid. Since $Y = \alpha/h_f \ll 1$, the expected increase of surface tension is very small and in equation (12), the surface tension is approximated by the one of an infinitely thick film.

Equation (12) has been discussed in several works (Aradian et al 2001; Chan et al 2011; Shah et al 2021). However, the characteristic lateral scale was chosen to be of the same order of magnitude as the radius of curvature of the Plateau border, thus eluding the question of the precise initial shape of the film. In the situation we consider, the natural horizontal scale for the pinching is the lateral characteristic length before

drainage, w given by equation (11), and much smaller than the radius of the Plateau border.

The scaling law of the thickness of the pinch is nevertheless expected to be the same as in previous analyses, whatever the chosen lateral scale. It has been found that $h \approx At^{-1/4}$ (Aradian et al 2001). More precisely, we denote h_0 the initial thickness, and t_0 the initial time of pinching. As emphasised above, the critical thickness reached before further fast piercing corresponds to the thickness at which van der Waals forces are effective. We denote respectively h_{vW} and $t_0 + \tau$ the critical thickness and the time at which it is reached. The film lifetime is $\tau = A^4(h_{vW}^{-4} - h_0^{-4}) \cong A^4 h_{vW}^{-4}$ and *does not depend on the initial thickness*, provided $h_{vW} \ll h_0$. The latter condition is readily verified if pinching occurs at the beginning of the drainage stage, i.e. $h_0 \approx h_f$.

Since the lifetime of a film only depends on the critical thickness h_{vW} , the latter is the natural vertical length scale, whereas the horizontal length scale remains the one of the pinch, w . Therefore, we introduce the dimensionless variable $\hat{h} = h/h_{vW}$ together with the previously introduced $\xi = z/w$ and equation (11) becomes

$$\tau \frac{\partial \hat{h}}{\partial t} + \frac{\partial}{\partial \xi} \left(\hat{h}^3 \frac{\partial^3 \hat{h}}{\partial \xi^3} \right) = 0, \quad (13)$$

where, using equation (11), the characteristic time τ is given by

$$\tau = \frac{3\alpha R_f^3}{V^* h_{vW}^3}, \quad (14)$$

in which the capillary velocity $V^* = \gamma/\mu$ has been introduced, for an immediate determination of the characteristic length defined above, $L = \tau V^*$.

With $\alpha = 0.1\text{nm}$, $h_{vW} = 100\text{nm}$, and $R_f = 1\text{mm}$, we find $L = \tau V^* = 300\text{m}$, which is less than one order of magnitude larger than the experimental lengths. We emphasize this value strongly depends on the chosen value of h_{vW} , which is rather arbitrary. In the following section, we compare the variations with α predicted by equation (13) with experimental data.

3.3 Experimental scaling of lifetime with length α

Importantly, equation (14) predicts a linear variation of lifetime, and thus of length L , with α , consistently with our experimental findings in foams (Tran et al 2020). As pointed out above, the absolute value of α is poorly determined, in particular in the case of mixtures of molecules with very different sizes; as a result, herein we focus on molecules rather symmetric in sizes. We report in figure 8 the experimental data that have been already presented but in a different form (Tran et al 2020): the value of length L determined in a Bikerman column is shown as a function of α . L is inferred from the measured foam height, as explained in the experimental section; α is computed from the variations of surface tension of the mixture with composition and the values of molar

volumes and extrapolated molar surfaces. Both variables are normalised by their maximum value, since we have shown that their maximum is reached for the same mixture composition. The expression of α as a function of surface tension is given elsewhere (Tran et al 2020).

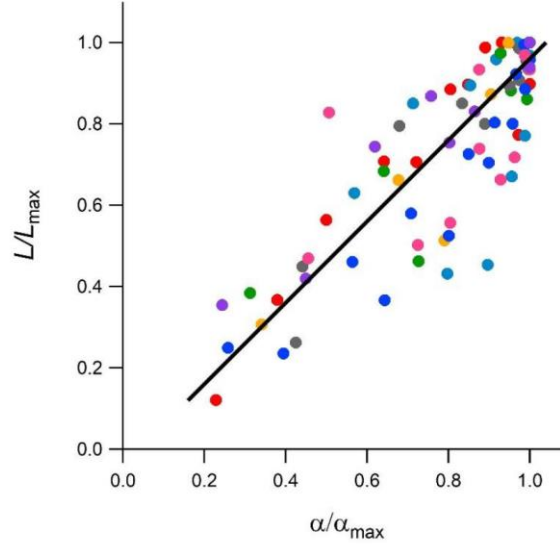


Figure 8: Length L as a function of length α for eight different liquid mixtures. Both L and α are normalized by their maximum values found in each mixture which are reached for the same composition. The full line is a guide to the eye. Red symbols: decane-toluene; Grey: nonane-toluene; Darker blue: octane-toluene; Lighter blue: heptane-toluene; Green: heptanol-cyclopentanol; yellow: hexanol-cyclopentanol; Pink: pentanol-cyclopentanol; Purple: pentanol-nonanol.

Although rather scattered, the overall linear increase of length L with α confirms the prediction of equation (14) and we attribute the dispersion to the poor determination of the molar surfaces. In order to further corroborate our analysis, we consider the relation between better determined quantities, i.e. the thickness of the film reached before drainage and length L , obtained using (10) and (14)

$$L = \frac{3h_f^2 R_f^2}{h_{vW}^3} \quad (15)$$

Therefore, the length L is predicted to depend on film thickness as well as on the radius of its curved part, R_f . As mentioned earlier, in foams, R_f corresponds to the radius of the Plateau border and is expected to be smaller than the curvature radius of the meniscus in single bubble experiments. However, it is difficult to fully determine the role of R_f on foam lifetimes because the latter is not constant but decreases with height. As a result, the radius of the Plateau border experienced by a bubble ascending the foam varies with time. Therefore, test of the variation with curvature predicted by equation (14) is made uneasy. In contrast, as explained in the experimental section, the film thickness can be directly measured in single bubble experiments and, in the following, we focus on the variations of L with h_f , which are both experimental data.

3.3 Experimental scaling of length L with thickness

In the experimental section, we have detailed measurements of the liquid film thickness when a bubble punctures. We have found bursting occurs for a very reproducible film thickness, which is, in addition, spatially homogeneous. These results suggest that drainage of a film is significant only at its pinched part, and that a bubble bursts before the other parts of the film have significantly drained. Because pinching is quickly followed by puncture, we expect that the thickness at the onset of bursting h_b is very close to the thickness reached at equilibrium, h_f , as drainage has a negligible effect everywhere but at the pinch. Since, in the same experiments, we measure lifetimes of bubbles in addition to thicknesses $h_b \approx h_f$, we can probe the relation between length L and film thickness at the onset of bursting. Figure 9 shows the variations of length L with thickness h_f for three different liquid mixtures. The length L spans almost one decade and its variations with thickness are consistent with the scaling predicted by equation (15), thus emphasizing the relevance of the analysis of the pinching dynamics we suggest.

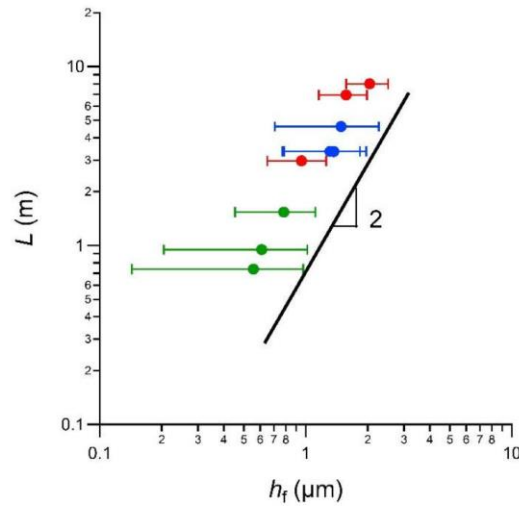


Figure 9: Length L as a function of film thickness at bursting, both measured in single bubble experiments performed with mixtures of decane and toluene (red circles), octane and toluene (blue circles) and heptanol and cyclopentanol (green circles). The error bars on h_f result from the uncertainty on the Taylor-Culick velocity.

In summary, taking advantage of the - relatively - simpler situation faced in liquid mixtures, we have shown that it is possible to describe the pinching dynamics of liquid films. In these systems, surface tension is thickness-dependent, which introduces a new length α making the problem very rich, with length scales ranging from molecular sizes to tens of meters. It is indeed tempting to compare our analysis with the ones in the literature for the widely studied soap films, i.e. made from aqueous surfactant solutions.

3.5 Comparison to soap films

In what precedes, we have assumed that film formation and drainage are decoupled stages of the life of a liquid film. Obviously, this description fails if the duration of film formation is of the same order as the one of drainage. We discuss in the following the mechanism of film formation in both limits, i.e, stretching with negligible drainage and drainage without stretching. The latter limit has been widely discussed in the literature, in light of the analogous problem of the formation of soap films from a reservoir (Mysels 1959; Seiwert et al 2014).

Mysels, Shinoda and Frankel (Mysels 1959) solved the problem of soap film entrainment by a solid frame from a reservoir in the case of an incompressible interface. They predicted the resulting film thickness follows a power law with the velocity at which the film is pulled from the reservoir. In some of the experiments that have been conducted since in aqueous surfactant solutions, deviations from the predicted law were observed, which were attributed to surface elasticity or viscoelasticity (Scheid et al 2010; Seiwert et al 2014). In the surfactant-free liquid mixtures we consider, the exchange of molecules between bulk and interfaces is limited by diffusion only. As a result, the characteristic time of equilibrium between bulk and film interfaces is given by h^2/D . This time is of the order of milliseconds, which is very short compared to the time needed for film formation. Therefore, the surface rheology can be considered as purely “elastic” in the usual acception of this term, referring to Gibbs’ elasticity. However, we emphasize surface elasticity is not sufficient to express the relation between the interfacial tension and the thickness of the film at the heart of our problem.

For an incompressible interface, Frankel’s law expresses the thickness of a film as a function of the pulling velocity (Mysels 1959):

$$h_{Fr} = 2.68l \left(\frac{U}{V^*} \right)^{2/3}, \quad (16)$$

where l is the characteristic length of the problem, similar to the Plateau border curvature. We can compare the thickness predicted by equation (16) to the thickness we predict in the absence of drainage. Depending on the physicochemical parameters and on the velocity of the film formation, two situations are encountered.

- $h_f \gg h_{Fr}$. In that case the stretching equilibrium cannot be reached since drainage efficiently thins the film down. As a result, the film formation is governed by drainage, and its thickness is h_{Fr} .
- $h_{Fr} \gg h_f$. In that case, drainage would lead to a film thickness larger than the one of the stretching mode. Film formation is therefore governed by stretching, and its thickness is h_f .

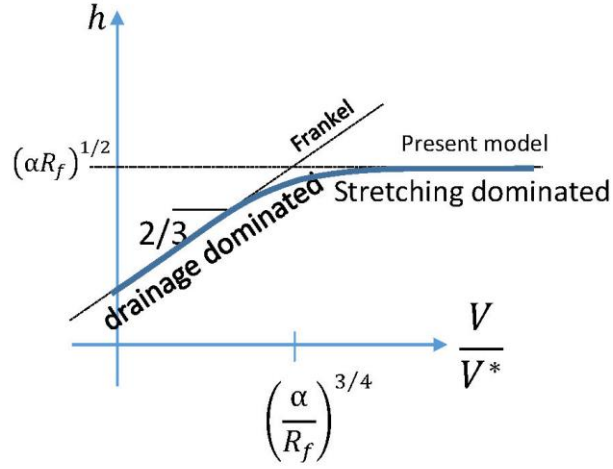


Figure 10: Thickness of a film of liquid mixture according to the velocity at which it is formed. At low velocities, drainage prevails over stretching and the thickness follows Frankel's law. At larger velocities, the film is stretched without significant drainage, and its thickness reaches a plateau value depending on both the radius of its curved part and the molecular length α . The regime examined herein is the high-velocity one.

Using equations (10) and (16), the crossover velocity between both regimes is obtained

$$V_C = V^* \left(\frac{\alpha}{R_f} \right)^{3/4}. \quad (17)$$

For liquid mixtures in which $\alpha \sim 0.1 \text{ nm}$ and $R_f \sim 1 \text{ mm}$, the crossover velocity is of the order of $10^{-4} \text{ m} \cdot \text{s}^{-1}$, which is in the lowest range of accessible pulling velocities (Seiwert et al 2014). As discussed in the appendix, for surfactant solutions, the length α with which they can be associated may be larger than the micron scale. In practice however, it is difficult to provide an estimate for α , particularly at concentrations below the critical micellar concentration (cmc), for which the dependence of surface tension with concentration is weak. A length $\alpha = 1 \mu\text{m}$ corresponds to a critical velocity $V_C \approx 1 \text{ m} \cdot \text{s}^{-1}$, a value that lies in the upper range of velocities reached in experiments. As a result, we expect the regime described by Frankel's laws to be generally met with surfactant solutions, except for very dilute solutions. In contrast, for liquid mixtures the experimental conditions always correspond to a regime with negligible drainage, in which an equilibrium of film tension is reached.

4. Conclusion

The lifetimes of bubbles and foams that are formed in liquid mixtures are much smaller than the ones in surfactant solutions but larger by at least three orders of magnitude than the ones in pure liquids of similar viscosities. A surfactant-like effect of one liquid for the other, resulting in a thickness-dependent surface tension, is at the origin of this enhanced stability. Because the molecules at stake are much smaller than surfactants,

the exchanges between bulk and interfaces are very fast and the interfacial rheology of liquid mixtures is much simpler than the one of surfactant solutions. The simple rheology allows drawing a full picture for the mechanisms of formation and death of films of liquid mixtures. As a single bubble approaches a liquid surface or, equivalently, bubbles come closer in a foam, the liquid film that is formed is first stretched. The stretching stage ends when a mechanical equilibrium is reached, which is made possible by the increase of surface tension in the flat parts of the films. However, a pressure difference remains between the film and the meniscus to which it is connected, leading to the pinching of the film, itself quickly followed by film bursting. The slowest stage consists in pinching, which duration therefore determines the lifetime of the film. We show that the analytical shape of the film in mechanical equilibrium can be derived, yielding in particular the characteristic lateral length of the problem. From the obtained lateral length and the equation for pinching dynamics, we suggest a scaling law for film lifetime, which is in agreement with experimental data. Finally, we compare liquid mixtures and surfactant solutions, and show why film dynamics differs in these systems.

Appendix

We provide an estimate of the length α in the case of surfactant solutions. We assume for the sake of simplicity that surface and bulk concentrations are related through the Langmuir adsorption isotherm

$$\frac{c}{c_\infty} = \frac{\Gamma}{\Gamma_\infty - \Gamma}, \quad (\text{A1})$$

where c is the surfactant bulk concentration and c_∞ the one at the critical micellar concentration (cmc), Γ the number of mole per interface unit and Γ_∞ the one at the cmc.

We use the ideal approximation for surface tension

$$\gamma = \gamma_0 - RT\Gamma, \quad (\text{A2})$$

together with surfactant conservation in which we have introduced the thickness of the surfactant layer at the surface, $\delta = \Gamma_\infty v_M$, with v_M is the molar volume of the surfactant,

$$c_0 V = c(V - 2S\delta) + 2S\Gamma, \quad (\text{A3})$$

and further using $h = 2V/S$, we finally obtain in the limit of dilute solutions, i.e. for $c_\infty v_M \ll 1$

$$\Gamma(h) = \Gamma(h = \infty) - \frac{2}{h} \frac{c_0 c_\infty \Gamma_\infty^2}{(c_\infty - c_0)^3} + \mathcal{O}\left(\frac{1}{h^2}\right). \quad (\text{A4})$$

We emphasize that, in contrast to liquid mixtures, surfactant solutions are usually very dilute.

With surfactants, the ratio of the surface and bulk concentrations is a length $\delta_s = \Gamma_\infty/c_\infty$, called thickness of the subsurface and in the micrometer range. Introducing the reduced concentration $\hat{c} = c_0/c_\infty$, we obtain from equations (A1) and (A4)

$$\alpha \cong \delta_s \frac{RT\Gamma_\infty}{\gamma_0} \frac{2\epsilon}{(1-\epsilon)^3} \quad (\text{A5})$$

Because $RT\Gamma_\infty/\gamma_0$ is in general of the order of unity, the value of α is in micrometer range, but it can be smaller far below the cmc and become considerably larger near the cmc.

References

- Aradian, A., Raphael, E. and de Gennes, P. G. 2001 "Marginal pinching" in soap films *Europhysics Letters*, **55**, pp 834-840.
- Bluteau, L., Bourrel, M., Passade-Boupat, N., Talini, L., Verneuil, E. and Lequeux, F. 2017 Water film squeezed between oil and solid: drainage towards stabilization by disjoining pressure *Soft Matter*, **13**, pp 1384-1395.
- Butler, J. A. V. 1932 The thermodynamics of the surfaces of solution *Proceedings of the Royal Society of London Series a-Containing Papers of a Mathematical and Physical Character*, **135**, pp 348-375.
- Champougny, L., Roche, M., Drenckhan, W. and Rio, E. 2016 Life and death of not so "bare" bubbles *Soft Matter*, **12**, pp 5276-5284.
- Chan, D. Y. C., Klaseboer, E. and Manica, R. 2011 Film drainage and coalescence between deformable drops and bubbles *Soft Matter*, **7**, pp 2235-2264.
- Chatzigiannakis, E., Jaansson, N. and Vermant, J. 2021 Thin liquid films: Where hydrodynamics, capillarity, surface stresses and intermolecular forces meet *Current Opinion in Colloid & Interface Science*, **53**, 101441.
- Chatzigiannakis, E. and Vermant, J. 2020 Breakup of Thin Liquid Films: From Stochastic to Deterministic *Physical Review Letters*, **125**, 158001.
- Connor, J. N. and Horn, R. G. 2003 The influence of surface forces on thin film drainage between a fluid drop and a flat solid *Faraday Discussions*, **123**, pp 193-206.
- Culick, F. E. C. 1960 COMMENTS ON A RUPTURED SOAP FILM *Journal of Applied Physics*, **31**, pp 1128-1129.
- Debregeas, G., de Gennes, P. G. and Brochard-Wyart, F. 1998 The life and death of "bare" viscous bubbles *Science*, **279**, pp 1704-1707.
- Denkov, N., Tcholakova, S. and Politova-Brinkova, N. 2020 Physicochemical control of foam properties *Current Opinion in Colloid & Interface Science*, **50**, 101376.
- Eriksson, J. C. 1964 On the thermodynamics of surface systems *Advances in Chemical Physics*, **6**, pp 145-174.
- Jain, R. K. and Ivanov, I. B. 1980 THINNING AND RUPTURE OF RING-SHAPED FILMS *Journal of the Chemical Society-Faraday Transactions II*, **76**, pp 250-266.
- Lhuissier, H. and Villermaux, E. 2012 Bursting bubble aerosols *Journal of Fluid Mechanics*, **696**, pp 5-44.
- Prigogine, I. and Marechal, J. 1952 THE INFLUENCE OF DIFFERENCES IN MOLECULAR SIZE ON THE SURFACE TENSION OF SOLUTIONS .4 *Journal of Colloid Science*, **7**, pp 122-127.
- Pugh, R. J. 1996 Foaming, foam films, antifoaming and defoaming *Advances in Colloid and Interface Science*, **64**, pp 67-142.

- Ross, S. and Nishioka, G. 1975 Foaminess of binary and ternary solutions *Journal of Physical Chemistry*, **79**, pp 1561-1565.
- Santos, M. S. C. S. and Reis, J. C. R. 2014 New Thermodynamics for Evaluating the Surface-phase Enrichment in the Lower Surface Tension Component *Chemphyschem*, **15**, pp 2834-2843.
- Scheid, B., Delacotte, J., Dollet, B., Rio, E., Restagno, F., van Nierop, E. A., Cantat, I., Langevin, D. and Stone, H. A. 2010 The role of surface rheology in liquid film formation *Epl*, **90**, pp 24002.
- Seiwert, J., Dollet, B. and Cantat, I. 2014 Theoretical study of the generation of soap films: role of interfacial visco-elasticity *Journal of Fluid Mechanics*, **739**, pp 124-142.
- Shah, M. S., Kleijn, C. R., Kreutzer, M. T. and van Steijn, V. 2021 Influence of initial film radius and film thickness on the rupture of foam films *Physical Review Fluids*, **6**, 013603
- Tran, H. P., Arangalage, M., Jorgensen, L., Passade-Boupat, N., Lequeux, F. and Talini, L. 2020 Understanding Frothing of Liquid Mixtures: A Surfactantlike Effect at the Origin of Enhanced Liquid Film Lifetimes *Physical Review Letters*, **125**, 178002.
- Tran, H. P., Delance, L., Passade-Boupat, N., Verneuil, E., Lequeux, F. and Talini, L. 2021 Foaming of Binary Mixtures: Link with the Nonlinear Behavior of Surface Tension in Asymmetric Mixtures *Langmuir : the ACS journal of surfaces and colloids*, **37**, pp 13444-13451

CONCLUSIONS & OUTLOOKS

Thin films of pure liquids are always unstable. Indeed, in the absence of surfactants at the liquid film's interfaces, the only contribution of Van der Waals forces results in attractive disjoining pressure, resulting in a rather quick drainage of the liquid film, on the scale of milliseconds. Among the well-known classical foaming phenomena, the Marangoni effect is critical for the liquid film's stability. The mechanisms by which the Marangoni flow inhibits the drainage of the liquid film have been discussed in the research literature. The long lifetime of air bubbles can be ascribed to the evaporation action of volatile liquids, the existence of surfactants, or contaminants. The common denominator among the aforementioned factors is the gradient of concentration of surface-active molecules in the liquid layer, which results in the Marangoni effect. However, surface tension variations able to immobilize the interfaces are extremely tiny and difficult to quantify precisely; they are estimated to be less than $mN \cdot m^{-1}$. They generate Marangoni flows that are not excessively vigorous but yet significant enough to prolong the foam's life by several seconds. Obviously, pure liquid cannot exhibit Marangoni effects and thus cannot foam. However, mixtures of simple liquids—as reported in the literature – do foam. The reported thin film persistence for these mixes can range from a few seconds to tens of seconds.

We carried out experiments with various liquids mixtures. Experiments were conducted to quantify this foaming effect for a variety of different liquid mixtures. The foamability of mixtures is determined by their physico-chemical nature. In agreement with the literature, we discovered that for each mixture, there is a component ratio of the liquids that results in maximum amount of foaming. Following that, in addition to nature, the effect of the size of the air bubbles on the mixture's foaming was examined. We discovered that mixes with same characteristics and compositions create more stable foams when the bubbles are smaller. Finally, we undertook tests to determine the thickness of liquid thin films, with a particular emphasis on the link between this thickness and the degree of foaming of the liquid mixes under study. The lifetime of this liquid layer is proportional to the square of its thickness, as demonstrated experimentally. The majority of the mixtures examined were capable of producing foam. We categorize mixtures as symmetric or asymmetric as well as attempt to construct a model that allows for simple and reliable predictions.

The case of symmetric mixtures is the simplest. This corresponds to mixtures of molecules almost identical in size. More precisely, both their molar volumes and molar surfaces have to be almost similar. We propose that the stabilizing mechanism for liquid films in mixtures is based on the fact that species concentrations are different in the bulk and at air interfaces. At the interface, the species with the lowest surface tension is always more concentrated than in the bulk. This concentration difference leads to a sublinear variation in surface tension with composition in symmetric mixtures. We show that this results in a thickness-dependent surface tension for the mixture and thus to foaming. Indeed, this is a surfactant-like behavior, in which the species with the lowest interfacial tension acts as a surfactant for the other species. We also show that the Marangoni effect induced by this thickness dependent surface tension controls the morphology of the film/Plateau boarder geometry before drainage and gives an analytical solution for the film thickness. Experimentally, we observe that there is a link between the foam lifetime, foamability and film thickness at the beginning of bursting. We observe that the foam lifetime is related with mixture composition for all mixtures investigated, whether polar or non-polar liquids.

Then we discuss asymmetric liquid mixtures, which are liquids consisting of molecules of different sizes, thus of different molar surfaces and volumes. For asymmetric mixes, the model employed for symmetric mixtures fails to describe the surface tension. We thus turn to ideal solution theory. In that frame we show that the species with the lowest surface tension are always more concentrated near the interface than in the bulk. But species with a higher molecular size cover a greater surface area and hence have a more complicated effect on the surface tension. This may result either in superlinear or sublinear variations of the surface tension. This is in agreement with our observation, asymmetric mixtures' surface tensions may vary in a sublinear or superlinear manner depending on their surface ratios. However, regardless of the sign of the nonlinearity, the surface concentration of the species with the lowest surface energy is always greater than the bulk concentration. And it is in fact this phenomenon that causes the mixtures to foam. Our theoretical model, on the other hand, does not quantitatively predict these mixtures' foamability. The limitation of our model is due to the difficulty to identify liquids' molar surfaces, and likely to the fact that the ideal solution frame neglects the fugacity of the different species in bulk and at interfaces.

Finally, we provide a theoretical model for the hydrodynamics of film thinning, that fits the experimental results. We show that hydrodynamics can explain why the lifetime of bubbles formed in liquid mixtures varies like the square of the thickness of the liquid layer.

To summarize, the foaming ability of mixtures is related to the concentration difference between the bulk and surface of the species with the lowest surface energy. It leads to a thickness dependent surface tension. Drainage of the film/Plateau border connection controls the life-time of the film. We have discussed both the effect of physico-chemistry and of hydrodynamics and provides various relations between surface tension, film thickness, and lifetime. Within the framework of this thesis, we demonstrated the ubiquitous nature of foaming in oil mixtures. This work has advanced our understanding of the stabilizing mechanism of oil foams, which has significant implications for operations involving liquid-gas mixtures, such as oil transport in pipes, lubricants in electric motors or food processing.

APPENDICES

Appendix A: Foaming systems – Measurement of liquid fraction in the foam Φ_L

In this Appendix, we will look at how to determine the liquid fraction in the foam Φ_L .

The drainage equation that characterizes the spatiotemporal evolution of the liquid fraction $\Phi_L(z, t)$ is provided below [3]:

$$\frac{\partial \Phi_L}{\partial t} + \vec{\nabla} \left[\frac{\kappa}{\mu} \left(\rho \vec{g} + \vec{\nabla} \left(\frac{\gamma}{R_f} \right) \right) \right] = 0 \quad \text{Eq.A.1}$$

where ρ : liquid density, R_f : curvature radius, κ : permeability, γ : surface tension.

According to literature [3], the expression for the curvature radius is:

$$R_f = \delta_b D_b \Phi_L^n \quad \text{Eq.A.2}$$

where, D_b is the bubble diameter and n is $1/2$ in the case of dry foam or 0.45 in the case of wet foam. In addition, δ_b is a geometric factor equal to 1.76.

- $Q = 0$

Eq.A.1 becomes:

$$\frac{\partial}{\partial z} \left(\frac{\gamma}{R_f} \right) = \rho g \quad \text{Eq.A.3}$$

Substituting **Eq.A.2** into the above equation, we thus obtain:

$$\Phi_L^n = \frac{\gamma}{\delta_b D_b \rho g (z + Z_0)} \quad \text{Eq.A.4}$$

where Z_0 is a constant.

A length of a capillary may be introduced $l_c = \frac{\gamma}{\delta_b D_b \rho g}$. In investigations with the Bikerman columns and $D_b = 1.6 \text{ mm}$, we find that $l_c \sim 1 \text{ mm}$.

In order to determine Z_0 , we examine the gas fraction at the bottom of the foam. We suppose that the foam in our case is a closing packet of bubbles, leads to $\Phi_B(z = 0) = 0.64$. Therefore,

$$\Phi_L(0) = 1 - \Phi_B = 0.36 \text{ and } Z_0 = \frac{l_c}{\Phi_L(0)^{\frac{1}{n}}} \approx 1.5 \text{ mm.}$$

This leads to the height dependence of the liquid fraction:

$$\Phi_L = \left(\frac{l_c}{z + \frac{l_c}{\Phi_L(0)^n}} \right)^{\frac{1}{n}} \quad \text{Eq.A.5}$$

Thus, the mean value of Φ_L along the foam height H is:


$$\langle \Phi_L \rangle = \frac{1}{H} \int_0^H \Phi_L(z) dz = \frac{n}{1-n} \left(\frac{l_c}{H} \right)^{1/n} \quad \text{Eq.A.6}$$

With a foam height H of around 5 – 10 mm (see **1.1.3**), we compute $\langle \Phi_L \rangle$ to be approximately 0.01 – 0.05, which is the dry foam area. This finding is compatible with the definition of dry foam [3] and the experimental data obtained for $Q \rightarrow 0$, see **Figure 1-8**.


- $Q \neq 0$

The drainage equation is as follows:


$$\frac{\partial \Phi_L}{\partial t} + \frac{\rho}{\mu} \vec{g} \vec{\nabla} \kappa + \vec{\nabla} \left(\frac{\kappa}{\mu} \left[-\frac{\gamma}{R_f^2} \vec{\nabla} R_f + \frac{1}{R_f} \vec{\nabla} \gamma \right] \right) = 0 \quad \text{Eq.A.7}$$



Gravity contribution



Capillarity contribution



Marangoni effect

We neglect the Marangoni which is tiny as well be explained below.

With dry foam $R_f = \delta_b D_b \Phi_L^{1/2}$, **Eq.A.7** becomes:

$$\frac{\partial \Phi_L}{\partial t} + \frac{\rho}{\mu} \vec{g} \vec{\nabla} \kappa - \vec{\nabla} \left(\frac{\kappa}{\mu} \frac{\gamma}{\delta_b D_b} \Phi_L^{-3/2} \vec{\nabla} \Phi_L \right) = 0 \quad \text{Eq.A.8}$$

By projecting upward along the vertical z axis, and remarking that the bubbles move upward with a velocity U , we obtain the following steady state relation:

$$\frac{\partial}{\partial z} \left[U \Phi_L - \frac{\kappa}{\mu} \left(\rho g + \frac{\gamma}{\delta_b D_b} \Phi_L^{-\frac{3}{2}} \frac{\partial \Phi_L}{\partial z} \right) \right] = 0 \quad \text{Eq.A.9}$$

We can integrate the previous equation. Taking into account the fact that the flow at the interface is zero, we obtain the following expression:

$$U \Phi_L - \frac{\kappa}{\mu} \left(\rho g + \frac{\gamma}{\delta_b D_b} \Phi_L^{-\frac{3}{2}} \frac{\partial \Phi_L}{\partial z} \right) = 0 \quad \text{Eq.A.10}$$

Permeability is the critical property that defines the entire system. To simplify, we propose that the foam in this study is an assembly of spheres, and hence the Carman – Kozeny model was

used. It is an empirical permeability equation that yields a relatively consistent approximation for the permeability coefficient.

Permeability κ is expressed as follows [3]:

$$\kappa = \frac{\Phi_L^3}{C_K A_s^2} \quad \text{Eq.A.11}$$

where C_K and A_s are respectively the stacking factor and the effective surface area for this model. Given that the foam is assumed to be a collection of spherical bubbles, C_K equals 5 and the effective surface area $A_s \sim \frac{\Phi_L^{1/2}}{D_b}$. Thus, the permeability $\kappa \sim \Phi_L^2 D_b^2$.

We obtain a differential equation of Φ_L over z by substituting κ into **Eq.A.10**:

$$\frac{\partial \Phi_L}{\partial z} - A_1 \Phi_L^{1/2} + A_2 \Phi_L^{3/2} = 0 \quad \text{Eq.A.12}$$

where $A_1 = \frac{\delta_b \mu U}{\gamma D_b}$ and $A_2 = \frac{\delta_b D_b \rho g}{\gamma}$.

The solution for the liquid fraction in the foam is:

$$\Phi_L(z) = \frac{A_1}{A_2} \tanh^2 \left[\frac{1}{2} \sqrt{A_1 A_2} (z - cste) \right] \quad \text{Eq.A.13}$$

where $\frac{A_1}{A_2} = \frac{\mu U}{\rho g D_b^2}$.

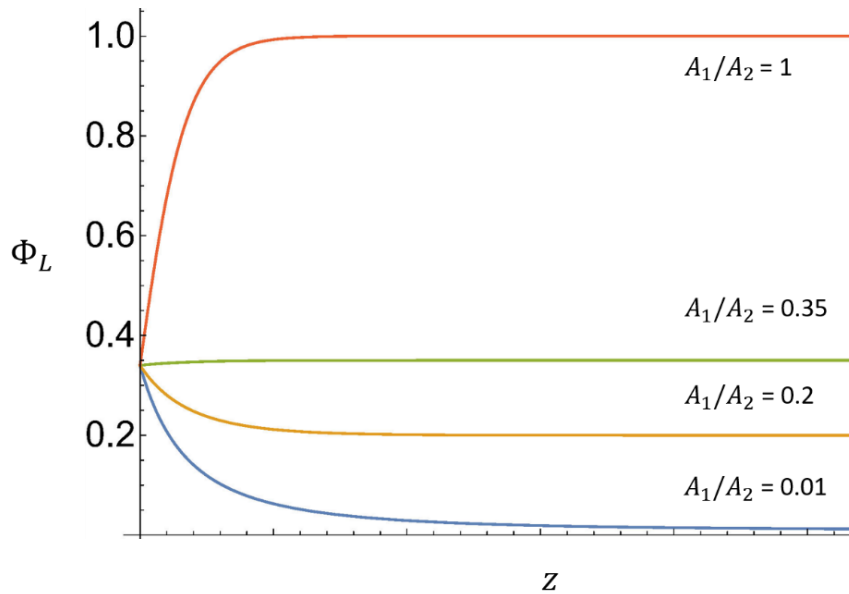


Figure A-1 : Φ_L as a function of z .

We display Φ_L as a function of z for various values of the $\frac{A_1}{A_2}$ ratio, as shown in **Figure A-1**. For $\frac{A_1}{A_2} > 1$, we can observe that the Φ_L grows with the height of the foam and reaches the value of

1. This makes no sense in terms of physics, the liquid fraction in the foam will progressively fall as the foam height increases. The physical solutions are for $\frac{A_1}{A_2} < 1$ (for example, $\frac{A_1}{A_2} = 0.35, 0.2, 0.01$). This ratio is dependent on the injection rate Q and the size of bubbles in the foam D_b . We can see that with a fixed value of Q , the ratio $\frac{A_1}{A_2}$ is inversely proportional to D_b .

Appendix B: Viscosity measurements

The viscosities of studied binary mixtures were computed using the empirical Kendall-Monroe equation [15]:

$$\mu = \left(x_1 \mu_1^{\frac{1}{3}} + x_2 \mu_2^{\frac{1}{3}} \right)^3 \quad \text{Eq.B.1}$$

where μ is the mixture's viscosity; μ_i and x_i are the viscosity and molar fraction of species i , respectively.

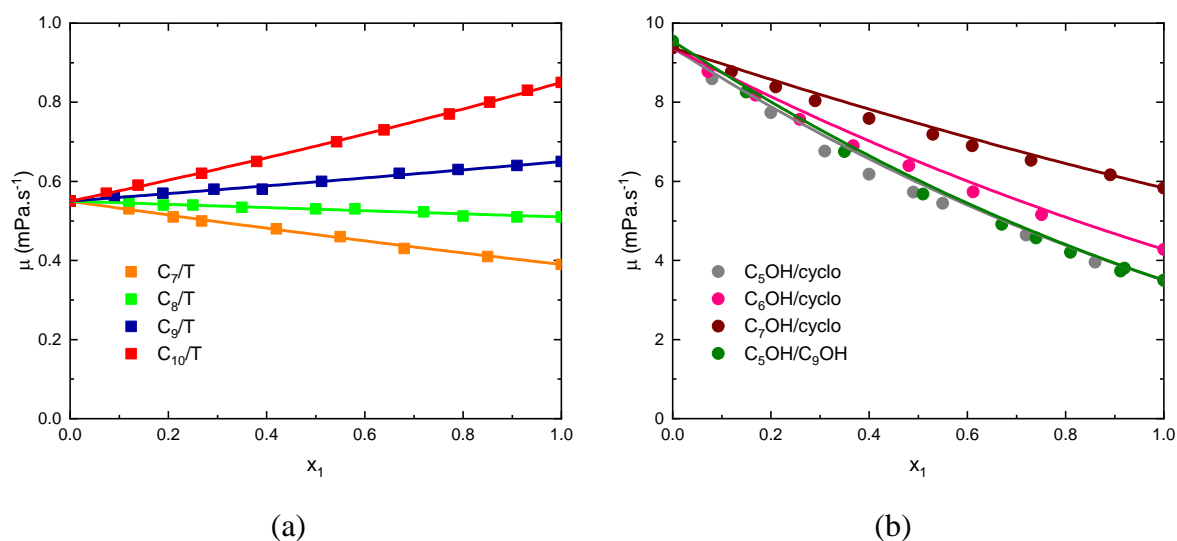


Figure B-1 : Measurement of viscosity μ as a function of molar fraction of liquid 1 x_1 in the binary mixtures. (a) of linear alkanes and Toluene; (b) of linear alcohols and Cyclopentanol/ of 2 linear alcohols. The predicted mixture's viscosities by Kendall-Monroe model are shown as solid lines.

To verify the validation of this model, we used a rheometer to measure the viscosity of the mixtures using alkane/Toluene and alcohol/Cyclopentanol (Low Shear 400, Lamy Rheology). The predicted values by Kendall-Monroe model are satisfactory with the experimental results obtained for estimating the mixture's viscosity, see **Figure B-1**. Likewise, **Figure B-2** illustrates the findings achieved using a PDMS/Decane mixture.

Note that the literature has several models [48–53] for describing the viscosity of a mixture. We select Kendall Monroe's model because it provides a simple equation for the mixture's viscosity that is quite accurate in comparison to the experiments.

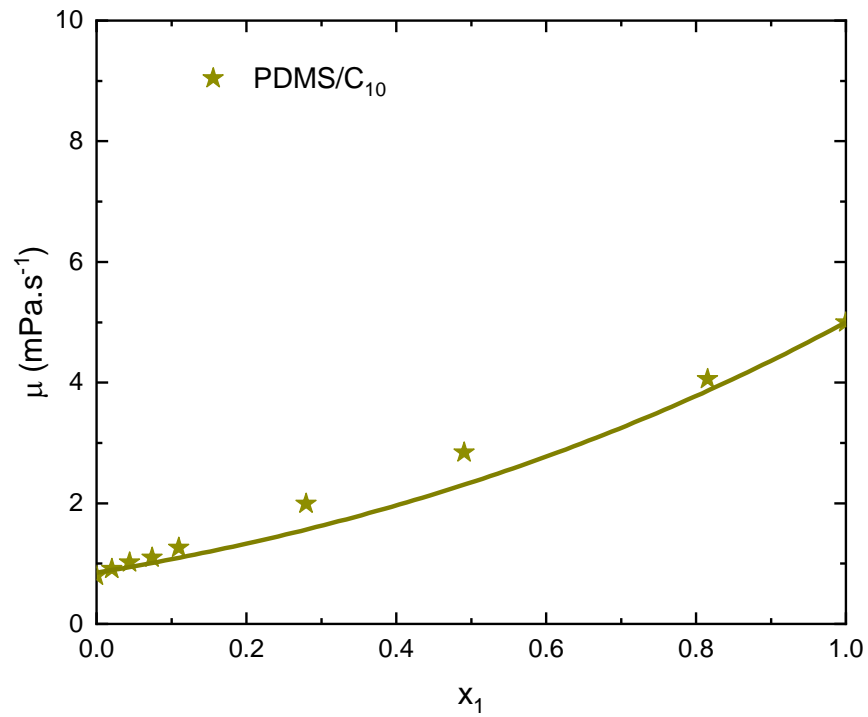


Figure B-2 : Measurement of viscosity μ of mixture PDMS/Decane as a function of molar fraction of Decane.

Appendix C: Estimation of bubble diameters based on creaming phenomena

In the following Appendix, we use the Richardson-Zaki model [14] from the creaming phenomena to analyze the size of the bubbles created by the Ultra Turrax set-up.

The bubble volume fraction in the liquid column is Φ_B . The flux of gas being imposed in the experiment – the average flux of gas is related to the rising speed of the air bubbles by:

$$U_{\text{exp}} \Phi_B = \frac{Q}{\pi R^2} \quad \text{Eq.C.1}$$

where U_{exp} is the experimental value of the bubble rising. Using the experimental values $\Phi_B = 0.3$, flowrate $Q = 100 \mu\text{L} \cdot \text{s}^{-1}$ and column radius $R = 10^{-2} \text{ m}$ gives us: $U_{\text{exp}} = 10^{-3} \text{ m} \cdot \text{s}^{-1}$.

We generate extremely small air bubbles ranging in size from $250 \mu\text{m}$ to $500 \mu\text{m}$ using the Ultra Turrax system. This results in the regime of low Reynolds numbers:

$$Re = \frac{\rho U_{\text{exp}} D_b^{UT}}{\mu} = 0.25 \quad \text{Eq.C.2}$$

where mixture's density $\rho = 10^3 \text{ kg/m}^3$ and mixture's viscosity $\mu = 10^{-3} \text{ Pa} \cdot \text{s}$.

The Reynolds number is small, i.e., $Re < 1$. Consequently, Stokes flow is the sort of fluid flow in the Ultra Turrax experiments.

The density difference between the air and liquid mixture results in air bubble creaming. The velocity of a single bubble is the Stokes' velocity:

$$v_{\text{stokes}} = \frac{1}{18} \frac{\rho g D_b^{UT^2}}{\mu} \quad \text{Eq.C.3}$$

In a bubbly liquid environment, the average creaming rate of bubble assembly is dependent on the volume fraction of gas Φ_B . This rate can be expressed as follows:

$$\langle v \rangle = v_{\text{stokes}} \cdot f(\Phi_B) \quad \text{Eq.C.4}$$

where $f(\Phi_B)$ is a hindered function of Φ_B .

Richardson - Zaki model [14] established that the empirical expression for this function is as follows:

$$f(\Phi_B) = (1 - \Phi_B)^5 \quad \text{Eq.C.5}$$

Meanwhile, the conservation of air flowrate provides us with the following:

$$Q = \langle v \rangle \Phi_B \pi R^2 \quad \text{Eq.C.6}$$

We can estimate the diameter of bubbles using the equations above:

$$\langle D_b \rangle = 0.34 \text{ mm} \quad \text{Eq.C.7}$$

The image analysis approach determined the bubble size D_b^{UT} to be 0.25 mm . The values above indicate that the two techniques, measurement by image analysis or estimate using creaming phenomena, provide comparable results.

Appendix D: Independence of bubble swelling time on injected flowrate

We return to the single bubble experiment in this Appendix. From the time the bubble forms until it bursts, the process is separated into two stages: the swelling stage and the unchanged-size stage. We shall demonstrate together that the duration of swelling is completely independent of the injected flowrate.

The bubble swelling stage is schematized in **Figure D-1 (a)**. V_0 denotes the volume of gas contained within the needle. Similarly, the volume of the bubble is indicated by V_b . The diameters of the needle and bubble are represented by D_0 and D_b , respectively. Ψ is defined as the angle formed by Oz and the needle outlet wall.

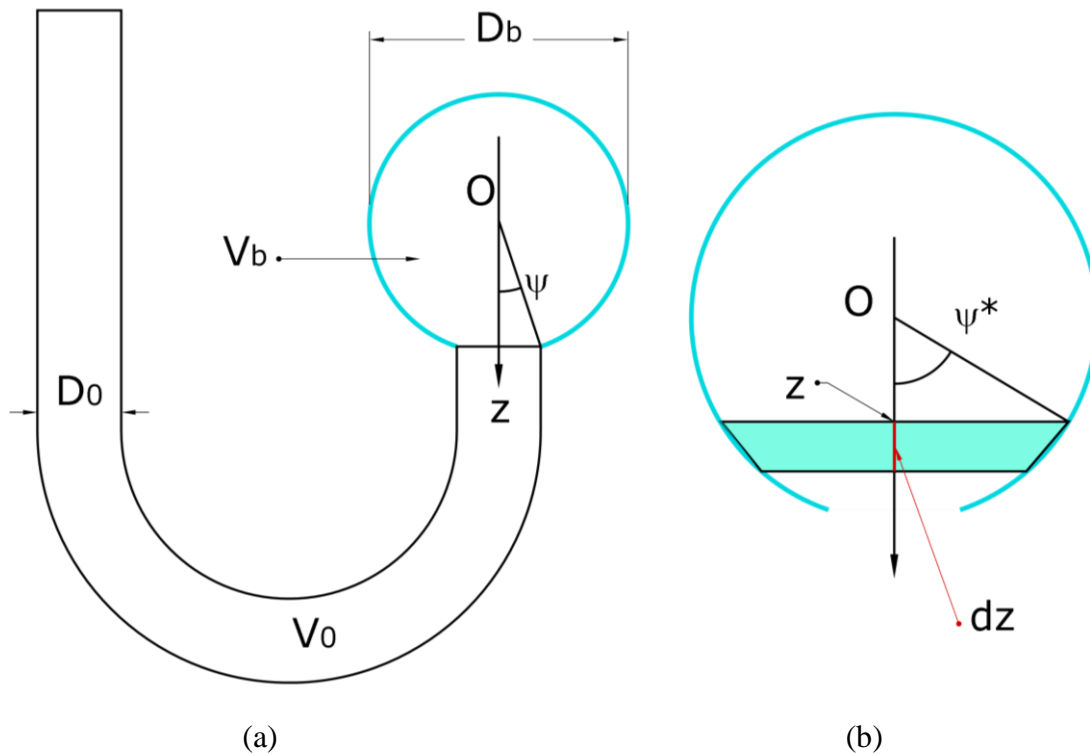


Figure D-1 : A bubble is swelling at the air/liquid interface during the injection of air into a bath of studied mixture. At all times, the bubble is attached to the needle. Liquid thin film in blue.

To determine the V_b , we split the bubble into air layers of small volume dV_b in the z direction. The thickness of these layers is dz . And their surface area is $S_z = \frac{\pi D_b^2}{4} \sin^2 \Psi^*$, where Ψ^* is the angle between Oz and the liquid thin film of this air layer, as schematized in **Figure D-1 (b)**.

We have:

$$dV_b = \frac{\pi D_b^2}{4} \sin^2 \Psi^* dz \quad \text{Eq.D.1}$$

Note that $z = \frac{D_b}{2} \cos \Psi^*$. So, $dz = -\frac{D_b}{2} \sin \Psi^* d\Psi^*$.

The integral of V_b over the angle Ψ^* can be expressed as followed:

$$V_b = \int_0^{V_b} dV_b = - \int_{\pi}^{\Psi} \frac{\pi D_b^3}{8} \sin^3 \Psi^* d\Psi^* \quad \text{Eq.D.2}$$

We can get the bubble volume V_b :

$$V_b = \frac{1}{6} D_b^3 \pi \cos^4 \frac{\Psi}{2} (-2 + \cos \Psi) \quad \text{Eq.D.3}$$

D_0 and D_b are connected by the expression $D_b = \frac{D_0}{\sin \Psi} = \frac{1}{\sin \Psi}$. To keep things simple, we set D_0 to 1.

Eq.D.3 becomes:

$$V_b = \frac{1}{6} \frac{\pi \cos^4 \frac{\Psi}{2} (-2 + \cos \Psi)}{\sin^3 \Psi} \quad \text{Eq.D.4}$$

The total volume of gas contained in the needle and bubble is as follows:

$$V = V_0 + V_b \quad \text{Eq.D.5}$$

The air pressure inside the bubble can be written:

$$P = P_0 + \Delta P \quad \text{Eq.D.6}$$

with $\Delta P = \frac{8\gamma}{D_b} = 8\gamma \sin \Psi$ is the Laplace pressure.

Using the ideal gas law $PV = cste$ and combining the above equations **Eq.D.4**, **Eq.D.5**, **Eq.D.6**, we finally obtain:

$$PV = P_0 V_0 + 8\gamma \sin \Psi \left[V_0 - \frac{\frac{1}{6} \pi \cos^4 \frac{\Psi}{2} (-2 + \cos \Psi)}{\sin^3 \Psi} \right] \quad \text{Eq.D.7}$$

Following that, we depict PV as a function of angle Ψ , as seen in **Figure D-2**. **Figure D-2 (a)** represents the case where the volume of the needle is ignored, whereas **Figure D-2 (b)** depicts the scenario when the volume of the needle is substantially bigger than the volume of the bubble.

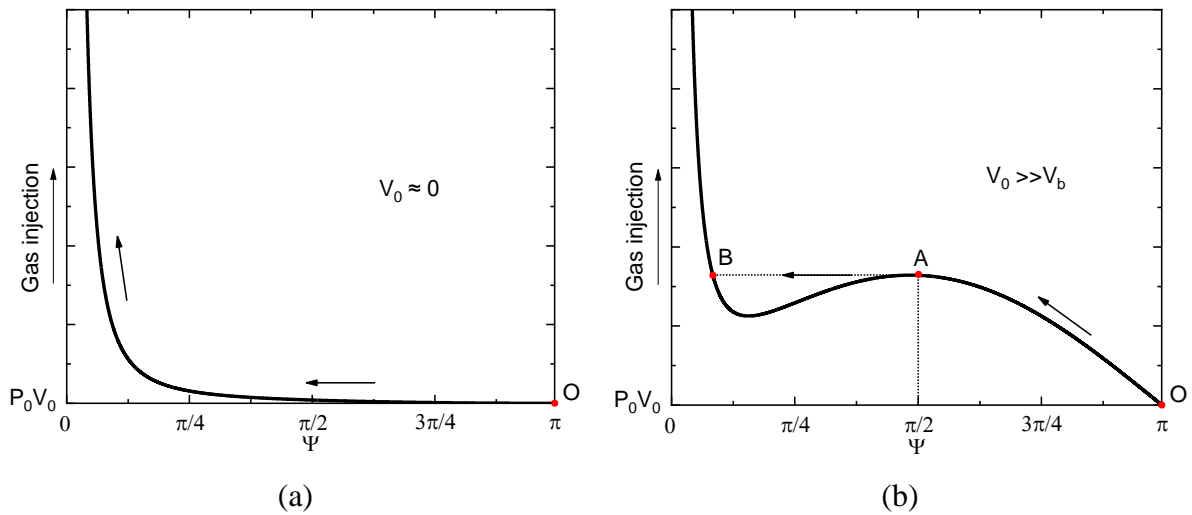


Figure D-2 : PV as a function of angle Ψ in a single bubble experiment - (a) The needle's gas volume exceeds the bubble volume; (b) The needle's gas volume is ignored. The arrow indicates the direction in which the bubble is expanding.

When the needle volume is ignored, we observe the bubble expanding in response to the rate of air injection, see **Figure D-2 (a)**. During the swelling phase, the PV curve is continuous in this condition. This is implausible. Because the volume of the needle, as well as the capacity of the reservoir, is substantially bigger in practice as compared to air bubbles of millimeter diameters.

Consider the latter situation, see **Figure D-2 (b)**; this is an actual experiment. The bubbles gradually increase throughout the swelling phase. The OA curve, which has $\Psi(t=0)$ is π , describes this process. Meanwhile, PV achieves a local maximum at point A, i.e., $\Psi = \pi/2$. Then there is instability; PV abruptly switches from A to B. This is the process of bubble bursting, which is determined by the gas's viscosity. To conclude, the duration of the swelling phase is independent of the injected flowrate of the syringe and this also explains why the size of the air bubble is entirely dependent on the needle's diameter.

Appendix E: Determination of x_1^{max} for symmetric mixtures

In this Appendix, we will look at how to calculate the maximum foam position x_1^{max} for symmetric mixtures.

To determine x_1^{max} , we must first examine the variation of foamability.

As described in **Chapter 2**, we utilized α as a length to quantify the foamability of mixtures.

Foaming length α is expressed as:

$$\alpha = \frac{2}{\gamma} \frac{\partial \gamma}{\partial x_1} \frac{v}{\sigma} (x_1 - \Gamma_1) \quad \text{Eq.E.1}$$

First, we'll try to figure out $\partial \gamma / \partial x_1$.

The surface tension of binary liquid mixtures can be fitted with their compositions using the equation below:

$$x_1 e^{\sigma_{fit} \frac{\gamma - \gamma_1}{RT}} + x_2 e^{\sigma_{fit} \frac{\gamma - \gamma_2}{RT}} = 1 \quad \text{Eq.E.2}$$

where γ_i is the surface tension of liquid i ($i = 1, 2$). And σ_{fit} is the area per mole, which, in a first approximation, is assumed to be the same for both liquids in the symmetric mixtures.

The derivative $\partial \gamma / \partial x_1$ can be determined from **Eq.E.2**:

$$\frac{\partial \gamma}{\partial x_1} = \frac{RT}{\sigma_{fit}} \left(e^{\sigma_{fit} \frac{\gamma - \gamma_2}{RT}} - e^{\sigma_{fit} \frac{\gamma - \gamma_1}{RT}} \right) \quad \text{Eq.E.3}$$

Because $\Gamma_1 = x_1 e^{\sigma_{fit} \frac{\gamma - \gamma_1}{RT}}$, γ can be deduced:

$$\gamma = \gamma_1 + \frac{RT}{\sigma_{fit}} \ln \frac{\Gamma_1}{x_1} \quad \text{Eq.E.4}$$

Substituting **Eq.E.4** into **Eq.E.2**, we may obtain the following relation between the surface molar fraction Γ_1 and the molar fraction x_1 :

$$\Gamma_1 = \frac{x_1}{x_1 + (1 - x_1) e^{\frac{\sigma_{fit}}{RT}(\gamma_1 - \gamma_2)}} \quad \text{Eq.E.5}$$

Additionally, by substituting **Eq.E.4** into **Eq.E.3**, we finally obtain:

$$\frac{\partial \gamma}{\partial x_1} = \frac{RT}{\sigma_{fit}} \frac{\Gamma_1}{x_1} \left(e^{\frac{\sigma_{fit}}{RT}(\gamma_1 - \gamma_2)} - 1 \right) \quad \text{Eq.E.6}$$

Eq.E.1 becomes:

$$\alpha = \frac{2vRT}{\sigma_{fit}^2} \left(1 - e^{\frac{\sigma_{fit}}{RT}(\gamma_1 - \gamma_2)} \right) \frac{\Gamma_1}{\gamma x_1} (\Gamma_1 - x_1) \quad \text{Eq.E.7}$$

By calculating the derivative of α with respect to x_1 , we may determine how foamability varies with mixture composition. The maximum foam position x_1^{max} corresponds to $d\alpha/dx_1 = 0$.

This means:

$$\frac{d}{dx_1} \left[\frac{G(x_1)}{\gamma} \right]_{x_1^{max}} = \frac{G'\gamma - G\gamma'}{\gamma^2} = 0 \quad \text{Eq.E.8}$$

where $G(x_1) = \left(\frac{\Gamma_1^2}{x_1} - \Gamma_1 \right)$.

If the condition $\Delta\gamma \ll \gamma$ is satisfied, we show in the following that $G'\gamma - G\gamma' \approx G'\gamma$. Actually, the order of magnitude of surface tension's difference in the film is expected to be $1 \text{ mN} \cdot \text{m}^{-1} \ll \gamma$. Furthermore, in the case of foaming symmetric mixtures, despite the fact that $\Gamma_1 > x_1$, the difference in molecule concentration between the bulk and the surface is not significant. That means $G(x_1) \gtrsim 1$. Hence, $G'\gamma - G\gamma' \approx G'\gamma$. The challenge now is to find x_1 such that $G'(x_1) = 0$.

Thus, we get:

$$2\Gamma_1\Gamma_1'x_1 - \Gamma_1'x_1^2 - \Gamma_1^2 = 0 \quad \text{Eq.E.9}$$

We recall **Eq.E.5** and find the derivative $\Gamma_1'(x_1) = d\Gamma_1/dx_1$:

$$\Gamma_1' = \frac{\Gamma_1^2}{x_1^2} e^\lambda \quad \text{Eq.E.10}$$

where $e^\lambda = e^{\frac{\sigma_{fit}}{RT}(\gamma_1 - \gamma_2)}$.

Substituting **Eq.E.10** into **Eq.E.9**, we finally obtain the maximum foam position x_1^{max} for symmetric mixtures:

$$x_1^{max} = \frac{e^\lambda}{1 + e^\lambda} \quad \text{Eq.E.11}$$

Note that e^λ is always smaller than 1 because $\gamma_1 < \gamma_2$. As a result, x_1^{max} is always less than 0.5 in foaming symmetric mixtures. This is shown in **Figure 2-7** as well.

Appendix F: A linear link between surface tension γ and surface molar fraction Γ cannot reflect asymmetric mixtures.

Table 9 : Molar surface σ_i were calculated using the cuboid molecule approximation from the molar volumes v and values of σ_{fit} obtained from Eq.F.2 for all binary mixtures

Mixture	Liquid 1	Liquid 2	σ_1 ($km^2 \cdot mol^{-1}$)	σ_2 ($km^2 \cdot mol^{-1}$)	σ_{fit} ($km^2 \cdot mol^{-1}$)
<i>Symmetric mixtures</i>	Heptane (C ₇)	Toluene (T)	0.24	0.19	0.56
	Octane (C ₈)	Toluene (T)	0.25	0.19	0.74
	Nonane (C ₉)	Toluene (T)	0.27	0.19	1.14
	Decane (C ₁₀)	Toluene (T)	0.28	0.19	1.63
	Pentanol (C ₅ OH)	Cyclopentanol (Cyclo)	0.19	0.17	0.48
	Hexanol (C ₆ OH)	Cyclopentanol (Cyclo)	0.21	0.17	0.52
	Heptanol (C ₇ OH)	Cyclopentanol (Cyclo)	0.23	0.17	0.93
	Pentanol (C ₅ OH)	Nonanol (C ₉ OH)	0.19	0.26	0.68
<i>Asymmetric mixtures</i>	Heptane (C ₇)	Hexadecane (C ₁₆)	0.24	0.37	-0.32
	Decane (C ₁₀) (50°C)	Eicosane (C ₂₀) (50°C)	0.29	0.43	-0.16
	PDMS	Decane (C ₁₀)	0.75	0.29	2.23

In **Chapter 2**, we assumed a basic phenomenological relation between surface tension γ and the molar fractions of each species on the surface Γ_i ($i = 1, 2$) for symmetric mixtures:

$$\gamma = \Gamma_1\gamma_1 + \Gamma_2\gamma_2 \quad \text{Eq.F.1}$$

To begin, and for the sake of simplification, we also applied this model to asymmetric mixtures.

We demonstrate in this Appendix that a linear relation cannot be applied to this circumstance.

The surface tensions of all binary liquid mixtures were fitted with their compositions using the equation below:

$$x_1 e^{\sigma_{fit} \frac{\gamma - \gamma_1}{RT}} + x_2 e^{\sigma_{fit} \frac{\gamma - \gamma_2}{RT}} = 1 \quad \text{Eq.F.2}$$

We can determine the values of σ_{fit} for all mixes using **Eq.F.2**, see **Table 9**.

The table above also includes the values for the molar surfaces σ_1, σ_2 obtained from the molar volumes using the cuboid molecule approximation. As can be seen, the more different these liquids are, equivalent to a larger surface ratio σ_2/σ_1 , the greater the value of σ_{fit} . Additionally, σ_{fit} frequently deviate significantly from the theoretical values of σ_1 and σ_2 . This is readily apparent when Decane/Toluene or PDMS/Decane mixes are used.

As discussed in **Chapter 2**, we used α as a length to characterize the foaming ability of the mixtures. The expression for foaming length α :

$$\alpha = \frac{2}{\gamma} \left(\frac{\partial \gamma}{\partial x_1} \right)_{x_1=x_1^0} \frac{v}{\sigma} (x_1^0 - \Gamma_1) \quad \text{Eq.F.3}$$

σ_{fit} in the table above is used to calculate the corresponding α for the asymmetric mixtures; same as in **Chapter 2** for symmetric mixtures.

We display, then, the foamability L_τ as a function in terms of α in **Figure F-1**. On this graph, however, there is no master curve. The distinction between symmetric and asymmetric mixtures was demonstrated most convincingly with PDMS/Decane or Decane/paraffin (Eicosane). Clearly, the simple model does not completely capture the foaming behavior of asymmetric mixtures. A single value σ_{fit} cannot accurately describe the difference in molar surface area of the liquids in a mixture. As a result, we employed Butler's model as described in **Chapter 3**.

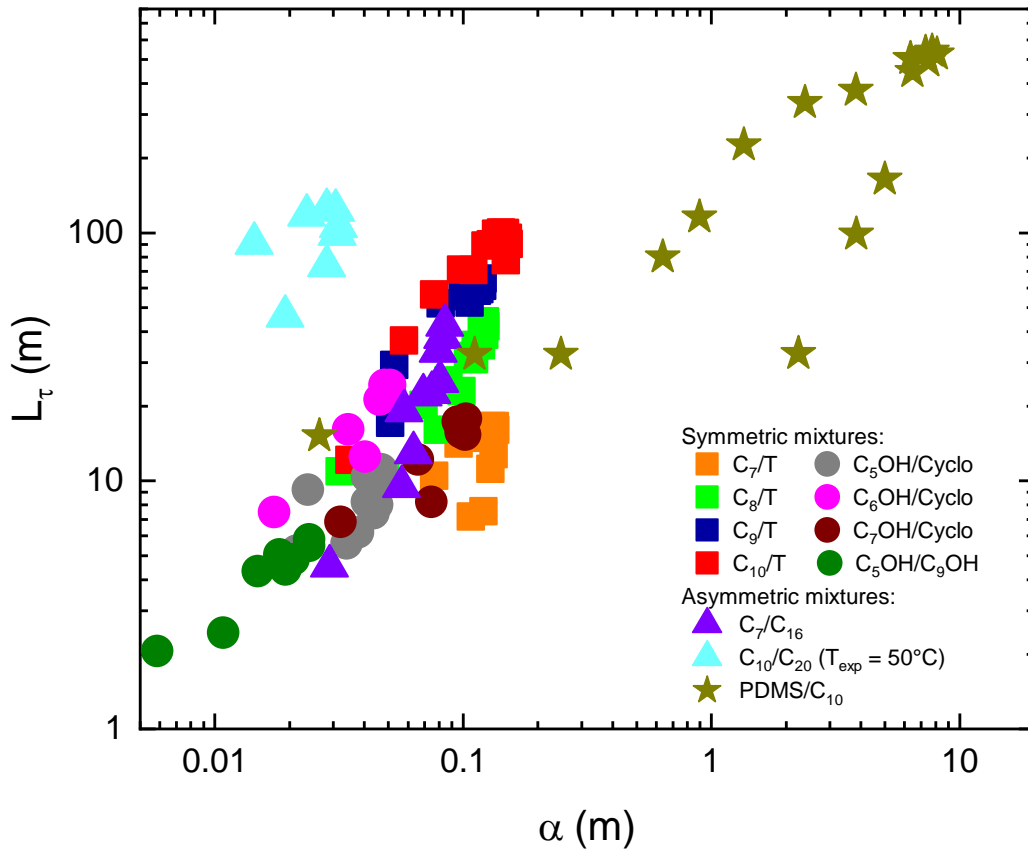


Figure F-1 : L_τ as a function of α for all liquid mixtures both symmetric and asymmetric.

We display, then, the foamability L_τ as a function in terms of α in **Figure F-1**. On this graph, however, there is no master curve. The distinction between symmetric and asymmetric mixtures was demonstrated most convincingly with PDMS/Decane or Decane/paraffin (Eicosane). Clearly, the simple model does not completely capture the foaming behavior of asymmetric mixtures. A single value σ_{fit} cannot accurately describe the difference in molar surface area of the liquids in a mixture. As a result, we employed Butler's model as described in **Chapter 3**.

RÉSUMÉ EN FRANÇAIS

INTRODUCTION

La formation de mousse dans les mélanges d'huile est un problème courant, par exemple dans les boîtes de vitesses des moteurs électriques. Des agents anti-mousses peuvent être utilisés, mais il est essentiel de comprendre les mécanismes de formation de la mousse. Les liquides purs ne forment pas de mousse en raison de la courte durée de vie des films liquides, où il n'y a aucun effet contre les interactions attractives de van der Waals [4,5]. La formation de mousse dans les mélanges liquides, en particulier les mélanges d'huile [8], est bien documentée. Cependant, l'effet de l'augmentation de le temps de vie des films liquides dans les mélanges n'a pas été expliqué en l'absence d'autres effets stabilisateurs connus [6,7]. Cette thèse propose un mécanisme pour l'augmentation du temps de vie des films liquides.

Dans le chapitre 1, nous présenterons les méthodes que nous avons utilisées pour mesurer le temps de vie des mousses dans des mélanges binaires dont la composition et la taille des bulles varient. Des expériences sur des bulles uniques formées à la surface d'un bain liquide nous ont permis de mesurer l'épaisseur du film liquide au moment de sa rupture. Dans le chapitre 2, nous discuterons et proposerons des modèles théoriques pour expliquer l'origine du moussage des mélanges de liquides de taille très similaire. Les mélanges plus compliqués, appelés mélanges binaires asymétriques, seront abordés plus en profondeur dans le chapitre 3. Enfin, dans le dernier chapitre, le chapitre 4, nous expliquerons comment modéliser le temps de vie des bulles.

CHAPITRE 1 : MÉTHODES EXPÉRIMENTALES

Détermination de la moussabilité des mélanges binaires à l'aide d'une colonne Bikerman

Nous avons réalisé des expériences avec différents mélanges de liquides. Des expériences ont été menées pour quantifier cet effet moussant pour différents mélanges de liquides en utilisant des colonnes de Bikerman [12,13]. Du gaz est injecté dans la colonne avec nos mélanges liquides binaires, à travers un matériau poreux, pour former de la mousse. Les expériences ont été réalisées dans un système fermé pour éviter l'effet de l'évaporation sur la capacité de moussage du mélange [7]. Pour chaque mélange binaire testé, la composition du mélange peut également être modifiée afin d'examiner son influence sur la hauteur de la mousse. La hauteur de la mousse H atteint en régime stationnaire a été mesurée pour chaque mélange. Le débit injecté Q et la hauteur initiale du liquide H_0 ont été fixés de façon à ce que la hauteur de la mousse ne dépende pas de la hauteur initiale du liquide et varie proportionnellement au débit.

A partir des valeurs de la hauteur expérimentale de la mousse H , nous pouvons calculer le temps de vie de la mousse, qui est le temps moyen que met une bulle pour se déplacer sur la hauteur de la mousse.

Ainsi, l'expression du temps de vie de la mousse est la suivante :

$$\tau = \frac{H\pi R^2}{Q}$$

où R est le rayon de la colonne.

La moussabilité est représentée par un temps de vie normalisée L_τ donnée par le produit du temps de vie τ par la vitesse capillaire $\frac{\gamma}{\mu}$:

$$L_\tau = \frac{\tau\gamma}{\mu}$$

où γ est la tension de surface et μ est la viscosité du mélange.

A travers les résultats obtenus, nous voyons que moussabilité est déterminée par la nature physico-chimique. En accord avec la littérature, nous avons découvert que pour chaque mélange, il existe une composition pour laquelle le temps de vie de la mousse est maximal [8].

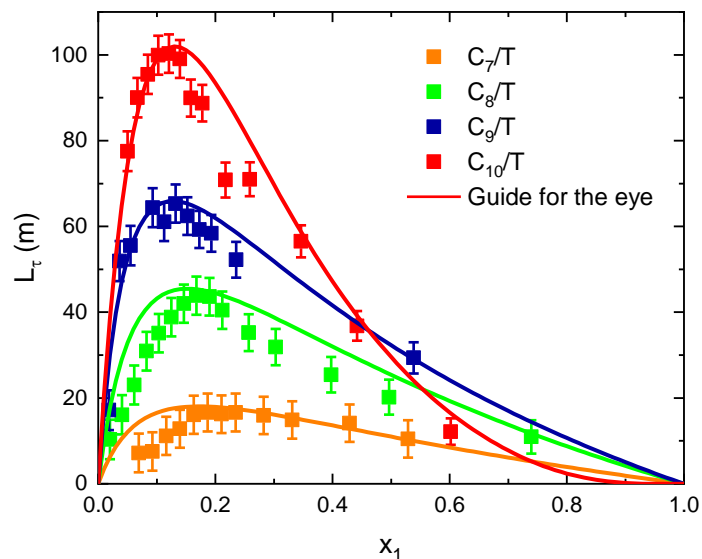


Figure 3 : Temps de vie expérimental normalisé de la mousse L_τ en fonction de la fraction molaire du liquide 1 x_1 dans les mélanges binaires d'alcane linéaires et de Toluène.

Variation de la taille de la bulle avec un montage Ultra Turrax

L'effet de la taille des bulles d'air sur le moussage du mélange a également été examiné. Dans la colonne Bickerman, la taille des bulles d'air formées est identique pour tous les mélanges $D_b = 1.6 \text{ mm}$. Faire varier la taille des bulles, nous avons développé un montage utilisant un dispositif Ultra Turrax qui permet de contrôler la taille des bulles.

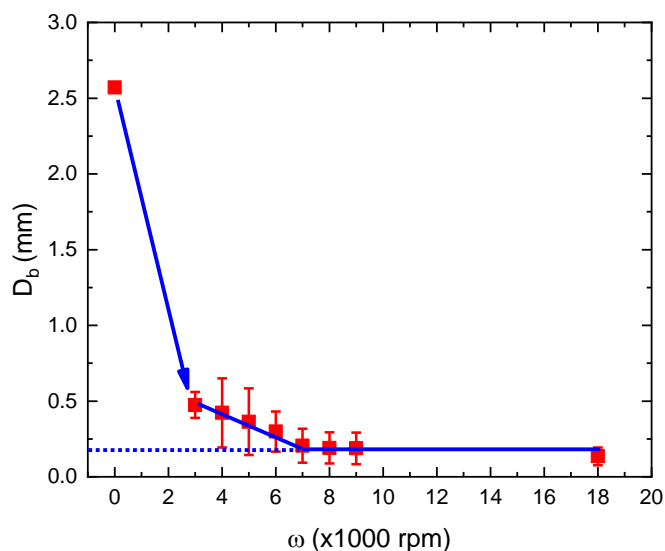


Figure 4 : Diamètre des bulles évalué par analyse d'image en fonction de la vitesse de rotation du dispositif Ultra Turrax à débit fixe $Q = 100 \mu\text{L} \cdot \text{s}^{-1}$. Le diamètre des bulles d'air est $D_b = 2.5 \text{ mm}$ lorsqu'aucun Ultra turrax n'est utilisé, soit $\omega = 0 \text{ rpm}$.

L'objectif de ce système expérimental est d'utiliser l'Ultra Turrax pour créer des bulles dont la taille est inférieure à celle de l'expérience précédente - la colonne de Bikerman. En effet, comme l'illustre la figure ci-dessus, nous pouvons fractionner les bulles d'air injectées dans la colonne des mélanges liquides étudiés en utilisant l'Ultra Turrax. La taille de ces bulles atteint un diamètre $D_b = 0.25 \text{ mm}$ à $\omega = 9000 \text{ rpm}$.

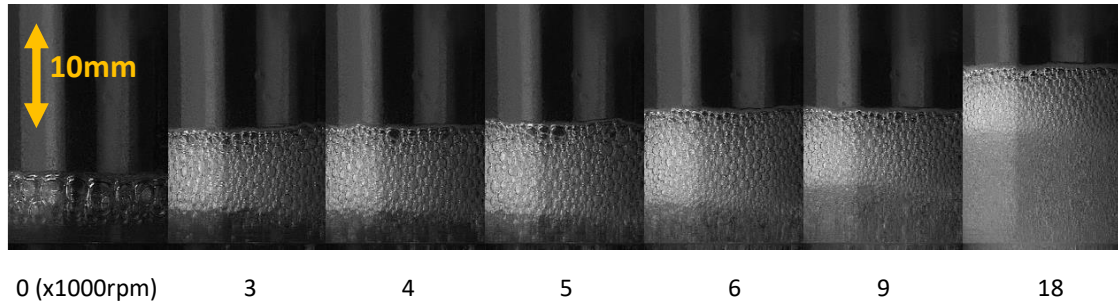


Figure 5 : Images expérimentales pour différentes vitesses de rotation du dispositif Ultra Turrax à un débit fixe $Q = 100 \mu\text{L} \cdot \text{s}^{-1}$.

Nous mesurons ensuite la hauteur de la couche de mousse créée par ces bulles d'air, de la même manière que les recherches antérieures, et nous tentons de comparer moussabilité en fonction de la taille des bulles.

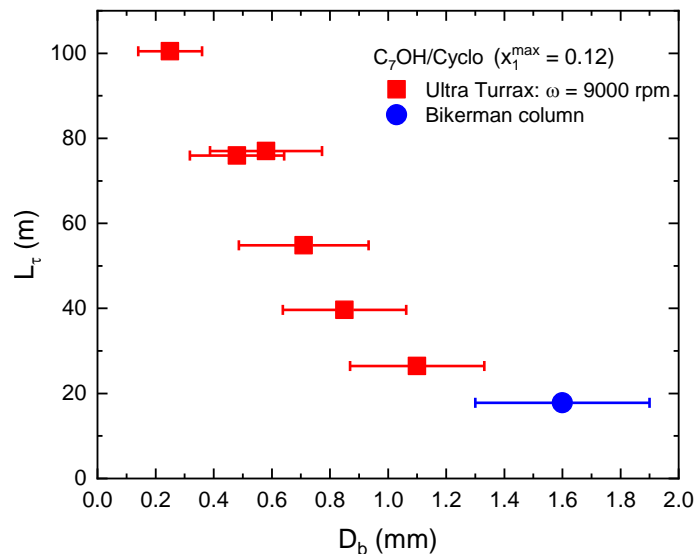


Figure 6 : Variations du temps de vie normalisée de la mousse L_τ en fonction du diamètre des bulles dans la mousse. Expériences : Ultra Turrax - carrés rouges et expérience : Bikerman - cercle bleu. Mélange Heptanol/Cyclopentanol (à $x_1 = 0.12$).

Nous avons découvert que les mélanges ayant les mêmes caractéristiques et compositions créent des mousses plus stables lorsque les bulles sont plus petites.

Mesure de l'épaisseur et du temps de vie du film liquide par l'expérience d'une bulle unique

Comme nous l'avons vu dans les sections précédentes, l'expérience avec la colonne Bikerman a permis d'obtenir des données quantitatives sur la moussabilité. Les expériences macroscopiques, en revanche, rendent impossible l'estimation exacte de l'épaisseur des films minces liquides entre les bulles au moment de leur éclatement. Par conséquent, nous montrons comment déterminer cette épaisseur à l'aide d'expériences sur une bulle unique.

Lorsque la bulle éclate, le trou s'ouvre à une vitesse constante. Par conséquent, nous pouvons déduire cette vitesse d'ouverture du trou U_{TC} - la vitesse de Taylor-Culick. L'épaisseur du film est déterminée en utilisant la relation de Taylor-Culick entre la vitesse d'ouverture du trou U_{TC} et l'épaisseur du film h_b à l'éclatement [23,24]:

$$h_b = \frac{2\gamma}{\rho U_{TC}^2}$$

Les L_τ mesurés sont présentés dans la figure ci-dessous. Les temps de vie normalisés des bulles sont représentés en fonction l'épaisseur de la couche mince liquide. D'après cette figure, le film a une épaisseur de l'ordre du micromètre, et le temps de vie normalisée de la mousse change proportionnellement au carré de l'épaisseur de ce film.

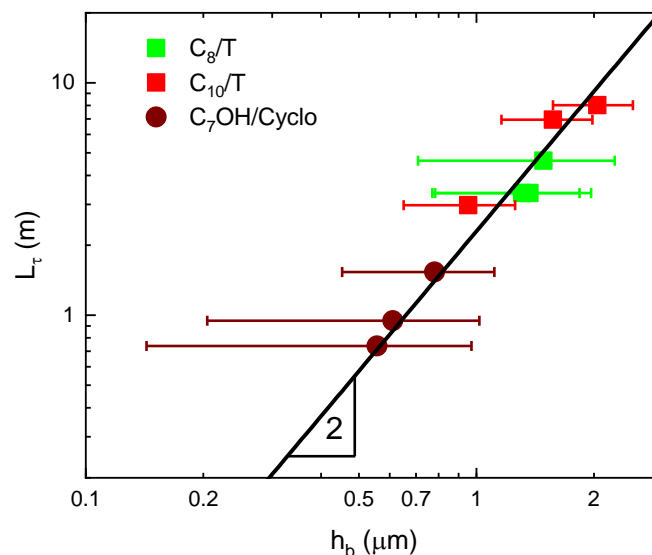


Figure 7 : Le temps de vie normalisé de la mousse L_τ en fonction de l'épaisseur du film liquide h_b pour les mélanges binaires étudiés. La ligne en trait plein est un guide pour l'œil.

Dans le chapitre 1, nous avons observé que la majorité des mélanges examinés étaient capables de produire de la mousse. Dans un premier temps, nous cherchons à décrire les comportements observés dans les mélanges « symétriques », c'est-à-dire composés de molécules dont les tailles sont proches.

CHAPITRE 2 : MÉLANGES BINAIRES SYMÉTRIQUES

Le cas des mélanges symétriques est le plus simple. Il correspond à des mélanges de molécules de taille presque identique. Plus précisément, leurs volumes molaires et leurs surfaces molaires doivent être presque similaires.

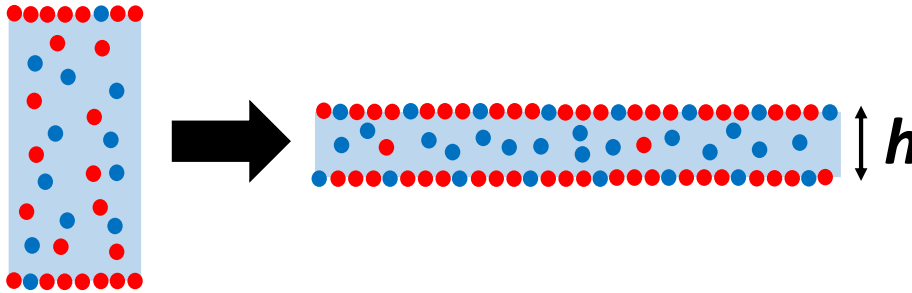


Figure 8 : Explication schématique de la tension superficielle en fonction de l'épaisseur d'un film de mélange liquide. Lorsque le film s'amincit à volume constant, les concentrations aux interfaces ne peuvent être maintenues constantes, ce qui conduit à un nouvel équilibre dans lequel la concentration interfaciale de l'espèce (rouge) ayant la plus petite tension superficielle est plus faible, et donc la tension superficielle est plus grande. L'épaisseur du film liquide est désignée par h .

Nous suggérons que le mécanisme de stabilisation des films liquides dans les mélanges est basé sur le fait que les concentrations des espèces sont différentes dans le volume et aux interfaces avec l'air. Les espèces ayant la plus faible tension superficielle sont toujours plus concentrées aux interfaces que dans le volume. En raison de ces différences de concentration, on s'attend à ce que la tension superficielle dépende de l'épaisseur des films minces : si un film s'amincit alors que son volume reste constant, la surface de ses interfaces augmente, ce qui modifie la répartition entre les interfaces et le volume, comme le montre la figure ci-dessus. En conséquence, les interfaces des films minces sont moins concentrées dans les espèces ayant la plus faible tension de surface par rapport à celles des grandes épaisseurs. Ceci conduit à une augmentation de la tension superficielle du film pour des épaisseurs décroissantes.

Dans ce qui suit, nous montrons que l'augmentation de la tension de surface peut s'écrire comme suit :

$$\gamma(h) = \gamma \left(1 + \frac{\alpha}{h} \right)$$

où γ est la tension superficielle du liquide dans un réservoir de liquide infiniment grand, h l'épaisseur locale du film. En outre, α est une longueur de mousse du mélange et dépend de sa composition.

Lorsque l'équilibre mécanique de la tension du film est atteint, la forme du film peut être déterminée analytiquement. Nous considérons un film d'épaisseur h_f relié à un bord de Plateau, voir la figure ci-dessous.

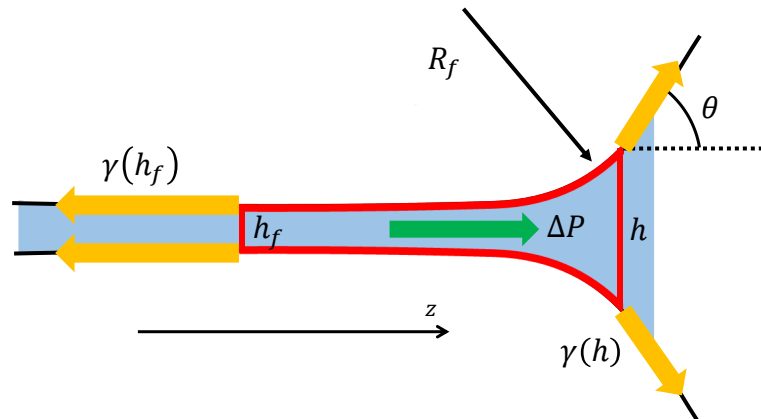


Figure 9 : Diagramme montrant les forces agissant sur un film fluide d'épaisseur h_f relié à une bordure de plateau dans la mousse. La tension superficielle plus élevée de la partie plate permet un équilibre mécanique même si les pressions ne sont pas équilibrées. Un équilibre de tension le long de l'axe z peut être écrit sur la partie du film en rouge.

La tension du film s'écrit : $2\gamma(h) \cos[\theta(z)] + \Delta P(h)h(z)$. L'équilibre du film impose que cette tension soit constante. Dans la partie plate du film pour laquelle $\theta = 0$ et $\Delta P(h) = 0$, la constante est simplement deux fois la tension interfaciale. On a donc pour tout z :

$$2\gamma(h_f) = 2\gamma(h) \cos[\theta(z)] + \Delta P(h)h(z)$$

où $\theta(z)$ est l'angle local du film avec la direction de l'axe z . $\Delta P(h) = \gamma(h)d^2(h/2)/dz^2$ est la différence de pression de Laplace entre le gaz et le liquide dans le ménisque écrite dans l'approximation de la couche mince avec des termes de premier ordre seulement.

Comme elle correspond à l'épaisseur atteinte lorsqu'un équilibre de tension est atteint, il est possible d'obtenir l'expression de h_f qui ne dépend que de la longueur α et du rayon de courbure du bord de Plateau R_f :

$$h_f = \sqrt{\alpha R_f}$$

Nous montrons également que l'effet Marangoni induit par cette tension superficielle dépendant de l'épaisseur contrôle la morphologie de la géométrie du film/le bord de Plateau avant le drainage et donne une solution analytique pour l'épaisseur du film.

Nous considérons ensuite les différences de concentration dans le volume et aux interfaces et nous calculons ensuite la longueur microscopique α . Cette différence de concentration conduit à une variation sous-linéaire de la tension de surface avec la composition dans les mélanges symétriques. Nous montrons que cela se traduit par une tension de surface dépendant de l'épaisseur du film et donc par la formation de mousse. En effet, il s'agit d'un comportement de type surfactant, dans lequel l'espèce ayant la tension interfaciale la plus faible agit comme un surfactant pour les autres espèces.

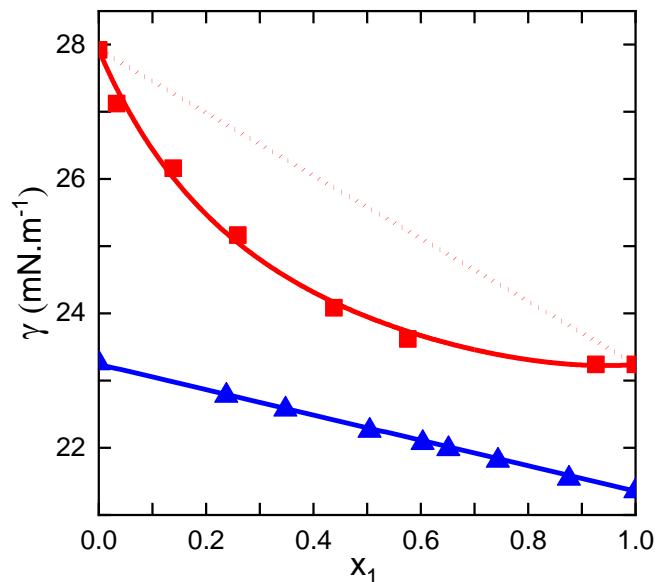


Figure 10 : Tensions de surface des mélanges Décane/Toluène (rouge) et Octane/Décane (bleu) en fonction de la fraction molaire de l'espèce ayant la tension de surface la plus faible (respectivement, Décane et Octane). Les lignes en trait plein sont des guides pour l'œil.

Ici, nous utilisons une relation phénoménologique très simple dans laquelle une relation linéaire entre la tension de surface γ et les fractions molaires de chaque espèce sur la surface Γ_i ($i = 1, 2$) est supposée [27]:

$$\gamma = \Gamma_1\gamma_1 + \Gamma_2\gamma_2$$

où γ et γ_i ($i = 1, 2$) sont les tensions de surface du mélange et des composants purs, respectivement.

Par ailleurs, il est possible de calculer α en utilisant les volumes et surfaces molaires des deux liquides et la dérivée de $\gamma(x_1)$:

$$\alpha = \frac{2}{\gamma} \left(\frac{\partial \gamma}{\partial x_1} \right)_{x_1=x_1^0} \frac{v}{\sigma} (x_1^0 - \Gamma_1)$$

Expérimentalement, nous observons qu'il existe un lien entre le temps de vie de la mousse, l'aptitude à la mousse et l'épaisseur du film au début de l'éclatement. Nous observons que le temps de vie de la mousse est lié à la composition du mélange pour tous les mélanges étudiés, qu'il s'agisse de liquides polaires ou non polaires et qu'il varie proportionnellement à la longueur α .

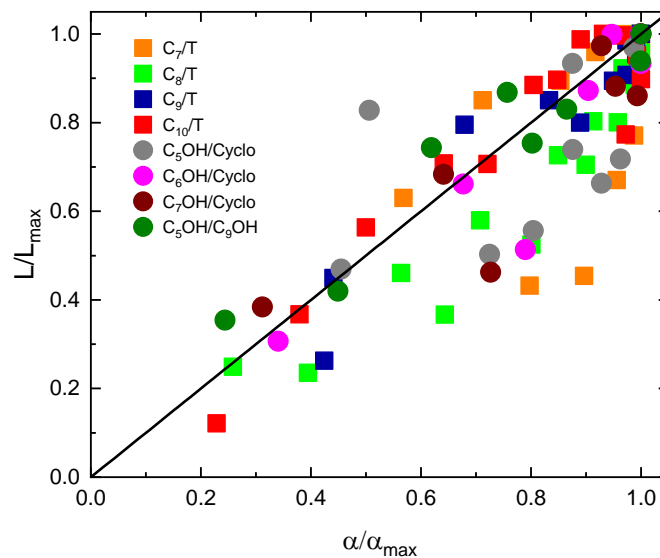


Figure 11 : L_τ en fonction de α pour 8 mélanges liquides différents. L_τ et α sont normalisés par leurs valeurs maximales trouvées dans chaque mélange qui sont atteintes pour une même composition. La ligne en trait plein est un guide pour l'œil.

CHAPITRE 3: MÉLANGES BINAIRES ASYMÉTRIQUES

Nous abordons ensuite les mélanges liquides asymétriques, qui sont des liquides constitués de molécules de tailles différentes, donc de surfaces et de volumes molaires différents. Pour les mélanges asymétriques, le modèle employé pour les mélanges symétriques ne parvient pas à décrire la tension de surface. Nous nous tournons donc vers la théorie de la solution idéale. Dans ce cadre, nous montrons que les espèces ayant la plus faible tension de surface sont toujours plus concentrées près de l'interface que dans le volume. Mais les espèces ayant une taille moléculaire plus élevée couvrent une plus grande surface et ont donc un effet plus complexe sur la tension de surface. Il peut en résulter des variations sur-linéaires ou sous-linéaires de la tension superficielle.

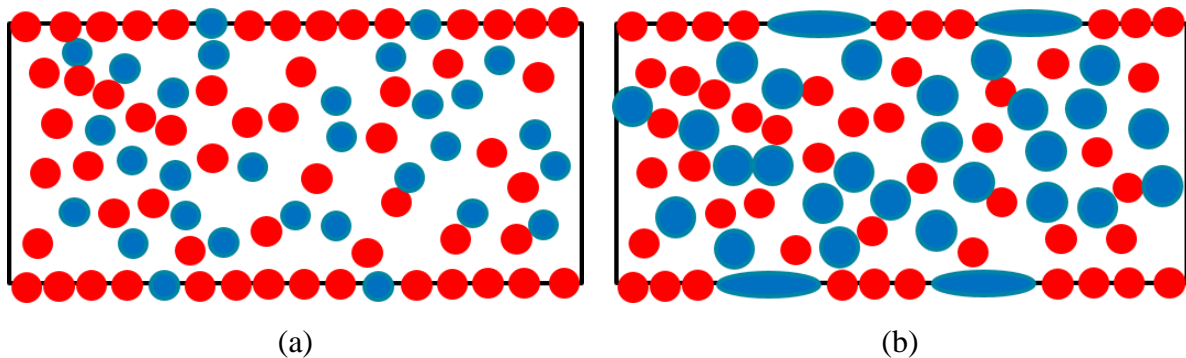


Figure 12 : (a) Film liquide de mélanges symétriques de molécules de tailles similaires.

La surface est enrichie en espèces ayant la plus faible tension superficielle (cercles rouges) par rapport au volume. (b) Film liquide de mélanges asymétriques composés de molécules de tailles très différentes. La surface est concentrée en espèces à faible tension superficielle (cercles rouges). L'espèce ayant l'énergie de surface la plus élevée (cercles bleus) a une taille moléculaire nettement supérieure, ce qui se traduit par une plus grande surface moléculaire.

Ceci est en accord avec notre observation, les tensions de surface des mélanges asymétriques peuvent varier de manière sous-linéaire ou sur-linéaire en fonction de leurs rapports de surface. Cependant, quel que soit le signe de la non-linéarité, la concentration en surface de l'espèce ayant la plus faible énergie de surface est toujours supérieure à la concentration au volume. Et c'est en fait ce phénomène qui provoque la formation de mousse dans les mélanges.

Dans le chapitre 1, nous avons utilisé un modèle phénoménologique assez simple, en supposant que la tension de surface γ est une fonction linéaire de la fraction molaire de surface Γ . La comparaison des données expérimentales et théoriques démontre que ce modèle est approprié pour les mélanges symétriques [37,38]. Cependant, pour les mélanges de molécules asymétriques, cette approche ne rend pas compte de manière adéquate des phénomènes observés tels que la sur-linéarité de la tension de surface.

L'approximation de la solution idéale a été introduite par Butler [21] pour décrire la partition surface/volume des mélanges idéaux. La relation entre la fraction volumique et la tension interfaciale s'écrit :

$$x_1 e^{\frac{\sigma_1}{RT}(\gamma-\gamma_1)} + x_2 e^{\frac{\sigma_2}{RT}(\gamma-\gamma_2)} = 1$$

où R est la constante du gaz idéal et T la température absolue.

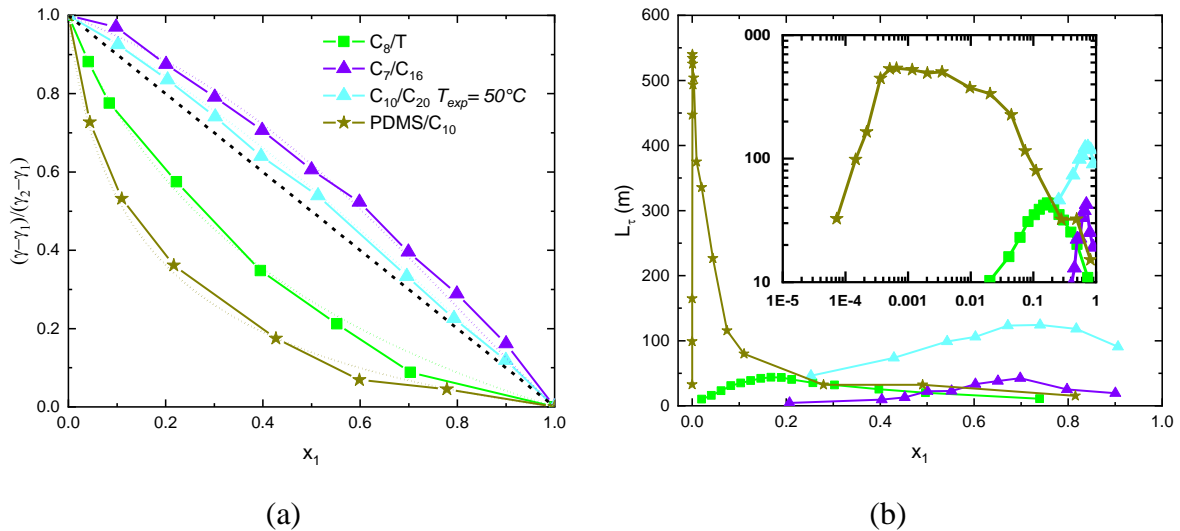


Figure 13 : (a) Tensions de surface normalisées de mélanges binaires en fonction de la fraction molaire du liquide 1 - l'espèce ayant la plus petite tension de surface. Les lignes pointillées montrent les tensions de surface calculées à partir du modèle de Butler. (b) L_τ avec les mêmes mélanges en fonction de la fraction molaire de l'espèce ayant la plus petite tension de surface. Inset: mêmes courbes en échelle log-log.

Dans le cas de mélanges asymétriques, on détermine l'expression de la longueur microscopique α qui caractérise la capacité à produire des mousses :

$$\alpha = \frac{RT}{2\gamma} \frac{(\Gamma_1 - x_1)^2}{(1 - x_1)x_1} \frac{v_1 x_1 + v_2 (1 - x_1)}{(\Gamma_1 \sigma_1 + (1 - \Gamma_1) \sigma_2)^2}$$

où σ_i et v_i sont la surface molaire et le volume molaire de l'espèce i dans le mélange liquide.

En revanche, notre modèle théorique ne permet pas de prédire quantitativement la moussabilité. La limitation de notre modèle est due à la difficulté d'identifier les surfaces molaires des liquides, et probablement au fait que le cadre de la solution idéale néglige la fugacité des différentes espèces en volume et aux interfaces [18,43].

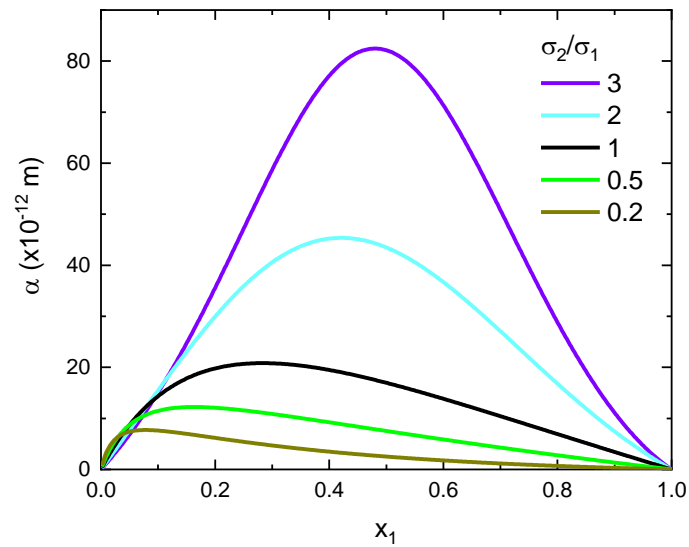


Figure 14 : Longueur α caractérisant l'augmentation de la tension superficielle lorsque l'épaisseur d'un film de mélange binaire diminue, en fonction de la composition du mélange.

CHAPITRE 4: HYDRODYNAMIQUE ET PERCEMENT DE FILMS LIQUIDES MINCES

Dans les chapitres précédents, nous avons montré que le moussage des mélanges liquides - sur la base de données expérimentales et de modèles théoriques - est dû à la répartition des molécules entre le volume et la surface. En effet, les couches de film liquide générées entre les deux bulles présentent une tension de surface dépendant de l'épaisseur. La différence de tension superficielle crée l'effet Marangoni, qui retarde le drainage dans les films minces. Cependant, ce drainage se produit toujours à la suite d'un déséquilibre de pression entre le film liquide et le bord de Plateau. Il en résulte un effet de pincement sur le film mince liquide.

Nous fournissons un modèle théorique pour l'hydrodynamique de l'amincissement du film, qui correspond aux résultats expérimentaux. Nous montrons que l'hydrodynamique peut expliquer pourquoi le temps de vie des bulles formées dans les mélanges liquides varie comme le carré de l'épaisseur de la couche liquide.

BIBLIOGRAPHIC REFERENCES

1. Arangalage, M. Moussabilité des mélanges d'huiles. (Sorbonne Université, 2018).
2. Derjaguin, B. V. & Obukov, E. V. *Acta Physicochim.* **5**, 1 (1936).
3. Cantat, I. *et al.* *Foams: Structure and Dynamics*. (Oxford University Press, 2013). doi:10.1093/acprof:oso/9780199662890.001.0001.
4. Derjaguin, B. & Landau, L. Theory of the stability of strongly charged lyophobic sols and of the adhesion of strongly charged particles in solutions of electrolytes. *Progress in Surface Science* **43**, 30–59 (1993).
5. Verwey, E. J. W. Theory of the Stability of Lyophobic Colloids. *J. Phys. Chem.* **51**, 631–636 (1947).
6. Lhuissier, H. & Villermaux, E. Bursting bubble aerosols. *J. Fluid Mech.* **696**, 5–44 (2012).
7. Chandran Suja, V. *et al.* Evaporation-induced foam stabilization in lubricating oils. *Proc Natl Acad Sci USA* **115**, 7919–7924 (2018).
8. Ross, S. & Nishioka, G. Foaminess of binary and ternary solutions. *J. Phys. Chem.* **79**, 1561–1565 (1975).
9. Ross, J. & Miles, G. D. An apparatus for comparison of foaming properties of soaps and detergents. *Oil Soap* **18**, 99–102 (1941).
10. Rusanov, A. I., Krotov, V. V. & Nekrasov, A. G. New Methods for Studying Foams: Foaminess and Foam Stability. *Journal of Colloid and Interface Science* **206**, 392–396 (1998).
11. Khristov, Khr., Exerowa, D., Christov, L., Makievski, A. V. & Miller, R. Foam analyzer: An instrument based on the foam pressure drop technique. *Review of Scientific Instruments* **75**, 4797–4803 (2004).
12. Bikerman, J. J. Methods of measuring foaminess. *Foams: Theory and Industrial Applications* (1953).
13. Bikerman, J. J. *Foams*. (Springer Berlin Heidelberg, 1973). doi:10.1007/978-3-642-86734-7.
14. Richardson, J. F. & Zaki, W. N. Sedimentation and fluidisation: Part I. *Trans. Inst. Chem. Eng.* **32**, 35–53 (1954).

-
15. Kendall, J. & Monroe, K. P. THE VISCOSITY OF LIQUIDS. II. THE VISCOSITY-COMPOSITION CURVE FOR IDEAL LIQUID MIXTURES. ¹. *J. Am. Chem. Soc.* **39**, 1787–1802 (1917).
 16. Iloukhani, H., Rezaei-Sameti, M. & Basiri-Parsa, J. Excess molar volumes and dynamic viscosities for binary mixtures of toluene+n-alkanes (C5–C10) at T=298.15K – Comparison with Prigogine–Flory–Patterson theory. *The Journal of Chemical Thermodynamics* **38**, 975–982 (2006).
 17. Szyszkowski, B. von. Experimentelle Studien über kapillare Eigenschaften der wässrigen Lösungen von Fettsäuren. *Zeitschrift für Physikalische Chemie* **64U**, 385–414 (1908).
 18. Matsumoto, M., Takaoka, Y. & Kataoka, Y. Liquid–vapor interface of water–methanol mixture. I. Computer simulation. *The Journal of Chemical Physics* **98**, 1464–1472 (1993).
 19. Vazquez, G., Alvarez, E. & Navaza, J. M. Surface Tension of Alcohol Water + Water from 20 to 50 .degree.C. *J. Chem. Eng. Data* **40**, 611–614 (1995).
 20. Rolo, L. I., Caço, A. I., Queimada, A. J., Marrucho, I. M. & Coutinho, J. A. P. Surface Tension of Heptane, Decane, Hexadecane, Eicosane, and Some of Their Binary Mixtures. *J. Chem. Eng. Data* **47**, 1442–1445 (2002).
 21. Butler, J. A. V. The thermodynamics of the surfaces of solutions. *Proc. R. Soc. Lond. A* **135**, 348–375 (1932).
 22. Champougny, L., Roché, M., Drenckhan, W. & Rio, E. Life and death of not so “bare” bubbles. *Soft Matter* **12**, 5276–5284 (2016).
 23. The dynamics of thin sheets of fluid. III. Disintegration of fluid sheets. *Proc. R. Soc. Lond. A* **253**, 313–321 (1959).
 24. Culick, F. E. C. Comments on a Ruptured Soap Film. *Journal of Applied Physics* **31**, 1128–1129 (1960).
 25. Howell, P. D. & Stone, H. A. On the absence of marginal pinching in thin free films. *Eur. J. Appl. Math.* **16**, 569 (2005).
 26. Koehler, S. A., Hilgenfeldt, S., Weeks, E. R. & Stone, H. A. Drainage of single Plateau borders: Direct observation of rigid and mobile interfaces. *Phys. Rev. E* **66**, 040601 (2002).
 27. Eberhart, J. G. The Surface Tension of Binary Liquid Mixtures ¹. *J. Phys. Chem.* **70**, 1183–1186 (1966).
 28. Shardt, N., Wang, Y., Jin, Z. & Elliott, J. A. W. Surface tension as a function of temperature and composition for a broad range of mixtures. *Chemical Engineering Science* **230**, 116095 (2021).

-
29. Gaines, G. L. Surface tension of polymer solutions. I. Solutions of poly(dimethylsiloxanes). *J. Phys. Chem.* **73**, 3143–3150 (1969).
 30. Suarez, J. T., Torres-Marchal, C. & Rasmussen, P. Prediction of surface tensions of nonelectrolyte solutions. *Chemical Engineering Science* **44**, 782–785 (1989).
 31. Nath, S. Surface Tension of Nonideal Binary Liquid Mixtures as a Function of Composition. *Journal of Colloid and Interface Science* **209**, 116–122 (1999).
 32. Kahl, H., Wadewitz, T. & Winkelmann, J. Surface Tension of Pure Liquids and Binary Liquid Mixtures. *J. Chem. Eng. Data* **48**, 580–586 (2003).
 33. Bagheri, A., Rafati, A. A., Tajani, A. A., Borujeni, A. R. A. & Hajian, A. Prediction of the Surface Tension, Surface Concentration and the Relative Gibbs Adsorption Isotherm of Non-ideal Binary Liquid Mixtures. *J Solution Chem* **42**, 2071–2086 (2013).
 34. Santos, M. S. C. S. & Reis, J. C. R. Thermodynamic evaluation of molar surface area and thickness of water + ethanol mixtures. *Journal of Molecular Liquids* **255**, 419–428 (2018).
 35. Prigogine, I. & Marechal, J. The influence of differences in molecular size on the surface tension of solutions. IV. *Journal of Colloid Science* **7**, 122–127 (1952).
 36. Queimada, A. J., Silva, F. A. E., Caço, A. I., Marrucho, I. M. & Coutinho, J. A. P. Measurement and modeling of surface tensions of asymmetric systems: heptane, eicosane, docosane, tetracosane and their mixtures. *Fluid Phase Equilibria* **214**, 211–221 (2003).
 37. Connors, K. A. & Wright, J. L. Dependence of surface tension on composition of binary aqueous-organic solutions. *Anal. Chem.* **61**, 194–198 (1989).
 38. Khosravi, D. & Connors, K. A. Solvent effects on chemical processes. 3. Surface tension of binary aqueous organic solvents. *J Solution Chem* **22**, 321–330 (1993).
 39. Belton, J. W. & Evans, M. G. Studies in the molecular forces involved in surface formation. II. The surface free energies of simple liquid mixtures. *Trans. Faraday Soc.* **41**, 1 (1945).
 40. Santos, M. S. C. S. & Reis, J. C. R. New Thermodynamics for Evaluating the Surface-phase Enrichment in the Lower Surface Tension Component. *ChemPhysChem* **15**, 2834–2843 (2014).
 41. Kaptay, G. Partial Surface Tension of Components of a Solution. *Langmuir* **31**, 5796–5804 (2015).
 42. Chang, T.-M. & Dang, L. X. Liquid–Vapor Interface of Methanol–Water Mixtures: A Molecular Dynamics Study. *J. Phys. Chem. B* **109**, 5759–5765 (2005).
 43. Aradian, A., Raphaël, E. & Gennes, P.-G. de. “Marginal pinching” in soap films. *Europhys. Lett.* **55**, 834–840 (2001).

-
44. Chatzigiannakis, E. & Vermant, J. Breakup of Thin Liquid Films: From Stochastic to Deterministic. *Phys. Rev. Lett.* **125**, 158001 (2020).
 45. Shah, M. S., Kleijn, C. R., Kreutzer, M. T. & van Steijn, V. Influence of initial film radius and film thickness on the rupture of foam films. *Phys. Rev. Fluids* **6**, 013603 (2021).
 46. Mysels, K. J., Frankel, S. & Shinoda, K. Soap films: studies of their thinning and a bibliography. *Pergamon press* (1959).
 47. Seiwert, J., Dollet, B. & Cantat, I. Theoretical study of the generation of soap films: role of interfacial visco-elasticity. *J. Fluid Mech.* **739**, 124–142 (2014).
 48. Tamura, M. & Kurata, M. On the Viscosity of Binary Mixture of Liquids. *BCSJ* **25**, 32–38 (1952).
 49. Grunberg, L. & Nissan, A. H. Mixture Law for Viscosity. *Nature* **164**, 799–800 (1949).
 50. Katti, P. K. & Chaudhri, M. M. Viscosities of Binary Mixtures of Benzyl Acetate with Dioxane, Aniline, and *m*-Cresol. *J. Chem. Eng. Data* **9**, 442–443 (1964).
 51. Hind, R. K., McLaughlin, E. & Ubbelohde, A. R. Structure and viscosity of liquids. Camphor + pyrene mixtures. *Trans. Faraday Soc.* **56**, 328 (1960).
 52. McAllister, R. A. The viscosity of liquid mixtures. *AIChE J.* **6**, 427–431 (1960).
 53. Heric, E. L. On the Viscosity of Ternary Mixtures. *J. Chem. Eng. Data* **11**, 66–68 (1966).

CONTACTS

SUJET : MOUSSABILITÉ DES MÉLANGES D'HUILES

Résumé :

La formation de mousse dans les mélanges d'huiles est un problème courant, par exemple dans les boîtes de vitesses de moteurs électriques. Des agents anti-mousses peuvent être utilisés, mais il est important de comprendre comment se forme la mousse. Les liquides purs ne forment pas de mousse en raison de la courte durée de vie des films liquides, où aucun effet ne s'oppose aux interactions attractives de van der Waals. Toutefois, l'effet permettant d'augmenter les temps de vie des films liquides dans les mélanges d'huiles, et en l'absence d'autres effets stabilisants connus, n'a pas été expliqué. Cette thèse propose un mécanisme à l'origine de cette augmentation. Nous avons mesuré le temps de vie de mousses dans des mélanges binaires dont la composition et la taille des bulles varient. Des expériences sur des bulles uniques formées à la surface d'un bain liquide ont permis de mesurer l'épaisseur du film liquide au moment de sa rupture. Nous démontrons que l'effet stabilisant est dû aux différences de concentration des espèces entre le volume et l'interface avec l'air : le liquide de tension de surface la plus faible a une concentration légèrement supérieure à l'interface et joue ainsi le rôle d'un tensioactif. Nous montrons ensuite comment ces différences de concentration sont reliées aux non-linéarités des variations de la tension de surface du mélange avec sa composition et quelles sont les conséquences sur le temps de vie des films liquides. Enfin, la rhéologie de surface de ces systèmes est plus simple que celle des films de savon et nous proposons une description quantitative de la formation, du drainage et de la rupture des films liquides.

Mots clés : moussabilité ; mousse d'huiles ; films liquides minces ; tension de surface ; temps de vie des mousses/bulles ; effet Marangoni

SUBJECT : FOAMABILITY OF OIL MIXTURES

Abstract :

Foaming in oil mixtures is a common problem, for example in electric motor gearboxes. Anti-foaming agents can be used, but it is important to understand how foam forms. Pure liquids do not form foams because of the short life of liquid films, where there is no effect against attractive van der Waals interactions. However, the effect at the origin of increased lifetimes of liquid films in oil mixtures, in the absence of other known stabilizing effects, has not been explained. This thesis proposes a mechanism for this increase. We have measured the lifetime of foams in binary mixtures of varying composition and bubble size. Experiments on single bubbles formed on the surface of a liquid bath allowed us to measure the thickness of the liquid film at the time of its rupture. We demonstrate the stabilizing effect is due to differences in species concentration between the volume and the interface with air: the liquid with the lowest surface tension has a slightly higher concentration at the interface and thus acts as a surfactant. We then show how these concentration differences are related to the non-linearities of the variations of the surface tension of the mixture with its composition and what are the consequences on the lifetimes of liquid films. Finally, we show that the surface rheology of these systems is simpler than that of soap films and propose a quantitative description of the formation, drainage and breakup of liquid films.

Keywords : foamability ; oil foam ; thin liquid films ; surface tension ; bubble/foam lifetimes ; Marangoni effect